DTU Library

Informed Sampling-based Collision and Grounding Avoidance for Autonomous Marine Crafts

Enevoldsen, Thomas Thuesen

Publication date:
2023

Document Version
Publisher's PDF, also known as Version of record

[Link back to DTU Orbit](#)

Thomas T. Enevoldsen

Informed Sampling-based Collision and Grounding Avoidance for Autonomous Marine Crafts

PhD Thesis, January 2023

Informed Sampling-based Collision and Grounding Avoidance for Autonomous Marine Crafts

Thomas T. Enevoldsen

Summary

Maritime technology has undergone significant developments in the past decades, but the frequency of collision and grounding incidents has not decreased. A majority of incidents are still attributed to human error [1]. This thesis focusses on algorithms for decision support and autonomous navigation that allow humans or an autonomous system to navigate safely.

A central element towards this is an effective collision and grounding avoidance system. Any vessel, autonomous or not, is required to adhere to the rules of safe navigation, the IMO COLREGs. The COLREGs describe the required navigational behaviours and describe the obligations between vessels when the risk of collision is imminent. The collision avoidance system must therefore comply with the COLREGs, to ensure safe navigation. Restrictions posed by the surrounding environment must also be accounted for to protect against grounding. The objective of this thesis is to research and develop novel collision and grounding avoidance algorithms, for use during fully or partial autonomous operation. To achieve these objectives, the thesis first investigates the COLREGs and general practises for safe navigation. Techniques within sampling-based motion planning (SBMP) are then used to develop a collision and grounding avoidance framework capable of considering the high-fidelity nature of the Electronic Navigational Charts (ENCs) and the complex nature of the COLREGs. Sampling-based motion planning is an established paradigm for solving challenging planning problems and is selected as the main approach to investigate the collision and grounding avoidance problem.

The thesis employs standard navigation methods to assess the risk of collision and to investigate which COLREGs are applicable in a given situation. Custom ship domains based on Lamé curves are proposed to bias the path planner toward finding route deviations in compliance with COLREGs rules 8 & 13-17. Conventional ideas within sampling-based motion planning are challenged to be able to extend the method from path planning to collision avoidance. When collision avoidance is performed, it is desired to leverage the underlying nominal path or route. This is done to ensure that the objectives encoded by the nominal route are included within the computed optimal deviation. As a result, novel cost functions were required to

calculate paths with minimum route deviation, which were subsequently developed and presented, leveraging ideas from existing track-control problems. Furthermore, a data-driven objective function, based on historical navigation information, is investigated to include the notion of "good seamanship" when computing route deviations, so that they mimic the behaviour of human navigators. Methods are investigated to increase the performance and convergence properties of sampling-based motion planning algorithms and are achieved by introducing novel sampling strategies. An informed sampling strategy is presented that accelerates the convergence towards solutions with minimum path deviation. In addition, a data-driven sampling strategy is proposed, which takes advantage of past experiences of others. This is shown to be effective in rapidly finding solutions within the vicinity of prior data. The informed and data-driven sampling strategies are demonstrated for cases related to marine crafts as well as general sampling-based motion planning problems.

The architecture and functional descriptions for an autonomy stack are presented in detail, with a specific emphasis on the role of the collision and grounding avoidance module to obtain partial or full autonomy. The *Short Horizon Planner* (SHP) is introduced as the module responsible for computing COLREGs compliant and safe route deviations.

In general, the proposed methods are demonstrated in the context of both the merchant fleet and for an autonomous harbour bus, the Greenhopper, primarily through high-fidelity simulations and hardware-in-the-loop testing using the proposed autonomy stack.

The research findings have been disseminated through publication or submission to international journals and also presented at international conferences. These scientific articles are part of the thesis.

Resumé

Navigation af skibe understøttes i stadig stigende grad af teknologi, men på trods af en løbende udvikling er antallet af uheld og ulykker forblevet uændret [1]. De fleste hændelser tilskrives menneskelige fejl. Denne afhandling bidrager til at udvikle den teknologi, der understøtter navigation fra at være brugerbetjent med stigende kompleksitet, til at blive smartere med præsentation af grundigt analyserede løsningsforslag. Med udgangspunkt i maskinel fortolkning af den navigationsmæssige situation bidrager afhandlingen med metoder til automatisk beregning af de manøvrer, der bør udføres for at undgå risiko for kollision eller grundstødning.

Til søs sætter internationale søvejsregler (COLREGs) rammen for forventet og påkrævet adfærd, hvis der er en risiko for kollision. Afhandlingen udvikler metoder og algoritmer, der beregner, hvordan der skal navigeres i en given situation, således at COLREGs regler overholdes samtidig med, at der tages højde for omgivelserne, herunder vanddybde.

Målet med afhandlingen er at udvikle nye metoder og algoritmer til sikker navigation, som beslutningsstøtte både for navigatører og som grundlag for autonom navigation for fartøjer hvor navigatøren ikke nødvendigvis befinder sig ombord. Arbejdet udvikler og videreudvikler metoder til anti-kollision, som er i stand til at tage højde for søkortinformation samt relevante søvejsregler. Forskningsarbejdet tager udgangspunkt i prøvebaseret bevægelsesplanlægning og bidrager med udvidelse og tilpasning til maritim navigation.

Afhandlingen udvikler specielle skibsdomæner baseret på Lamé-kurver for at kunne fjerne ruteforslag, som ikke er i overensstemmelse med COLREGs, og den udfordrer konventionelle idéer inden for prøvebaseret bevægelsesplanlægning fra at omhandle ruteplanlægning til også at understøtte kollisionsafvigelse. Tilpasningerne til det maritime domæne inkluderer både domænespecifikke kostfunktioner og funktioner baseret på maskinlæring, hvor algoritmerne lærer ud fra historiske data og kvantificerer begrebet "godt sømandskab". Som resultat efterlignes adfærden hos menneskelige navigatører samtidig med, at computerkraft udnyttes til at beregne de minimale afvigelser fra planlagt kurs, som tilmed undgår risici.

Afhandlingen undersøger ydermere konvergensegenskaberne af algoritmer, og udvikler en "oplyst" strategi (informed sampling strategy), som accelerer konvergens. Desuden udnyttes historiske AIS observationer til hurtigere at kunne finde løsninger på baggrund af data.

De omtalte metoder blev udviklet til brug både ombord på større skibe, som handelsflåden, samt til den autonome havnebus Greenhopper. Resultaterne blev primært vist igennem avancerede simuleringer af hele det autonome system, blev valideret på SIMAC's træningssimulator, og desuden implementeret og testet på den faktiske hardware.

Forskningsresultaterne er udgivet eller under bedømmelse i internationale tidsskrifter og konferencer. De videnskabelige artikler indgår i afhandlingen.

Preface

This thesis was prepared at the Automation and Control Group (AUT), Department of Electrical and Photonics Engineering of the Technical University of Denmark (DTU), in partial fulfillment of the requirements for acquiring the PhD degree in engineering. The project was funded by the Innovation Fund Denmark, the Danish Maritime Fund, Orients Fund, and Lauritzen Fonden through the Autonomy part of the ShippingLab project, grant number 8090-00063B. The electronic navigational charts were provided by the Danish Geodata Agency.

The project advisors were:

- Associate Professor Roberto Galeazzi (main supervisor), Department of Electrical and Photonics Engineering, Automation and Control Group, DTU.

- Professor Mogens Blanke (co-supervisor), Department of Electrical and Photonics Engineering, Automation and Control Group, DTU.

Part of the research was carried out at ETH Zürich with Professor Emilio Frazzoli as the supervisor.

This thesis consists of a summary report of all research findings gathered as a collection of published or submitted articles in peer reviewed scientific journals and published in conference proceedings in the period 2020-2023.

_____

Kgs. Lyngby, January 2023
Thomas T. Enevoldsen

List of Publications

Publications included in the thesis

(A) T. T. Enevoldsen, C. Reinartz, and R. Galeazzi, "COLREGs-Informed RRT* for Collision Avoidance of Marine Crafts," *2021 IEEE International Conference on Robotics and Automation (ICRA)*, 2021, pp. 8083–8089. DOI: `10.1109/ICRA48506.2021.9560909`.

(B) T. T. Enevoldsen and R. Galeazzi, "Grounding-aware RRT* for Path Planning and Safe Navigation of Marine Crafts in Confined Waters," *IFAC-PapersOnLine*, vol. 54, no. 16, pp. 195–201, 2021, 13th IFAC Conference on Control Applications in Marine Systems, Robotics, and Vehicles CAMS 2021. DOI: `https://doi.org/10.1016/j.ifacol.2021.10.093`.

(C) T. T. Enevoldsen, M. Blanke, and R. Galeazzi, "Sampling-based collision and grounding avoidance for marine crafts," *Ocean Engineering*, vol. 261, p. 112 078, 2022. DOI: `https://doi.org/10.1016/j.oceaneng.2022.112078`.

(D) T. T. Enevoldsen and R. Galeazzi, "Informed sampling-based collision avoidance with least deviation from the nominal path," *2022 IEEE/RSJ International Conference on Intelligent Robots and Systems (IROS)*, 2022, pp. 8094–8100. DOI: `10.1109/IROS47612.2022.9982202`.

(E) T. T. Enevoldsen and R. Galeazzi, "Guaranteed Rejection-free Sampling Method Using Past Behaviours for Motion Planning of Autonomous Systems," 2022, Under review. DOI: `https://doi.org/10.48550/arXiv.2109.14687`.

(F) T. T. Enevoldsen, M. Blanke, and R. Galeazzi, "Autonomy for Ferries and Harbour Buses: a Collision Avoidance Perspective," 2023, Under review. DOI: `https://doi.org/10.48550/arXiv.2301.02711`.

Publications not included in the thesis

(G) F. E. T. Schöller, T. T. Enevoldsen, J. B. Becktor, and P. N. Hansen, "Trajectory Prediction for Marine Vessels using Historical AIS Heatmaps and Long Short-Term Memory Networks," *IFAC-PapersOnLine*, vol. 54, no. 16, pp. 83–89, 2021, 13th IFAC Conference on Control Applications in Marine Systems, Robotics, and Vehicles CAMS 2021. DOI: `https://doi.org/10.1016/j.ifacol.2021.10.077`.

(H) P. N. Hansen, T. T. Enevoldsen, D. Papageorgiou, and M. Blanke, "Autonomous navigation in confined waters - a colregs rule 9 compliant framework," *IFAC-PapersOnLine*, vol. 55, no. 31, pp. 222–228, 2022, 14th IFAC Conference on Control Applications in Marine Systems, Robotics, and Vehicles CAMS 2022. DOI: `https://doi.org/10.1016/j.ifacol.2022.10.435`.

(I) C. Reinartz, T. T. Enevoldsen, R. Galeazzi, and O. Ravn, "A causal model-based planner for the reconfiguration of continuous processes," *2021 European Control Conference (ECC)*, 2021, pp. 1751–1756. DOI: `10.23919/ECC54610.2021.9655016`.

(J) C. Reinartz and T. T. Enevoldsen, "pyTEP: A Python package for interactive simulations of the Tennessee Eastman process," *SoftwareX*, vol. 18, p. 101 053, 2022. DOI: `https://doi.org/10.1016/j.softx.2022.101053`.

Acknowledgments

"Alle små åer i enge
gemmer en underlig drøm
om havet, det store, det frie,
som stilner den stridende strøm.

Når løbet er kæmpet til ende,
er havet det mål, de skal nå,
havet der frier fra alle
de kræfter, som tvinger en å."
 — Piet Hein, August 1934*, extract from*
 ÅEN OG HAVET[1], reproduced with kind
permission from Piet Hein A/S, Middelfart

At the beginning of 2020, the PhD ship set sail in calm waters, and the journey officially began. Already at this time, a storm was forming, and before anyone knew it, the COVID-19 pandemic would change the course of many ships in the coming years. Despite the endless unforeseen challenges associated with operating during a global pandemic, the ship still made it to its final destination, marking the end of the PhD voyage, with both the ship and the crew intact. The journey would not have been a success without the many "elder brethren", great companions and supporters along the way.

The first acknowledgement goes to my main supervisor Associate Professor *Roberto Galeazzi*, for not only supporting me but also for always believing in all of my ideas and work, throughout the course of our collaboration. His very valuable guidance and input always elevated our work to the next level, and the many publications would not have been the same without him. In the end, he has undoubtedly shaped my trajectory as an academic, and for that I am deeply grateful.

---

[1]Piet Hein, 1991, DIGTE FRA ALLE ÅRENE, p. 58

Table of Contents

List of Abbreviations

LWIR Long Wavelength Infrared. 10, 278

MARPOL International Convention for the Prevention of Pollution from Ships. 2

MASS Maritime Autonomous Surface Ships. 5, 6, 7, 8, 9, 25, 26, 27, 30, 31, 32, 33, 36, 38, 49, 50, 109, 110, 115, 117, 119, 120, 121, 122, 123, 275, 276, 281, 283, 285, 286

MMSI Maritime Mobile Service Identity. 90, 91, 102

MPC Model Predictive Control. 18, 20, 23, 151, 191, 192, 201

MSC Maritime Safety Committee. 6

MWS Middleware Simulator. 104, 105, 114, 116, 117, 285, 286

NED North-East-Down. 39, 45, 47, 62, 63, 66, 84, 85, 91, 111, 201, 202, 205

OCP Optimal Control Problem. 18, 19, 276, 277

PAD Predicted Area of Danger. 171, 201

PDF Probability Density Function. 83, 84, 85, 92, 93, 96, 157, 158, 252

PRM Probabilistic Roadmaps. 21, 227, 247

PSO Particle Swarm Optimizaton. 17

RADAR Radio Detection and Ranging. 153, 173

RCC Remote Control Center. 49, 104, 107, 288

ROT Rate of Turn. 50, 90

RRT Rapidly-exploring Random Trees. 19, 21, 22, 53, 55, 56, 70, 150, 151, 171, 192, 200, 228, 247

RRT* Optimal Rapidly-exploring Random Trees. 19, 21, 22, 23, 24, 29, 51, 53, 54, 55, 56, 57, 63, 68, 70, 73, 76, 77, 150, 151, 152, 155, 160, 162, 163, 164, 169, 170, 171, 178, 179, 181, 183, 192, 193, 200, 201, 226, 227, 228, 229, 235, 247, 248, 249, 257

RUT Route Server. 104, 107, 108, 285, 286

SAS Situation Awareness Service. 104, 107, 108, 109, 110, 115, 117, 285, 286

Chapter 1

Introduction

The world's population recently surpassed 8 billion people, further highlighting the importance of a continued acceleration of the green transition. More than ever, there is a demand for improved and sustainable logistic and mobility capabilities, to further facilitate the protection and preservation of the remaining natural precious resources and the environment.

One of the crucial available resources is the ocean, where its well-being is essential, as it is a key contributor and regulator for many of the processes that allow humans, and other life forms, to inhabit planet Earth. The oceans are not only responsible for absorbing carbon dioxide, but also serve as a regulating factor for climate, weather, drinking water, food sources, and much more [12].

In 2015, United Nations (UN) adopted the 17 Sustainable Development Goals (SDG), which are common goals to be reached by 2030, to ensure the well-being of the planet now and in the future. Here, the importance of the ocean is clearly emphasised by the fact that one of the SDGs is dedicated to saving and preserving life below water (SDG 14[1]). The oceans are related to additional SDGs, namely sustainable consumption and production (SDG 12[2]), and climate action (SDG 13[3]). One of the contributing factors to the detriment of the oceans are marine incidents related to groundings and collisions. In particular, incidents involving tankers and container vessels, due to their potential cargo, pose an increased risk of severe pollution [13]–[15].

Conventions are established to prevent both collision and grounding incidents

---

[1]UN SDG 14 - Life below water `https://www.un.org/sustainabledevelopment/oceans/` (Accessed November 22nd, 2022)

[2]UN SDG 12 - Responsible consumption and production `https://www.un.org/sustainabledevelopment/sustainable-consumption-production/` (Accessed November 22nd, 2022)

[3]UN SDG 13 - Climate action `https://www.un.org/sustainabledevelopment/climate-change/` (Accessed November 22nd, 2022)

and maritime pollution by International Maritime Organization (IMO) and United Nations Convention on the Law of the Sea (UNCLOS), which are the primary overseeing entities of the oceans. IMO, in particular, has both constructed and adopted several conventions that target ship owners, ship builders, and seafarers, in order to increase the safety and general well-being of the oceans.

One such convention is the International Convention for the Prevention of Pollution from Ships (MARPOL), which was first adopted in 1973, but has recently seen many additions and amendments to align with the expectations and desires of the SDGs. A significant addition was Annex VI, which places limits on the emissions and prohibits deliberate emission of ozone-depleting substances. Another convention is the Convention on the International Regulations for Preventing Collisions at Sea (COLREGs), which provides a unified rule-oriented approach to safe navigation practises, by establishing 41 rules for navigation and signalling equipment. This provides sailors and navigators with a common understanding of how to deconflict and mitigate potential collision and grounding risks [16]. Furthermore, as prescribed by the International Convention for the Safety of Life at Sea (SOLAS) [17, Chapter 5], modern integrated bridge systems onboard larger vessels comprise various technologies: Electronic Chart Display and Information System (ECDIS), Automatic Radar Plotting Aid (ARPA) radar systems, and for some vessels Automatic Identification System (AIS). All of which constitute unified measures to ensure the safe passage of marine vessels.

1.1 Marine incidents and casualties

Despite both the existence of extensive conventions and regulations, in combination with great technological advancements and strict vessel requirements, maritime incidents and casualties continue to occur. Within the past 3 months, several grounding incidents have occurred in Danish waters. Such as Ragna, a German container vessel, which grounded itself on October 28th, 2022, in the Little Belt area of Denmark[4]. Later on December 15th, 2022, the coaster, Scanlark, grounded itself west of the island of Samsø[5]. As recently as January 23rd, 2023, the Norwegian freight carrier, Peak Skorpo, grounded itself near Nakskov[6].

Both collision and grounding incidents continue to occur on a global scale,

---

[4]https://www.soefart.dk/article/view/877049/containerskib_pa_grund_i_lillebaelt_k aptajn_anholdt (Accessed January 30th, 2023)

[5]https://www.soefart.dk/article/view/887043/fragtskib_er_gaet_pa_grund_naer_samso (Accessed January 30th, 2023)

[6]https://www.soefart.dk/article/view/893277/fragtskib_gaet_pa_grund_ved_nakskov (Accessed January 30th, 2023)
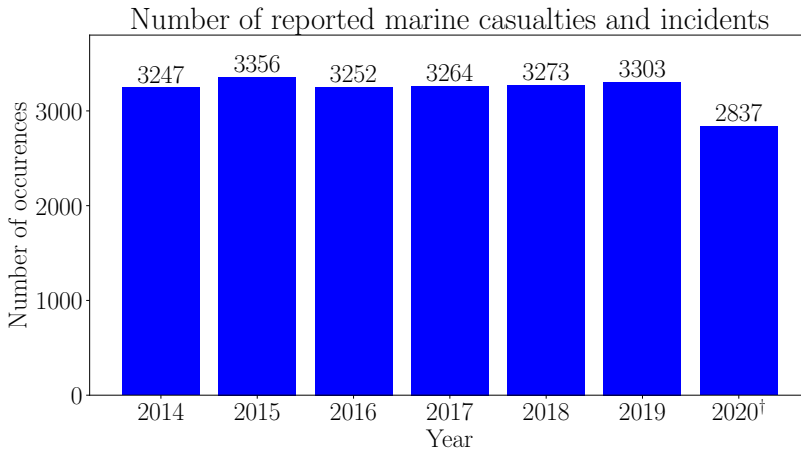
Figure 1.1: Statistics from European Maritime Safety Agency (EMSA) concerning the number of reported marine incidents and casualties, which have remained close to constant the past 7 years. †There is a small decrease in the number of reported incidents in 2020, this is linked with a reduction in maritime traffic due to and during the height of the COVID-19 pandemic. During March to June 2020 there was a worldwide recorded drop between -5.64 and -13.77% for container ships and -19.57% and -42.77% for passenger crafts [18].

involving vessels of great size. On the morning of August 7th, 2022, the container vessel BF TIGER collided with another cargo vessel, Xinghang, causing the latter vessel to sink[7]. On August 29th 2022, a bulk carrier named OS 35 collided with the Liquefied Natural Gas (LNG) tanker, ADAM LNG, with OS 35 being urged to purposely ground post-collision to minimise the risk of sinking[8].

The European Maritime Safety Agency (EMSA) reports[9] that the number of marine causalities[10] and incidents have remained steady over the past seven years, see Figure 1.1 [1, p. 13]. Navigational incidents that factor in a degree of human contribution, consisting of collision, contact, and grounding/stranding events, represent 43% of all incidents and casualties [1, p. 19]. Uğurlu *et al.* [19] showed that poor use of the integrated bridge system and other available equipment, combined

---

[7]https://www.soefart.dk/article/view/861393/fragtskib_synker_efter_kollision_med_maerskchartret_containerskib (Accessed January 30th, 2023)

[8]https://www.soefart.dk/article/view/864925/fragtskib_pa_grund_efter_kollision_med_lngfartoj (Accessed January 30th, 2023)

[9]The data is based on incidents/casualties with: vessels carrying flags from a EU member state, occurences within territorial waters of an EU member state, or other incidents within the interests of an EU member state [1, p. 4].

[10]Marine casualty refers to an event that results death, injury or loss of a person onboard a ship, abandonment or loss of a ship, stranding or collision, ship material damage, marine infrastructure damage, environmental damage. For further details, see EMSA [1, p. 12]
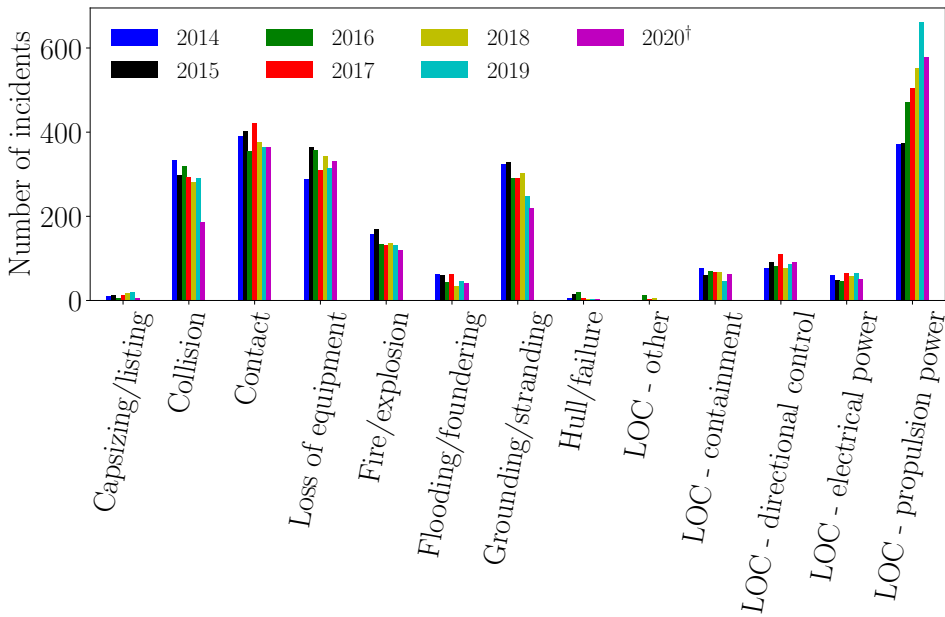
Figure 1.2: A categorical breakdown of the incident types. It is clear that the main contributing factor is Loss of Control (LOC) in the propulsion power. However, it is noteworthy that incidents including the human element, that is: collision, contact and grounding/stranding combined constitute a large part of the overall incidents. [†]As this bar chart represents the incidents over the same period as Figure 1.1, there is a decrease in the number of reported incidents in 2020, linked with the COVID-19 pandemic [18].

with poor assessment of the situation, is one of the leading causes of grounding events. During the 2014-2020 period, cargo ships were the most frequent type of vessel involved in incidents with other ships (49%), followed by passenger ships (22%), fishing vessels (14%), service ships (11%) and the final 4% classified as other ships [1, p. 20]. Marine incidents and causalities result not only in material and human losses, but also in great ecological damage [20]. It is worth noting that oil spills in particular have been at an all-time low in the past decade, although the most common causes are allisions and collisions (over 40%), seconded by grounding incidents [21].

Autonomous transportation systems seek to increase efficiency in terms of availability, mobility, safety, and emissions. The automotive industry has provably taken advantage of the technological by-products of vehicle autonomy for more than a decade, providing humans with important assistive technologies, such as various degrees of lane assistance, to improve safety [22]–[24].

Similarly, maritime autonomy seeks to further advance existing technology and

also take advantage of the knowledge gained from the shift toward Maritime Autonomous Surface Ships (MASS), thus bringing greater mobility capabilities and safer operations to existing fleets and new builds. Increasing safety and onboard navigation capabilities will ultimately lead to a decrease in maritime incidents and causalities related to human error. By reducing the occurrence of such events, there will be an overall positive impact on the environment, which is consistent with the objectives of the SDGs.

1.2 Autonomy for marine crafts

Recently, maritime autonomy has seen rapid developments, technological maturity, and many important demonstrations of the current state-of-the-art. Caccia [25] and Rivkin [26] surveyed major results and developments within MASS technologies, describing worldwide developments for commercial and defence applications, giving an older and more recent perspective, respectively.

The past five years have seen multiple instances and demonstrations of functioning MASS technology onboard large commercial vessels. In December 2018, Finferries and Rolls-Royce demonstrated autonomous capabilities onboard the Falco[11], the world's first fully autonomous ferry. In fall 2021, Sea Machines sent their 11m long vessel on a 1000nm autonomous voyage, which they titled "The Machine Odyssey"[12]. The journey took place from Cuxhaven, Germany and sailed north through Germany into the inner coastal waters of Denmark, before returning to Hamburg, Germany. Showing their situation awareness technology within inner coastal waters, and autonomously performing 31 collision avoidance manoeuvres. In 2020, the MEGURI2040[13] project was formed, which is a Japanese initiative to alleviate their ageing navigators, improve navigational safety, and increase mobility for their many island societies. In early 2022, six different demonstrations of their current autonomy initiatives took place, most notable was the fully autonomous (both birthing and navigation) container ship the Mikage[14]. Around the same time, a newly built fully autonomous car ferry, the SOLEIL[15], also demonstrated autonomous

---

[11]https://www.rolls-royce.com/media/press-releases/2018/03-12-2018-rr-and-finferries-demonstrate-worlds-first-fully-autonomous-ferry.aspx (Accessed November 21st, 2022)

[12]https://sea-machines.com/the-machine-odyssey/ and https://sea-machines.com/introducing-the-machine-odyssey-worlds-first-1000-nm-autonomous-voyage/ (Accessed November 21st, 2022)

[13]https://www.nippon-foundation.or.jp/en/what/projects/meguri2040 (Accessed November 21st, 2022)

[14]https://maritime-executive.com/article/first-autonomous-navigation-and-berthing-test-on-a-containership (Accessed November 21st, 2022)

[15]SOLEIL https://www.mhi.com/news/220117.html (Accessed November 21st, 2022)

navigation. During a 40 day voyage in spring 2022, IBM and ProMare achieved a fully unmanned and autonomous crossing of the Atlantic ocean, sailing from Plymouth, United Kingdom, to Halifax, Nova Scotia. The Mayflower[16] (also known as MAS400) demonstrated artificial intelligence-driven perception systems. Norwegian Yara Birkeland[17], a collaboration between KONGSBERG and Yara, aims to become the first zero-emission autonomous container feeder. The autonomy and approval activities of the class societies are expected to take place in 2023-2024.

Serious efforts within maritime urban mobility have also received some attention. In 2018, Wärtsilä unveiled an autonomous dock-to-dock system[18], where a ferry fully autonomously serviced three ports along its route. In fall 2022, the Norwegian autonomous ferry, Milliampere, was made available for tests with the public, highlighting the technology developed by NTNU and served as an important case study for inner-city mobility [27]. As a spin-off from the Milliampere effort, the company Zeabuz was formed, which takes advantage of the accumulated research experiences and aims to launch a ferry solution in 2023. Another Norwegian initiative, Hyke, is also working towards increasing mobility and accessibility. In the canals of Amsterdam, Roboat, which is a collaboration between MIT and Amsterdam Institute for Advanced Metropolitan Solutions (AMS), aims to provide autonomous waterborne mobility and service solutions, freeing clutter from the streets[28]–[30].

1.2.1 Autonomy for merchant vessels and ocean liners

The road to full maritime autonomy is not yet fully realised, as there are challenges both from a societal and legislative perspective [31]–[33]. However, the topic of autonomous shipping and MASS in general has now appeared on IMO's radar[19], as an increased interest is displayed in integrating and adopting current developments into its regulatory framework. This was made evident during the 105th session of IMO's Maritime Safety Committee (MSC), where it was agreed to develop a non-mandatory code for MASS, with the possibility for it to become mandatory, as an amendment to SOLAS, starting January 2028. The initial steps for developing this code are underway until June 2023 [34].

As a result, the shift towards autonomy within the merchant fleet will most likely

---

[16]Mayflower `https://www.mas400.com` (Accessed November 21st, 2022)

[17]Yara Birkeland `https://www.yara.com/knowledge-grows/game-changer-for-the-environment/` and `https://www.kongsberg.com/maritime/support/themes/autonomous-ship-project-key-facts-about-yara-birkeland/` (Accessed November 21st, 2022)

[18]`https://maritime-executive.com/article/waertsilae-conducts-autonomous-ferry-voyage-and-docking` (Accessed November 24th, 2022)

[19]`https://www.imo.org/en/MediaCentre/HotTopics/Pages/Autonomous-shipping.aspx` (Accessed November 25th, 2022)

be a gradual process. Instead, technologies emerging from the developments towards maritime autonomy will enable various degrees of automation and optimisation, through retrofits and installation of minor additions to the existing equipment. In the study by Rivkin [26], it was concluded that current state-of-the-art technologies are sufficient for MASS, which is also evident from the recent increase in efforts and demonstrations within the space of maritime autonomy.

The sensor and hardware stack required for basic autonomy can provide an electronic outlook, to complement existing systems onboard, such as the ARPA radar and ECDIS. By combining the electronic outlook with a certain degree of automatic situation awareness and by adding collision and grounding avoidance algorithms, one can create a rudimentary system for navigational decision support.

For a majority of the merchant vessels and ocean liners, a significant portion of their voyage is conducted in open waters, where the frequency of traffic and required manoeuvring is heavily reduced and the risk of grounding non-existent.

During these periods, a decision support system could allow the manned bridge to rest or perform other duties while on watch. The electronic outlook and situation awareness systems then maintain an overview of the surroundings and, if required, alert the crew in ample time, so that action can be taken to deconflict the situation. Such a system, when applied to open waters, could allow for a temporally unmanned bridge, and thereby enable partial autonomy. When navigating inland waterways or inner coastal waters, a decision support tool could allow pilots to virtually board ships, mitigating some of the safety risks associated with climbing aboard foreign ships.

In general, the use of decision support systems can enable safer operations by reducing human errors and fatigue. By reducing the human element, the frequency of incidents is subject to decrease, having an overall positive impact on the casualty statistics and the environment.

1.2.2 Autonomy for ferries and harbour buses

The operation of ferries and harbour buses poses a different set of challenges, compared to navigating large vessels in open water. Ferries and harbour buses generally operate within inner coastal and confined waters. A key difference for ferries and harbour buses, compared to merchant vessels, is that their operational region is clearly defined and limited to operating between the same ports at all times. In some circumstances, additional or modified regulations may be present when operating such ferries or harbour buses. In Danish waters, selected ferries must always yield for crossing traffic, irrespective of whether they approach from the port or starboard side [35], [36].

The simplified operating conditions for crafts, such as ferries and harbour buses, allow the development of tailored solutions to the particular problem at hand. However, these waters are typically occupied by experienced and inexperienced seafarers, due to the abundance of leisure crafts present within such waters. These challenges require that the autonomous system is capable of detecting abnormalities and safely addressing emergency scenarios. Acting in a human-predictable manner as expected by fellow sailors is crucial, as this is both according to the rules and for the sake of safe navigational practises.

If achieved, these autonomous ferry technologies can increase the available mobility and could be beneficial not only for urban scenarios, but in particular also for smaller island communities. In countries such as Denmark[20] and Japan[21], there exist many smaller island societies, many of which are threatened by the lack of service, as in some instances they are limited by the number of scheduled departures. Autonomous ferry solutions allow for increased or constant availability of certain routes by providing an on-demand service.

1.3   ShippingLab

ShippingLab is a Danish non-profit collaborative initiative for autonomous water-borne mobility and smart shipping solutions. The primary goal of the ShippingLab project is to create Denmark's first autonomous and environmentally friendly ship. The ShippingLab project is divided into three areas: digital ship operations, autonomy, and decarbonisation. The work package dedicated to autonomy aims to research and develop technologies for partial and fully autonomous solutions. Partial autonomy for larger crafts is achieved by developing a decision support system, which ultimately could allow for a temporary unmanned bridge. Full autonomy is being developed in the context of an electric autonomous ferry, the Greenhopper.

The partial and full autonomous solutions both use a custom autonomy stack, which is developed based on a modular and end-to-end system approach, with each module within the autonomy stack compartmentalised and clearly defined. Figure 1.3 provides a simplified overview of the MASS architecture, which roughly divides

---

[20]The Danish "Færge Analyse 2019" (*Ferry* Analysis 2019) states that Denmark consists of 391 islands, of which 72 are inhabited. To preserve island communities, local politicians argue that more ferry departures are needed to increase the mobility of island residents. `https://www.danishshipping.dk/publikationer/publikationer-om-skibsfart/download/Publications_Model_Publication/34/faergerederiernes-faergeanalyse-2019.pdf` (Accessed November 28th, 2022)

[21]According to the MEGURI2040 project, Japan has 400 inhabited island, with most of them only serviced twice a day. `https://www.nippon-foundation.or.jp/en/what/projects/meguri2040` (Accessed November 28th, 2022)
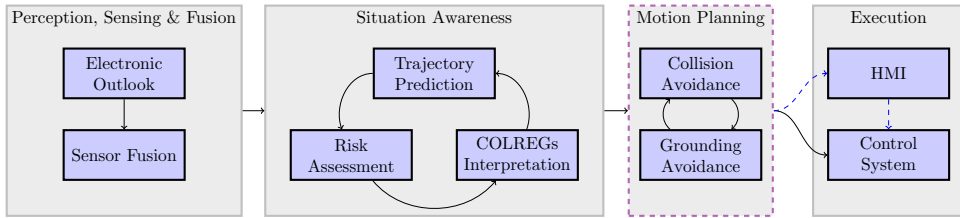
Figure 1.3: Simplified MASS architecture. The perceived information is fused, then subsequently assessed by the situation awareness. Based on the scenario at hand, a route deviation is computed by the collision and grounding avoidance system. The resulting deviation(s) are either sent to a decision support system (Human-machine Interface (HMI))) or directly to the vessel control system.

the system into four categories: Perception & Sensing, Situation Awareness, Motion Planning, and finally Execution.

The Perception, Sensing & Fusion stack is the combination of all available sensory information, which ultimately results in fused estimates of the vessel surroundings and the own ship itself. Perception and Sensing constitute all the information from the electronic outlook, which is composed by input from systems such as the ECDIS, radars, cameras, etc. Fusion is responsible for joining all sensor inputs to a coherent description of the vessel surroundings. Based on a continuous stream of information regarding the vessel surroundings, the Situation Awareness provides an assessment, by anticipating future evolution through predictions and risk assessment. A high-level COLREGs interpreter provides analysis that takes into account the perceived scenario and triggers requests for route deviations accordingly. Once a deviation has been called for, motion planning is executed in the form of a collision and grounding avoidance module, which responds with rule-compliant and safe trajectories to be subsequently executed by the navigator or vessel control system.

The Greenhopper

The demonstration of the autonomous technologies will take place onboard recently built vessel, the Greenhopper. The Greenhopper is a 12.2 m long double-ended battery-operated catamaran capable of carrying 25 passengers, two crew members, a baby carriage, one wheelchair and four bicycles. Figure 1.4 shows the Greenhopper manoeuvring in a Danish harbour.

The Greenhopper will provide an alternative service to cross the fjord, with a voyage duration of 5-7 minutes, over a distance of approximately 600 m. Figure 1.5 highlights the area of Limfjorden served by Greenhopper. The vessel can freely traverse the area, as it is not restricted by its draught. The westernmost land masses

Figure 1.4: The Greenhopper: a Danish autonomous ferry.
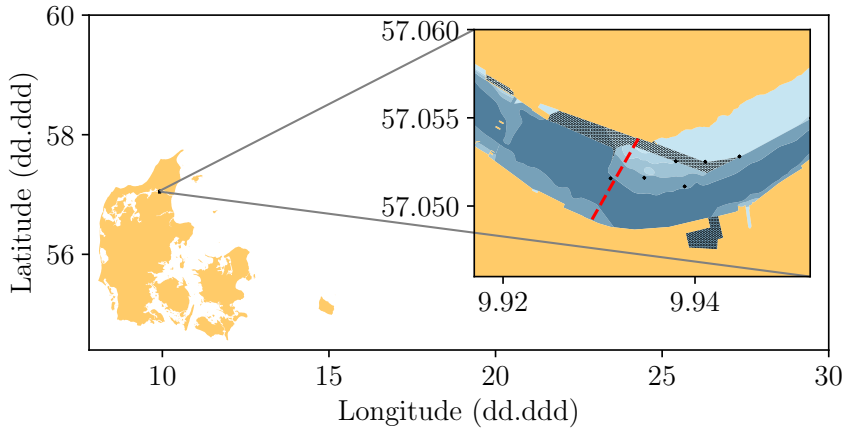
Figure 1.5: The Greenhopper area of operation, located at Limfjorden, Aalborg, Denmark. The dashed red line is the nominal route, crosses buoys and hatched areas dredged locations. Darker blues are deeper contours.

within the fjord are the pillars of the Limfjordsbroen (a bridge connecting Aalborg and Nørresundby). Furthermore, the Greenhopper serves as a research vessel to demonstrate autonomous capabilities, which have been researched and developed within the ShippingLab project.

The Greenhopper is equipped with the necessary sensors and actuators to achieve autonomous navigation. Two azimuth thrusters mounted in the fore and aft, along the centre line, allow the vessel to manoeuvre freely upon the surface of the water. On a mast are four RGB cameras and eight Long Wavelength Infrared (LWIR) cameras for electronic outlook. An X band radar, a Global Navigation Satellite System (GNSS)

receiver, a gyro compass, an AIS transponder and an Inertial Measurement Unit (IMU) for navigation and target vessel detection, and finally four W band radars and two 3D lidars for close quarter obstacle detection and docking. Most of the sensors are mounted on the mast, with the lidars and W band radars mounted on the railings; see Figure 1.4. Steering and waypoint commands are executed by a Voyage Control System (VCS). The system operates between a set of nominal waypoints, where the VCS will safely perform the required docking manoeuvres and voyage sequences. When a deviation is required, the existing route can be either augmented or completely replaced, such that a collision situation can be appropriately deconflicted.

1.4 Research objectives

Marine vessels perform long or short passages based on an underlying nominal route, optimised so that the port of call is met, bad weather is avoided, passenger transport is maximised, and criteria such as fuel and energy efficiency is optimised. However, the nominal route depicts an ideal voyage and, for good reason, is incapable of considering the varying presence of target vessels and traffic conditions that may arise locally along the route. During the voyage, when the conditions invalidate the current course and speed, a navigator must assess the unfolding situation and then, based on his experience and the COLREGs, choose to alter the speed or course. The navigator performs a deviation that is a trade-off between loss of performance, with respect to following the previously optimal conditions of the nominal route, and safety.

During the operation of an autonomous vessel, the given system must be equipped such that a workflow similar to that of a human navigator can be achieved. The unfolding scenario must be correctly assessed and dealt with. A central element for such an operation is an effective collision and grounding avoidance system, which is capable of reporting whether there is a feasible route deviation, when called upon. Then, depending on whether the system is partially or fully autonomous, the proposed route deviation is presented to the human navigator as assistance or executed directly by the autonomous system.

This thesis constitutes the work carried out in relation to the ShippingLab autonomy work package, which focusses primarily on the research and development of the motion planning module (see Figure 1.3). Therefore, the main research objectives are to investigate collision and grounding avoidance methodologies for fully and partially autonomous marine crafts. In the context of the thesis, the collision and grounding avoidance module will also be called Short Horizon Planner (SHP), as

this is the internal name of the module within the ShippingLab autonomy stack. The developed methods are presented, when applicable, in the context of both generic merchant vessels and an autonomous harbour bus (Greenhopper).

As such, one could ask the following questions:

1. What constitutes COLREGs-compliance and safe navigation practises, and how are they adequately incorporated into autonomy?

2. What is "good seamanship" and what role does it play for automated collision and grounding avoidance?

3. Given the available information about the surroundings, how does one plan safe and COLREGs-compliant route deviations?

4. Without compromising accuracy, how can one aid in grounding avoidance using the Electronic Navigational Charts (ENCs)?

5. What are the requirements to deploy autonomous collision and grounding avoidance?

On the basis of the above questions, the thesis posed the following research objectives:

1. Research methods to generate COLREGs-compliant route deviations while optimising common criteria set by seafarers and considering safe navigation practises.

2. Research methods to achieve grounding avoidance and increased navigational safety by leveraging the information available to seafarers.

3. Develop and integrate the collision and grounding avoidance module (the Short Horizon Planner) into an autonomy stack.

4. Investigate the underlying requirements for full or partial autonomous operation in the future, both from a technological and societal perspective, in the context of collision and grounding avoidance.

To achieve the research objectives, the thesis investigated the state-of-the-art literature and extended the existing body of knowledge with novel methods and tools based on theoretical developments and practical implementations. To ensure that the outcomes align with practise, expert knowledge from professional seafarers was actively included as part of both the design and validation procedures. The solutions were engineered according to both theory and practise to ensure maximum applicability of the obtained solutions. Using a software framework that mimics the

autonomy stack, the performance of the developed methods was extensively evaluated using software-in-the-loop testing. This allowed for assessing the feasibility of the solutions prior to being deployed on real hardware.

1.5   Thesis outline

The majority of the thesis consists of an article collection that compiles the four conference and two journal publications carried out during the project. The content of the dissertation prior to the attached articles serves as a summary of the proposed novelty, as well as an elaboration of certain parts of the techniques and methodologies.

Following this chapter, Chapter 2 presents the state-of-the-art methods and results within the realm of collision and grounding avoidance strategies for marine crafts, general sampling-based motion planning, and sampling strategies for sampling-based motion planners. Chapter 3 presents an overview of the main contributions of the thesis and describes how each of the papers addresses the previously asked research questions. Chapter 4 discusses safe navigation practises and the COLREGs, for both large and small marine crafts, with a particular emphasis on the rules applicable to the merchant crafts and the autonomous harbour bus, the Greenhopper. Methods for assessing the risk of collision and applying the given COLREGs are described, along with custom ship domain to enforce the applicable rules. Chapter 5 presents the sampling-based motion planning framework tailored towards achieving collision and grounding avoidance for marine crafts. The primary sampling strategies, problem constraints, and objective functions are presented, which all constitute the framework for computing optimal route deviations in compliance with both grounding avoidance and the COLREGs. Chapter 6 describes two advanced sampling techniques, which take advantage of the concept of an informed set to increase the convergence rate of sampling-based motion planning algorithms. Chapter 7 attempts to quantify "good seamanship" as both an objective function and a sampling strategy. By leveraging historical AIS data, the past experience of human navigators is included in the collision and grounding avoidance framework. Chapter 8 presents the modular composition of the autonomous system, more specifically the autonomy stack. Detailed descriptions of the developments for the ShippingLab project are presented, where various modules of the stack are introduced and their interconnection discussed, especially from the perspective of the Short Horizon Planner (SHP), the collision and grounding avoidance module. Finally, Chapter 9 provides a conclusion to the dissertation and summarises the project outcomes, concluding with a discussion about the potential future work.

Chapter 2

State of the art

The following chapter contains an overview of the state of the art, which serves as a summary of the most fundamental and recent advances within both the selected methodologies and research area.

First, the literature surrounding collision and grounding avoidance for marine crafts is detailed, whilst emphasising the use of and compliance towards the COL-REGs [16], with a detailed account of the COLREGs given later in Chapter 4). Second, an overview of the literature concerning both general and various topics within Sampling-based Motion Planning (SBMP) is presented, highlighting important contributions from the field of SBMP.

2.1 Collision and grounding avoidance for marine crafts

The following is an overview of the literature within collision and grounding avoidance, a particular note will be made regarding COLREGs-compliance, therefore, unless stated, a given work neglects the COLREGs.

Tam *et al.* [37] detailed some of the earlier efforts within collision avoidance for close range encounters. Various ship domains are compared, which at the time were used for enforcing the COLREGs. Later, Huang *et al.* [38] published an exhaustive review of the current state-of-the-art within collision avoidance, where a broad survey of current algorithms and techniques for collision avoidance are highlighted, analysed and discussed.

Most recently, a two-part series by Vagale *et al.* [39], [40] detailed various aspects of the path planning and collision avoidance for autonomous marine crafts, where both methods and algorithms have been presented, analysed, and compared. They mention that the current regulations (i.e COLREGs) potentially need updating to accommodate the emerging autonomous marine crafts. Furthermore, the authors

argue that there is a need for a rigorous framework for assessing the capabilities of the autonomous marine crafts.

Campbell *et al.* [41] surveyed existing autonomous collision avoidance strategies for surface vessels, with one of the notable shortcomings being the inability to deal with complex encounters, such as a multiple vessel scenarios, due to the requirement of human-like decision making. The authors also argued that there is a challenge in quantifying COLREGs, which are intended for single vessel encounters and human interpretation.

A similar point is argued by Tam and Bucknall [42], who also discussed the limitations of COLREGs during multiple vessel encounters and proposed a priority-based system that behaves equivalent to a human officer-on-watch. The authors also proposed and emphasised the need for a deterministic collision avoidance scheme, compared to competing stochastic methods, and argued that marine navigation requires consistency in its proposed manoeuvres and solutions.

2.1.1   COLREGs-compliant collision and grounding avoidance

Benjamin and Curcio [43] discussed legal aspects of COLREGs and their possible interpretation by humans. Simulations were provided for dealing with rules 14-17 using a multi-objective optimisation approach based on interval programming [44]. The method is later extended and field tested, also considering rule 8 [45], [46]. Larson *et al.* [47] (and later also in [48]), detailed a complete collision avoidance scheme for autonomous surface vessels, from chart consideration to sensors for obstacle avoidance. Target vessels are avoided using predicted areas of danger and COLREGs-compliance is dealt with by computing the relative bearing towards a given vessel and applying rules 13-15 as needed.

Using fuzzy relational products, Lee and Kim [49] detailed a method to generate paths compliant with rules 13-15. Perera *et al.* [50] detailed a decision-making system for collision avoidance based on fuzzy logic, where the own ship is capable of adhering to rules 13-15 and standing on when required.

Blaich *et al.* [51] proposed using Lee's algorithm [52], which is based on breadth-first search, to solve the collision avoidance problem. Using the ship domain proposed by Goodwin [53], the authors are able to enforce COLREGs rules 13-15. Later, Blaich *et al.* [54] instead proposed using an A* algorithm for increased performance. Campbell and Naeem [55] presented the heuristic rule-based A* (R-RA*) algorithm integrated together with a decision-making framework, which determines the current COLREGs situation using the relative bearing. COLREGs-compliance to rules 13-15 is enforced at the output of the algorithm when the optimal path is delivered. This work was extended in [56] by including target vessel detection, as well as

hardware-in-the-loop testing using a real bridge simulator. Naeem *et al.* [57] used a modified A* to generate COLREGs-compliant paths according to rules 8 and 14, considering vessel dynamics, static and dynamic objects. Singh *et al.* [58] used an A* algorithm to compute collision free paths, without considering the COLREGs, instead the algorithm considers ocean currents.

Ant Colony Optimisation (ACO) was leveraged by Lazarowska [59] to create a collision avoidance scheme. The proposed method uses a hexagonal ship domain to enforce COLREGs rules 8 & 14-15. In Lazarowska [60], a database of path primitives was generated, which were then selected based on the given scenario. COLREGs-compliance is achieved by only storing path primitives that deviate towards the starboard side. Later Lazarowska [61] conducted a comparison study between the two previous proposed methods, applied to recorded data.

Ni *et al.* [62], [63] proposed using Genetic Algorithms (GA) to compute COLREGs-compliant trajectories, enforcing rules 8 & 13-15. Tsou [64] also applied a GA to compute compliant paths, using predicted areas of danger to adhere to rules 13-15, whilst also considering the true polygons from the underlying Electronic Navigational Chart (ENC).

Hu *et al.* [65] proposed a multi-objective optimisation approach, which was solved using Particle Swarm Optimizaton (PSO). COLREGs-compliant paths, considering rules 2(b), 8 & 13-17, are generated despite non-cooperative targets by considering the element of *good seamanship*. These results were later extended in [66], where instead a hierarchical multi-objective variant of PSO was used. The proposed method and implementation were demonstrated using a high-fidelity bridge simulator.

Xue *et al.* [67] proposed using Artificial Potential Fields (APF) to adhere to rules 13-17, both in open and confined waters, using the relative bearing to determine the given COLREGs scenario. Lee *et al.* [68] proposed instead to combine the APF-like approach with a fuzzy logic scheme. This resulted in a system capable of dealing with rule 8, by simply yielding towards starboard for all collision scenarios. [69] detailed a modified APF algorithm, capable of generating COLREGs-compliant paths that enforce rules 13-15, while considering multiple target vessels and static obstacles.

Wilson *et al.* [70] used a line-of-sight algorithm to calculate risks and achieve collision avoidance in a two vessel encounter. Kuwata *et al.* [71] used the Velocity Obstacle (VO) method together with a hazard evaluator to deal with both static and moving obstacles. The proposed method is compliant with rules 8 & 13-15, since the method yields for obstacles that neglect the COLREGs. The VO method and a generalised extension was further investigated by [72], [73], where by disallowing port side manoeuvres COLREGs-compliance towards rules 14 & 15 was achieved.

When casting the collision avoidance problem as an Optimal Control Problem (OCP), it is possible to use methods from control theory, such as Model Predictive Control (MPC). Eriksen and Breivik [74] detailed a method that complied with rule 8, while minimising the deviation from a nominal course, while taking into account static and dynamic obstacles. Using an elliptical COLREGs penalty function and the branching-course MPC algorithm, Eriksen *et al.* [75] proposed a method that complies with rules 8, 13 & 17, whilst favouring trajectories that comply with rules 14 & 15. Eriksen *et al.* [76] further extends on the previous method, proposing a hybrid architecture that combines various levels of collision avoidance and is capable of adhering to COLREGs rules 8 & 13-17. Johansen *et al.* [77] presented a scenario MPC-based scheme that optimises a finite number of course and propulsion commands, by forward simulating the vessel and guidance dynamics of the system, in order to yield COLREGs-complaint manoeuvres (rules 8 & 13-18), utilising short-term linear predictions of the target vessels. Hagen *et al.* [78] expanded upon this, by presenting an extension that no longer relies on accurate knowledge of the underlying dynamics of the vessel, allowing the collision avoidance system to be used to retrofit vessels with existing guidance systems. Kufoalor *et al.* [79] extended the scenario-based MPC approach to include uncertainties manifesting in real radar information, with an exhaustive field verification of the scenario-based method and the surrounding system detailed in [80], discussing adherence towards COLREGs rules 2, 5-8 & 13-19, under the assumption of straight-line target vessel predictions. In Abdelaal *et al.* [81], the authors proposed a non-linear MPC trajectory tracking and collision avoidance scheme, which is compliant with COLREGs rules 13-15, based on straight-line target vessel predictions. This is enforced through a soft constraint on the yaw rate, such that starboard manoeuvres are favoured.

Garrido *et al.* [82] and Chen *et al.* [83] used the Fast Marching Method (FMM) to compute global paths in the presence of both static obstacles and environmental disturbances; however, dynamic obstacles and COLREGs-compliance were not considered. Tan *et al.* [84] proposed using Fast Marching Square (FMS) to remedy the weaknesses of FMM, which consists of running FMM twice with different objectives. COLREGs-compliance towards rules 13-17 is achieved while considering straight-line predictions from the target vessels.

Svec *et al.* [85] proposed a combined 4D lattice and MPC-based collision avoidance scheme. They propose using a probabilistic worst-case estimate of the target vessel locations and checks for adherence to COLREGs rules 13-15. [86] presented a congestion metric and a 5D lattice planner for collision avoidance in both open and confined waters, adhering to COLREGs rules 13-15. Bergman *et al.* [87] demonstrated a two-step collision avoidance scheme, which complied with COLREGs 8 &

13-17. A lattice-based planner driven by a database of motion primitives computes suboptimal trajectories, which are later used as a warm-start and subsequently refined by an OCP.

Chiang and Tapia [88] presented a non-holonomic Rapidly-exploring Random Trees (RRT) collision avoidance algorithm that, based on vessel dynamics, generates dynamically feasible and suboptimal paths, due to the lack of optimiser. Using a virtual obstacle region, compliance with COLREGs rules 14 & 15 is achieved. In Zaccone *et al.* [89] and Zaccone [90] an Optimal Rapidly-exploring Random Trees (RRT*) algorithm was demonstrated, capable of finding collision free paths between an initial and goal state, which adhere to COLREGs rules 13-15. The proposed method considers the kinematic constraints of own ship, while optimising with respect to path length, number of actions and distance towards obstacles. Zhang *et al.* [91] utilises RRT as both a global and a local path planner to generate the required trajectories. Collision avoidance and COLREGs-compliance is achieved using the concept of Quaternion Ship Domains Silveira *et al.* [92]. Cao *et al.* [93] presented an RRT-based algorithm for computing paths within inland waterways, considering only static obstacles posed by the ENC. Due to using a non-optimising SBMP algorithm, they propose using a path smoothing step in order to achieve higher quality paths.

Liang *et al.* [94] proposed a method for global route plans based on ENC data and techniques within computational geometry. Based on water depths, a graph was extracted through triangulation, in order to feed an algorithm that yielded a global path consisting only of the vital waypoints. The authors highlight the importance of using real ENC data, rather than approximations. Blindheim and Johansen [95] presented an open-source library for manipulating, visualising, and simulating ENC information in the context of autonomous marine crafts. The library is applied in [96] for computing paths based on a dynamic risk metric, obtained from the shallow water conditions posed by the ENC.

2.1.2 Autonomy for ferries and harbour buses

Reddy *et al.* [97] provided insight into the many benefits of using zero-emission autonomous ferries for countries with plenty of waterways. Many countries have ample coastlines and island societies, where autonomous ferries and harbour buses can significantly impact urban mobility. Autonomous passenger ferries are presented as providing greater flexibility compared to manned ferries, better cost effectiveness, and also providing an environmentally friendly alternative transport.

Brekke *et al.* [27] provided a summary of the developments efforts related to the milliAmpere platform. The vessel featured various path planning and collision

avoidance schemes capable of computing route deviations in the face of target vessels. Bitar *et al.* [98] presented a three-phase method for conducting automatic crossings, while separating the stages into undocking, voyage, and transit. The presented work computes trajectories for the three phases in order to perform the crossing, considering only static obstacles. Thyri *et al.* [99] proposed using path-velocity decomposition method to generate trajectories in highly trafficked areas within confined waters, solving the planning problem in velocity space. The method leverages a set of predefined paths, which are feasible in static conditions, with an online phase recomputing paths with respect to dynamic obstacles.

Thyri *et al.* [100] and Thyri and Breivik [101] demonstrated a COLREGs-compliant collision avoidance algorithm based on control barrier functions, adhering with rules 8 & 13-17. Compliance is achieved using their proposed ship domain, which depending on the COLREGs scenario, shapes the obstacles environments. The method is demonstrated onboard both an autonomous ferry and a leisure craft.

In Amsterdam, The Netherlands, Roboat is developing an autonomous vessel for both urban mobility and logistics [28]–[30]. Vries *et al.* [102] demonstrated COLREGs-compliant collision avoidance for the Roboat, with respect to rule 13-15, through the use of a MPC solution in combination with a cost function penalising certain manoeuvres with respect to the given target vessel.

Koschorrek *et al.* [103] presented a collision avoidance scheme for an autonomous river crossing ferry, where a hybrid A* algorithm computes the path for the crossing. Their case study takes place on the Rhine river, where local law states that any crossing vessel must yield for incoming traffic, therefore the COLREGs are not explicitly considered. For the same vessel, a trajectory generator is proposed based on path-velocity decomposition [104].

Yuan *et al.* [105] demonstrated a two-stage collision avoidance scheme for a ferry crossing an inland waterway, using a dynamic risk model to assess the situation. As their work is applied to the waterways within the republic of China, local laws dictate that ferries must yield for all traffic travelling along the river. Mei and Arshad [106] used APF to perform along river navigation, considering rules 13 & 14 by biasing towards either port or starboard, with the latter occurring if a head-on scenario is identified.

Hjelmeland *et al.* [107] proposed using adaptive stress testing to explore points failure present within a collision avoidance system, as doing so preventively may reduce the risk of incidents while deploying an immature system. Adaptive stress testing uses reinforcement learning to converge to common failure modes such that they can be analysed and subsequently addressed. The techniques presented are applied in the context of an autonomous ferry.

2.2 Sampling-based motion planning

Ever since Probabilistic Roadmaps (PRM) (Kavraki *et al.* [108], [109] and Geraerts and Overmars [110]) and Rapidly-exploring Random Trees (RRT) (LaValle [111]) were introduced, Sampling-based Motion Planning (SBMP) algorithms have seen massive adoption within the various robotics communities. Sampling-based algorithms have numerous advantages over traditional grid-based algorithms, as they do not require an explicit representation of the state space or problem constraints, as the algorithms generate and check feasibility incrementally by sampling the space.

Probabilistic Roadmaps (PRM) build a single graph of the state space, ideal for static scenarios, allowing for multiple queries from various starting and goal states. RRT instead builds a directed graph rooted at the starting node, rapidly exploring the entire space. Due to the nature of both algorithms, the resulting paths are suboptimal, as both graphs are built without considering an optimisation step.

Kuffner and LaValle [112] proposed RRT-connect, where instead of growing a tree from only the starting node, a tree is grown from both the start and goal state, increasing the rate of convergence. LaValle and Kuffner [113] presented both an exhaustive description of RRT, as well as a kinodynamic variant. Pepy *et al.* [114] proposed including the full dynamical model within RRT, thus ensuring that the path found to be dynamically feasible.

Optimal SBMP came to be when Karaman and Frazzoli [115] (Karaman and Frazzoli [116]) presented a groundbreaking contribution, namely RRT* and PRM*, which combatted the lack of optimality by including an optimisation whilst building the graphs. These algorithms allow for the inclusion of problem-specific optimisation metrics. The generated paths are asymptotically optimal in probability [117].

Typically, SBMP algorithms are used for path planning. However, during collision avoidance, an underlying path or trajectory exits. Vonásek *et al.* [118] proposed the use of an initial path from a Voronoi graph to guide the RRT exploration. Lan and Di Cairano [119] detailed an implementation that computed paths with curvature similar to the nominal trajectory. Tang *et al.* [120] biased the sampling towards guide points, which were placed along a discretised representation of the nominal trajectory. Lin *et al.* [121] repaired infeasible parts of the nominal trajectory to compute feasible deviations.

The performance of SBMP algorithms is strongly influenced by the choice of sampling strategy and distribution. The original technique proposed by LaValle [111] was to uniformly sample the state space, as this guarantees that a solution is found, if it exists. Later, Urmson and Simmons [122] proposed using a heuristic such that the tree is biased towards exploration and toward lower-cost areas of the

state space. Véras *et al.* [123] reviewed various sampling techniques used for both RRT and RRT* algorithms, the authors labelled each technique with a particular biasing objective: goal-biased, obstacle-biased, region-based, path-biased, passage-biased, search/sampling space reduction and sample biasing through alternative distributions. Gammell and Strub [117] provided an overview of current techniques used in state-of-the-art SBMP.

2.2.1   Sampling space reduction

By adaptively reducing the sampling space to encompass only states of increased value or such that the probability of sampling states that may improve the solution is increased, the performance is bound to increase.

Abbasi-Yadkori *et al.* [124] proposed utilising knowledge of the free space, in order to form a non-convex region. By directly sampling the non-convex region (using a hit-and-run sampling technique), it is guaranteed that the obstacle states are not sampled. Using prior knowledge of the space or problem at hand is commonly known as importance sampling [125]. Importance sampling is a (a priori) non-uniform sampling technique, where utilising prior knowledge allows for increased convergence speed to a solution. Importance sampling is not limited to the SBMP literature, but is also present for other motion planning techniques [126]–[129].

Gammell *et al.* [130] (Gammell *et al.* [131]) popularised search space reduction when they introduced the Informed RRT*, also referred to as the L^2 informed set. It leverages the L^2 norm to bound the sampling space by n-dimensional symmetric ellipses, once an initial solution is found. By directly sampling the ellipsoid, each sample has a greater likelihood, compared to uniformly sampling the space, of improving the current solution. The informed set decreases in volume as the cost (Euclidian distance) decreases. The informed sampling strategy maintains the same probabilistic guarantees for both completeness and optimality as RRT*.

Current research continues to investigate methods to form and fully utilise informed subsets and search space reduction techniques in general to accelerate the convergence properties of the different SBMPs. In Mandalika *et al.* [132], using the notion of a beacon, smaller sets within the bounding n-dimensional hyperspheroid are formed, densifying the original informed set and focussing the search. Similarly, Joshi and Panagiotis [133] also proposed identifying subregions within the informed set. Kunz *et al.* [134] argued that the L^2 informed subset is ineffective for systems with kinodynamics constraints. Instead, the informed set is subdivided and sampled using hierarchical rejection sampling. Yi *et al.* [135] proposed a technique for leveraging arbitrarily shaped informed sets, including non-convex spaces. Asymptotic optimality for these general informed spaces is

shown using a sampling strategy based on Markov Chain Monte Carlo. Li *et al.* [136] demonstrated a scheme where the L^2 subset is slid along the current solution, forming multiple local search space reductions along the path. Locally reducing the search space allowed for optimising smaller segments of the current solution. Ryu and Park [137] proposed finding a suboptimal path quickly, in this case using a gridmap, such that the L^2 informed subset [130] is applied from the first sample.

Informed RRT*, other than improving both convergence rate and overall performance of RRT*, turned out to be an integral part of future SBMP algorithms and spawned new powerful algorithms such as Batch Informed Trees (BIT*), AIT* and regionally accelerated BIT* (RABIT*) [138]–[140].

2.2.2 Learning-based sampling spaces

Data-driven sampling distributions and strategies allow motion planning systems to leverage past data to speed up convergence and increase path quality. Iversen and Ellekilde [141] presented a sampling technique in which an uniform distribution is continuously updated with data from past experiences and paths. Then Kernel Density Estimation (KDE) is used to bias the uniform search space toward the data. Lehner and Albu-Schäffer [142], [143] instead proposed using Gaussian Mixture Model (GMM) to bias generated samples toward regions containing past solutions, continuously updating an initial distribution. Chamzas *et al.* [144] decomposed the state space into subregions, forming local task-specific sampling spaces based on task knowledge, with the spaces represented by GMMs. Zhang *et al.* [145] created a rejection sampling strategy by leveraging previous solutions from similar working environments to increase sampling efficiency and computational costs in new, but similar, environments. Arslan and Tsiotras [146] generated samples and classified whether or not it was in collision, then using a KDE approach, the distribution is estimated based on the feasible samples from the classifier.

Ichter *et al.* [147] trained a conditional variational autoencoder on past experiences from a robotic system. Samples biased towards the data were generated using the latent layer, pushing the search towards previously explored areas. The authors combine their proposed sampling strategy with a conventional uniform sampling scheme to ensure that the SBMP optimality guarantees are maintained. Ichter and Pavone [148] extended the previous method to also include both a learning-based sampling strategy, local steering, and collision checking within the autoencoder. Li *et al.* [149] combined historical data, deep neural networks and MPC to create a learning-based kinodynamic motion planner. Due to the use of imitation learning, the planner is capable of computing new paths that comply with kinodynamic constraints.

2.2.3   Additional sampling-based motion planning algorithms

Since the introduction of RRT*, countless variations of the algorithm have appeared. Noreen *et al.* [150] highlighted and detailed the strengths and weaknesses of 20 RRT* variants. Paden *et al.* [151] and Claussmann *et al.* [152] surveyed the use of motion planning techniques for autonomous urban and highway vehicles, respectively, detailing the use of SBMP. Park and Kuipers [153] and Pharpatara *et al.* [154] proposed a non-holonomic RRT* for specifically aerial and ground vehicles, respectively.

Recently, Gammell and Strub [117] surveyed and highlighted the state-of-the-art within optimal SBMP. Some notable algorithms besides RRT* includes BIT* [138], Fast Marching Trees (FMT*) [155], Regionally accelerated BIT* (RABIT*) [140], Advanced BIT* [156]. Most of which leverage and build upon the results presented in Gammell *et al.* [130], as these class of algorithms specialise in minimising between two states, rather than mapping the optimal path from the root to any state within the space. Additional SBMP algorithms, but not limited to, can be found in [139], [157]–[159].

Chapter 3

Summary of main contributions
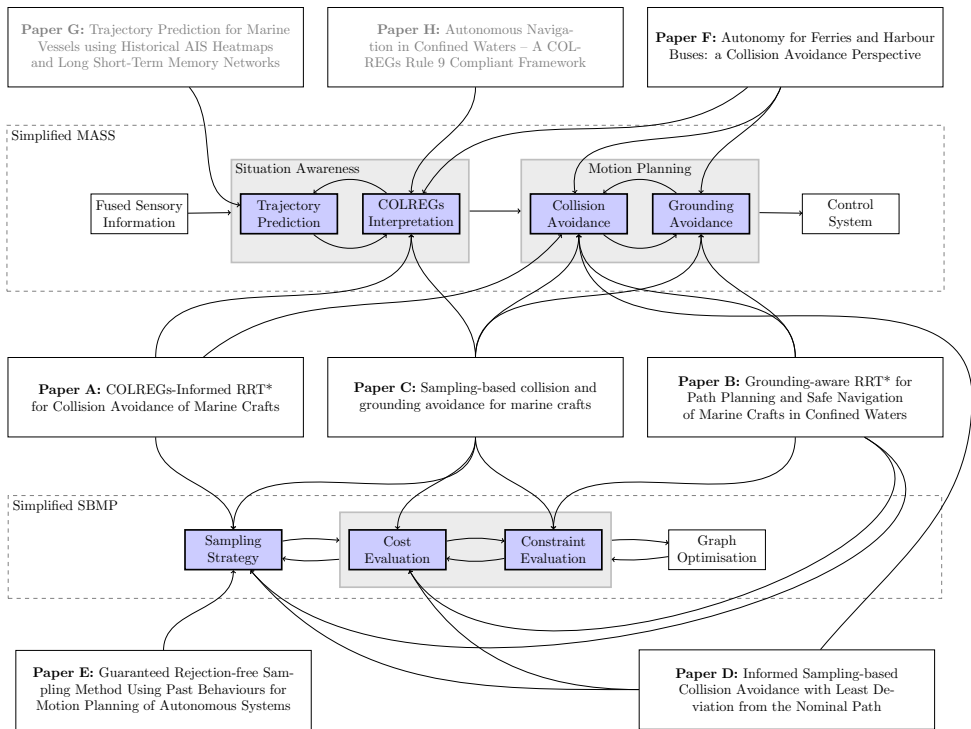
Figure 3.1: Graphical overview of each contribution. The paper contributions are divided in two categories: COLREGs-compliant collision and grounding avoidance techniques for Maritime Autonomous Surface Ships (MASS) and advanced methods and techniques for Sampling-based Motion Planning (SBMP). The work from the two greyed out papers, Paper G [8] and Paper H [9], was also carried out during the PhD project in relation to MASS, but are not included in the thesis.

3.1   Summary

The research contributions of this thesis are divided into two topics, namely i) COLREGs-compliant collision and grounding avoidance for MASS, ii) advanced sampling strategies and objective functions for sampling-based collision avoidance. Figure 3.1 presents a graphical overview of the various contributions, which are ordered alphabetically with respect to their publishing order. The work has been disseminated in four conference papers (Paper A, Paper B, Paper D, Paper F) and two journal publications (Paper C, Paper E).

The work within Paper A, Paper B, Paper C and Paper F directly concerns the development of collision and grounding avoidance techniques for autonomous marine crafts, with the former three utilising a sampling-based collision and grounding avoidance framework, and the latter a deterministic lattice-based approach. Paper D and Paper E are instead proposed as general methods and techniques to improve the convergence properties and solution cost of SBMP algorithms. The contributions are presented in the context of general motion planning problems, with applications including, but also well beyond, MASS.

The contributions directly associated with MASS are as follows. Paper A focusses on open water sampling-based collision avoidance for ocean-going vessels using a tailored informed sampling strategy. Paper B and Paper C detail a sampling-based collision and grounding avoidance framework for larger vessels that navigate in confined and inner coastal waters. Novel objective functions for minimal path deviation and data-driven "good seamanship" are proposed. Paper C proposed custom ship domains to achieve partial adherence to the COLREGs. Paper F detailed the autonomy stack for the Greenhopper autonomous harbour bus, highlighting the various developments and modules within the proposed stack. The paper also discussed maritime autonomy from the perspective of collision avoidance, highlighting some of the challenges regarding autonomous operation using automated electronic outlook, situation awareness and collision avoidance. A deterministic lattice-based collision avoidance algorithm is presented to combat some of the prior shortcomings.

Paper A, Paper B, Paper C and Paper F successfully address the research objectives posed in the thesis. Contributions from the papers have resulted in a COLREGs-compliant collision and grounding avoidance scheme, which considers various elements of safe navigation. The SBMP approach allows the scheme to efficiently include high-fidelity information present within the ENCs, along with custom ship domains that describe various COLREGs scenarios. Navigational experience from previous sailors is used to integrate measures of "good seamanship" within the planning loop, resulting in route deviations that exhibit behaviours similar to those

of real human navigators. During the implementation of the collision and grounding avoidance module for the Greenhopper, several challenges with the stochastic approach of SBMP were discovered. Instead, a deterministic collision avoidance scheme was created that takes advantage of ideas from SBMP, to efficiently and effectively compute route deviations.

Both Paper D and Paper E were byproducts of the developments towards the collision and grounding scheme for the MASS. They both present techniques to improve the performance of the SBMP scheme to increase its convergence rate and overall effectiveness. Paper D proposed an informed sampling strategy that hones the sampling effort to increase the convergence speed of sampling-based collision avoidance problems. It presents a generalised objective function for minimum path deviation, while extending the conventional informed sampling strategy to work with piece-wise linear path segments. Paper E presented a novel data-driven sampling strategy, which leverages a combination of historical data and the known obstacle environment to generate rejection-free samples that are guaranteed to be feasible with respect to the static conditions. As mentioned previously, the contributions within those papers are applicable to general robotic systems; however, the proposed methods are demonstrated in the context of autonomous marine crafts, specifically related to inner coastal collision and grounding avoidance.

3.2 Journal articles

(C) T. T. Enevoldsen, M. Blanke, and R. Galeazzi, "Sampling-based collision and grounding avoidance for marine crafts," *Ocean Engineering*, vol. 261, p. 112 078, 2022. DOI: `https://doi.org/10.1016/j.oceaneng.2022.112078`.

This article presents the proposed COLREGs-compliant sampling-based collision and grounding avoidance framework for autonomous marine crafts. Sampling-based methods are highly effective at solving high-fidelity motion planning problems, such as those posed by MASS when considering complex environmental constraints. Conventionally, SBMP is used to plan paths without knowledge of an underlying nominal route. Therefore, in order to leverage SBMP techniques for collision avoidance, a novel cost function is proposed to calculate the minimum cross-track error. This allows the framework to compute routes with minimum deviation, ensuring that the properties of the nominal route are preserved. COLREGs-compliance is achieved using custom ship domains based on Lamé curves, which allow the SBMP algorithm to reject states that violate rules 8, 13-17. The framework is demonstrated in

the context of inner coastal and confined waters, subject to encounters with multiple vessels.

Chronologically, this work is published after Paper A and Paper B, both of which also concern SBMP for marine crafts, therefore, it is natural that this work builds upon the ideas present within those two papers.

(E) T. T. Enevoldsen and R. Galeazzi, "Guaranteed Rejection-free Sampling Method Using Past Behaviours for Motion Planning of Autonomous Systems," 2022, Under review. DOI: https://doi.org/10.48550/arXiv.2109.14687.

The article presents a novel data-driven sampling strategy, which is able to leverage historical data to generate rejection-free samples within the static obstacle space. The sampling strategy is capable of generating samples from the underlying distribution of the historical data or approximately uniformly sample the domain described by the past data. The work leverages techniques within computational geometry and multivariate kernel density estimation to form the proposed sampling strategy. This allows behavioural traits to be encoded within the sampling strategy itself, which results in solutions that mimic the behaviour found within previously planned paths, demonstrations, etc. The work is presented in the context of general robotic systems that are able to leverage past experiences to guide the search for new ones. One of the case studies in the article concerns the computation of routes in confined waters for an autonomous vessel, using AIS as the historical data. The required constraints to achieve the desired navigational safety are shown to be encoded directly in the sampling space, when generating the strategy based on historical data, allowing the samples to adhere to a representation of "good seamanship".

3.3 Peer reviewed conference papers

(A) T. T. Enevoldsen, C. Reinartz, and R. Galeazzi, "COLREGs-Informed RRT* for Collision Avoidance of Marine Crafts," *2021 IEEE International Conference on Robotics and Automation (ICRA)*, 2021, pp. 8083–8089. DOI: 10.1109/ICRA48506.2021.9560909.

This paper presents a novel informed sampling strategy that directly generates samples from within a COLREGs-compliant subset. The paper argues that in open water conditions, when there is a risk of collision between two vessels, the situation can be deconflicted by deviating within a space described by an annulus for overtaking scenarios and a half-annulus for head-on and crossing scenarios. Using inverse transform sampling, there is a direct uniform sampling

strategy for generating samples within the annulus and half-annulus subsets. The ideas are further extended by using techniques from informed sampling strategies, where the annulus is replaced by a concentric elliptical annulus, which decreases in size as the cost of the solution improves. This significantly increases the rate of convergence and computational time of the algorithm, when compared to the baseline rectangular and informed sampling strategies.

(B) T. T. Enevoldsen and R. Galeazzi, "Grounding-aware RRT* for Path Planning and Safe Navigation of Marine Crafts in Confined Waters," *IFAC-PapersOnLine*, vol. 54, no. 16, pp. 195–201, 2021, 13th IFAC Conference on Control Applications in Marine Systems, Robotics, and Vehicles CAMS 2021. DOI: `https://doi.org/10.1016/j.ifacol.2021.10.093`.

This paper presents a novel objective function to achieve grounding-aware collision avoidance and path planning. The objective function is computed based on historical AIS data using a multivariate kernel density estimate, which attempts to quantify the average behaviour of past navigators within confined waters of a selected geographic region. The probabilistic description of past behaviours is used to penalise deviations that are too far from the average behavioural pattern of vessels of a similar size. Based on the data, it is shown that this ensures an adequate safety margin toward the shallow water contours. In combination with the objective function, depth contours which satisfy the navigable area by own ship are extracted, and subsequently triangulated to allow uniform sampling of the arbitrarily non-convex areas. The objective function and the sampling strategy are demonstrated in a confined water scenario using the SBMP algorithm RRT*.

(D) T. T. Enevoldsen and R. Galeazzi, "Informed sampling-based collision avoidance with least deviation from the nominal path," *2022 IEEE/RSJ International Conference on Intelligent Robots and Systems (IROS)*, 2022, pp. 8094–8100. DOI: `10.1109/IROS47612.2022.9982202`.

This paper presents the concept of informed sampling strategies for collision avoidance, that is, computing paths with minimum deviation, rather than solving the conventional path planning problem. To this end, both a novel objective function and an informed sampling strategy is proposed to minimise towards a prescribed nominal path, while adaptively limiting the search space. The work extends the informed sampling strategy proposed by Gammell *et al.* [130], which uses a single ellipsoidal subset to focus its search. Instead, this paper proposed using a union of ellipsoids placed along the nominal path. Both the proposed objective function and the informed sampling strategy

are suitable for computing paths with minimal deviation for n-dimensional systems that have piece-wise linear nominal paths. The proposed methods are demonstrated on case-studies related to autonomous marine crafts navigating in confined waters, showcasing its ability to rapidly converge to solutions with minimal route deviation along routes consisting of several legs.

(F) T. T. Enevoldsen, M. Blanke, and R. Galeazzi, "Autonomy for Ferries and Harbour Buses: a Collision Avoidance Perspective," 2023, Under review. DOI: `https://doi.org/10.48550/arXiv.2301.02711`.

This paper details and summarises the ShippingLab development effort for materialising a collision avoidance module within an autonomy stack, for the Greenhopper, an autonomous harbour bus. It discusses a collision avoidance perspective to maritime autonomy, in the shift toward MASS. The autonomy stack and its various modules are introduced; in particular, the development of a Short Horizon Planner (SHP) is given in great detail. The paper outlines the inherent difficulties related to achieving COLREGs-compliance, further discussing apparent operational constraints and challenges for MASS, such as autonomous ferries or harbour buses.

A deterministic lattice-based planning algorithm is presented, as an alternative to the previous SBMP-based algorithms, to remedy some of the shortcomings of the stochastic framework.

Chapter 4

Rules and practises for safe navigation

A fundamental requirement for any fully or partially autonomous marine craft is the adherence to the rules for safe navigation. The IMO Convention on the International Regulations for Preventing Collisions at Sea (COLREGs), the marine "rules-of-the-road", provides such a collection of rules, constituting a framework for a common understanding among seafarers.

Furthermore, the consideration, interpretation, and implementation of the COL-REGs within collision avoidance schemes for MASS is paramount, in order to secure the ability to be fully commissioned and adopted. The first paragraph of the COL-REGs specifically states that the rules within apply to all ocean-going (seagoing) vessels [16, Part A - rule 1].

This chapter details the rules most relevant to collision avoidance and subsequently introduces the concepts and methods developed to ensure compliance with the selected rules. Concepts for safe navigation and COLREGs-compliance is discussed both in the context of larger ocean-going vessels and for the Greenhopper harbour bus; therefore, the rules are mostly discussed assuming that at least one of the vessels (own ship) is power-driven. The COLREGs are present to varying degree in most contributions of this thesis (Paper A, Paper B, Paper C and Paper F). This chapter discusses the primary method, which was first proposed in Paper C and later refined in Paper F, to achieve partial adherence to the COLREGs.

The description and interpretation of the COLREGs are presented following the work by Cockcroft and Lameijer [160] and the IMO document [16].

4.1   COLREGs for collision avoidance

The IMO COLREGs play a crucial role in ensuring safe passage for the worlds many fleets. The convention forms a common ground for safe navigation, standardising lights and shapes for situation assessment, both in clear and poor visibility, light and sound signals for communication among vessels, and most importantly, navigational responsibilities in the face of collision risks.

The COLREGs consists of 41 rules divided into six sections [16]:

- Part A - General (Rules 1-3)

- Part B - Steering and Sailing (Rules 4-19)

- Part C - Lights and Shapes (Rules 20-31)

- Part D - Sound and Light signals (Rules 32-37)

- Part E - Exemptions (Rule 38)

- Part F - Verification of compliance (Rules 39-41)

Part A defines the general aspects of the convention, such as to whom and where the rules apply. Here, rule 1 denotes that all vessels on the high seas must adhere to the rules specified within the COLREGs. Rule 1 further states that the rules shall not interfere with special rules specified by local governments, harbours, specific passages of water, etc. Part C & D refer to specific signalling hardware, and are therefore largely unrelated to the collision avoidance aspects of MASS [16], [160].

In Part B are the *Steering and sailing rules*, which encompass the most important rules from a collision avoidance perspective, namely rules 4-19. There are different rules and obligations depending on the visibility conditions and whether encounters occur between power-driven vessels, sailboats, or a mixture. An overview of the most important rules is available in Table 4.1, which are paraphrased from IMO [16] and Cockcroft and Lameijer [160]. The remainder of this section includes a description of selected rules and their application to collision avoidance.

Rule 4 states that rules 4-10 are general and apply during any visibility conditions. Rule 5 & 6 are crucial for safe navigation, as rule 5 refers to the required look-out. On manned crafts, this is achieved by combining human eyesight with the navigational aids available on the bridge. Maintaining a sufficient look-out is crucial for mitigating collision risks and acting in ample time when such risks occur. For autonomous marine crafts, the responsibility of maintaining an appropriate look-out is situated within the situation awareness, driven by all the sensory inputs. Rule 6 states that all vessels must proceed at a safe speed at all times, and this rule in particular is
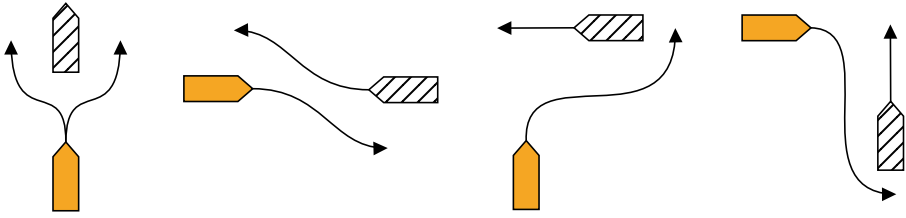
Figure 4.1: Visualisation of the encounters described by COLREGs rules 13-15, i.e. overtaking, head-on and crossing scenarios. The solid coloured vessel is in a give-way situation.

heavily dependent on environment and scenarios in which the vessel is currently operating within. Ocean-going vessels that cross the Atlantic Ocean are capable of cruising at great speeds, depending on traffic conditions, because of the vast open waters. For inner coastal and confined waters, the safe speed is highly dependent on the traffic conditions, the draught restrictions, and possibly also on the navigational experience of the surrounding seafarers.

Rule 7 & 8 refer to the determination of the prevailing risk of collision, and the requirement to act accordingly. Rule 7 states that every vessel must use all available means to determine if a collision risk exists, specifically that one should assume so, if there is any doubt. Rule 8 describes the actions to avoid collision and that such actions should be performed according to the rules of Part B and be "positive", as in, performed in ample time and according to good seamanship.

Assessing the existence of a risk of collision onboard a MASS (rule 7) is typically situated within a situation awareness system. If there is some uncertainty or ambiguity in the scenario at hand, the collision avoidance scheme can evaluate whether a deviation is necessary given the specified safety margins. Acting in ample time, according to rule 8, also requires that the collision avoidance scheme is triggered as early as a collision risk is deemed to exist.

In the current state-of-the-art, there is a general consensus that the minimal requirement to ensure compliant and safe navigation practises is the adherence towards rules 8 & 13-17 [161]. Methods for collision and grounding avoidance typically claim compliance with the COLREGs, when, at the very least, rules 13-15 are considered. More recently, researchers have begun describing algorithms as partially adhering to the COLREGs, since the COLREGs encapsulate more than just the rules of navigation.

The reason being that rules 13-15 are the most actionable rules from a collision avoidance point of view, as these rules represent the three most common encounter types between two vessels, namely: overtaking (rule 13), head-on (rule 14), and crossing (rule 15). Rule 14 & 15 apply only to an encounter between two power-

driven vessels. Figure 4.1 visualises rules 13-15, where the solid coloured vessel has the give-way obligation.

Rule 13 states that any vessel performing an overtaking manoeuvre must stay out of the way of the vessel that is being overtaken. Rule 14 describes that when two power-driven vessels meet at a (near) reciprocal course both vessels are obliged to deviate toward starboard, so the vessels pass one another on their respective port sides. Rule 15 concerns crossing scenarios for two power-driven vessels, where if a vessel approaches from the starboard side of the own ship, own ship must keep out of the way and avoid passing in front of the other vessel. Rule 16 & 17 describes the required actions by the give-way and stand-on vessel respectively. With the give-way vessel urged to take early and clear action and the stand-on vessel requested to maintain its course and speed, if possible. Clear action refers to the execution of few manoeuvres, as well as alterations that are clearly visible to the look-out onboard the target vessel.

It is important to note that rules 14 & 15 assume that the encountered vessel is capable of performing its manoeuvre obligation. However, if a crossing takes place in confined waters such as a narrow channel, certain crafts may be restricted in their manoeuvrability. Whenever a restricted vessel is part of the encounter, rule 9 applies and states that one must not impede the passage of a manoeuvrability restricted craft. Assessing whether a given vessel is restricted in its manoeuvrability comes down to many factors, the simplest of which is that the vessel itself signals or broadcasts that it is restricted. This is possible using lights, flags, and AIS.

Rule 18 summarises the responsibilities between vessels. For power-driven vessels (rule 18(a)), it is required that they keep out of the way of sailing vessels, vessels engaged in fishing, vessels not under command, and vessels that are manoeuvrability restricted. The remaining parts of rule 18 describe similar responsibilities for sailing vessels, fishing vessels, etc.

4.1.1   Circumstantial rules and local amendments

As part of rule 1(b) and 1(c) [16], some local governments have amended or altered rule 15. Examples of this include Canadian waters, where rule 15 (crossing scenarios) has been modified so that any vessel crossing a river must yield to power-driven vessels travelling along it, with only one exception on the St. Lawrence River at the Île Rouge [162, Rule 15(b)]. Similarly, in Germany, all ferries crossing the Rhine River must always give-way for traffic sailing along the river [103]. The Canadian collision avoidance rules also modify and amend several other rules, with a notable example being their modifications to rule 9. Here it is specified that vessels travelling with the current in a narrow channel shall disregard its obligation to yield and instead

stand-on. The stand-on vessel must through sound signal the desired side the give-way vessel shall pass. The give-way vessel travelling upstream must acknowledge the requested passage and subsequently safely execute the manoeuvre [162, Rule 9(k)]. Within Danish waters, there are minor amendments to the COLREGs, such as specific rules for three ferry routes [35, §19]. Here it is clearly stated that the crossing ferries must adjust their voyage so that they avoid the risk of collision with vessels travelling along the waters. This means that regardless of whether the target vessel approaches from the port or starboard side, the crossing ferry must disregard the usual obligation to rule 15, and yield for any traffic the ferry may impede. It further states that should a risk of collision arise, then the COLREGs are to be followed.

Local amendments are not only limited to changes in the COLREGs, as local governments can also alter the requirements for the equipment carried onboard a given craft, as stated in SOLAS, "Administrations may exempt ships from the application of the requirement" [17, Chapter 5, 1.3]. This is the case with the requirement to carry AIS, where normally SOLAS requires it onboard vessels greater than 300GT (gross tonnage) engaged on international voyages, and 500GT vessels and all passenger vessels irrespective of their voyage [163]. However, in Denmark, certain passenger or region-specific vessels, such as the Greenhopper, are exempt from carrying it [164].

4.1.2 Good seamanship and the ordinary practises of seamen

The term *good seamanship*, or some derivative of it, is both mentioned within and in the context of the COLREGs. Rule 2 on responsibility states that one must always follow the COLREGs, but also, if necessary, disregard them to mitigate the prevailing incident. Choosing to deviate from the COLREGs when needed is described as applying *good seamanship* or *acting within the ordinary practise of seamen*.

Cockcroft and Lameijer [160] provides further examples of practises that may be considered ordinary or applicable during special circumstances. Here, an element of good seamanship is to properly make use of the available equipment onboard. For example, correctly adjusting the radar in restricted weather conditions and navigating with functioning equipment. Or by correctly considering the squatting or banking phenomena when navigating within shallow waters.

As pointed out by Porathe [165], the COLREGs are written as generally as possible, so that the interpretation of the rules depends on the given situation at hand and also the experience and cultures of those involved.

There are multiple instances of very generalised formulations within the COL-REGs, such as rule 8, which states in relation to actions to avoid collision "if the circumstances admit, be positive, made in ample time and with due regard to the

observance of good seamanship" [16, Rule 8(a)]. Similarly, rule 16, which concerns the actions of all give-way vessels, states that one must "take early and substantial action to keep well clear" [16, Rule 16]. Here, phrasing such as "circumstances", "ample time", "early and substantial action" are up for interpretation, posing as additional challenges for implementing the COLREGs for MASS.

Other examples include rule 15, which simply states that when two vessels are crossing, during instances where there may be a risk of collision, the vessel with the other to its starboard side must give-way and "avoid crossing ahead of the other vessel" [16, Rule 15]. To comply with such a requirement, one must assess what the limits are for crossing ahead of a given vessel. If both vessels are large merchant crafts, then one should definitely not cross at one ship length in front of the other; similarly, one should not necessarily give-way if the give-way vessel could safely pass in front at a distance of multiple nautical miles.

Rule 17, concerns the behaviour of the stand-on vessel, and states that if the give-way vessels fails to perform a manoeuvre to mitigate the imminent collision risk, the stand-on vessel must instead do so "as soon as it becomes apparent to her that the vessel required to keep out of the way is not taking appropriate action in compliance with these Rules" [16, Rule 17(a-(ii))]. This essentially translates to that one must be capable of detecting abnormal events and incidents and in sufficient time be able to mitigate the prevailing risks.

The vagueness of *good seamanship* and *ordinary practises* creates additional requirements and proves to be quite challenging, not only for MASS, but also for human navigators, as they even need concrete scenarios to properly evaluate with respect to the COLREGs.

The adherence towards the COLREGs, during any foreseeable incident, builds upon human experiences and past lessons learnt, as there are no specific details regarding what constitutes ample time or distance, sufficient reaction time, or what constitutes a "circumstance". Porathe [165] argued that good seamanship also depends on the local environment and that one could attempt to quantify it from the perspective of a specific operating region in which the MASS is to be deployed. However, such a solution may only be feasible for systems with very well-defined use-cases or small regions of operation. Extending the COLREGs to include guidelines or expected safety distances, reaction times, local and cultural behaviours, etc., may alleviate some of the ambiguity present within the rules. However, it is virtually impossible to sufficiently cover all possible encounters, cultures, and edge-cases. Porathe [165] argued that the COLREGs should be reconsidered so that *good seamanship* and *the ordinary practise of seamen* are expressed in varying degrees of "negligence" with respect to the rules.

Table 4.1: Common COLREGs used in collision and grounding avoidance. Rules are paraphrased from [16] and [160].

Rules	Explanation
Rule 5	*Look-out*: The vessel must at all times maintain a look-out using sight and hearing, such that a full understanding of the unfolding situation and risk of collision is maintained.
Rule 6	*Safe speed*: The vessel must navigate with a safe speed, such that it can effectively avoid collisions and also maintain an adequate stopping distance.
Rule 7	*Risk of collision*: Every vessel must use all means available to determine if a risk of collision exists. If in doubt, then it is deemed that a risk of collision exists.
Rule 8	*Action to avoid collision*: The give-way vessel must perform its alterations in such a way that the change in behaviour is easily observable to other vessels. The rule also recommends that, if possible, fewer and larger course change(s) is preferred over speed changes and smaller frequent course adjustments.
Rule 9(d)	*Narrow channels*: A crossing vessel shall not impede the passage of a vessel that can only safely navigate within the channel or fairway.
Rule 13	*Overtaking scenario*: The vessel being overtaken must maintain its course and speed, whereas the overtaking vessel may overtake on either side of the stand-on vessel.
Rule 14	*Head-on scenario*: Both vessels must perform a manoeuvre such that they pass one-another on their respective port sides.
Rule 15	*Crossing scenario*: A vessel must give-way to another vessel, if the second vessel approaches from starboard side. The vessel that has the right of way must keep the current course and speed.
Rule 16	*Give-way vessel behaviour*: The give-way vessel should take early action and remain a safe distance from the stand-on vessel.
Rule 17	*Stand-on vessel behaviour*: The stand-on vessel is urged to maintain constant course and speed, and not attempt to avoid collision unless it is clear that the give-way vessel is not abiding by the COLREGs.
Rule 18(a)	*Responsibilities between vessels*: Except when rules 9, 10 & 13 apply, a power-driven vessel must keep out of the way of sailing vessels, manoeuvrability restricted vessels, vessels engaged in fishing and vessels not under command.

4.2   Assessing the risk of collision

In order for the autonomous system to correctly apply the COLREGs, and ultimately
perform COLREGs-compliant collision avoidance, it is crucial that the MASS is
capable of assessing whether or not the risk of collision exists. If so, then the
applicable COLREGs rule must be identified and correctly communicated to the
system. Human navigators use several tools and concepts to determine when there
is a risk of collision and subsequently which COLREGs to apply.

4.2.1   Target vessel assumptions

To adequately enforce the COLREGs, the presence of a prediction scheme is assumed,
which is capable of providing the anticipated trajectories of the target vessels that are
present within the given scenario. In some circumstances, such as for ocean-going
vessels, straight-line predictions are more than sufficient; however, the methods for
COLREGs-compliance presented in Section 4.3 accept arbitrarily shaped trajectories
as input.

   Such a trajectory, be it straight-line or arbitrary, for the i-th target vessel consists
of the north-east position and heading over time t

$$\text{TV}_i = \{N_i(t), E_i(t), \psi_i(t)\}. \tag{4.1}$$

Furthermore, it is assumed that the length of the target vessel is available and
whether or not the target vessel is restricted (i.e. to determine if rule 9 applies).

4.2.2   Closest Point of Approach (CPA) and Time to CPA (TCPA)

Two important metrics for determining whether there is a risk of collision are Closest
Point of Approach (CPA) and Time to Closest Point of Approach (TCPA), both of
which are automatically calculated and visualised on advanced navigational aids
onboard the bridge, such as ECDIS.

   Given the current course, speed and position of the own ship and surrounding
target vessels, it is possible to compute the corresponding CPA value, which repre-
sents the distance at which the own ship and the given target vessel will be at their
closest, typically given in metres or nautical miles. TCPA is then the time, in seconds
or minutes, until the own ship and target vessel reach the point of CPA.

   For computing first the TCPA, let

$$\mathbf{p}_{\text{OS}} = [N_{\text{OS}}, E_{\text{OS}}]^T \tag{4.2}$$

be the position of own ship and

$$\mathbf{p}_{\text{TV}} = [N_{\text{TV}}, E_{\text{TV}}]^T \tag{4.3}$$
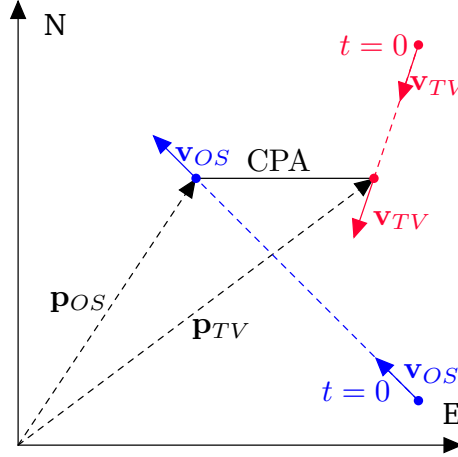
Figure 4.2: Vector definitions for the derivation of CPA and TCPA for two vessels, assuming constant speed and heading.

the position of the target vessel, with $N_{(\cdot)}$ and $E_{(\cdot)}$ representing the north and east coordinates in the North-East-Down (NED) tangential plane, respectively. Then let

$$\mathbf{v}_{\text{OS}} = [V_{\text{OS}} \cos(\psi_{\text{OS}}),\ V_{\text{OS}}(\sin \psi_{\text{OS}})]^T \tag{4.4}$$

be the own ship and similarly

$$\mathbf{v}_{\text{TV}} = [V_{\text{TV}} \cos(\psi_{\text{TV}}),\ V_{\text{TV}} \sin(\psi_{\text{TV}})]^T \tag{4.5}$$

the target vessels velocity vectors, where $V_{(\cdot)}$ represents the speed of the vessel and $\psi_{(\cdot)}$ its corresponding heading angle, also in NED, see Figure 4.2. Using the position and velocity vectors for both vessels at the current time, TCPA is given by

$$\text{TCPA} \triangleq -\frac{(\Delta \mathbf{p}(0))^T \Delta \mathbf{v}}{(\Delta \mathbf{v})^T \Delta \mathbf{v}} \tag{4.6}$$

where $\Delta \mathbf{v} = \mathbf{v}_{\text{OS}} - \mathbf{v}_{\text{TV}}$ is the relative velocity and $\Delta \mathbf{p}(0) = \mathbf{p}_{\text{TV}}(0) - \mathbf{p}_{\text{OS}}(0)$ the relative position at $t = 0$. Assuming that both vessels maintain constant speed and heading, their respective positions at $t = \text{TCPA}$ are expressed as

$$\mathbf{p}_{\text{OS}}(\text{TCPA}) = \mathbf{p}_{\text{OS}}(0) + \mathbf{v}_{\text{OS}} \cdot \text{TCPA} \tag{4.7}$$

$$\mathbf{p}_{\text{TV}}(\text{TCPA}) = \mathbf{p}_{\text{TV}}(0) + \mathbf{v}_{\text{TV}} \cdot \text{TCPA} \tag{4.8}$$

with CPA defined as

$$\text{CPA} \triangleq \left\| \Delta \mathbf{p}(\text{TCPA}) - \frac{(\Delta \mathbf{p}(0))^T \Delta \mathbf{v}}{(\Delta \mathbf{v})^T \Delta \mathbf{v}} \Delta \mathbf{v} \right\|. \tag{4.9}$$

(a) No limit violated   **(b)** CPA $\leq d_{\text{act}}$ **(c)** CPA $\leq d_{\text{act}} \wedge$ TCPA $\leq t_{\text{act}}$
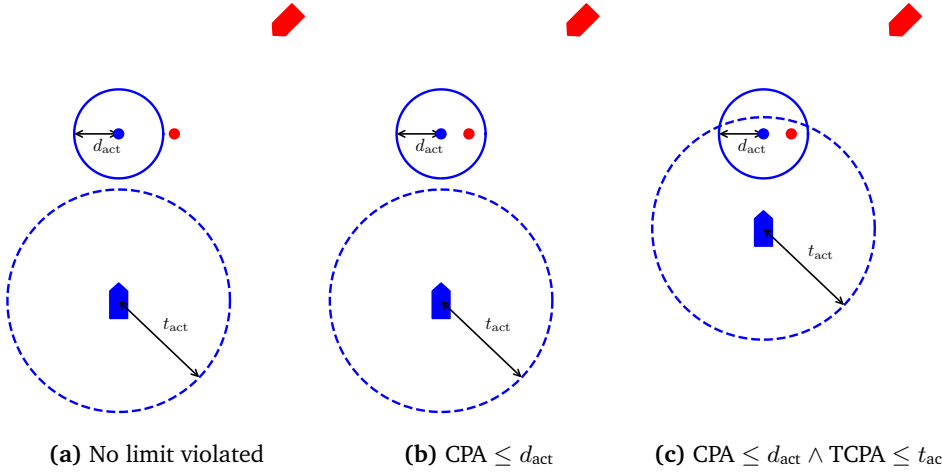
Figure 4.3: Visual demonstration of the CPA and TCPA limits, d_{CPA} and t_{act} respectively. The blue and red dots are the CPA points for the blue and red vessel, respectively.

Evaluating Equation 4.9 yields a value representing how close the two vessels will be at $t = $ TCPA. Figure 4.2 visualises the CPA between two vessels approaching at different, but constant speeds. The application of CPA and TCPA is depicted in Figure 4.3, where three different scenarios have been visualised. If the CPA limit d_{act} is not violated (Figure 4.3a) then the own ship proceeds as usual. Once the value of CPA is less than some chosen limit, a collision risk is imminent. However, if the TCPA value is large, such that t_{act} is not yet violated, this means that the violation of the CPA limit is in a distant enough future to warrant no action (Figure 4.3b). Vessels typically wait until both the CPA and TCPA limits are violated (Figure 4.3c), before initiating a manoeuvre.

4.2.3   Applying the correct COLREGs

Once a risk of collision is deemed to exist (i.e. CPA $\leq d_{\text{act}}$) and it is deemed that a deviation must be computed (i.e. TCPA $\leq t_{\text{act}}$), either based on CPA and TCPA, or from another source of situation awareness (such as [166], [167]), the next step is to determine the applicable COLREGs to the scenario at hand.

By computing the relative bearing between the own ship and the given target vessel,

$$\beta_{\text{rel}} = \arctan2(E_{\text{TV}} - E_{\text{OS}}, N_{\text{TV}} - N_{\text{OS}}) \tag{4.10}$$

it can be evaluated to determine where the target is located with respect to the own ship. The relative bearing is mapped to four sectors, as shown in Figure 4.4, namely port, starboard, overtaking, and head-on sectors. Once the relative bearing has been

Head-on sector

$\beta = 0^o$

$\beta = -3.5^o$

Port sector   Starboard sector

$\beta = -112.5^o$ $\beta = 112.5^o$

Overtaking sector
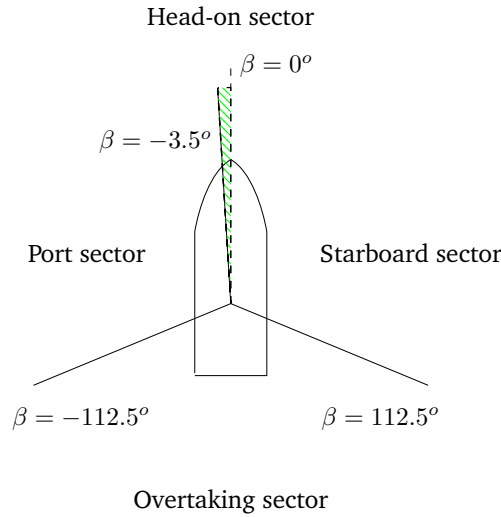
Figure 4.4: Division of the relative bearings into four sectors, in order to determine the applicable COLREGs rule (13-15), based on the relative position between own ship and the target vessel. Uncertainty associated with the head-on sector is indicated by the gridded area. For further details see Papageorgiou *et al.* [166]. The ship domain by Goodwin [53] utilises the same divisions for its sectors.

computed and the correct section identified, the COLREGs can be applied. If the target vessel is identified to be a sailing vessel, the own ship must give-way (Rule 18(a)), regardless of where the vessel is located with respect to the own ship.

Rule 13 (overtaking) states that a vessel is overtaking when it approaches another vessel from a direction of more than 22.5 degrees abaft its beam [160]. Therefore, for relative bearings $-112.15° \leq \beta_{rel} \leq 112.5°$, it means that the own ship is being overtaken, and must therefore stand-on and adhere to Rule 17. However, if $-3.5° \leq \beta_{rel} \leq 3.5°$ and the headings of both vessels are similar, the own ship is the overtaking vessel. If instead the headings of the two crafts are different by 180 degrees, rule 14 (head-on) instead applies, since the two vessels are approaching on a (nearly) reciprocal course. It is important to be mindful of rule 9 during a head-on encounter, as if the target vessel is only capable of navigating within a narrow stretch of water, the give-way action of the own ship may have to compensate for the target vessels inability to give-way.

For relative bearings $3.5° \leq \beta_{rel} \leq 112.5°$, the target vessel approaches from the starboard side, which means that rule 15 (crossing) applies, and own ship must yield for all vessels coming from starboard. As the own ship has the give-way responsibility, it must do so according to the practises specified in rule 16. Under normal circumstances, if $-3.5° \leq \beta_{rel} \leq -112.5°$, the own ship would
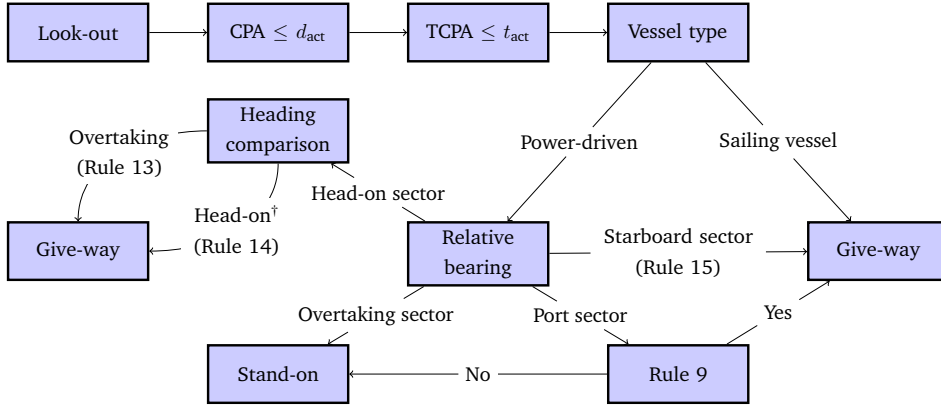
Figure 4.5: An overview of the workflow from identifying a risk of collision to applying the relevant COLREGs to a given unfolding scenario. CPA and TCPA are computed based on the current position of the target vessel(s) at $t = 0$, as described in Equation 4.6 and 4.9. [†]Rule 9 may apply also in the head-on scenario, where the target vessel is unable to fulfil its give-way obligation. Therefore own ship must be mindful of this when planning its own manoeuvre.

instead be the stand-on vessel. However, should the target vessel be restricted in its manoeuvrability (rule 9), the own ship instead has the give-way responsibility and must act accordingly.

The entire workflow for collision risk assessment procedure and the application of COLREGs is visualised in Figure 4.5.

4.3   Ship domains for enforcing the COLREGs

Once the risk of collision has been identified and the vessel with the obligation to give-way has been assigned, a corresponding safe and COLREGs-compliant manoeuvre must be performed. The essence of achieving COLREGs-compliance for collision avoidance algorithms is penalisation or pruning of solutions that violate the give-way obligations, cause risk of collision, and cause discomfort for the target vessels.

A ship domain, in its simplest form, represents a metric for determining whether two vessels enter too close quarters and thereby violate each others comfort. The terminology was introduced by Fujii and Tanaka [168], who defined it as no-go zones around target vessels. Goodwin [169] later proposed a similar idea, where the area or domain surrounding a given ship was divided into three sectors (the same divisions as in Figure 4.4), with different safety distances for each of the sectors. It is argued that the size of the ship domain is influenced by the physical properties of the vessel (length, width, speed, etc.), the current traffic and weather conditions, and finally the experience of the onboard navigator. Coldwell [170] proposed the use of

an elliptical ship domain, which differs based on the current COLREGs scenario at hand. The dimensions of the domain are based on the length of the ship, with scaling factors determined through statistical analysis of gathered radar data. Similarly, Hansen *et al.* [171] presented an elliptical ship domain for confined waters, where the scaling factors were determined by AIS data from the given area and the length of the target vessel.

Various methods exist in the literature for enforcing the COLREGs. One of the most common methods is to use a modified ship domain around the given target vessel, which can report whether or not a given state or configuration of the own ship violates a given rule with respect to the target vessel. Inspired by this, Campbell and Naeem [55] used an occupancy grid to generate obstacle regions. Similarly, Chiang and Tapia [88] presented a virtual obstacle approach, where, depending on the applicable rule, a region towards the starboard side was completely blocked or a region in front of the vessel. Smierzchalski and Michalewicz [172] and Lazarowska [59] leveraged hexagonal representations for the target vessel domains, which are biased toward the starboard side of the target vessel. Zaccone *et al.* [89] presented a vectorial approach to reject points that violate the give-way constraints.

Depending on the objective or details of the collision avoidance scheme, binary checks such as those presented above may be insufficient. Instead of checking for violation of a domain for a given COLREGs rule, Eriksen *et al.* [76] and Zhu *et al.* [173] proposed potential function based cost terms, which penalise non-compliant trajectories.

As discussed in Section 4.1, there are three primary scenarios where that requires the own ship to give-way or deviate from its nominal route, in order to adhere to the COLREGs. Since the head-on and crossing scenarios require that manoeuvres are performed to the starboard side, the ship domain for those scenarios must be designed such that computed solutions deviate toward starboard or are safely able to perform a port side manoeuvre. For overtaking scenarios, passing on either side is acceptable, as long as it is safe according to the given circumstances.

4.3.1   Enforcing crossing and overtaking scenarios using Lamé curves

For crossing scenarios, COLREGs rule 15, requires that a manoeuvre toward starboard is performed, so that the own ship passes behind the target vessel. However, if CPA is large, it may be possible to pass in front of the target vessel, without causing discomfort and a risk of collision. Overtaking scenarios instead require that the own ship initiates the manoeuvre with ample distance, passing the target vessel at a safe margin, either on the port or starboard side. Own ship must also ensure that a safe distance towards the target vessel is kept, once the overtaking manoeuvre has been

(a) Overtaking (Rule 13)   **(b)** Crossing (Rule 15)
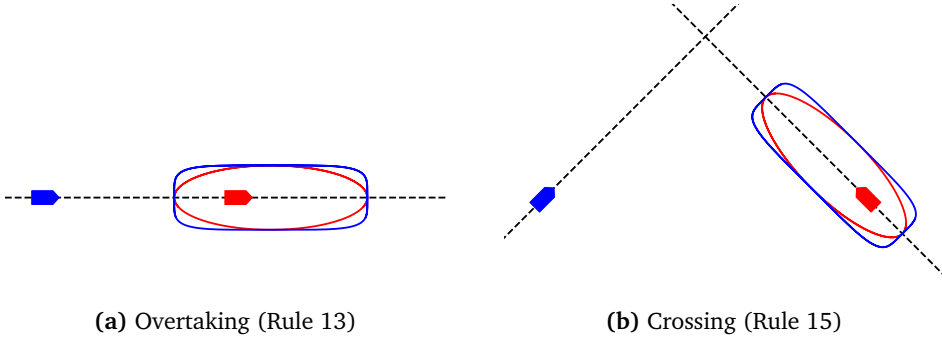
Figure 4.6: Lamé curve (super ellipse) representations of COLREGs rule 13 and 15. The rules for overtaking and crossing scenarios are enforced using a ship domain represented by a single super ellipse. By increasing parameter p, the area increases and converges towards a rectangle (blue curve $p = 5$, red curve $p = 2$).

completed.

Compliance with both these rules, rule 13 and 15, can be achieved by using a ship domain described by a single super ellipse (Lamé curve), given by

$$h_{\text{OT, GW},p} \triangleq \left| \frac{\bar{E}_i(t)}{a_L} \right|^p + \left| \frac{\bar{N}_i(t)}{b_L} \right|^p \leq 1 \qquad (4.11)$$

where $\bar{N}_i(t)$ and $\bar{E}_i(t)$ represent the difference in coordinates between the own ship and the i-th target vessel, a_L and b_L are some scalar values determined based on the length of the target vessel, and p a scalar deciding the shape of the super ellipse. The ship domain for rule 13 and 15, at two different values p, is visualised in Figure 4.6, where placing the proposed ship domain around the target vessel allows penalising solutions that fall within it. Evaluation of Equation 4.11 results in a binary indication of whether or not a given point, or a sequence of points, is in violation of the ship domain.

In order to evaluate whether the own ship violates the domain of a given target vessel, their difference in coordinates is computed. Given the known trajectory for the own ship and the predicted trajectory for the target vessel, and some static offset parameters, the difference in coordinates for the i-th target vessel is given by

$$\begin{aligned} \Delta E_i(t) &= E_{\text{OS}}(t) - E_{\text{TV},i}(t) \\ \Delta N_i(t) &= N_{\text{OS}}(t) - N_{\text{TV},i}(t). \end{aligned} \qquad (4.12)$$

To account for the heading of the target vessel, the resulting difference in coordinates is rotated counter-clockwise by the heading of the corresponding i-th target vessel,

$$\begin{bmatrix} \bar{E}_i(t) \\ \bar{N}_i(t) \end{bmatrix} = R_-(\psi(t)) \begin{bmatrix} \Delta E_i(t) \\ \Delta N_i(t) \end{bmatrix} + c_L \qquad (4.13)$$

(a) Transforming the domain.   **(b)** Checking for point violation.
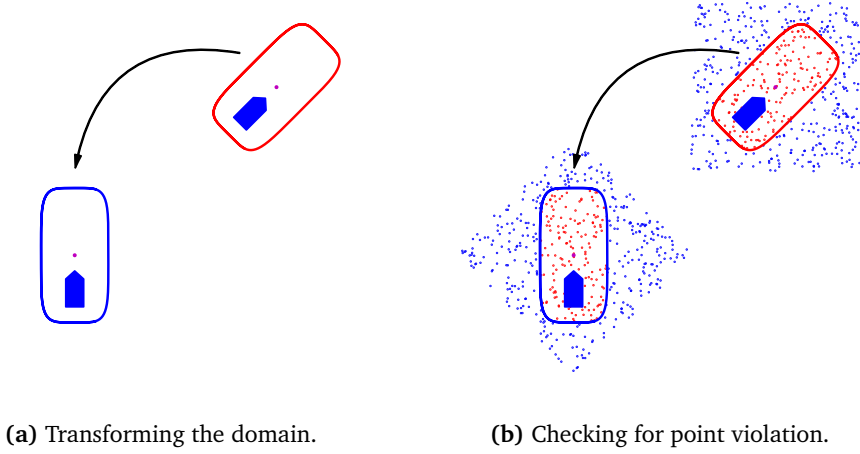
Figure 4.7: Visualising how coordinates in the NED frame are transformed into the local coordinates, such that the domain can be evaluated. In Figure 4.7a the red ellipse is the domain for the vessel at an arbitrary north-east position and heading, with the blue ellipse representing the local coordinates described by Equation 4.12. Figure 4.7b evaluates whether random points in NED are within the domain in the local coordinates, correctly labelling the ones in violation.

with rotation matrix

$$R_- \left(\psi \right) = \begin{bmatrix} \cos(\psi) & \sin(\psi) \\ -\sin(\psi) & \cos(\psi) \end{bmatrix} \tag{4.14}$$

where $c_L = [E_{\text{offset}}, N_{\text{offset}}]^T$, which represents the offset in the north and east directions, in difference coordinates, respectively. Without using the offsets, the geometric centre of the domain would be equal to $E_{\text{TV},i}(t)$ and $N_{\text{TV},i}(t)$.

The rotated coordinate pair $\bar{N}_i(t)$ and $\bar{E}_i(t)$ are then used to evaluate the condition presented in Equation 4.11, in order to determine whether the given COLREGs is violated. Figure 4.7 visualises the procedure, where 500 random positions in NED coordinates are transformed and evaluated for a randomly located target vessel, which is prior to the transform described by its position and heading in NED.

Remark 4.1. *In Paper C, the offsets for the difference in coordinates were originally introduced as part of Equation 4.12. However, to make offsetting the shape more intuitive, the offsets are instead applied after computing the rotated difference in Equation 4.13.*
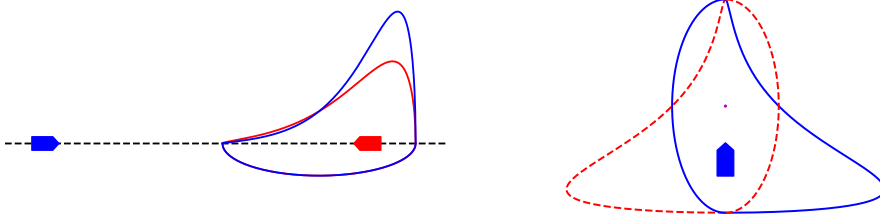
(a) Combination of two Lamé curves describing the domain for COLREGs rule 14.

(b) Each individual Lamé curve is symmetric. The dashed components are discarded.

Figure 4.8: By leveraging two Lamé curves, it is possible describe an adequate ship domain for rule 14. Figure 4.8a shows the proposed ship domain described by Equation 4.17, with two different parameters for c (see Equation 4.16). Figure 4.8b shows underlying (symmetric) Lamé curves, with the solid curves resulting from posing restrictions on $\bar{E}(t)$.

4.3.2   Enforcing head-on scenarios using two different elliptical curves

When encountering a head-on scenario, rule 14, it is expected that both the own ship and the target vessel yield and perform manoeuvres toward their respective starboard sides. A ship domain that encapsulates this behaviour requires a degree of asymmetry, as the ship domain must prevent the own ship from performing a port side manoeuvre, unless it is capable of doing so at a sufficiently safe distance. Such a domain can be obtained by combining two modified Lamé curves (see Figure 4.8a), given by the following modified ellipse equation

$$h_{\text{HO},c} \triangleq \left(\frac{\bar{E}_i(t)}{a_L} \right)^2 g_c\left(\bar{N}_i(t)\right) + \left(\frac{\bar{N}_i(t)}{b_L} \right)^2 \leq 1 \tag{4.15}$$

where $\bar{N}_i(t)$ and $\bar{E}_i(t)$ represent the difference in coordinates between the own ship and the i-th target vessel (given by Equation 4.12) and a_L and b_L are some scalar values determined based on the length of the target vessel.

To penalise passing on the starboard side of the target vessel, its elliptical ship domain must be extended along its major axis (in local coordinates). This is achieved by transforming Equation 4.15, using a transform such as

$$g_c\left(\bar{N}_i(t)\right) = e^{c\bar{N}_i(t)}, \quad c \geq 0. \tag{4.16}$$

where $c \geq 0$ is a scalar value and $\bar{N}_i(t)$ the difference in north coordinates described by Equation 4.12.

(a) Transforming the domain.   **(b)** Checking for point violation.
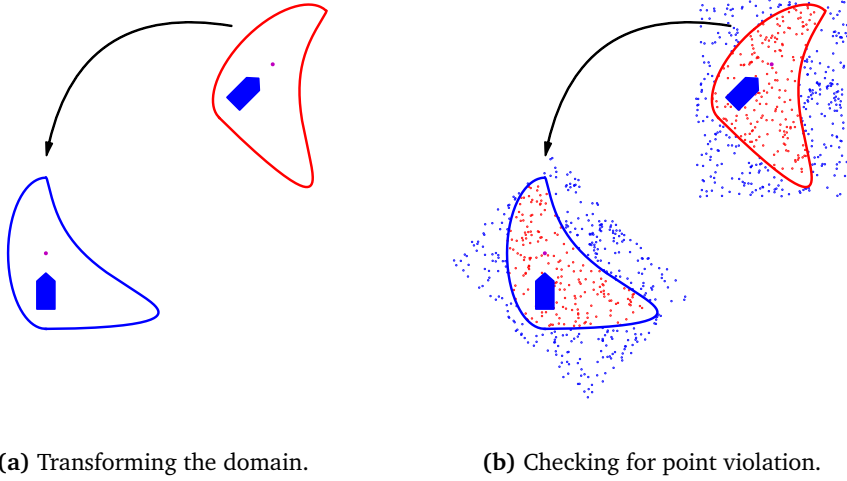
Figure 4.9: Visualising the coordinate transformation from the NED frame to the local coordinates. In Figure 4.9a the red ellipse is the domain for vessel at an arbitrary north-east position and heading, with the blue ellipse representing the local coordinates described by Equation 4.12. Figure 4.9b evaluates whether random points in NED are within the domain described by the local coordinates, correctly labelling the ones in violation.

The transform extends the proposed ship domain along both directions of the major axis because of the inherent symmetric properties of the ellipse. Therefore, the asymmetric ship domain must be constructed using two halves of the different elliptical curves (see Figure 4.8b),

$$
h_{\mathrm{HO}}(t) = \begin{cases} \left(\frac{\bar{E}_i(t)}{a_L}\right)^2 e^{c\bar{N}_i(t)} + \left(\frac{\bar{N}_i(t)}{b_L}\right)^2 \leq 1 & \text{if } \bar{E}_i(t) \geq 0 \\ \left(\frac{\bar{E}_i(t)}{a_L}\right)^2 + \left(\frac{\bar{N}_i(t)}{b_L}\right)^2 \leq 1 & \text{if } \bar{E}(t) < 0 \end{cases} \tag{4.17}
$$

where, based on conditions for the positive and negative values of the local coordinate $\bar{E}_i(t)$, the violation of the respective domain is checked. The solid blue curve in Figure 4.8b represents the domain described by Equation 4.17. Depending on the chosen offset (in Equation 4.12), the comparison in the if statement should instead be with respect to E_{offset}.

As with the domains for rule 13 and 15, Figure 4.9 visualises the procedure, where 500 random positions in NED coordinates are transformed and evaluated for a randomly located target vessel, which is initially described by its position and heading in NED, to determine whether rule 14 is violated for a given set of coordinates.

(a) Overtaking (13)   **(b)** Head-on (14)   **(c)** Crossing (15)
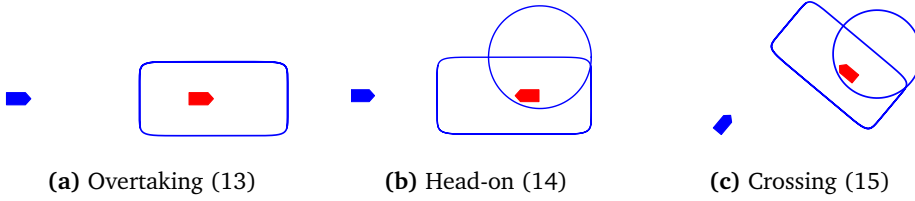
Figure 4.10: Ship domains for computing COLREGs-compliant path alterations, combining a Lamé curve and circular constraint. The dimensions based on the length of target vessel.

4.3.3   Enforcing head-on scenarios using a Lamé curve and circle

The Lamé curve (Equation 4.11) and the transformed ellipse (Equation 4.17) constitute scalable ship domains to calculate collision avoidance manoeuvres according to COLREGs rules 13-15. However, selecting sensible parameters, especially for Equation 4.17, poses a great challenge, compared to simply scaling by a factor of ship length (as in Equation 4.11).

Therefore, a simpler approach consists of combining a Lamé curve with a simple circular constraint, as visualised in Figure 4.10. By using only the Lamé curve, one is still able to comply with rule 13 & 15, and with the addition of the circular constraint, also with rule 14. The Lamé curve is the same as in Equation 4.11, i.e.,

$$h_{\text{Lamé}} \triangleq \left| \frac{\bar{E}_i(t)}{a_L} \right|^p + \left| \frac{\bar{N}_i(t)}{b_L} \right|^p \leq 1 \tag{4.18}$$

with the circular constraint given by

$$h_{\text{circle}} \triangleq \bar{E}_i(t)^2 + \bar{N}_i(t)^2 \leq r_L^2 \tag{4.19}$$

where r_L is the radius of the circular constraint and is scaled based on the length of the target vessel.

As with the previous methods, the domains are evaluated using difference in co-ordinates (as described in Equation 4.13), although with a different offset parameter c_L, for both the Lamé curve and the circle. Determining adherence towards rule 13 & 15 can be achieved simply by evaluating $h_{\text{OT,GW}} = h_{\text{Lamé}}$, with rule 14 requiring both conditions to be evaluated $h_{\text{HO}} = h_{\text{Lamé}} \lor h_{\text{circle}}$. If the conditions are asserted to be true, the positions of own ship violate the domain of the target vessel and thereby the associated rule.

Remark 4.2. *The formulation of the Lamé curve together with the circle is presented differently in Paper F, compared to that of Equations 4.18 and 4.19. For the sake of coherence of the thesis chapter, the constraints have been reformulated to fit the notation of the chapter. However, it should be noted that the two formulations result in the same outcome in terms of ship domain.*

4.4 Discussion

Correct interpretation and adherence towards the COLREGs is, beyond dispute, a crucial component of MASS. As current rules are built on ambiguities and interpretations, the complete adherence to all situations proves to be quite a challenge. The proposed ship domains provide a simple yet powerful tool for determining whether a proposed trajectory adheres to the given applicable COLREGs rule. The domains allow experts to choose safety limits scaled by ship lengths, stopping distances, and other relevant metrics, for scaling according to desired safety measures.

However, one of the downsides of modelling the COLREGs as a constraint, rather than a cost, is that the feasibility of the problem decreases. During some circumstances, a rule compliant manoeuvre may not exist, and therefore computing a non-compliant (or less compliant) deviation might be necessary to mitigate the prevailing risk of collision. One instance of this could include requiring entering very close quarters or passing the target vessel incorrectly, in order to resolve the conflict, either by violating the COLREGs or the chosen safety margins. One could instead argue that by representing the COLREGs as constraints, the collision avoidance scheme is instead able to report whether a deviation exists within the prescribed safety limits. If not, then the system can send a request for help from a human proxy, either onboard or at a Remote Control Center (RCC). Adhering to the COLREGs usually consists of multiple steps, most of which are beyond the typical scope of collision avoidance. To perform adequate evasive manoeuvres, it is required that the human navigator or MASS correctly assesses the situation at hand, identifies the relevant COLREGs and then plans a remedial action if necessary.

Achieving partial COLREGs-compliance onboard ocean liners traversing open waters is simple, compared to vessels operating within confined and inner coastal waters. In open waters, the radar system is capable of detecting incoming target vessels well in advance of their CPA. Then applying the ship domains is as simple as predicting their straight-line trajectories, and extracting their ship length and navigational status from their AIS messages. More often than not, it can be safely assumed that vessels that navigate within open waters will continue along their straight path for a foreseeable future and carry an AIS transponder. The AIS messages can inform the MASS about the target vessel's operations and whether it is restricted in its manoeuvrability. If so, then rule 18 applies, and the MASS is responsible for keeping out of the way. Navigators onboard large crafts, such as container vessels and bulk carriers, look multiple nautical miles and minutes ahead, such as a range of 10-15 nm and 20 minutes ahead. These crafts are therefore able to initiate their give-way obligations well in advance, at a TCPA of 10-15 minutes. If for some reason

the collision avoidance scheme is unable to compute a feasible deviation, a proxy can be notified while there are still more than 10 minutes until CPA. In open waters, evasive actions are (almost) always preferred and sufficient for dealing with the risk of collision, as reducing speed is not desired whilst cruising onboard large crafts.

Within confined and inner coastal waters applying the COLREGs is a completely different story, as there is not only a significant variation in traffic conditions, but also a wider range of vessel types, sizes and navigational experience. In these waters, straight-line predictions may no longer be a sufficient representation of the future intents and actions of the target vessels, as traffic conditions and potential draught constraints pose additional challenges. Without the straight-line assumption, the presented situation awareness is no longer capable of computing the collision risk using the conventional descriptions for CPA and TCPA. Instead, other metrics and systems are required for both predicting the trajectories and for assessing the scenario at hand. Research efforts exist that explore alternative method for computing CPA and TCPA that also leverage the Rate of Turn (ROT) and Speed over Ground (SOG) for increased accuracy [174]. Moreover, the occurrence of vessels restricted in manoeuvrability is greatly increased, as large merchant vessels typically must traverse inner coastal waters to arrive at their port of call. Hansen *et al.* [9] demonstrated a situation awareness framework for including rule 9, where it was highlighted that a river crossing ferry cannot blindly follow rule 15, without considering the manoeuvrability constraints of other vessels.

In general, it is expected that the behaviour and actions of a MASS are predictable to human navigators, since both manned and autonomous craft must co-exist. Therefore, it is important to also consider the culture and local interpretation of the rules so that the behavioural outcomes of the collision and grounding avoidance scheme align with local seafarers, both experienced and inexperienced. A complicated aspect of applying the COLREGs is doing so during instances where the MASS must not only assess behavioural traits based upon the type of vessel or geographic region of operation, but also estimate and assess the manoeuvrability of the encountered vessel. Especially during instances where the target vessel is not equipped with AIS. A risk of collision may arise if a given target vessel incorrectly assumes that the MASS is capable of determining whether or not a special rule or circumstance applies, such as the application of COLREGs rule 9.

Depending on the purpose of the given MASS, one could expect that local rules may be altered to accommodate its operation or the needs of surrounding vessels. As there are local rules for some ferries in Denmark, one could speculate that by introducing similar obligations for the Greenhopper, that is, that the Greenhopper must yield for all traffic, the ambiguity of the given COLREGs scenario decreases.

Chapter 5

Sampling-based motion planning for marine crafts

A combined collision and grounding avoidance scheme is instrumental for ensuring the computation of safe and compliant route deviations. To ensure safe operation, all interactions with target vessels must be handled according to the COLREGs. Furthermore, the available information from sources such as the ENC must be adequately processed and represented to ensure grounding avoidance.

This chapter introduces sampling-based motion planning (SBMP) in the context of marine crafts. First, the general formulation of the n-dimensional SBMP problem is presented, with an accompanying description of the primary algorithm, RRT*. Then, the SBMP problem is subsequently specialised for the maritime domain, where various relevant constraints and objectives functions are introduced.

The primary content of the chapter details the developed SBMP framework, which is specifically tailored for marine crafts. The chapter contains additional details about the contributions in Paper B and Paper C, regarding the extraction and manipulation of high-fidelity information available from the ENC.

The chapter presents the novel objective function for SBMP problems originally introduced in Paper C, in the form of minimising the route deviation from a prescribed nominal, rather than the typically path length metric. A vector-based approach inspired by track-control is first introduced (Paper C), with a simpler variant provided toward the end (Paper D).

The main research outcomes are presented in the context of partial or full autonomy for larger marine crafts, such as the merchant fleet, where it is assumed that the vessel is currently at cruising speed.
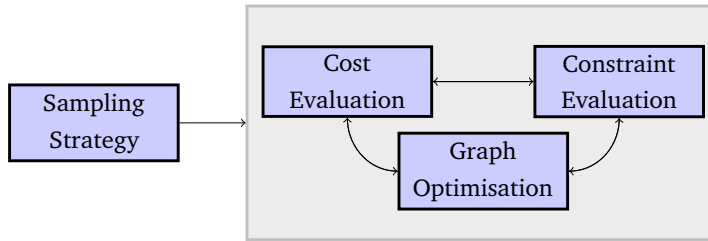
Figure 5.1: The sampling strategy for generating a random state or configuration from the state space. The SBMP algorithm then evaluates its feasibility and eventual cost, before adding it to the tree (or graph) that approximates the free space. Depending on the chosen SBMP method, the addition of the new state to the tree is an iterative process, in order to ensure optimal edge connections.

5.1   Optimal sampling-based motion planning

Planning problems are usually described as computing a sequence of feasible states that connect a starting configuration to the target (or goal) configuration. For these problems, it is commonly assumed that there is no prior knowledge of how to reach the goal state, which instead must be discovered by the algorithm. By introducing an element of optimisation, one can instead obtain an optimal sequence of states.

In the realm of solving continuous planning problems, the two most common methods for approximating the state space (or search space) are either graph-based and sampling-based approximations.

Graph-based approximations are typically a deterministic class of algorithms, and are known to be resolution complete and resolution optimal. This means that both the quality of the solution and the ability to report the existence of a solution depend on the selected resolution. A finer graph (or grid) resolution unavoidably impacts the computational time. When building a discrete representation of the environment, each point is evaluated to determine whether it violates the given obstacles and constraints. For complicated state spaces, this poses a significant computational challenge.

Sampling-based motion planning (SBMP) instead incrementally estimates an approximation of the state space by randomly sampling states and checking their feasibility. Since the checks are performed as the representation of the state space (or search space) is being built, it allows for the implementation of black-box constraint and collision checking. SBMP has been able to conquer applications where explicit representation of the obstacles and/or constraints is both infeasible or practically impossible [175, Chapter 5].

Figure 5.1 visualises the simplified procedure of a SBMP algorithm, where a

sampling strategy samples random states that are used to generate candidate nodes for the graph. These nodes, once identified, are iteratively evaluated by cost metrics, constraint models and a graph optimiser, in order to build an optimal representation of the free space.

5.1.1   Optimal SBMP problem formulation and definition

As the concept of sampling-based motion planning (SBMP) works for arbitrary dimensions, the following definitions reflect this. The formulation of the optimal SBMP is based on [130].

Let $\mathcal{X} \subseteq \mathbb{R}^n$ be the n-dimensional state space, with $x \in \mathcal{X}$ denoting a n-dimensional state vector. The state space $\mathcal{X}$ is composed of two subsets, namely: the free space $\mathcal{X}_{\text{free}}$ representing all valid states for the given system, and the obstacle set $\mathcal{X}_{\text{obs}}$ containing all violating states, with $\mathcal{X}_{\text{free}} = \mathcal{X} \backslash \mathcal{X}_{\text{obs}}$. Importantly, all states within $\mathcal{X}_{\text{free}}$ are feasible with respect to both system and environmental constraints.

Let $x_s \in \mathcal{X}_{\text{free}}$ be some initial feasible state at time $t = 0$ and $x_e \in \mathcal{X}_{\text{free}}$ be the desired feasible final state at some time $t = T$, where T is some unknown value. Then, let $\sigma : [0,1] \mapsto \mathcal{X}_{\text{free}}$ be a sequence of feasible states that constitutes the path that connects x_s to x_e through $\mathcal{X}_{\text{free}}$, and Σ the set of all feasible and nontrivial paths, with a given path denoted by $\sigma \in \Sigma$.

The objective of optimal sampling-based motion planning (SBMP) is to find the optimal path σ^*, which minimises a cost function $c(\cdot)$, while connecting x_s to x_e through feasible states $x \in \mathcal{X}_{\text{free}}$,

$$\sigma^* = \arg\min_{\sigma \in \Sigma} \left\{ c(\sigma) \mid \sigma(0) = x_s, \, \sigma(1) = x_e, \forall s \in [0,1], \, \sigma(s) \in \mathcal{X}_{\text{free}} \right\}. \qquad (5.1)$$

5.1.2   Optimal Rapidly-exploring Random Trees (RRT*)

A very popular method to solve the optimal SBMP problem is using an algorithm called RRT*, which was originally proposed by Karaman and Frazzoli [116] as an optimising version of RRT by LaValle [111]. Both RRT and RRT* are probabilistically complete, which means that with enough samples generated, the probability of finding the solution converges to one [175], while RRT* is also asymptotically optimal [116]. Essentially, RRT* is a method of generating a directed graph, or tree, through the free (or feasible) space, forming optimal connections (edges) between the starting state and every other state in the free space $\mathcal{X}_{\text{free}}$, keeping track of nodes that fall within the target (or goal) region, to report the best found solution.

Consider the directed graph $\mathcal{T} = (\mathcal{V}, \mathcal{E})$, consisting of the set of nodes $\mathcal{V}$ and the set of edges $\mathcal{E}$. Candidate nodes and edges are generated as follows. First, a uniformly random sample x_{rand} is generated based on an approximation of $\mathcal{X}$,

---

Algorithm 5.1: RRT* (formulated based on [116] and [130])

    Given : x_s, x_e

1 $\mathcal{V} \leftarrow \{x_s\}, \quad \mathcal{E} \leftarrow \emptyset, \quad \mathcal{T} = (\mathcal{V}, \mathcal{E})$;

2 **for** $i = 1 \dots N$ **do**

3      $x_{nearest} \leftarrow$ NearestNode$(\mathcal{T}, x_{rand})$;

4      $(x_{new}, x_{new}) \leftarrow$ ExtendTowards$(x_{nearest}, x_{rand})$;

5   **if** Feasible$(x_{nearest}, x_{new}, x_{new})$ **then**

6          $\mathcal{T} \leftarrow$ InsertNode$(\mathcal{T}, x_{new})$;

7          $X_{near} \leftarrow$ Near$(\mathcal{T}, x_{new}, r)$;

8          $x_{min} \leftarrow x_{nearest}$;

9          $c_{min} \leftarrow$ Cost(x_{min}) + Line(x_{min}, x_{new});

10   **for** $\forall x_{near} \in X_{near}$ **do**

11            $c_{new} \leftarrow$ Cost(x_{near}) + Line(x_{near}, x_{new});

12   **if** $c_{new} < c_{min}$ **then**

13   **if** Feasible$(x_{near}, x_{new}, x_{new})$ **then**

14                  $x_{min} \leftarrow x_{near}$;

15                  $c_{min} \leftarrow c_{new}$;

16         $\mathcal{E} \leftarrow \mathcal{E} \cup \{x_{min}, x_{new}\}$;

17   **for** $\forall x_{near} \in X_{near}$ **do**

18            $c_{near} \leftarrow$ Cost(x_{near});

19            $c_{new} \leftarrow$ Cost(x_{new}) + Line(x_{new}, x_{near});

20   **if** $c_{new} < c_{near}$ **then**

21   **if** Feasible$(x_{new}, x_{near}, x_{near})$ **then**

22                  $x_{parent} \leftarrow$ Parent(x_{near});

23                  $\mathcal{E} \leftarrow \mathcal{E} \setminus \{x_{parent}, x_{near}\}$;

24                  $\mathcal{E} \leftarrow \mathcal{E} \cup \{x_{new}, x_{near}\}$;

25 **return** $\mathcal{T}$;

---

typically sampled uniformly between a minimum and maximum value of the state x. By uniformly sampling the space, the completeness of RRT* is preserved, which means that it correctly reports the feasibility and returns optimal solutions. Once x_{rand} is computed, the nearest node $x_{nearest}$ to x_{rand} within the current graph is located. As the graph grows in size, finding the nearest neighbour is computationally expensive. This is typically remedied by using efficient data structures, such as a k-d tree [176], in order to speed up the search. Additional speed can be gained by sacrificing accuracy, by using an approximate nearest-neighbour algorithm [177].

Then, using a steering function, a node x_{new} is generated in the direction of x_{rand} from $x_{nearest}$ and its resulting edge is formed. If the edge between x_{new} and $x_{nearest}$ is feasible with respect to $\mathcal{X}_{free}$, the node x_{new} and resulting edge is added to the tree. An edge is deemed feasible if the connection is collision free, both with static and dynamic obstacles, and also adheres to the underlying system constraints, be it

geometric, kinematic or dynamic constraints. As previously described, one of the strengths of SBMP algorithms comes from the ability to perform efficient feasibility checks, as these can be represented and implemented in an entirely black-box fashion if desired. The feasibility checker needs to simply return true or false, to indicate whether the new node and subsequent edge should be formed [175].

Once the edge between x_{new} and $x_{nearest}$ has been formed, the optimising step determines whether more suitable parent and child nodes exists within a ball of radius r from x_{new}. This step is called rewiring, as neighbouring nodes and edges are checked whether they form lower costs edges (or paths). Once all nodes within the ball have been checked, the rewiring is complete and the process starts over by generating another uniform sample.

The overview of the RRT* algorithm is provided in Algorithm 5.1, and with the step-by-step procedure visually presented in Figure 5.2. Given some initial tree $\mathcal{T}$ (Figure 5.2a) spanning $\mathcal{X}_{free}$, connecting the starting state x_s to feasible states in $\mathcal{X}_{free}$. Generate a random sample x_{rand} (Figure 5.2b) and find the nearest node x_{near} within $\mathcal{T}$, and steer towards it, generating a new node x_{new} (Figure 5.2c). If the edge connecting x_{near} and x_{new} is feasible, add both the node and edge to the tree (Figure 5.2d). If one cycles these steps (Figures 5.2a-5.2d), the RRT algorithm is obtained. Due to random sampling, RRT is capable of efficiently exploring the entire state space and ultimately converges to the goal region, given that a feasible solution exists. Should a solution exist, the method is guaranteed to find it as the number of samples goes towards infinity. However, despite an infinite number of samples, the obtained solution is by no means optimal, as nodes are simply attached to the nearest node in the tree. The algorithm only guarantees that every feasible state is connected to the starting node, whilst adhering to the constraints of the problem.

The previously described optimisation, or rewiring step, takes place in Figures 5.2e-5.2h. Figure 5.2e visualises the process in which all nodes within a ball of radius r are checked, to determine whether there are lower cost parents, compared to simply using the node $x_{nearest}$. Figure 5.2f rewires the edge to a different node, as it results in a lower overall cost. Then, in Figure 5.2g, all nodes within the ball are checked again, but instead for candidate child nodes that minimise the path. Similarly, a child node is identified with less cost, and therefore the graph is rewired (Figure 5.2h).

The method continues to expand the tree until either: a maximum amount of samples or valid nodes have been generated, it reaches a time limit, or until a certain cost is reached. Finding a suitable stopping cost is challenging; therefore, sample, node, or time limits are typically selected.
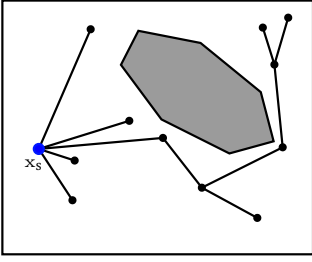
(a) The current tree $\mathcal{T}$ at some i-th iteration, mapping paths from x_s to $\mathcal{X}_{\text{free}}$.
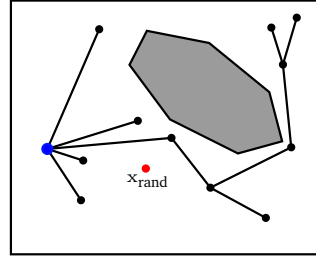
(b) Random uniformly generated sample x_{rand} from within $\mathcal{X}$.
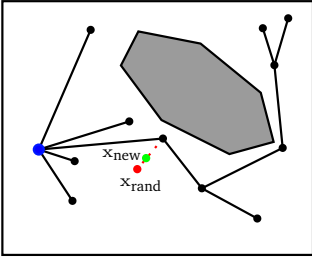
(c) Generating a new candidate node x_{new} by steering toward sample x_{rand}.
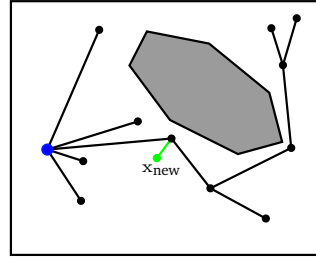
(d) As the connecting edge from the tree to x_{new} is feasible, the node is added.
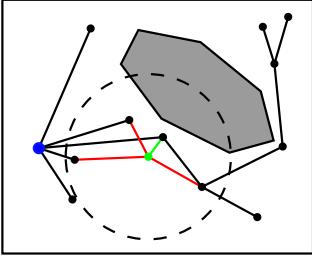
(e) Candidate parent nodes within a radius r of x_{new} are checked.
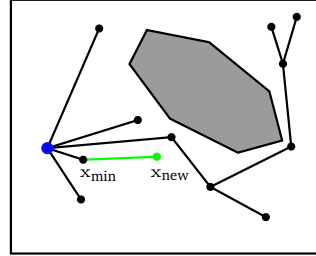
(f) A lower cost and feasible parent node is identified, therefore the tree is rewired.
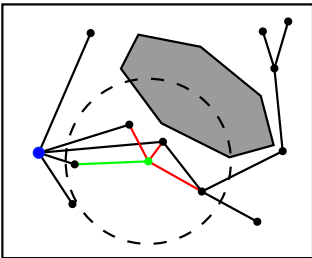
(g) Candidate child nodes within a radius r of x_{new} are checked.
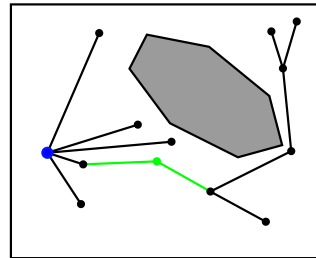
(h) A lower cost and feasible child node is identified, therefore the tree is rewired.

Figure 5.2: The bounding box represents $\mathcal{X}$, the polygon $\mathcal{X}_{\text{obs}}$, with the remaining space $\mathcal{X}_{\text{free}} = \mathcal{X} \setminus \mathcal{X}_{\text{obs}}$. Figures 5.2a-5.2d represents the explorative graph generation of RRT [111], by adding the optimising steps from Figures 5.2e-5.2h the algorithm becomes RRT* [116].
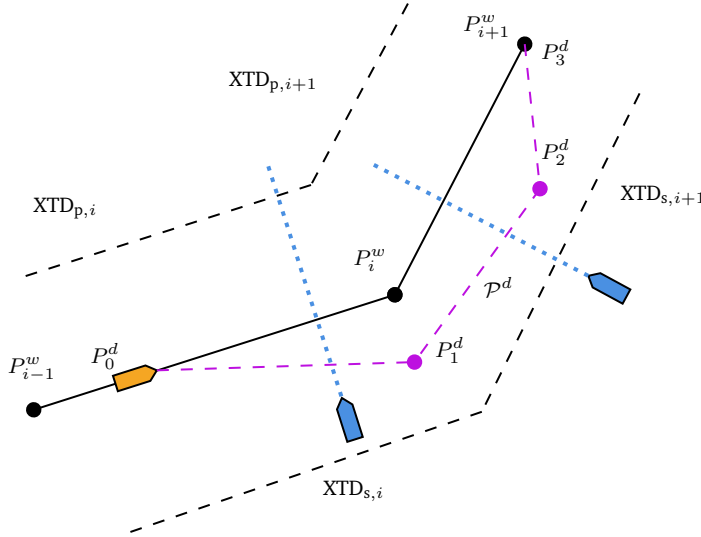
Figure 5.3: Given some nominal path $\mathcal{P}^w$, with the own ship travelling along it. At some point, the system detects that a deviation must occur, therefore the collision and grounding avoidance scheme is called, such that an adequate route deviation is computed. Located at some point P_0^d along the nominal route, own ship computes a deviation (dashed purple lines) consisting of four waypoints (including its initial waypoint), with the final waypoint representing the reentry to point to the nominal path (P_3^d). The waypoints P_0^d and P_3^d are equal to the exit P_s and reentry P_e respectively. The collision and grounding avoidance scheme is designed to work at any arbitrary location along the nominal route.

5.2 Sampling-based motion planning for marine crafts

For larger marine crafts, such as the merchant fleet, the gradual adoption of autonomous technologies will most likely be achieved through retrofitting. Onboard such crafts, there exist low-level controls schemes, such as autopilots and waypoint controllers, which allow navigators to simply provide a sequence of waypoints that the vessel must follow. Leveraging a SBMP algorithm such as RRT* seems natural, as the graph (or tree) generation is tailored towards generating sequences of waypoint-like outputs. Furthermore, it is possible to constrain the solution according to the underlying requirements or restrictions posed by the existing track-control scheme.

As mentioned, SBMP typically concerns finding a previously unknown path through a given environment, returning a sequence of feasible states that brings the system from the start to the goal. However, for systems such as marine crafts, there often already exists an underlying nominal route that has been optimised with respect to local weather forecasts, grounding safety margins, for its port of call, etc.

It is therefore natural to consider the existence of this nominal route, and

instead shift the objective of the motion planning problem to minimise the resulting route deviation from the nominal, as the nominal route not only encodes crucial information, but a resulting deviation that is similar in nature to the nominal may also preserve some safety aspects encoded within the predefined route. Therefore, for marine crafts, the SBMP is reformulated as finding the minimal deviation from the nominal route.

Let $\mathcal{P}^w : [0, 1] \mapsto \mathcal{X}$ define the nominal sequence of waypoints, and $\mathcal{P}^d : [0, 1] \mapsto \mathcal{X}$ describe the sequence of waypoints constituting a potential route deviation, where $\mathcal{P}^d \in \Sigma$ and Σ constitute all feasible deviations. $P_s \in \mathcal{X}_{\text{free}}$ describes the initial waypoint at $t = T$, or exit point, along the nominal route, and $P_e \in \mathcal{X}_{\text{free}}$ the final waypoint, which represents the reentry point to the nominal route, at some unknown time $t = T_f$. The planning problem is then given by

$$\mathcal{P}^{d*} = \underset{\mathcal{P}^d \in \Sigma}{\arg\min} \left\{ c\left(\mathcal{P}^d\right) \mid \mathcal{P}^d(0) = P_s, \, \mathcal{P}^d(1) = P_e, \, \forall s \in [0, 1], \, \mathcal{P}^d(s) \in \mathcal{X}_{\text{free}} \right\} \quad (5.2)$$

where the objective is to compute the optimal route deviation $\mathcal{P}^{d*} \in \mathcal{X}_{\text{free}}$ that minimises some objective function $c(\mathcal{P}^d)$, connecting the current position of own ship P_s to a suitable reentry point P_e along the nominal route. Figure 5.3 visualises the before-mentioned quantities, in the face of two approaching target vessels from starboard, where $P_0^d = P_s$ and $P_3^d = P_e$.

As in the general SBMP, the free space $\mathcal{X}_{\text{free}} = \mathcal{X} \backslash \mathcal{X}_{\text{obs}}$ is occupied by constraints within $\mathcal{X}_{\text{obs}}$. Importantly, all states within $\mathcal{X}_{\text{free}}$ are feasible with respect to both the system and environmental constraints.

The obstacle subset $\mathcal{X}_{\text{obs}}$ is formed as the union over all constraints, namely,

$$\mathcal{X}_{\text{obs}} = \mathcal{X}_{\text{obs}}^{\text{OS}} \cup \mathcal{X}_{\text{obs}}^{\text{ENC}} \cup \mathcal{X}_{\text{obs}}^{\text{TV}}, \qquad \mathcal{X}_{\text{obs}}^{\text{TV}} = \bigcup_{i=1}^{n} \mathcal{X}_{\text{TV},i}(t) \qquad (5.3)$$

with $\mathcal{X}_{\text{obs}}^{\text{OS}}$ containing states that violate the manoeuvring constraints of own ship, $\mathcal{X}_{\text{obs}}^{\text{ENC}}$ the grounding and buoy collision states, and finally $\mathcal{X}_{\text{obs}}^{\text{TV}}$ the target vessel constraints, which is the union of n vessels, such that all n are considered simultaneously.

For larger marine crafts, as evasive manoeuvres are preferred over speed changes, one can attempt to solve the collision avoidance problem by assuming constant speed. This simplifies the SBMP problem, as it is no longer necessary to solve a two-point boundary value problem within the steering function, as assuming constant speed allows the steering and rewiring to be considered purely geometrically. Therefore, coupled with P_s are the initial velocity and heading of own ship, which are used as initial conditions for the planning problem. In some instances, it may be desired, or even required, to evaluate the effect of a speed change. This can be achieved by

running multiple SBMP solvers in parallel, each with a different speed as the initial condition.

5.2.1 Own ship constraints

As the vessel dynamics are not directly considered whilst planning the route deviations, alternative constraints must be posed in order to ensure the validity of the proposed route.

One such constraint is to ensure that the angle between two consecutive segments is feasible for execution by the underlying track-control scheme. Furthermore, two consecutive waypoints must be spaced by at least twice the wheel-over distance.

Additional constraints could include discarding solutions that fall outside of the specified Cross-track Distance (XTD). The XTD serves as an alarm limit for navigators, notifying them when the vessel gets too far from the nominal route (see Figure 5.3). The distance is set for each leg along the nominal route and is tighter in critical or confined waters, as violating the XTD indicates a potential grounding risk. However, grounding avoidance is ensured by including the ENC as a separate constraint, $\mathcal{X}_{\text{obs}}^{\text{ENC}}$, which is covered in Section 5.3.

As noted previously, if required, one could include the vessel dynamics such as by solving a two-point boundary value problem.

5.2.2 Target vessel constraints and COLREGs-compliance

As it is assumed that the collision and grounding avoidance scheme receives the anticipated target vessel trajectories, once the situation awareness deems necessary (i.e. the CPA and TCPA limits are violated), it is possible to leverage said trajectories for ensuring both obstacle avoidance and COLREGs-compliance. By encoding the trajectories with the applicable COLREGs domain (as determined in Section 4.2.3 and Section 4.3), the target vessel trajectory at each time-step spatially occupies regions that violate the COLREGs from the perspective of the own ship.

The set $\mathcal{X}_{\text{obs}}^{\text{TV}}$ that describes the constraints of the target vessel that is formed as the union of the encoded spatial constraints for each target vessel $\mathcal{X}_{\text{TV},i}(t)$, as follows,

$$\mathcal{X}_{\text{obs}}^{\text{TV}} = \bigcup_{i=1}^{n} \mathcal{X}_{\text{TV},i}(t). \tag{5.4}$$

5.3 The Electronic Navigational Chart (ENC)

An essential component to achieve grounding avoidance is the inclusion of the information contained within the Electronic Navigational Chart (ENC). For chart

```
ENCFILE.000
├─ ⋮
├─ BOYCAR
│  ├─ 00-{shape, category, colour(s), (lon, lat)}
│  └─ ⋮
├─ ⋮
├─ DEPARE
│  ├─ 00-{min-depth, max-depth, polygon ((lon, lat), ...)}
│  └─ ⋮
├─ DRGARE
│  ├─ 00-{min-depth, max-depth, polygon ((lon, lat), ...)}
│  └─ ⋮
├─ ⋮
├─ LNDARE
│  ├─ 00-{polygon ((lon, lat), ...)}
│  └─ ⋮
└─ ⋮
```
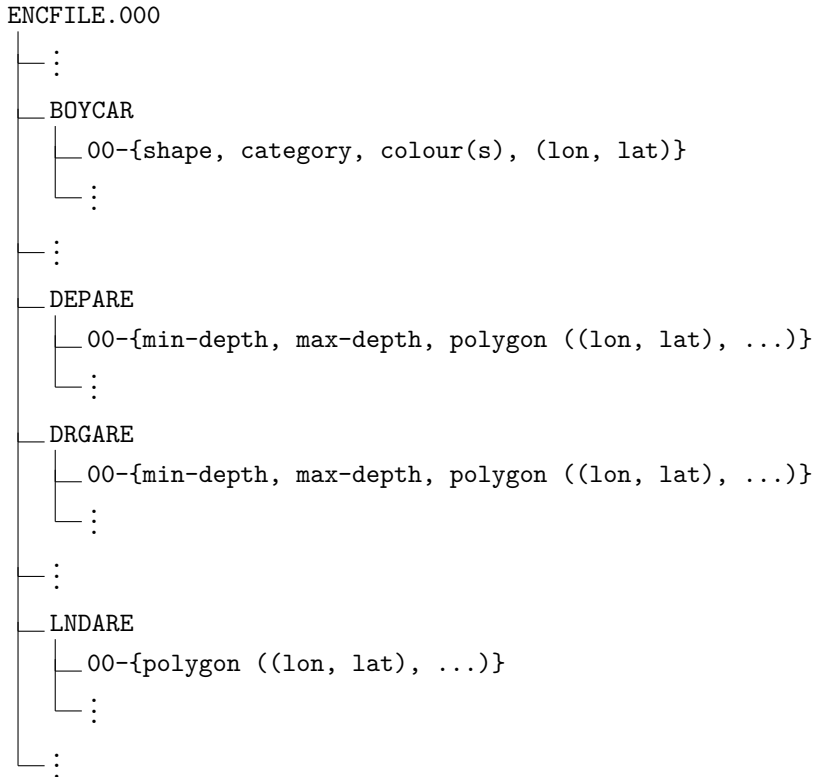
Figure 5.4: This figure visualises a subset of the most relevant layers, and a subset of the information contained within each geo object. Each layer may contain multiple objects, such as DEPARE, which contains geometries for varying water depths. Each object within the DEPARE layer contains not only the latitude and longitude for each polygon, but also associated depths values describing both the shoalest and deepest measured depths. Similarly, the buoy layer describes the anchored location of the respective buoy, as well as relevant information about its shape and descriptors. For further details regarding the various ENC layers and attributes, see [178].

information to be certified as an ENC, the information must be in the S-57 format, which is the current standard set by the International Hydrographic Organization (IHO) for use with ECDIS. The S-57 standard consists of up to 160 different geo object (short for geographic object) classes, describing anything from land and depth contours, to buoy locations, fairways, offshore platforms, bridge pylons, etc. Each geo object is typically referred to as a layer, as certain ones can be switched on and off when using the ECDIS. To achieve complete grounding avoidance, it is important to use the charts, in order to generate a feasible area of operation in which the vessel can safely navigate within.

(a) Geofiltered (black).   **(b)** Cropped contours.
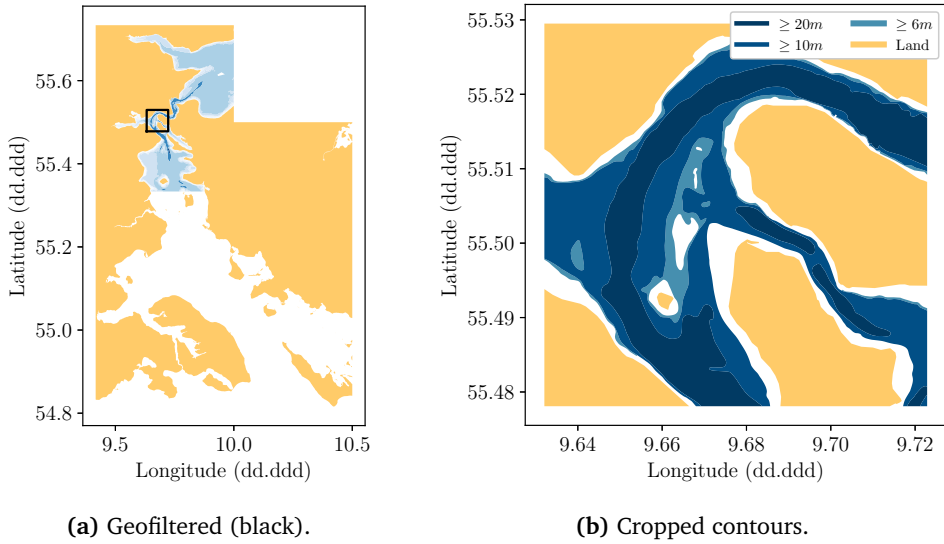
Figure 5.5: Using a geofilter (black square in Figure 5.5a) to extract ENC data. The resulting polygons are filtered by the draught restriction of own ship and further reduced to the region of the filter (Figure 5.5b). White contours in Figure 5.5b are depths shoaler than 6m.

Two of the most important layers, or geo objects, are the depth contours, also called DEPARE, and the dredged areas, called DRGARE. It is not necessary to consider the land contours (LNDARE) during motion planning, as they do not intersect the depth contours, which means that if a point is registered as outside the depth or dredge contours, the point must be on land or in a similarly untraversable position. The land contours do, however, help with visualising the case-studies. Additionally, there are separate layers for each type of buoy, with the most important being: cardinal buoys (BOYCAR), lateral buoys (BOYLAT) and safe water buoys (BOYSAW). The buoy geo objects consist of information related to their position and appearance, and it is therefore possible to deduce the relevant information about navigational requirements and safety. Figure 5.4 partially details the object information available from each layer, with the geometries being the most relevant to ensure grounding avoidance. For further details about the various ENC layers and attributes, see [178].

Each of the layers contain a collection of polygons that describe the geometries, with associated attributes. For the depth contours, minimum and maximum depth values are attached to each polygon, and it is therefore possible to extract only the depth contours with depths feasible for the draught of own ship. Similarly, the dredged areas contain polygons and their associated dredged depth. The polygons within each layer can be represented by arbitrary and often non-convex polygons.

Simply extracting all the geometries of the chart may be infeasible, as ENCs

may cover large geographical areas and therefore the vast amount of data used to represent the given polygons may result in a large computational burden. To extract more manageable polygon information, it is desirable to reduce the polygons to a subset that describes the area of interest, both in terms of geography and water depths.

To do so, all contours with a feasible water depths are extracted, then a geofilter is applied to the charts to discard all polygons that fall strictly outside the filter. Such a geofilter is described by region of desired latitude and longitude values, that is

$$\mathcal{G}^{\mathrm{geo}} = \{(\lambda_i, \phi_i) \mid \lambda_{\min} \leq \lambda_i \leq \lambda_{\max} \wedge \phi_{\min} \leq \phi_i \leq \phi_{\max}\}, \tag{5.5}$$

which describes all latitude and longitude pairs (λ_i, ϕ_i), within the minimum desired latitude ($\lambda_{\min}$) and longitude ($\phi_{\min}$) values, and the maximum desired latitude ($\lambda_{\max}$) and longitude ($\phi_{\max}$) values. Application of the filter yields a set of polygons $\mathcal{X}^{\mathrm{ENC,geo}}$, which are all contours (in geodetic coordinates) where at least one of the points falls within the specified filter $\mathcal{G}^{\mathrm{geo}}$.

However, the extracted polygons within $\mathcal{X}^{\mathrm{ENC,geo}}$ may still represent very large areas, as is evident in Figure 5.5a, where a geofilter (black square) has been applied to the ENC, yet most of the extracted polygon information lies outside the area of interest. To remedy this, the intersection between the filter and extracted polygons is computed in order to form new polygons that are bounded by the geofilter,

$$\mathcal{X}^{\mathrm{ENC,geo}}_{\mathrm{cropped}} = \mathcal{X}^{\mathrm{ENC,geo}} \backslash \mathcal{G}^{\mathrm{geo}} \tag{5.6}$$

An example of cropped (or bounded) polygon set $\mathcal{X}^{\mathrm{ENC,geo}}_{\mathrm{cropped}}$ is visualised in Figure 5.5b. The coordinates within the cropped polygons are then transformed from geodetic coordinates to NED, resulting in the feasible set of contours $\mathcal{X}^{\mathrm{ENC}}_{\mathrm{free}}$. Once the these contours have been extracted, cropped and transformed to NED, the obstacle subset for the SBMP problem can be calculated the complement set

$$\mathcal{X}^{\mathrm{ENC}}_{\mathrm{obs}} = \left(\mathcal{X}^{\mathrm{ENC}}_{\mathrm{free}}\right)^{\complement} \tag{5.7}$$

which represent the set used for rejecting samples that violate the draught restrictions of own ship.

However, directly using the extracted contours may result in route deviations that are arbitrarily close to the infeasible regions and shallow waters, as the polygons simply provide an indication of whether or not a given point is feasible. Instead, prior to generating $\mathcal{X}^{\mathrm{ENC}}_{\mathrm{obs}}$, one can modify $\mathcal{X}^{\mathrm{ENC}}_{\mathrm{free}}$ by eroding the polygon boundary and dilating the holes. As the buoys within the ENC are only represented as a single point, the dilation also serves as a margin to avoid collision with the given buoy. The amount of dilation (and erosion) for each contour or buoy can differ as desired.

(a) Contour extraction.

(b) Erosion and dilation of feasible contours.
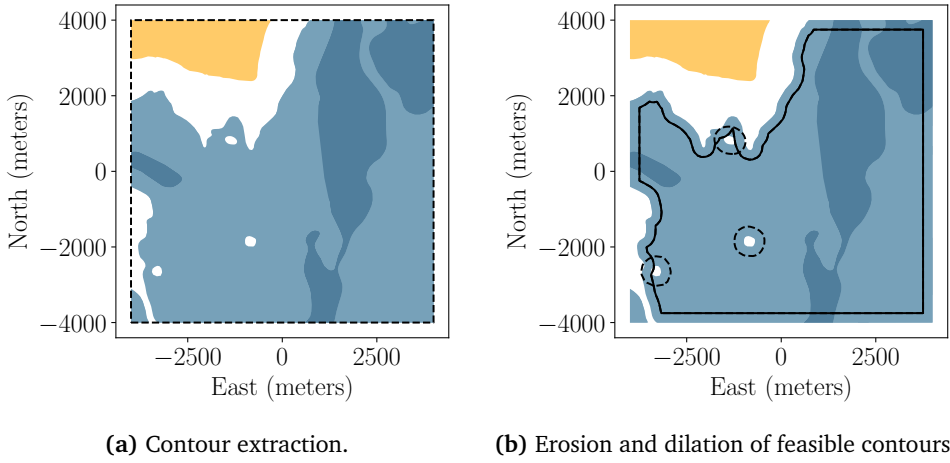
Figure 5.6: Extraction of the feasible depth contours ($\mathcal{X}_{\text{free}}^{\text{ENC}}$) using the geofilter (dashed black rectangle). Once extracted, the perimeter is eroded and the holes dilated, in order to add a safety margin towards shallow waters.

Doing so creates an additional safety margin towards the infeasible contours, thereby enhancing safety and providing additional grounding avoidance. Figure 5.6a demonstrates contour extraction within a rectangular approximation of the state space (the dashed rectangle) after converting to NED, with 5.6b detailing the addition of safety margins through erosion and dilation, where the solid line indicates the erosion of the boundary and the dashed lines the dilation of the holes.

5.3.1 Uniform sampling of feasible ENC contours

To maintain the guarantees and properties of the solutions of SBMP, such as by using RRT*, the most common sampling strategy involves uniformly sampling an approximation of $\mathcal{X}_{\text{free}}$. For marine crafts, such an approximation can be obtained from the previously applied geofilter (Equation 5.5), as it already approximates the region of interest from the ENC. By converting the $\mathcal{G}^{\text{geo}}$ to NED coordinates, the resulting region becomes a rectangular approximation $\mathcal{X}_{\text{rect}}$ of $\mathcal{X}_{\text{free}}$, bounded by its minimum and maximum north-east coordinates. To generate samples, the north and east coordinates are uniformly drawn from within approximation $\mathcal{X}_{\text{rect}}$, as follows

$$(N, E) \sim \mathcal{U}(\mathcal{X}_{\text{rect}}), \tag{5.8}$$

where (N, E) is the north-east coordinate pair, and $\mathcal{U}$ represents a uniform distribution, sampled between the limits of each dimension. However, simply using a rectangular approximation of the free space may yield very poor performance, depending on the ratio between feasible and infeasible water depths.
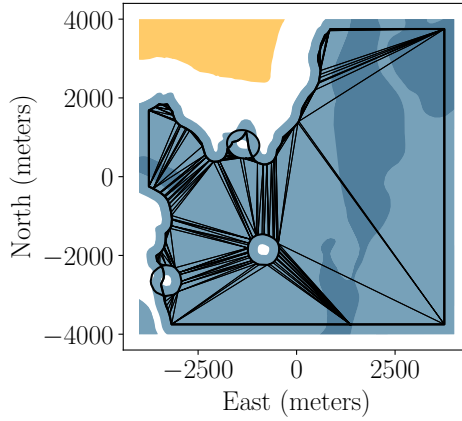
Figure 5.7: Triangulated space.

The reason why one most often uniformly samples an approximation of the state space is that a representation of $\mathcal{X}_{\text{free}}$ is typically unavailable for most planning problems. However, for marine crafts, the ENC contains a high-fidelity description of the free space, which is traversable for the given craft under nominal conditions. Therefore, one could instead leverage this information to generate samples directly within the feasible chart contours, in order to increase the efficiency of the SBMP algorithms.

The feasible contours were previously extracted and merged into a single polygon, through the formation of $\mathcal{X}_{\text{free}}^{\text{ENC}}$, in order to form the environmental constraint $\mathcal{X}_{\text{obs}}^{\text{ENC}}$. By generating samples within the description of the free space ($\mathcal{X}_{\text{free}}^{\text{ENC}}$), one can be sure that a given state is valid with respect to the problem at hand. Depending on the particular planning problem, $\mathcal{X}_{\text{free}}^{\text{ENC}}$ is most likely described by a non-convex polygon. Therefore, in order uniformly sample such a polygon, one can either use rejection sampling techniques, methods for directly sampling non-convex polygons (such as [124]), or decomposition techniques (such as triangulation [179]).

By computing the triangulation of $\mathcal{X}_{\text{free}}^{\text{ENC}}$, the non-convex polygon is decomposed into a set of triangles, all of which can easily be uniformly sampled. Constrained Delaunay Triangulation (CDT) is a proven method for computing the triangulation of non-convex polygons, and ensures that a finite set of non-overlapping triangles are returned [180]. Furthermore, CDT ensures that all triangles are guaranteed to remain within the polygon, even for non-convex polygons with holes.

Once the triangulated contours have been obtained, uniformly generating samples within a given triangle is achieved as follows

$$P = \left(1 - \sqrt{r_1}\right) A + \sqrt{r_1}\left(1 - r_2\right) B + \sqrt{r_1} r_2 C \tag{5.9}$$

where P represents a coordinate within the triangle composed of vertices (A, B, C), $r_1 \sim \mathcal{U}(0, 1)$ and $r_2 \sim \mathcal{U}(0, 1)$ [179]. However, one must first select which triangle to sample, which is achieved by weighting each triangle within the triangulated set by their area and selecting them accordingly, such that larger triangles are samples more often than smaller ones.

Remark 5.1. *It should be noted that the polygon resolution of the contour geometries found within the ENC is typically very high. Therefore, it can be beneficial for the sake of performance to simplify the polygons, such as by using a line simplification method. A common and efficient approach is using the Douglas-Peucker algorithm [181], however, one should be aware that topology is not necessarily preserved.*

5.4 Performance metrics

As both grounding avoidance and COLREGs-compliance are modelled as constraints for the marine craft SBMP problem, the performance metrics (or objective functions) can focus on quantities related solely to the own ship.

This section first introduces the most common cost function used for SBMP, namely the path length. Then a novel objective function that minimises the path deviation is presented.

Additional performance metrics, such as speed loss, can be found in Paper C. A data-driven performance that encapsulates and encodes past behaviours of other seafarers is presented later in Chapter 7.

5.4.1 Minimal path length

When planning a route deviation from a single segment along the nominal route, minimising the total length of the path is comparable and simpler than computing the deviation in terms of cross-track error or equivalent. Therefore, depending on the initial and reentry point along the nominal track, it may be favourable to simply consider the path length.

Given a computed route deviation $\mathcal{P}^d$, consisting of m waypoints (P_s and P_e included), the length of the path is calculated as

$$c_l\left(\mathcal{P}^d\right) = \sum_{i=1}^{m-1} \|P_i^d - P_{i-1}^d\|_2, \quad \forall P_i^d \in \mathcal{P}^d. \tag{5.10}$$

5.4.2 Minimal path deviation (cross-track error)

When traversing inner coastal or confined waters, collision avoidance manoeuvres may be required along multiple legs, rather than a single segment. As track control
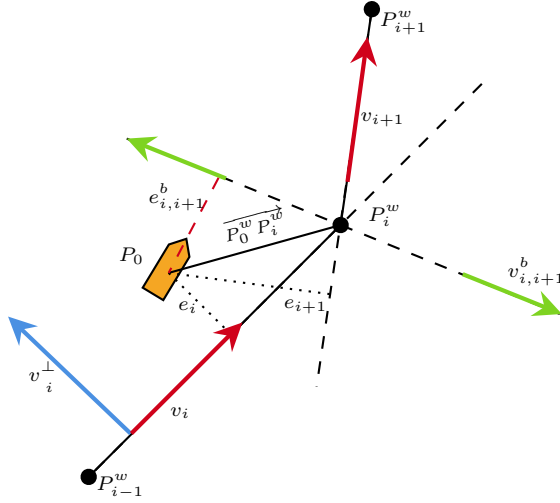
Figure 5.8: The required vectors for computing the cross-track error (CTE) towards a given leg. The bisecting line (Equation 5.14) provides the condition for selecting which leg to minimise towards, in this case either v_i or v_{i+1}.

schemes continuously steer the vessel along these segments, minimising the Cross-track Error (CTE) (sometimes known as XTE) to the nominal route, one could leverage a similar idea as an objective function. As the proposed SBMP implicitly defines the time component, the minimisation between the nominal and deviation is simply computed by evaluating the spatial differences between the two routes. All of the following vector quantities for describing the cross-track error are visualised in Figure 5.8.

Consider therefore a path segment, $\overline{\boldsymbol{P}_{i-1}^w \boldsymbol{P}_i^w}$, which is defined by two waypoints. Let $\boldsymbol{P}_{i-1}^w$ and $\boldsymbol{P}_i^w$ denote the position vectors of the waypoints P_{i-1}^w and P_i^w respectively, expressed in the NED frame. The direction vector for a given path segment $\overline{\boldsymbol{P}_{i-1}^w \boldsymbol{P}_i^w}$, $\boldsymbol{v}_i$, is defined as

$$\boldsymbol{v}_i = \left(\cos\left(\psi_i\right), \sin\left(\psi_i\right)\right), \tag{5.11}$$

with its corresponding perpendicular vector

$$\boldsymbol{v}_i^{\perp} = \left(-\sin\left(\psi_i\right), \cos\left(\psi_i\right)\right). \tag{5.12}$$

Given the current position of own ship, $\boldsymbol{P}_0$, and the current path segment $\boldsymbol{v}_i$, performing an inner product

$$\boldsymbol{e}_i = \boldsymbol{P}_0 \boldsymbol{P}_i^w \cdot \boldsymbol{v}_i^{\perp}, \tag{5.13}$$

yields the cross-track error between the current position of the own ship and a given leg. Given instances with multiple legs, such as $\boldsymbol{v}_i$ and $\boldsymbol{v}_{i+1}$ in Figure 5.8,

a mechanism is required to determine the leg towards which the cross-track error should be minimised.

Using the bisecting line between v_i and v_{i+1},

$$v^b_{i,i+1} = \frac{(v_{i+1} + v_i)}{\|v_{i+1} + v_i\|} \tag{5.14}$$

and then by computing and checking the signed distance to the said bisecting line $v^b_{i,i+1}$

$$e^b_{i,i+1} = \overrightarrow{P_0 P^w_i} \cdot \left(v^b_{i,i+1}\right)^\perp, \tag{5.15}$$

it is possible to determine whether to minimise the cross-track error towards v_i and P_i, or instead v_{i+1} and P_{i+1}. Therefore, the cross-track error for a given waypoint P^d_i along the proposed deviation $\mathcal{P}^d$ is given by

$$e_{P^d_i} = \begin{cases} P^d_i P^w_i \cdot v^\perp_i & \text{if } e^b_{i,i+1} \le 0 \\ P^d_i P^w_{i+1} \cdot v^\perp_{i+1}, & \text{if } e^b_{i,i+1} > 0 \end{cases}. \tag{5.16}$$

The cross-track error along the entire deviation, $\mathcal{P}^d$ (excluding P^d_s and P^d_e as they have zero deviation), is computed as the sum of all errors

$$c_e\left(\mathcal{P}^d\right) = \sum_{i=1}^{m-2} e_{P^d_i}, \quad \forall P^d_i \in \mathcal{P}^d. \tag{5.17}$$

An alternative formulation for minimum deviation is an objective function that computes the minimum distance towards nominal route, while considering the nominal path in its entirety. Given the entire nominal route and a computed deviation, the corresponding error between the two is given by

$$c_d\left(\mathcal{P}^d\right) \triangleq \sum_{k=1}^{m-2} \min \left\|\mathcal{P}^w - P^d_i\right\|_2, \quad \forall P^d_i \in \mathcal{P}^d \tag{5.18}$$

this will result in solutions that tend towards the nominal path. As the nominal path is likely to consist only of few waypoints, for better results, a linearly interpolated version of $\mathcal{P}^w$ should instead be used. The minimum distance calculation for high resolution paths, in Equation 5.18, can be sped up by using k-d trees for the nearest neighbour search.

Remark 5.2. *It should be noted that, depending on the expansion distance of the SBMP algorithm, the nominal route leg length, and the chosen steering function, minimising the cross-track error can result in "corner cutting" in the transition between two legs. A potential remedy for this behaviour is achieved by linearly interpolating both the nominal route $\mathcal{P}^w$ and the route deviation $\mathcal{P}^d$ prior to computing the cost term in Equation 5.18.*
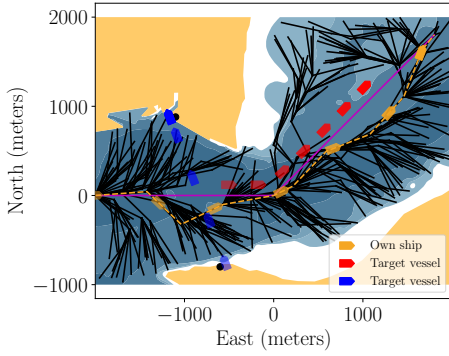
(a) Two vessel scenario, one crossing and one overtaking, within inner coastal waters.
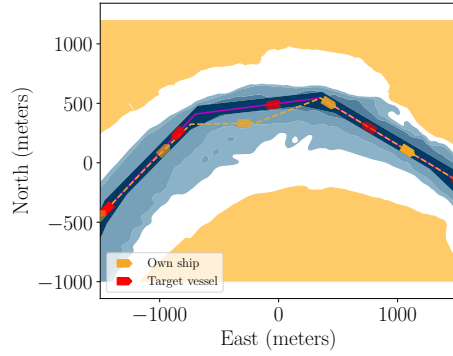
(b) Multi-leg single vessel head-on scenario within a narrow dredged passage.
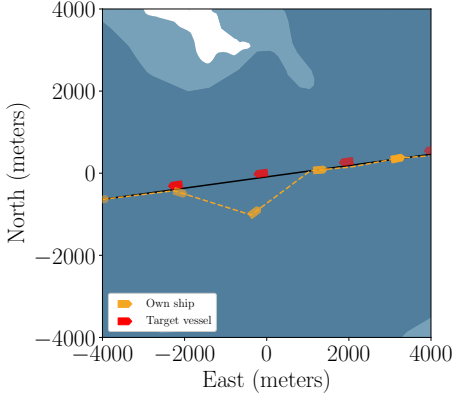
(c) Single leg and single vessel head-on scenario.
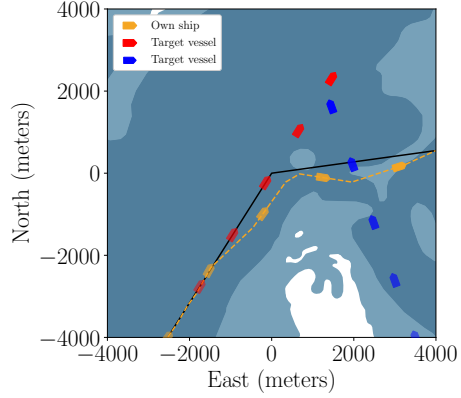
(d) Overtaking and crossing scenarios over two legs.

Figure 5.9: Four different case-studies of the proposed sampling-based collision and grounding avoidance framework for marine crafts. Figure 5.9a visualises the directed graph (or tree) generated by RRT*, which maps the starting configuration to all other feasible states, returning the minimum path between the exit and reentry points. COLREGs-compliance is achieved by leveraging the ship domain (Section 4.3) applicable to the encounter at hand. The scenarios in Figures 5.9b, 5.9c and 5.9d present encounters of varying complexity, both from a collision and grounding avoidance perspective.

5.5   Collision and grounding avoidance for merchant crafts

The proposed sampling-based collision and grounding avoidance framework is presented and demonstrated in the context of larger crafts, such as the merchant fleet. As the presented methods assume cruising-like conditions, the case studies only considers scenarios where own ship is in transit.

To achieve COLREGs-compliant collision and grounding avoidance, the collision risk assessment (Section 4.2) and the proposed ship domains (Section 4.3) are combined with the proposed SBMP framework from this chapter. The case studies presented in Figure 5.9 assume that external sensor fusion and situation awareness systems have detected the surrounding target vessels, assessed the situation and triggered a route deviation. The target vessels information is then passed to the collision and grounding avoidance scheme so that a safe and COLREGs-compliant manoeuvre is computed.

The four scenarios presented in Figure 5.9 use a combination of the minimum path length and the minimum cross-track error metrics presented in Section 5.4. In Figure 5.9c, the scheme successfully deconflicts a head-on scenario according to the safety margins set by the ship domain (Equation 4.17). By combining the minimum path length and cross-track error, the scheme remains on the nominal track until a deviation is required, doing so yields a trade-off between the path length and cross-track error, compared to simply deviating immediately, which would have resulting in a path of minimum length. Figure 5.9b demonstrates the scheme in a highly constrained environment, with multiple legs. As the depth contours pose severe restrictions, it is highly desirable that the collision and grounding scheme respects the nature of the nominal route. This results in a deviation that takes place shortly before transitioning to the second legs.

As the collision and grounding avoidance scheme relies on external predictions and assessment, the scheme also works with multiple target vessels. Figures 5.9a and 5.9d show the calculation of routes in the face of two target vessels, where both an overtaking and crossing scenario must be taken into account. The deviation successfully deconflicts the scenario at hand, mitigating the risk of collision, whilst ensuring safe passage with respect to the infeasible depth contours.

5.6   Discussion

The chapter presented the contributions of the thesis that constitute the core sampling-based collision and grounding avoidance framework, which is capable of producing safe and COLREGs-compliant route deviations for large marine crafts traversing confined and inner coastal waters. The resulting deviations from the framework are suitable for both decision support and autonomous operation. Several route suggestions can be generated by introducing weights in the objective functions or by modifying the safety constraints. Generating a single route deviation and executing it enables the autonomous system to autonomously deconflict potential collision risks that may occur throughout its voyage.

As described previously, SBMP algorithms typically focus on finding the shortest path between two states, whereas for collision avoidance, one would prefer to compute optimal deviations from the underlying nominal route. To facilitate this, novel cost functions for computing minimum deviation paths, combining concepts from SBMP and track-control, were presented, such that the proposed framework is capable of respecting the existence of a nominal route and minimise towards it.

To ensure safe navigation, the predicted target vessel trajectories, together with the proposed ship domains, formed a subset of the obstacles space that represented states that are in violation with the COLREGs. Furthermore, grounding avoidance was achieved by considering the complex nature of the depth contours available from within the ENCs. Various techniques from computational geometry were used to add safety margins, reduce polygon complexity, and produce uniform samples of non-convex regions, in order to leverage the ENC information within the SBMP framework.

The efficacy of the proposed framework consisting of performance metrics, sampling space, and constraints was successfully demonstrated using the SBMP algorithm RRT* in various scenarios in complex environments, considering multiple vessels. If required by the problem at hand, it is possible to construct the tree such that it considers the underlying vessel dynamics. This adds additional computational time, as two-point boundary-value problems must be solved at each edge formation.

Sampling-based algorithms, such as RRT*, are able to quickly report the existence of a feasible solution. However, as the solution tends towards optimality in probability, choosing when to stop the search for a solution becomes rather challenging. Depending on the complexity of the problem, such as the ratio between $\mathcal{X}_{\mathrm{free}}$ and $\mathcal{X}_{\mathrm{obs}}$, running the algorithm for a fixed number of samples may produce solutions of varying quality, as in some instances a good solution can be found with little or no samples, whereas other times more samples may be required. To further complicate the matter, as the number of samples added to the tree increases, so does the complexity of the required computations. This results in increased computational time for larger graphs, whereas smaller ones result in faster nearest neighbours searches and rewiring steps. Therefore, a suitable termination strategy is needed for the use of SBMPs in practical applications. The algorithm either needs to be terminated after a fixed amount of samples, or after a certain runtime. A greater amount of samples may be required in cluttered environments to achieve a similar size tree as in non-cluttered ones, and choosing a fixed amount of samples will most likely result in a non-constant runtime.

One of the downsides, when using RRT* (and RRT), is that the method maps the starting state to all other states in the free space $\mathcal{X}_{\mathrm{free}}$, as demonstrated in Figure

5.9a. This means that a lot of computational effort is spent exploring every aspect of the space, which does not necessarily improve the solution at hand. Furthermore, mapping of unnecessary states also increases the overall size of the graph, adding additional computational complexities. Mapping the starting state to all other states is not an issue when using discrete graph-based algorithms, such as A*, as here a heuristic guides the search such that the least amount of exploration is wasted. This issue for SBMP can be remedied by introducing more advanced sampling techniques or heuristics. Both are explored in subsequent chapters of the thesis.

The impact of computational speeds, stopping conditions, and overall predictability is important when it comes to the practical application of the proposed collision and grounding avoidance system, since the route deviations are computed based on constant or static information about the future trajectories of the target vessels and environmental conditions. Great computational times may lead to solutions that are outdated, with respect to the scenario at hand, therefore, the vessel needs to know what manoeuvre is required and to perform it as soon as possible. Thus, if the unfolding scenario changes, the system can recompute the deviation to ensure the validity and safety of the calculated deviation. Efficient and rapid replanning in the face of new information from the sensor fusion and situation awareness modules allows for a degree of uncertainty in the perceived situations.

Grounding avoidance was achieved by considering the shallow water contours as restrictions to ensure that only route deviations within traversable areas were computed. By extracting and preprocessing (adding safety margins) the feasible contours along the nominal route prior to departure, one is able to incorporate the high-fidelity nature of the ENCs without the need for tuning parameters. However, within the ENC are many additional navigational aids and requirements that one must adhere to, to comply with the COLREGs and the navigational practises of other seafarers. Buoys not only serve as regional indicators, but also indicate desired behaviour of incoming ships. A fully compliant collision and grounding avoidance scheme should also adhere to the desired behaviour indicated by the buoys, e.g. following the instructions of the cardinal and lateral buoys.

The current framework simply avoids colliding with the buoys, as they extracted from the ENC and simply treated as obstacles. Since the proposed method computes minimally deviation route alterations, within the feasible contours, the framework is able to disregard the buoys that indicate fairways and shallow waters, and lateral buoys, as the nominal route encodes the correct lane of passage. However, special circumstance may require stricter adherence to buoys.

Chapter 6

Informed sampling techniques

As discussed in the previous chapter, one of the shortcomings of SBMP methods, such as RRT*, is that graph generation connects and optimises all feasible connections throughout the state space. For certain problems, such as those of higher complexity and dimensions, the uniform sampling strategy tends to waste a lot of sampling effort, both when generating infeasible samples and when performing unnecessary exploration of the entire space. For certain planning problems, such as collision avoidance, a clear predefined goal or nominal route exists, which instead could be leveraged to hone the search, as one could instead seek paths in the neighbourhood of said nominal. Such a focused search would yield lower cost solutions within the same amount of sampling effort, which ultimately results in a greater convergence speed toward the optimal solution.

This chapter introduces the concept of an informed subset and informed sampling strategies, which are proven sampling techniques for achieving rapid convergence to the optimal solution. Informed sampling strategies focus on generating samples by adaptively reducing the search space, as the current solution improves. Doing so increases the overall probability that the newly generated samples are capable of improving the cost of the current solution. Gammell *et al.* [130] popularised the first informed sampling strategy for RRT*, where they proposed an adaptive sampling space to find paths of minimum length. Here, the sampling space is shaped as a hyperellipsoid, scaled with respect to the current best found solution. This particular formulation and idea serve as the theoretical basis for the remaining chapter, which will present additional informed sampling strategies, as the main contributions from Paper A and Paper D.

The core content of the chapter introduces a novel informed sampling strategy that leverages the existence of an underlying nominal route (or path), in order to form an informed subset that can be used for collision avoidance. This particular

sampling strategy is the primary contribution of Paper D, which aims to increase the performance of using SBMP for collision avoidance, specifically to calculate paths with minimal deviation along piece-wise linear segments. The chapter further introduces the COLREGs-informed subset and sampling strategy, which is the presented novelty in Paper A. The sampling technique is tailored for marine crafts and the adherence towards COLREGs rules 13-15.

6.1   Common sampling techniques and sample biasing

To preserve the feasibility and optimality guarantees of SBMP algorithms, one can choose to generate uniformly distributed random samples of the free space $\mathcal{X}_{\text{free}}$ [111], [115]. Generating a uniformly random state x_{rand} from $\mathcal{X}_{\text{free}}$, is given by

$$x_{\text{rand}} = \mathcal{U}\left(\mathcal{X}_{\text{free}}\right) \tag{6.1}$$

where $\mathcal{U}(\cdot)$ is a uniform distribution. Since directly sampling the free space is infeasible, as it requires exact information of the problem, an approximation is instead used, typically consisting of the minimum and maximum values for each state, as described in Section 5.1.2. The approximation is equivalent to a rectangle in $\mathbb{R}^2$ and hyperrectangle in $\mathbb{R}^n$, with the sampling routine denoted as

$$x_{\text{rand}} = \mathcal{U}\left(\mathcal{X}_{\text{rect}}\right). \tag{6.2}$$

When the space is always only uniformly sampled $\mathcal{X}$, the probability of connecting the found path directly to the goal state x_{e} is very low. Therefore, a goal region is typically used in order to increase the probability that a solution is found.

To further improve the performance and convergence of SBMP algorithms, the uniform sampling scheme is typically combined with a sample biasing routine. There are a number of proven biasing strategies for SBMP algorithms, with the primary categories including: goal-biasing, obstacle-biasing, path-biasing, passage-biasing. The general idea is to introduce a heuristic to guide the search, in a honed or explorative manner [113], [117], [122], [123].

Goal biasing is an effective strategy that ensures that the tree growth is biased towards the goal region and that the calculated path connects to the actual goal state [113]. The main idea behind goal biasing is to use a uniformly distributed random variable, e.g. $u \sim \mathcal{U}(0, 1)$, compared to some scalar value, such as $0 \leq \delta \leq 1$. Then, based on the comparison between the two, either uniformly sample the rectangular approximation or attempt a direct connection to the goal,

$$x_{\text{rand}} = \begin{cases} \mathcal{U}\left(\mathcal{X}_{\text{rect}}\right), & \text{if } \delta < u \\ x_{\text{e}} & \text{otherwise} \end{cases}. \tag{6.3}$$
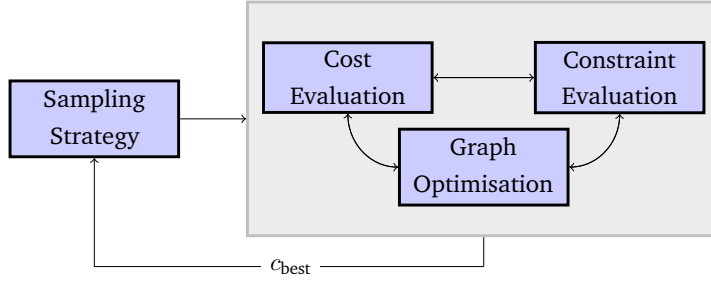
Figure 6.1: An updated visualisation of the previously presented SBMP workflow, as detailed in Figure 5.1, here the SBMP receives feedback about how each sample affects the cost of the current best found solution. Section 6.2 introduces feedback of the solution cost to adaptively reduce the search space, that is, to focus the sampling effort, as the current found solution cost improves. This allows the sampling strategy to hone the search and thereby accelerate the convergence to the optimal solution.
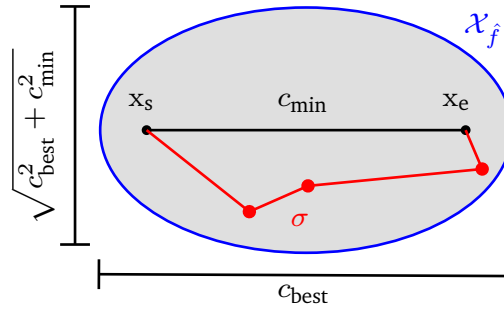
Figure 6.2: Visual representation of the informed subset as proposed by [130]. Once an initial solution has been obtained, the sampling space reduces to a bounding ellipsoid, thereby increasing the probability future states improve the current solution cost.

Once the path has been connected to the goal, the sampling strategy can be switched to exclusively sampling $\mathcal{X}_{\text{rect}}$.

6.2 Informed sampling

In addition to guiding or biasing the generated samples, additional performance can be obtained by performing an online reduction or modification to the sampling space or strategy. One particular class of these sampling strategies is called search space reduction or informed sampling. The main purpose of search space reduction is to reduce the sampling space in order to increase the probability that newly generated states improve the current best found solution. In order achieve a reduction, the sampling strategy requires a sense of feedback, such as the current graph develop-

ment or solution cost, in order to alter or focus its search. Figure 6.1 visualises the feedback structure of a simplified SBMP workflow, where in this case the current cost of the solution c_{best} is fed back into the sampling strategy.

Informed sampling strategies were popularised by Gammell *et al.* [130] (Gammell *et al.* [131]), who introduced Informed RRT*, and were some of the first to demonstrate effective search space reduction. They define several important sets, such as the omniscient set, $\mathcal{X}_f$, which is the set of states that can possibly improve the cost of the current solution, that is,

$$\mathcal{X}_f = \{ \mathrm{x} \in \mathcal{X}_{\text{free}} \,|\, f(\mathrm{x}) < c_{\text{best}} \} \tag{6.4}$$

where c_{best} is the cost of the current solution and $f(\mathrm{x})$ the combined cost-to-go and cost-to-come in order to pass through the state x going from x_{s} to x_{e}. They further state that exact knowledge of $\mathcal{X}_f$ requires exact knowledge of the planning problem.

For problems that seek to find solutions of minimum path length (minimising the Euclidian distance), it is possible to create a bounded space that is scaled by the current solution cost, once an initial solution has been obtained. Gammell *et al.* [130] showed that an admissible estimate of $\mathcal{X}_f$ is described by the equation for an n-dimensional hyperspheroid,

$$\mathcal{X}_{\hat{f}} = \{ \mathrm{x} \in \mathcal{X} \,|\, \|\mathrm{x}_{\text{s}} - \mathrm{x}\|_2 + \|\mathrm{x} - \mathrm{x}_{\text{e}}\|_2 \leq c_{\text{best}} \} \tag{6.5}$$

which is a special hyperellipsoid. The traverse diameter of the hyperellipsoidal set is scaled by the cost of the current solution c_{best} and its other diameter by $\sqrt{c_{\text{best}}^2 - c_{\text{min}}^2}$, with c_{min} representing the minimum achievable cost between the starting and the goal state. All quantities are visualised in Figure 6.2.

As the informed set is admissible, it guarantees that any state that may improve the solution is contained within it, which ensures that the optimal solution is included in the current search space. As the hyperellipsoid is a function of the current solution cost, the size of the informed set inevitably shrinks in size as the solution cost improves. Furthermore, it is possible to analytically generate samples that fall within the informed set, see [117], [130].

To apply the informed set, an initial solution cost is required in order correctly dimension it. Therefore, one typically uses the approximation $\mathcal{X}_{\text{rect}}$ until an initial solution is obtained. Depending on the cost of the initial solution, it may be a disadvantage to immediately switch to the informed set, as it may be significantly larger than the original approximation. To compare the two sets, the Lebesgue measure ($\lambda(\cdot)$) is computed, as it allows one to quantify the size of n-dimensional subsets.
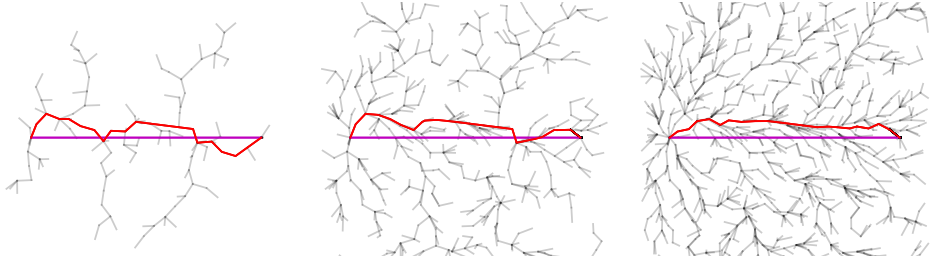
(a) $N = 200$, $c_l(\sigma) = 1.2299$ **(b)** $N = 800$, $c_l(\sigma) = 1.1580$ **(c)** $N = 1500$, $c_l(\sigma) = 1.0632$
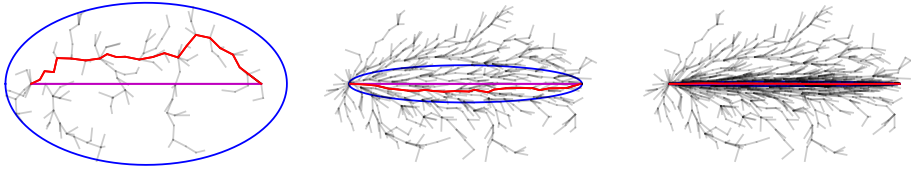
(d) $N = 200$, $c_l(\sigma) = 1.2233$ **(e)** $N = 800$, $c_l(\sigma) = 1.0130$ **(f)** $N = 1500$, $c_l(\sigma) = 1.0001$

Figure 6.3: Comparison between the rectangular approximation and an informed sampling strategy applied to RRT*. Figures 6.3a-6.3c details the performance of the rectangular approximation ($\mathcal{X}_{\text{rect}}$), which exhibits the previously described behaviour of mapping the starting state to every other state. Figures 6.3e-6.3f demonstrates the effectiveness of the informed set ($\mathcal{X}_{\hat{f}}$), where performing online search space reduction increases the probability that a given sample may improve the current found solution. For the same number of samples, the informed algorithm practically converges to the optimal solution, compared to the rectangular approximation. The cost function $c_l(\cdot)$ is the path length as described in Equation 5.10.

Once the Lebesgue measure of the informed set is smaller than that of the approximation,

$$\lambda\left(\mathcal{X}_{\hat{f}}\right) < \lambda(\mathcal{X}_{\text{rect}}) \tag{6.6}$$

the informed sampling strategy kicks in. The Lebesgue measure of the hyperrectangle is simply its volume, where the measure of the informed set $\mathcal{X}_{\hat{f}}$ is given by [131]

$$\lambda\left(\mathcal{X}_{\hat{f}}\right) = \frac{c_{\text{best}}\left(c_{\text{best}}^2 - c_{\text{min}}^2\right)^{\frac{n-1}{2}}}{2^n} \frac{\pi^{\frac{n}{2}}}{\Gamma\left(\frac{n}{2} + 1\right)}. \tag{6.7}$$

The effectiveness of the informed set is clearly demonstrated in the example study shown in Figure 6.3. Here, the same problem is solved with and without the use of the informed sampling strategy (applied to the RRT* algorithm). Simply using the rectangular approximation (Figures 6.3a-6.3c) causes the graph to explore unnecessary parts of the free space, where once the informed set kicks in (Figures
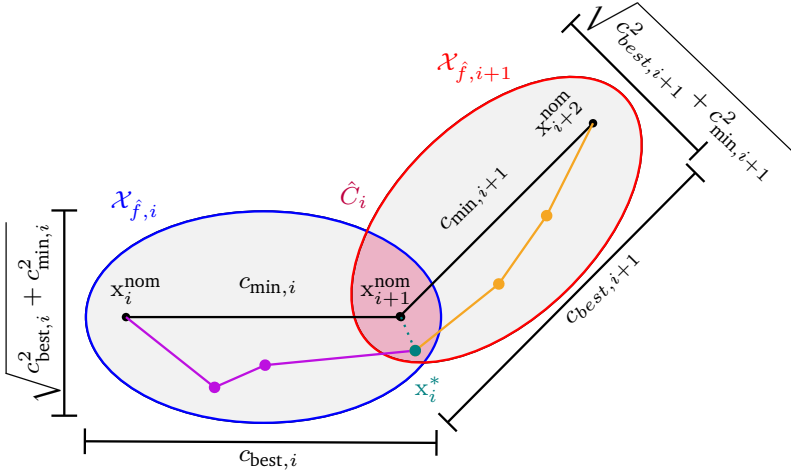
Figure 6.4: The visualisation of the informed set for increasing the probability of generating samples for minimising the path deviation. With a nominal path consisting of m states, and therefore $m-1$ piece-wise linear segments, the informed set is described by the union of $m-1$ hyperellipsoids.

6.3d-6.3f) the solution rapidly converges to its minimum as the sampling space actively reduces and hones the generated samples.

6.3 Informed sampling for minimal path deviation

The informed sampling strategy as presented in Section 6.2 only works for minimising the path length. However, for collision avoidance applications, it is highly desirable to instead minimise towards an existing nominal path, as previously discussed and presented in Chapter 5, specifically Section 5.4.2.

For certain motion planning applications, such as the case studies presented for marine crafts, the underlying nominal route consists of several piece-wise linear segments. During ideal or nominal conditions, the minimal deviating solution is equivalent to the sum of each path length along each segment. By applying this idea to the informed set, one can extend it such that for each linear segment, an informed subset is formed.

Given the piece-wise linear nominal path σ^{nom}, which consists of m states $x_i^{\mathrm{nom}} \in \sigma^{\mathrm{nom}}$, and the current best found path deviation σ^{dev} with states $x_i^{\mathrm{dev}} \in \sigma^{\mathrm{dev}}$, which is described by

$$\sigma^{\mathrm{dev}} = \left(x_k^{\mathrm{dev}}\right)_{k=1}^{N} \tag{6.8}$$

where N is the length of the deviation including the exit and reentry states, $x_1^{\mathrm{dev}} = x_{\mathrm{s}}$

and $x_N^{\text{dev}} = x_e$. The informed subset for minimal path deviation then consists of the union of $m - 1$ ellipsoids along each nominal path segment, that is,

$$\mathcal{X}_{\hat{F}} = \bigcup_{i=1}^{m-1} \mathcal{X}_{\hat{f},i} \tag{6.9}$$

where each set is described by the pair-wise waypoints of σ^{nom}

$$\mathcal{X}_{\hat{f},i} = \{x \in \mathcal{X} \mid \|x_i^{\text{nom}} - x\|_2 + \|x - x_{i+1}^{\text{nom}}\|_2 \leq c_{\text{best},i}\}, \tag{6.10}$$

with each subset $\mathcal{X}_{\hat{f},i}$ described and scaled by its own local best solution cost $c_{\text{best},i}$. For planning problems where $m = 2$, the proposed method defaults to that of Gammell *et al.* [130], as the nominal path consists only of a single leg.

As noted previously, the original informed subset is admissible, which means that it guarantees that it includes all states that may possibly improve the current solution. This guarantee must also be maintained for the proposed informed sampling space $\mathcal{X}_{\hat{F}}$. By dividing the current found path deviation σ^{dev} so that the local path cost $c_{\text{best},i}$ shares part of its length with neighbouring ellipsoids, one can guarantee that the path in its entirety will remain within the entire informed set $\mathcal{X}_{\hat{F}}$. Figure 6.4 visualises two neighbouring ellipsoids along a nominal path, where each local cost shares the common state x_i^*.

Between the starting state x_s and the end state x_e there are $m - 2$ states along the nominal path x^{nom} that connects them. Then $\mathcal{N}$ is a finite sequence of common states between two neighbouring ellipsoids, which are obtained by calculating the nearest states in σ^{dev} to each of the $m - 2$ nominal states x_i^{nom}, that is,

$$\mathcal{N} = ((x^*, k)_j)_{j=1}^{m-2} \tag{6.11}$$

where the nearest neighbour computation is given by

$$x^* = \underset{x^{\text{dev}} \in \sigma^{\text{dev}}}{\arg\min} \left\|x^{\text{dev}} - x_i^{\text{nom}}\right\|_2, \quad \forall i = 2, \ldots, m - 1 \tag{6.12}$$

with k the index of the state x^* in the path deviation σ^{dev}. When $m > 2$, the local cost $c_{\text{best},i}$ for each informed set is given by

$$\mathcal{C}_{best} = \left(c_{\text{best},i} = c_l(\rho_i) \quad \forall i = 1, \ldots, m - 1\right) \tag{6.13}$$

where $c_l(\cdot)$ is the path length of the local segment ρ_i, which is given by

$$\rho_i = \begin{cases} \left(x_s, x_2^{\text{dev}}, \ldots, x_i^*, x_{i+1}^{\text{nom}}\right) & \text{if } i = 1 \\ \left(x_i^{\text{nom}}, x_{i-1}^*, x_{k_{i-1}+1}^{\text{dev}}, \ldots, x_i^*, x_{i+1}^{\text{nom}}\right) & \text{if } 1 < i < m - 1 \\ \left(x_i^{\text{nom}}, x_{i-1}^*, x_{k_{i-1}+1}^{\text{dev}}, \ldots, x_{N-1}^{\text{dev}}, x_e\right) & \text{if } i = m - 1 \end{cases} \tag{6.14}$$

Equation 6.14 describes how the current path deviation is divided among the various informed subsets, so that they all have a state in common. Figure 6.4 details the various components of the proposed informed set, where the current path deviation is divided into two subpaths, before being used to scale the ellipsoid along their respective linear segments.

Once $X_{\hat{F}}$ and $\mathcal{C}_{\text{best}}$ are constructed, it can be guaranteed that a given route deviation σ^{dev} and all states that can improve the deviation are contained within the set $X_{\hat{F}}$. The samples within the ellipsoids are generated as described in [131], where the ellipsoids are selected and sampled based on their relative measures, with rejection sampling applied based on their proportional membership to ensure uniformity.

6.3.1   Sample biasing using the nominal route

Similar to the goal-biasing strategy, performance can be increased for finding the initial solution by biasing the search toward the waypoints within the nominal path.

Equation 6.3 is extended to include every state within the nominal route, except the starting state, such that

$$
x_{\text{rand}} = \begin{cases} \mathcal{U}\left(\mathcal{X}_{\text{space}}\right), & \text{if } \delta < u \\ \mathcal{U}\left(\left(x_1^{\text{nom}}, \dots, x_m^{\text{nom}}\right)\right), & \text{otherwise} \end{cases} \tag{6.15}
$$

where $\mathcal{X}_{\text{space}}$ is the current sampling space (e.g. $\mathcal{X}_{\text{rect}}$ or $\mathcal{X}_{\hat{F}}$). Despite activating the informed set, it may still be favourable to continue to randomly select samples from the nominal route, as this allows the exploration to converge to the exact same waypoints, should they be feasible.

Figure 6.5 shows the convergence of the computed deviation towards the nominal route in the obstacle free case. The proposed method is further demonstrated in Figure 6.6 where the deviation computes a tight path around the obstacles, while minimising the path deviation.

6.3.2   Switching condition

As with the original informed sampling strategy, presented in Section 6.2, a switching condition is required to determine if the informed set should be activated. Similarly to the condition in Equation 6.6, the Lebesgue measures of X_{rect} and the informed subset $\mathcal{X}_{\hat{F}}$ can be compared,

$$
\lambda\left(\mathcal{X}_{\hat{F}}\right) < \lambda\left(\mathcal{X}_{\text{rect}}\right) \tag{6.16}
$$

(a) $n = 80$ **(b)** $n = 180$ **(c)** $n = 400$
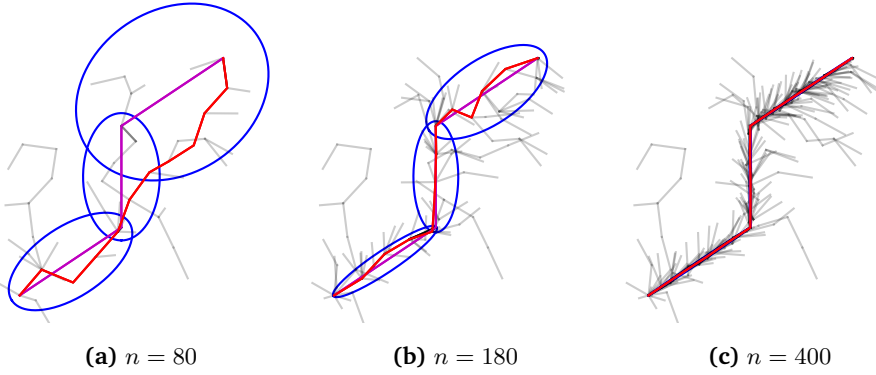
Figure 6.5: Several iterations using the proposed informed sampling strategy (blue ellipses) in order to compute a the minimal path deviation (red), which eventually fully converges to the nominal path (magenta).

(a) $n = 250$, $c_d(\sigma) = 895$ **(b)** $n = 500$, $c_d(\sigma) = 285$ **(c)** $n = 750$, $c_d(\sigma) = 229$
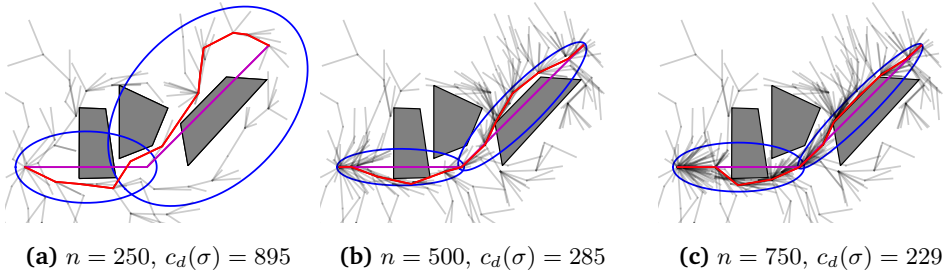
Figure 6.6: Solution to a planning problem where the nominal route is blocked by several obstacles. The proposed informed sampling strategy focuses the graph generation to remain within the neighbourhood of the nominal route (magenta). As the number of samples increase, the computed path deviation (red) converges towards the nominal. The cost function $c_d(\cdot)$ for minimal deviation is described in Equation 5.18.

where the Lebesgue measure of $\mathcal{X}_{\hat{F}}$ is given by

$$\lambda\left(\mathcal{X}_{\hat{F}}\right) = \sum_{i=1}^{m-1} \lambda\left(\mathcal{X}_{\hat{f},i}\right) - \sum_{i=1}^{m-2} \lambda(C_i) \tag{6.17}$$

with $C_i = \mathcal{X}_{\hat{f},i} \cap \mathcal{X}_{\hat{f},i+1}$. The Lebesgue measure of the informed subset consists of the sum of each $m - 1$ individual Lebesgue measure, minus the $m - 2$ intersections.

Computing the measure of the i-th ellipsoid is trivial, as one simply uses the measure defined previously in Equation 6.7, replacing the costs by the ones corresponding to the i-th ellipsoid. Calculating an exact value for the intersection measure proves quite challenging, as there is no apparent analytical solution. Therefore, an
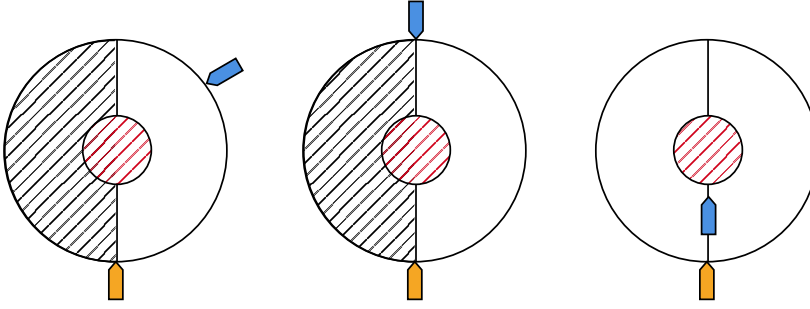
Figure 6.7: Geometric definition of the COLREGs-compliant subsets, for crossing, head-on and overtaking scenarios respectively, based on annuli and half-annuli.

estimate for each intersection, $\hat{C}_i$, is used as a substitute

$$\lambda\left(\hat{\mathcal{X}}_{\hat{F}}\right) = \sum_{i=1}^{m-1} \lambda\left(\mathcal{X}_{\hat{f},i}\right) - \sum_{i=1}^{m-2} \lambda\left(\hat{C}_i\right). \qquad (6.18)$$

The simplest and most conservative estimate is to set $\hat{C}_i = 0$, which results in an overestimated measure, as it contains twice the intersection for each pair of ellipsoids. If the measure for each $\mathcal{X}_{\hat{f},i}$ is small compared to that of $\mathcal{X}_{\text{rect}}$, the poor estimate is insignificant. The downside of the simple estimate is the inaccuracy in complicated environments, where the initial computed deviation may result in large distances towards each segment. For some planning problems, the suboptimal choice of the heuristic for $\hat{C}_i$ may cause the informed sampling strategy to remain inactive. In these instances, the planning problem is instead solved using the uniform approximation of the free space $\mathcal{X}_{\text{rect}}$, which results in worst-case performance equivalent to that of the underlying SBMP algorithm. More details on the performance of the proposed informed sampling strategy are found in Paper D (Section D.4), where despite the suboptimal heuristic, the informed subset achieves approximately twice the performance in the selected case studies.

6.4   COLREGs-informed sampling

The two previously described informed sampling strategies are defined for general n-dimensional systems. The informed sampling routine for minimum path deviation is suitable for various systems, especially for marine crafts, as they, more often than not, operate with predefined nominal routes. This section introduces a final informed sampling strategy, one that is tailored to marine systems, in particular to single vessel encounters in open waters, where own ship is travelling along a straight leg.

In these waters, the possible encounters between the own ship and a single target vessel are clearly described by COLREGs rules 13-15, namely: crossing, head-on and overtaking. Once the risk of collision has been deemed to exist (Section 4.2), the relevant COLREGs scenario identified (Section 4.2.3), and the t_{act} has been violated, a manoeuvre can be planned and executed. Once these three conditions are true, one can decompose the three common COLREGs scenarios into geometric no-go zones, with respect to the required manoeuvres, as shown in Figure 6.7. For the crossing and head-on scenarios, it is expected that the own ship performs a manoeuvre towards starboard, which can be expressed as avoiding a central collision zone, resulting in deviations taking place within a region shaped as a half-annulus. During overtaking scenarios, the same idea applies; however, as own ship is free to manoeuvre both towards port and starboard, the region is simply an annulus.

Half-annulus and annulus subsets provide better approximations of the sampling space, compared to the rectangular approximation $\mathcal{X}_{rect}$. Furthermore, by introducing an informed version of the set, leveraging ideas from Section 6.2, the resulting sampling strategy involves generating samples within a concentric elliptical annulus, which decreases in size as the solution improves. The two proposed sets, the annulus and the concentric elliptical annulus, are called the COLREGs-compliant subsets.

6.4.1   Uniformly sampling the annulus subset

The annulus is described by an inner radius (r_{min}) and an outer radius (r_{max}), where the objective is to uniformly generate samples within the area defined by the radial area between the two previously mentioned radii, which is achieved by applying the inversion method for non-uniform random variate generation [182, Chapter 2].

Given the following Probability Density Function (PDF)

$$f(x) \triangleq \underbrace{\frac{A_{inner}}{A_{circle}}}_{c_i} + 2\underbrace{\frac{A_{outer}}{A_{circle}}}_{c_o} x \qquad (6.19)$$

where $A_{inner} = \pi r_{min}^2$ represents the area of the inner circle, $A_{outer} = \pi \left(r_{max}^2 - r_{min}^2 \right)$ the area of annulus itself and $A_{circle} = \pi r_{max}^2$ the area covered by the outer circle. By integrating Equation 6.19, the following Cumulative Distribution Function (CDF) is obtained,

$$F(x) \triangleq c_i x + c_o x^2. \qquad (6.20)$$

The inverse CDF is obtained by solving $F \left(F^{-1} \left(u \right) \right) = u$ for $F^{-1}(u)$, where $u \sim \mathcal{U}(0, 1)$ represents a realisation of the uniform distribution. Substituting all parame-

ters for $F^{-1}(u)$ yields the following expression,

$$F^{-1}(u) = \frac{-r_{\min}^2}{2\left(r_{\max}^2 - r_{\min}^2\right)} + \sqrt{\left(\frac{r_{\min}^2}{2\left(r_{\max}^2 - r_{\min}^2\right)}\right)^2 + \frac{r_{\max}^2}{r_{\max}^2 - r_{\min}^2}u}, \quad (6.21)$$

which is used to generate a radius

$$r = r_{\min} + F^{-1}(u)(r_{\max} - r_{\min}), \quad (6.22)$$

in combination with an angle $\theta \sim \mathcal{U}(0, 2\pi)$. Finally, these two values are transformed to produce uniformly distributed points in the NED plane

$$N = r\cos\theta, \quad E = r\sin\theta. \quad (6.23)$$

The generated samples can be limited to the half annulus by reducing the range of $\theta \sim \mathcal{U}(0, 2\pi)$ accordingly.

6.4.2   Uniformly sampling the concentric elliptical annulus subset

As with the annulus, it is desirable and possible to generate uniformly random samples within the concentric elliptical annulus. Limiting the sampling effort to parts of the concentric elliptical annulus, an informed sampling strategy similar to Section 6.2 is obtained, which directly only considers the COLREGs-compliant subset.

The maximum radius of the ellipse depends on the angle, therefore $r_{\max}$ becomes angle dependent, $r_{\max}(\theta)$, namely

$$r_{\max}(\theta) = \frac{ab}{\sqrt{(b\cos\theta)^2 + (a\sin\theta)^2}} \quad (6.24)$$

where $a = \frac{1}{2}c_{\text{best}}$ is the major semiaxis and $b = \frac{1}{2}\sqrt{c_{\text{best}}^2 - c_{\min}^2}$ the minor semiaxis, respectively.

To ensure uniformity, samples should be generated with greater likelihood at points where the difference between the inner and outer radii is greatest, that is, $r_{\max}(\theta) - r_{\min}$. The resulting PDF for this expression is given by

$$f(\theta)d\theta = \frac{dA}{A} \quad (6.25)$$

with dA corresponding to the differential area with respect to $d\theta$,

$$dA = \frac{1}{2}\left(r_{\max}^2(\theta) - r_{\min}^2\right)d\theta, \quad (6.26)$$

and A describes the entire area of the concentric elliptical annulus,

$$A = \pi(ab - r_{\min}^2). \quad (6.27)$$

By combining Equation 6.24 with Equation 6.25, the following PDF is obtained, for the random variable θ,

$$f(\theta)d\theta = \frac{1}{2A}\left(\frac{(ab)^2}{(b\cos\theta)^2 + (a\sin\theta)^2} - r_{\min}^2\right)d\theta. \tag{6.28}$$

When integrating with respect to θ, the resulting CDF becomes

$$F(\theta) = \frac{ab\tan^{-1}\left(\frac{a\tan\theta}{b}\right) - \theta r_{\min}^2}{2A}. \tag{6.29}$$

Due to the structure of

$$\frac{ab\tan^{-1}\left(\frac{a\tan\theta}{b}\right) - \theta r_{\min}^2}{2A} = u, \tag{6.30}$$

calculating the inverse CDF is infeasible, as there is no exact solution. Instead, a numerical approximation, in this case Newton-Raphson,

$$\theta_{k+1} = \theta_k + \frac{f(\theta_k)}{f'(\theta_k)} \tag{6.31}$$

where

$$f(\theta_k) = \frac{ab\tan^{-1}\left(\frac{a\tan\theta_k}{b}\right) - \theta_k r_{\min}^2}{2A} - u \tag{6.32}$$

$$f'(\theta_k) = \frac{1}{2A}\left(\frac{(ab)^2}{(b\cos\theta_k)^2 + (a\sin\theta_k)^2} - r_{\min}^2\right). \tag{6.33}$$

is used to generate an approximate value of θ given a realisation of the uniform random variable $u \sim \mathcal{U}\left(0, 0.24\bar{9}\right)$. The closed interval $\left[0, 0.24\bar{9}\right]$ is selected due to a singularity in $\tan(\cdot)$ at $\pm\pi/2$. Once a value for the angle θ is obtained, the radius and subsequent points in NED are generated as in Equations 6.22 and 6.23, respectively.

As with the prior informed strategies, it may not be immediately favourable to sample using the informed subset. Therefore, the area of the annulus compared to the concentric elliptical annulus must be evaluated to ensure optimal switching. Since the relative area of both shapes is the same with or without considering them as annuli, one can simply compare the following ratio

$$\frac{A_e}{A_c} < 1 \Leftrightarrow c_{\text{best}}\sqrt{c_{\text{best}}^2 - c_{\min}^2} < r_{\max}^2. \tag{6.34}$$

where A_e and A_c describe the area of an ellipse and a circle, respectively.

Figure 6.8 demonstrates the COLREGs-informed sampling strategy, which solves a crossing scenario simply by seeking deviations within the space of starboard manoeuvres. Detailed performance information can be found in Paper A (Section A.5), where the proposed COLREGs-informed sampling routine significantly outperforms the baseline, which is a rectangular approximation and the original informed strategy by Gammell *et al.* [130].
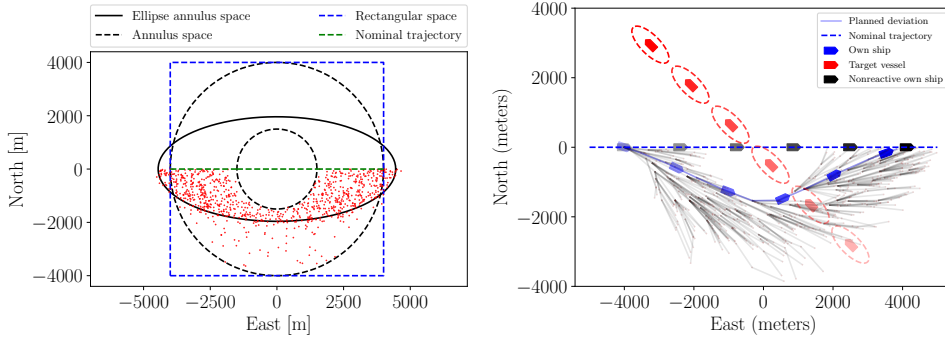
(a) Comparison between the different sampling approximations.

(b) Solving a crossing scenario using the COLREGs-informed subset.

Figure 6.8: The COLREGs-informed sampling routine is visualised in Figure 6.8a, where samples are initially generated within the lower annulus, before switching to sampling within the lower concentric half-elliptical annulus, once a feasible path has been found. Figure 6.8b details the resulting graph and path deviation for dealing with a crossing scenario.

6.5   Discussion

This chapter presented two novel informed sampling strategies, both of which adaptively reduce the search space as the current best found solution improves. By confining the sampling space to smaller regions, the probability increases that newly formed edges will improve the solution cost. The performance can be further improved by leveraging the smaller sampling space in order to prune the edges and nodes that fall outside it, in order to decrease the computational time associated with the nearest neighbour searches. Tree pruning is demonstrated in several state-of-the-art SBMP algorithms [117], [130], [138].

As demonstrated in both Chapter 5 and this chapter, using SBMP is viable to solve collision avoidance problems, especially for systems such as marine crafts, by introducing relevant cost functions and sampling strategies.

Combining the previously defined performance metric for minimum path deviation, together with the proposed informed set that consists of the union of several informed subsets, allows for a tight and rapid convergence to the predefined nominal path, and thereby satisfies the requirements posed by the collision avoidance problem. Compared to simply generating paths using the rectangular approximation, informed sampling routines ensure increased performance and solution quality for the same amount of sampling effort. This is important to make sure that once the search is stopped, either after a fixed time or number of samples, the resulting path deviation resembles the optimal one as much as possible.

The proposed informed sampling routine for minimal path deviation is demonstrated using a suboptimal heuristic for the Lebesgue measure. Despite this, the performance increase still amounts to approximately twice that of the rectangular approximation. By providing a better estimate of $\hat{C}$, the sampling strategy is expected to further outperform the baseline.

The COLREGs-informed sampling strategy significantly reduces the search space for a very specific SBMP problem, namely for marine crafts subject to single-vessel encounters. The strategy effectively limits the search to only concern starboard deviations for rules 13 & 14, increasing the rate of convergence.

Selecting the placements and size of the original annulus proves rather challenging for larger CPA values, as one needs to ensure that the annulus is placed along the nominal trajectory of its own ship, whilst ensuring that the point of CPA for both vessels is included in the restricted zone, that is, the zone containing the risk of collision. For use in practise, a robust method for selecting the geometric centres should be developed. During open water conditions, it is typically assumed that the target vessel maintains a constant course and speed, as there is no immediate incentive to deviate. Therefore, one could further argue that for such a simple case, where there are no draught restrictions or other complex constraints, using SBMP to solve these single-vessel encounters might be overkill. Once the placement and inner geometries of the annulus are identified, the problem could instead be solved geometrically by inserting an additional waypoint, such as in [166].

Importantly, both proposed informed sampling strategies are activated once they are favourable. This means that for complicated planning problems, if the given informed strategy does not activate, the overall performance is never worse than that of the SBMP algorithm itself, which is already limited by the default rectangular approximation. Therefore, there is no significant computational disadvantage in including one of the informed sampling strategies within a given collision avoidance framework.

Chapter 7

Encoding navigator behaviour and best practises

Operating a vessel within both the regulatory and cultural frameworks sees the requirement of *good seamanship*, and that one's navigational practises adhere to those required by *ordinary practises of seamen* [160]. This is important because autonomous operation must coexist with human navigators in a world where there is no favourable treatment for the autonomous vessel. Autonomous systems are expected to act as a human would, in order to ensure consistent adherence to the safe navigational frameworks.

One could argue that the element of good seamanship comes into play once the risk of collision is imminent, as this may require the vessel, whether autonomous or not, to deviate from its nominal operation. Therefore, it is vital to include elements of predictability and human-like actions in the deviation proposed by automated collision and grounding avoidance schemes, so that the vessel acts according to the expectations of human navigators, local culture, and regulations.

This chapter presents the primary contributions from Paper B and Paper E, where recorded AIS information is leveraged to encode past experiences of human navigators, so that the collision and grounding avoidance behaviours of the autonomous vessel generate route deviations that reflect this. The past experiences were represented in both cases using various techniques within multivariate Kernel Density Estimation (KDE).

In Chapter 5, grounding avoidance was taken into account by eroding and dilating the contours from the ENC according to some desired safety distance, allowing the charts to be modelled as constraints to serve as binary collision checks. For scenarios without a nominal route, this means that the calculated deviations can come arbitrarily close to the safety margins. To prevent this, Paper B presented a

data-driven objective function that describes regions of the state space where vessels of similar sizes and types typically operate. This allows the collision and grounding avoidance framework to penalise route deviations that fall outside the space of past behaviours.

Paper E also uses past experiences to form a data-driven sampling strategy, which directly generates feasible samples within the constraints posed by the problem and historical data. Using the ENC information together with the historical data, the presented sampling strategy is capable of generating uniform and rejection-less samples, in the vicinity of the historical data, of arbitrarily shaped non-convex polygons.

All KDEs within the thesis, Paper B and Paper E were computed using the Python toolbox KDEpy [183].

7.1   Collecting and processing past navigational experiences

When humans gain experience and knowledge, it is often based on previous experiences or the actions demonstrated by others. Junior navigators and other trainees gain a lot of their knowledge by learning practical lessons from experienced navigators. In modern times, many of these demonstrated actions are recorded by local AIS stations, set out to monitor the world's fleets. AIS is used as a navigational aid by many vessels, especially larger ones, as it is mandatory, as it transmits static and dynamic information, which plays a vital role in both manual and automatic collision and grounding avoidance [163].

The static information includes the Maritime Mobile Service Identity (MMSI), the IMO number, the length and beam of the vessel, the type of vessel, and the location of the antenna. The location of the antenna is used to correctly visualise the dimensions the of vessel, with respect to the broadcasted location, within the ECDIS system. All static information is setup during installation and therefore remains the same for all voyages unless the vessel is physically altered. The dynamic information provides time stamped values for latitude, longitude, heading, Course over Ground (COG), Speed over Ground (SOG), Rate of Turn (ROT), and navigational status. The navigational status can be used to signal whether or not the given craft is underway, at anchor, restricted in manoeuvrability (COLREGs rule 9) etc. The dynamic information is generated and broadcast automatically based on the sensory equipment onboard the given vessel. Finally, AIS is also capable of transmitting voyage specific information, such as draught, cargo type, and port of call.

As was evident in Chapter 4, the information contained in AIS is a crucial aid to determine both the risk of collision and which COLREGs rule applies to a given

situation.

There exist various services that record and make historical data available. In Denmark, the Danish Maritime Authority has made the recorded AIS available for free, every day, since 2006. As much of this data is recorded within the confined and inner coastal waters of Denmark, it is bound to contain many complex patterns and behavioural trends. These data can be used to find paths in local waters of a similar nature to those executed by local sailors, as past experiences within the AIS data encode safe, human, "average", and predictable behaviour.

Based on the available Danish AIS data for some chosen time period, a historical database $\mathcal{A}$ is constructed, where each element represents an individually recorded AIS message. The messages within the database contain the previously described information; however, only a subset of the entries are desired. Therefore, a reduced message m_i, is given by

$$\mathrm{m}_i = \begin{bmatrix} \mathrm{MMSI}_i & t_i & \mathrm{SOG}_i & D_i & \lambda_i & \phi_i \end{bmatrix} \tag{7.1}$$

with the vessel MMSI, timestamp, SOG, draught, latitude, and longitude.

As $\mathcal{A}$ represent historical data for all Danish waters, a subset limited to a specific geographical region $\mathcal{R}$ is extracted,

$$\mathcal{R} = \{(\lambda_i, \phi_i) \mid \lambda_{\min} \leq \lambda_i \leq \lambda_{\max} \wedge \phi_{\min} \leq \phi_i \leq \phi_{\max}\} \tag{7.2}$$

bounded by minimum and maximum values for latitude and longitude. The data set can be further limited by removing messages from stationary vessels and search and rescue helicopters, as these do not represent the navigational behaviour of the vessels. The desired SOG range is described by

$$\mathcal{V} = \{\mathrm{SOG}_i \mid \mathrm{SOG}_{\min} < \mathrm{SOG}_i < \mathrm{SOG}_{\max}\}. \tag{7.3}$$

In addition, the data can be reduced according to the vessel length, type, draught, etc. In this chapter, it is desired to compare the behaviours of the vessel confined to certain depth contours. This is achieved by only selecting messages where the draught is greater than or equal to some draught $\bar{D}$.

Reducing $\mathcal{A}$ according to the three aforementioned criteria results in the reduced subset of AIS messages $\bar{\mathcal{A}}$,

$$\bar{\mathcal{A}} \triangleq \{\mathrm{m}_i \in \mathcal{A} \mid (\lambda_i, \phi_i) \in \mathcal{R} \wedge \mathrm{SOG}_i \in \mathcal{V} \wedge D_i \geq \bar{D}\}. \tag{7.4}$$

When the data set is reduced from $\mathcal{A}$ to $\bar{\mathcal{A}}$, unless otherwise stated, the geodetic coordinates are transformed into NED.

7.2   Quantifying navigational behaviour and best practise

Given the vast amounts of historical information, the next step involves quantifying the behaviour found within the data and generating a suitable representation. For motion planning applications, these experiences could be modelled as objective functions or as heuristics to guide the search for solutions.

7.2.1   Multivariate kernel density estimation

A prime candidate for describing the average, or most likely, behaviour of prior navigators is using multivariate KDE, which is a nonparametric method for estimating an unknown PDF that represents the distribution of the historical data. It is assumed that the historical data contain realisations of the true underlying p-variate distribution $f(\mathrm{x})$.

Let $X = \{\mathrm{x}_i \in \mathbb{R}^p \,|\, \mathrm{x}_i \sim f,\, i = 1, \ldots, n\}$ be some p-dimensional data set with n realisations, then the p-variate KDE is given by [184]

$$\hat{f}_X(\mathrm{x}, \mathrm{H}) = \frac{1}{n} \sum_{i=1}^{n} |\mathrm{H}|^{-1/2} K(\mathrm{H}^{-1/2}(\mathrm{x} - \mathrm{x}_i)) \tag{7.5}$$

with the i-th element $\mathrm{x}_i = [x_{i1}, x_{i2}, \ldots, x_{ip}]^T \in X$ from the data set containing realisations from $f(\mathrm{x})$, an arbitrary element $\mathrm{x} = [x_1, x_2, \ldots, x_p]^T \in \mathbb{R}^p$, the chosen $p \times p$ bandwidth matrix with $\mathrm{H} = \mathrm{H}^T > 0$, and kernel function $K(\cdot)$. For the remaining chapter, the subscript for the KDE represents the data set on which it was computed, i.e. $\hat{f}_X(\mathrm{x}, \mathrm{H})$ was computed based on historical data X.

For large data sets, the impact of selecting a given kernel decreases, compared to the importance of choosing a suitable bandwidth matrix, as it determines the amount and direction of the resulting kernel smoothing [185, Section 6.2.3]. For certain dimensions and underlying distributions of the data, rule-based selection of the optimal bandwidth is possible. For one-dimensional data with unimodal or normal features, the application of Silverman's or Scott's rule can be utilised to find the bandwidth [186]. If the one-dimensional data has multiple modes then the ISJ (Improved Sheather-Jones) algorithm is capable of computing the optimal bandwidth [187].

Such rule-based bandwidth selectors are not applicable to multivariate KDEs. Either one must manually tune the bandwidth matrix or utilise a data-driven approach to calculate both the optimal kernel function and the bandwidth matrix [184], [188], [189]. For p dimensions, there are $p(p+1)/2$ bandwidth parameters to freely select. However, bandwidth selection is typically restricted to a single bandwidth parameter, or to a selection of parameters along the diagonal, that is, $\mathrm{H} = h^2 \mathrm{I}_p$ with $h > 0$ or $\mathrm{H} = \mathrm{diag}\{h_1^2, h_2^2 \ldots, h_p^2\}$ with $h_i > 0$, where I_p is the p-dimensional identity matrix.

(a) AIS data plotted on the depth contours.

(b) KDE based on $\bar{\mathcal{A}}$ for $\bar{D} \geq 3$m.

(c) KDE based on $\bar{\mathcal{A}}$ for $\bar{D} \geq 6$m.

(d) KDE based on $\bar{\mathcal{A}}$ for $\bar{D} \geq 9$m.
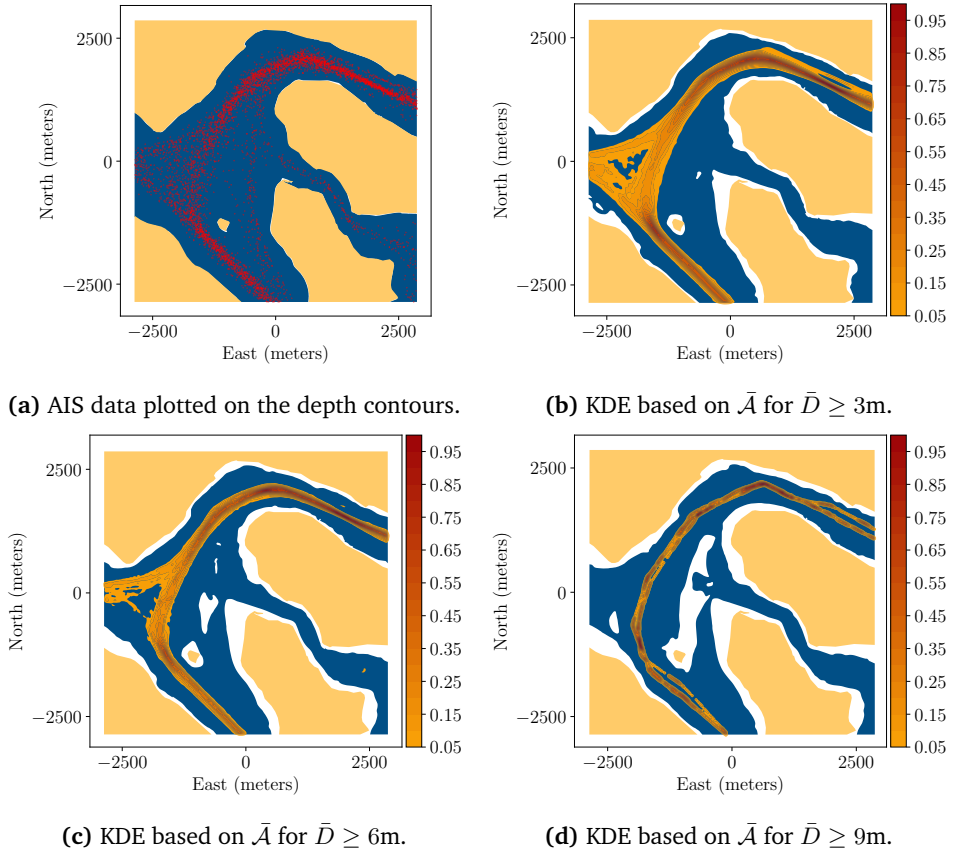
Figure 7.1: Resulting PDFs from computing the KDEs based on historical AIS data. The geographical area, or the region of interest, $\mathcal{R} = \{(\lambda_i, \phi_i) \mid 55.48° \leq \lambda_i \leq 55.53° \wedge 9.64° \leq \phi_i \leq 9.72°\}$, and the speeds $\mathcal{V} = \{\text{SOG}_i \mid 0.5\text{kn} < \text{SOG}_i < 50\text{kn}\}$, from the Danish Little Belt area. As the required draught increases, the area of the feasible contours shrinks.

7.2.2 AIS-based KDEs according to vessel draught

In general, there is expected to be a correlation between the draught of a given vessel and the feasible depths from within the ENC it traverses, since the vessel will only be able to navigate safely within depths that are equal to or deeper than its draught. For confined waters, it is interesting to investigate the actual traversed areas by certain sizes of vessels, to estimate the typical safe navigational behaviours across different water depths. By generating various instances of the reduced AIS data set $\bar{\mathcal{A}}$ (Equation 7.4) based on increasing values of the draught, namely $\bar{D} \geq 3$, 6 and 9 metres, three different KDEs were obtained. The multivariate normal kernel function, together with a hand-tuned bandwidth model, $\text{H} = h^2 \text{I}_p$, was used to compute the estimates of $\hat{f}_{\bar{\mathcal{A}}}(\text{x}, \text{H})$.

Along with the corresponding feasible depth contours, for each of the draughts, Figure 7.1 visualises the respective KDE, where dark blue areas are waters deeper than the feasible depths, white and yellow indicating shallow waters and land masses, respectively. As the draught of the vessels increases, the amount of feasible water depth decreases. Interestingly enough, even when visualising the raw data (Figure 7.1a) compared to the smallest draught of 3m (Figure 7.1b), the vast majority of traffic travels west around the most central island. This indicates that there is a passage of deeper waters; which is confirmed by further restricting the draught to 6 and 9 metres, in Figures 7.1c and 7.1d respectively. It is also evident that the vessel travels as close to the middle of the feasible contours as possible, in order to ensure safe distances toward shallow waters on either side of the craft. Both of these behaviours indicate that there is valuable experience available within the historical data that the autonomous system could leverage to act as the surrounding vessels would expect it to.

7.2.3   Data-driven behaviour performance metric

A simple way to directly use the KDE within the collision and grounding avoidance framework is to include it as an additional cost term in the objective function.

In its current form, evaluating points or samples, within the KDE calculated by Equation 7.5, yields the density value in the given region. Since the proposed SBMP tries to minimise a given cost, complementary KDE values are instead computed,

$$\bar{F}(\mathrm{x}) = 1 - \frac{\hat{f}(\mathrm{x}, \mathrm{H})}{\max\left(\hat{f}(\mathrm{X}, \mathrm{H})\right)} \tag{7.6}$$

where the calculated KDE is first normalised by the maximum value of the data set, before subtracting it from 1. This is to penalise deviations from high densities, essentially creating a cost valley towards dense regions of the KDE. Figure 7.1 can instead be interpreted as having the lowest cost at the highest densities.

An objective function corresponding to a "good seamanship" metric, evaluated for some candidate path deviation σ of length m is given by

$$c_g(\sigma) = \sum_{i=1}^{m-1} \bar{F}(\mathrm{x}_i), \quad \forall \mathrm{x}_i \in \sigma. \tag{7.7}$$

For a more impactful evaluation, one should interpolate σ to ensure that the deviation is considered in its entirety, rather than just the waypoints ($\mathrm{x}_i \in \sigma$). The objective function proposed in Equation 7.7 is highly suitable for cases where no nominal route encodes safe conditions. It should therefore be used in conjunction with the
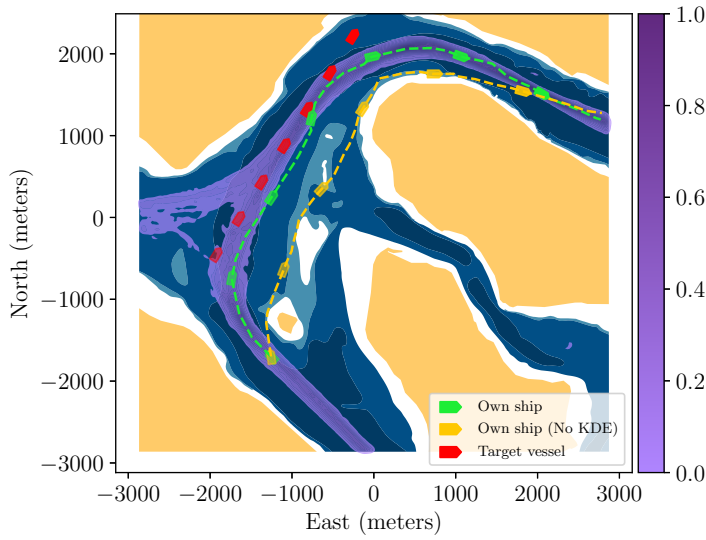
Figure 7.2: Application of the computed KDE as an objective function for "good seamanship", as it penalises manoeuvres that lie outside the space of typical deviations. An overtaking encounter is unfolding, where own ship is overtaking within the waters around Skærbæk, Fænø and Middelfart, in the Little Belt area in Denmark. The scenario compares the proposed objective function from Equation 7.8, with simply minimises with respect to $c_l(\sigma)$.

desire for minimal path length, in order to trade off between performance and safety,

$$c(\sigma) = w_1 c_g(\sigma) + w_2 c_l(\sigma) \tag{7.8}$$

with scalar weights w_i, the "good seamanship" metric $c_g(\sigma)$, and the evaluation of the path length $c_l(\sigma)$.

Figure 7.2 demonstrates the application of the objective function proposed in Equation 7.8. Here, an optimal path between some starting state and a desired end state is computed. By simply planning according to the path length, using the contour descriptions as constraints, the resulting path lies unnecessarily close to the safety margins of the contours. By instead taking into account the past behaviours from the area, a more human navigator-like path maintains an adequate distance from shallow waters and only approaches the safety limit when yielding for the target vessel. The highest densities of the KDE are equal to the lowest cost.

7.3 Sampling strategy leveraging past navigational experiences

This section describes a sampling strategy that takes advantage of the KDE descriptions of past navigational experiences, to generate feasible samples that are
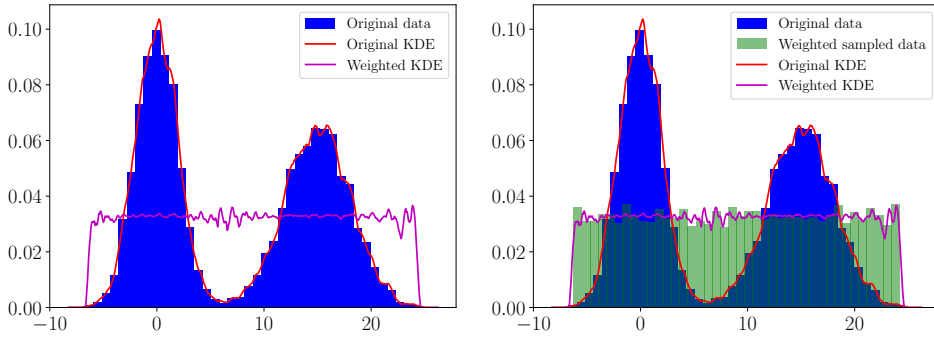
(a) Comparison between the two KDEs.   **(b)** Approximate uniform sample generation.

Figure 7.3: Generating samples from the weighted KDE to uniformly sample the domain.

guaranteed to fall within the safety margins imposed by the contours.

7.3.1   Approximately uniformly sampling a KDE

Since the generated KDEs represents a nonparametric estimate of the underlying PDF, one can not simply perform inverse transform sampling as one typically would. As the calculated KDE $\hat{f}_X(x, H)$ is composed of a collection (or mixture) of the selected kernel function $K(\cdot)$ with parameters H, at each of the data points in X, one can instead regenerate the underlying distribution by uniformly sampling the data set X and applying the kernel function.

Given the data set $X = \{x_1, x_2, \ldots, x_n\}$ consisting of n values, used to generate the estimated PDF, create a list $\mathcal{K} = \{k_1, k_2, \ldots, k_m\}$ of m indices, uniformly sampled from the discrete uniform distribution $\mathcal{U}_d(1, n)$. A sample s_k is then generated by biasing each of the k-th samples from X

$$s_k = x_k + t_k, \quad \forall k \in \mathcal{K} \tag{7.9}$$

by t_k, which is generated from the kernel function $K(\cdot)$ with the bandwidth parameter H [185], [190]. This corresponds to biasing the kernel sample by some mean value. For the Gaussian kernel, t_k is a realization of a Gaussian distribution with 0 mean and variance H, this amount to s_k is also being a Gaussian random variable, but instead with mean x_k and variance H.

Using Equation 7.9 to generate samples will, as the number of samples tends to infinity, regenerate the estimated distribution $\hat{f}_X(x, H)$. For motion planning applications, it is instead desired to uniformly sample the domain described by the KDE, as uniform exploration of the free space is the typical objective of SBMPs, in order to find feasible and eventually optimal solutions.

By instead creating the set of indices $\mathcal{K}$ weighted by the reciprocal of the densities, the generated samples will approximately uniformly represent the domain of the data set X, as the number of samples tends towards infinity. The density for each data point x_i within the set X is extracted

$$\omega_i = \hat{f}_X(\mathrm{x}_i, \mathrm{H}), \quad \forall \mathrm{x}_i \in X \tag{7.10}$$

forming $\mathcal{W} = \{\omega_1, \omega_2, \ldots, \omega_n\}$, reselecting the indices $k_i \in \mathcal{K}$ weighted by the reciprocal of the corresponding weights $\omega_i \in \mathcal{W}$, results in a selection of data points that eventually will approximately uniformly cover the domain described by X, as captured by $\hat{f}_X(\mathrm{x}, \mathrm{H})$.

A toy example is visualised in Figure 7.3, where a KDE is calculated for the original data (blue histogram), by extracting the weights $\mathcal{W}$ and computing a weighted KDE one can visualise the resulting uniform sampling of the KDE domain. Figure 7.3b approximately uniformly generates samples that cover the domain described by the original KDE.

7.3.2 Guaranteed rejection-less sampling of past experiences

The following section details the generation a KDE, which, when sampled using the method described in Section 7.3.1, is capable of generating samples that are guaranteed to be present within the free space, meaning that they are feasible with respect to environmental constraints. Paper E presents a theorem and a formal proof to generate the proposed guaranteed rejection-less sampling strategy, presented for general n-dimensional systems. This section formulates the strategy in terms of the SBMP for marine crafts and instead emphasises the application.

Consider a collection of AIS data $\bar{\mathcal{A}}$ for $\mathcal{X} \subseteq \mathbb{R}^2$, reduced according to the geographic region of interest, and containing only the coordinates of the ships with draughts greater than or equal to that of own ship. The initial set of infeasible depth contours for the vessels contained within the data set is described by $\mathcal{X}_{\mathrm{obs},0}^{\mathrm{ENC}}$ (as defined previously in Equation 5.3). The nominal free space given the initial constraints of the problem is given by

$$\mathcal{X}_{\mathrm{free}}^0 = \left\{ \mathrm{x} \in \mathcal{X} \,|\, \bar{\mathcal{A}}(\mathrm{x}) \cap \mathcal{X}_{\mathrm{obs},0}^{\mathrm{ENC}} = \emptyset \right\}. \tag{7.11}$$

As with the erosion and dilation procedure described in Section 5.3, safe navigation practises require maintaining a safe distance from shallow water contour lines. Therefore, the set of ENC obstacles is modified to include this safety distance, with $\mathcal{X}_{\mathrm{obs},1}^{\mathrm{ENC}}$ reflecting such.

(a) $\bar{\mathcal{A}}$ and $\mathcal{X}_{\text{free}}^0$.

(b) Safety constrained free space $\mathcal{X}_{\text{free}}^1$ and $\bar{\mathcal{A}}$.

(c) KDE, $\hat{f}_{\bar{\mathcal{A}}}(\mathrm{x}, \mathrm{H})$ based on $\bar{\mathcal{A}}$ and $\mathcal{X}_{\text{free}}^0$.

(d) Erosion and dilation of $\mathcal{X}_{\text{obs},1}^{\text{ENC}}$ based on the selected bandwidth H, to form $\mathcal{X}_{\text{obs},2}^{\text{ENC}}$, and ultimately $\mathcal{X}_{\text{free}}^2$.
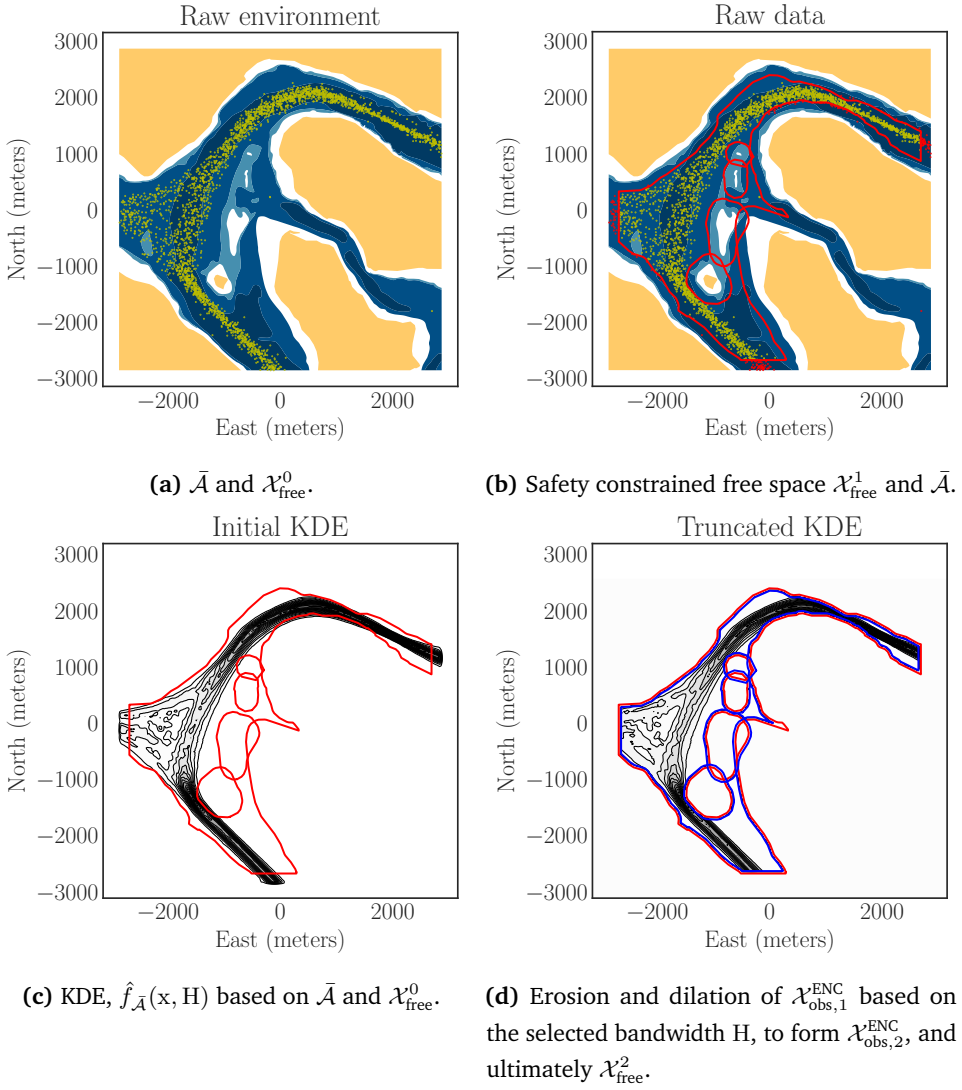
Figure 7.4: Visualising the extracted AIS data for vessels with certain draughts. Figure 7.4a displays part of the data on the corresponding feasible depth contours from the ENC, where darker blues indicate deeper water. Figure 7.4b imposes the updated free space upon $\bar{\mathcal{A}}$, in order to take the desired safety margins into account. Figure 7.4c visualises the computed KDE on the nominal set of data $\bar{\mathcal{A}}$ for some chosen bandwidth H. Figure 7.4d shows the free space subject to erosion and dilation according to H, it also shows the truncation procedure of the KDE as described in Equation 7.14.

This results in a new set describing the free space, as the prior one is constrained,

$$\mathcal{X}^1_{\text{free}} = \left\{ \mathrm{x} \in \mathcal{X} \,|\, \bar{\mathcal{A}}(\mathrm{x}) \cap \mathcal{X}^{\text{ENC}}_{\text{obs},1} = \emptyset \right\} \tag{7.12}$$

meaning that $\mathcal{X}^0_{\text{free}} \cap \mathcal{X}^1_{\text{free}} \neq \emptyset$. Figure 7.4 visualises the AIS data set $\bar{\mathcal{A}}$ together with the nominal free space $\mathcal{X}^0_{\text{free}}$ and the updated free space that includes the safety margins $\mathcal{X}^1_{\text{free}}$.

The objective is now to compute a KDE that encapsulates the space of past behaviours, such that if they are resampled, they will ensure that the own ship navigates safely within the desired limits. Importantly, a finite support kernel function $K(\cdot)$ must be used, to ensure that the samples generated using Equation 7.9 remain within the free space of the planning problem. This ensures the rejection-less nature of the sampling strategy. Examples of finite support kernels include the box and Epanechnikov's kernel [185, Section 6.2.3].

Firstly, a KDE, $\hat{f}_{\bar{\mathcal{A}}}(\mathrm{x}, \mathrm{H})$, is calculated based on the data set $\bar{\mathcal{A}}$, which only considers the nominal environment $\mathcal{X}^0_{\text{free}}$, if desired, the KDE could also be computed on feasible data within the safety margins, that is, $\bar{\mathcal{A}}^1 = \bar{\mathcal{A}} \cap \mathcal{X}^1_{\text{free}}$. Figure 7.4c visualises the aforementioned KDE, computed using $\bar{\mathcal{A}}$. Based on the chosen bandwidth matrix H, the free space is further reduced to form a final set, which yields

$$\mathcal{X}^2_{\text{free}} = \left\{ \mathrm{x} \in \mathcal{X} \,|\, \bar{\mathcal{A}}(\mathrm{x}) \cap \mathcal{X}^{\text{ENC}}_{\text{obs},2} = \emptyset \right\} \tag{7.13}$$

where $\mathcal{X}^{\text{ENC}}_{\text{obs},2}$ is the result of eroding and dilating $\mathcal{X}^{\text{ENC}}_{\text{obs},1}$ with respect to the chosen bandwidth. This means that by construction $\mathcal{X}^2_{\text{free}} \subset \mathcal{X}^1_{\text{free}}$. By reducing the historical data to only include states that fall within the free space described by Equation 7.13, $\bar{\mathcal{A}}^2 = \bar{\mathcal{A}} \cap \mathcal{X}^2_{\text{free}}$, the data set now describes the valid values within the KDE, which when sampled, will generate feasible points within $\mathcal{X}^1_{\text{free}}$.

To apply the approximate uniform sampling strategy described in Section 7.3.1, the previously calculated KDE $\hat{f}_{\bar{\mathcal{A}}}(\mathrm{x}, \mathrm{H})$ densities outside of $\mathcal{X}^2_{\text{free}}$ must be truncated and the entire KDE normalised. This ensures that the updated KDE, $\bar{f}_{\bar{\mathcal{A}}}(\mathrm{x}, \mathrm{H})$, only describes the valid regions of the free space according to the data $\bar{\mathcal{A}}^2$.

The truncation procedure occurs as follows,

$$\bar{f}_{\bar{\mathcal{A}}}(\mathrm{x}, \mathrm{H}) = \begin{cases} \hat{f}_{\bar{\mathcal{A}}}(\mathrm{x}, \mathrm{H}), & \forall \mathrm{x} \in \bar{\mathcal{A}}^2 = \bar{\mathcal{A}} \cap \mathcal{X}^2_{\text{free}} \\ 0, & \text{otherwise} \end{cases} \tag{7.14}$$

and after normalising the updated KDE is given by $\hat{f}_{\bar{\mathcal{A}}^2}(\mathrm{x}, \mathrm{H})$

$$\hat{f}_{\bar{\mathcal{A}}^2}(\mathrm{x}, \mathrm{H}) = \frac{\bar{f}_{\bar{\mathcal{A}}}(\mathrm{x}, \mathrm{H})}{\int_{\mathbb{R}^2} \bar{f}_{\bar{\mathcal{A}}}(\mathrm{s}, \mathrm{H}) \, \mathrm{d}\mathrm{s}}. \tag{7.15}$$

Extracting the densities (or weights) from $\hat{f}_{\bar{\mathcal{A}}^2}(\mathrm{x}, \mathrm{H})$ and sampling data points from $\bar{\mathcal{A}}^2$, one ensures that the generated samples fall within $\mathcal{X}^1_{\text{free}}$ in a rejection-less

(a) Sampling $\hat{f}_{\bar{A}^2}(\mathrm{x}, \mathrm{H})$ directly.

(b) Weighted sampling $\hat{f}_{\bar{A}^2}(\mathrm{x}, \mathrm{H})$.

(c) Solving a SBMP using the approximately uniform sampling strategy.
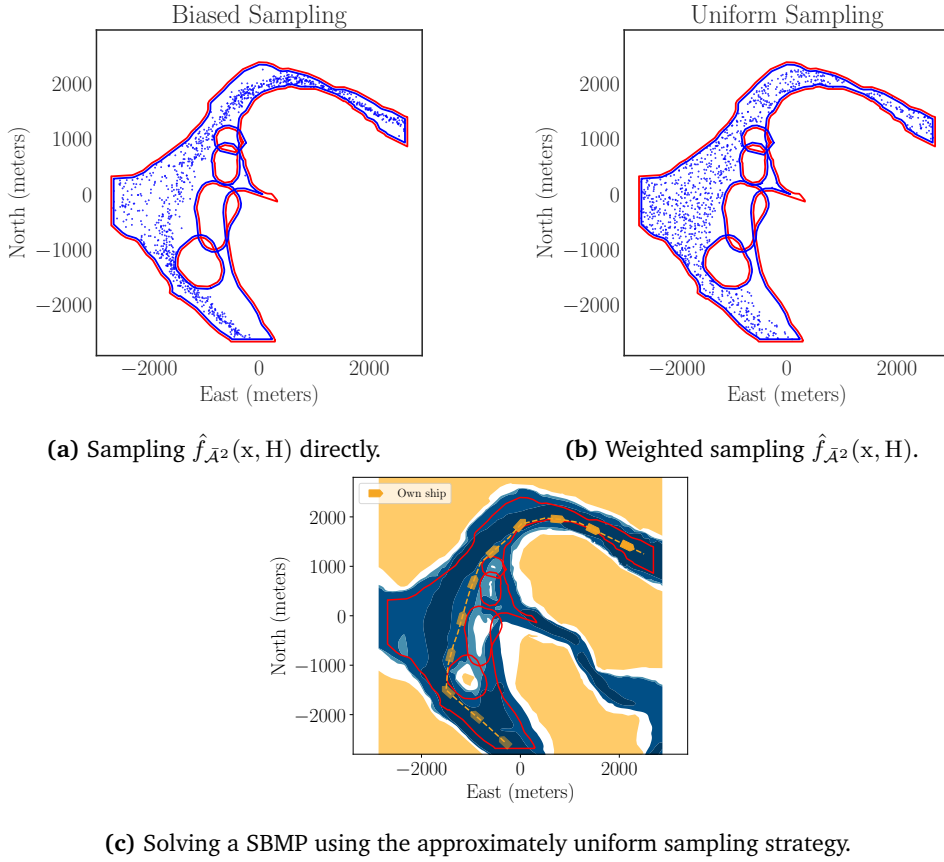
Figure 7.5: Demonstration of two different sampling strategies leveraging the computed KDE $\hat{f}_{\bar{A}^2}(\mathrm{x}, \mathrm{H})$. Figure 7.5a shows the generation of samples that are biased towards the high density areas of the underlying historical data, where Figure 7.5b visualises the computed uniformly distributed samples over the domain of $\hat{f}_{\bar{A}^2}(\mathrm{x}, \mathrm{H})$. Figure 7.5c shows the application of the approximately uniform sampling strategy for generating a safe path for own ship travelling confined waters, ensuring that it adheres towards the desired safety measures.

and approximately uniform manner. Recall that $\mathcal{X}_{\text{free}}^1$ describes the free space that accounts for the desired safety margins toward the shallow water contours (the red polygon in Figures 7.4b and 7.4c).

Figure 7.5 demonstrates the proposed rejection-less sampling strategy, both to generate samples biased toward the distribution of $\hat{f}_{\bar{A}^2}(\mathrm{x}, \mathrm{H})$, and for generating the approximately uniform coverage of the domain of $\hat{f}_{\bar{A}^2}(\mathrm{x}, \mathrm{H})$. Figure 7.5a shows the direct sampling of the KDE by uniformly selecting data points from $\bar{A}^2$, resulting in a biased sampling routine that primarily generates new samples in the vicinity of the underlying historical data. This particular sampling routine is equivalent to

the bias obtained by solving the SBMP using the behaviour-driven objective function proposed in Section 7.2.3. Figure 7.5b details the application of the weighted sampling of $\bar{\mathcal{A}}^2$ according to the reciprocal of the density values $\hat{f}_{\bar{\mathcal{A}}^2}(\mathrm{x}, \mathrm{H})$, resulting in an approximately uniform sampling of the domain represented by $\mathcal{X}^1_{\mathrm{free}}$. In Figure 7.5c, the strategy visualised in Figure 7.5b is used to efficiently solve a SBMP problem, using past behaviours to bias the search for solutions.

7.4   Discussion

The chapter presented two methods for including past behaviours and data-driven experiences from human navigators within the collision and grounding avoidance framework, through the use of recorded AIS information and multivariate KDEs.

Multivariate Kernel Density Estimation (KDE) was selected due to its low complexity for representing non-parametric distributions, as the model itself depends only on a bandwidth matrix and a kernel function. As the KDE is composed by a mixture of the chosen kernel function, generating and evaluating samples and points require very simple operations. By estimating densities, one can encode a representation of the "navigators best practises", either as an objective function or sampling strategy, for ultimately biasing the solutions towards those with human likeness. An important aspect of navigational safety is to comply with the obligations set by the regulations, e.g. COLREGs, to act predictably for humans and in ways that human-operated vessels would. By encoding the navigational behaviour as densities, a simple and concise model for the overall distribution of the data is obtained. However, the simplicity also decreases the amount of information one may be able to infer from the AIS data, where other learning-based method such as techniques from deep learning may be able to extract additional information.

The results showed that the safety margins and "average" vessel behaviours with respect to shallow waters can be extracted from local the AIS data using the multivariate KDEs. Based on the description and potential applications of "good seamanship" as described in Section 4.1.2, one could argue that there is much more to it than the results presented within this chapter. Important elements within "good seamanship" that this chapter fails to address include quantifying the best navigational practises that must be applied when two vessels interact, such as detecting when a given vessel chooses not to comply, or how to "avoid crossing ahead of the other vessel" when in a give-way scenario with unknown comfort limits. An important element that still needs to be addressed is quantifying the ability to detect "circumstances", abnormal events, and incidents, which fall outside the scope of the COLREGs, in sufficient time to be able to mitigate the prevailing risks.

The presented methods perform a very rudimentary analysis and operation on the AIS data, as they are simply sorted by draught, in order to yield positional information corresponding to certain vessel sizes. Draught was selected as an important metric as it is the main component to ensure grounding avoidance. However, assuming that the vessels determine their respective safe water depths using only the reported draught may have been a non-conservative estimate, as vessels also specify an under keel clearance for additional safety and also to account for tide variations and squat effects. Therefore, it could be beneficial to perform a more detailed and in-depth analysis of the AIS data, as it may be possible to extract additional behaviours. The data also contains additional information that could indicate certain behavioural traits, such as cargo type, port of call, navigation status, length, width, etc. It is also worth noting that depending on the selected geographical area, very few vessels can be responsible for the majority of the produced AIS information, such as local ferries and dredgers. Balancing the data based on the MMSI values could increase the generality of the extracted data. As the AIS information simply encodes past positions, with no description or indication of the respective vessels nominal route or objective at the time, the amount of information that can be inferred about collision avoidance is limited. One should instead investigate the AIS data in relation to their nominal routes, as this could allow for the generation of additional metrics relating to reaction times, deviations, abnormalities, etc.

The effectiveness of a sampling strategy, such as the one presented in this chapter, is highly dependent on the quality of the underlying data. During instances where the historical data only represents a small subset of the actual free space, for certain constraint and obstacle configurations, the feasibility of the planning problem may decrease. Therefore, to preserve the feasibility and eventually asymptotic optimality of the underlying SBMP algorithm, it is necessary to regularly sample a larger space (such as the rectangular approximation $\mathcal{X}_{\mathrm{rect}}$). This trade-off is common within data-driven or learning-based sampling strategies, as the reduced sampling region does not ensure the existence of feasible and optimal solutions [147].

This chapter investigated "good seamanship" from a grounding avoidance perspective, leaving collision avoidance mostly unexplored. Overall, there is valuable information to be extracted from historical AIS data, which ultimately can provide beneficial input to collision and grounding avoidance frameworks. By encoding the navigational cultures within the planning scheme, the resulting paths and deviations more accurately represent and exhibit behaviours expected by human navigators, which may ultimately increase safety.

Chapter 8

Autonomy for marine crafts

This chapter concerns all the developments related to the materialisation of a collision and grounding module, called the Short Horizon Planner (SHP), within a software architecture for autonomous navigation. An outline of the proposed autonomy stack is given, highlighting the various modules and core functionalities present within the system. The interconnection and sequencing of various procedures is described in order to demonstrate the logic present within the proposed system.

The resulting autonomy stack and modules are capable of acting as a decision support system or as a fully autonomous navigation system. The results in this chapter concern the development and commissioning efforts related to the autonomous harbour bus, the Greenhopper, with the primary results and experiences obtained from both high-fidelity simulation and sea trials.

The ideas, discussions, research, and developments of the technology within the autonomy stack are attributed to all ShippingLab collaborators who in some form have contributed. In particular, the general architecture and autonomous supervisor structure was proposed and discussed in [191]–[194]. Elements of the electronic outlook, such as object detection, object tracking, and water segmentation, were investigated in [195]–[202]. Advanced techniques for robust and cyber-resilient sensor fusion were presented in [203], [204]. Situation awareness and anticipating target vessel behaviour were covered in [8], [9], [166], [167], [205]. The collision and grounding avoidance module builds on the ideas and developments presented in this thesis. Primarily the content from Paper F, as it directly concerns the methods developed for the autonomous system onboard the Greenhopper.
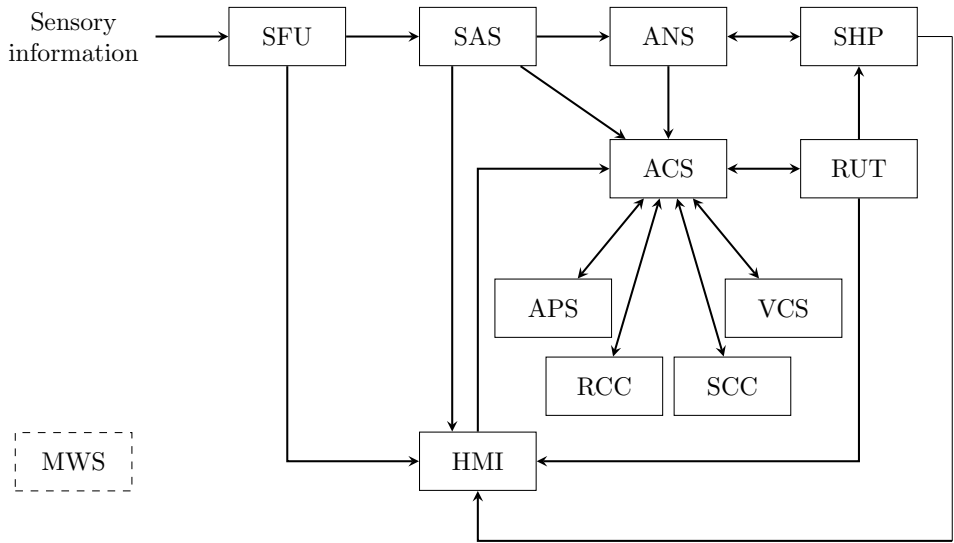
Figure 8.1: A graphical overview of all the modules present within the autonomy stack developed during the ShippingLab project. Each of the module acronyms is explained in Table 8.1. The modules communicate using a custom middleware solution with a publisher-subscriber architecture, adhering to strict interface specifications.

Table 8.1: Modules from within the autonomy stack and their acronyms.

Acronym	Module name
ACS	Autonomous Coordination Supervisor
ANS	Autonomous Navigation Supervisor
APS	Autonomous Platform Supervisor
HMI	Human-machine Interface
RCC	Remote Control Center
RUT	Route Server
SAS	Situation Awareness Service
SCC	Shore Control Center
SFU	Sensor Fusion
SHP	Short Horizon Planner
VCS	Voyage Control System
MWS	Middleware Simulator

8.1 The autonomy stack

This section presents the central elements of the ShippingLab autonomy stack. The stack contains more than 11 modules, each serving a specific computational purpose within the system. Figure 8.1 visualises the interconnection between the modules, with Table 8.1 summarising the acronyms of the modules. This section provides a description of the development process and the custom middleware solution, followed by descriptions of the central modules.

8.1.1 Development process and middleware

The backbone of the autonomy stack is a custom middleware solution, simply referred to as "the middleware", which enables publish–subscribe communication, allowing multiple modules to subscribe to a single module. Once messages are received by the subscribing modules, an immediate acknowledgement is recorded to monitor the integrity of the system. The middleware allows the various modules to be located across a network, in order to distribute load among the hardware nodes, whilst also increasing fault-tolerance. Built into the middleware are redundancies in the form of both network, module, and hardware node redundancy. The middleware is capable of automatically detecting problems with the network by actively monitoring package acknowledgements throughout the system. Each node serves its own instance of the middleware, so that should a given hardware node fail, the entire communication stack remains operational. Furthermore, the system is capable of having hot and cold instances of each module running along side the active ones. For further details on additional features of the middleware and the reasoning behind design choices, see [192]–[194].

The autonomy stack functionality is divided into separate modules, allowing concurrent development of all of the components. Through several iterations, interfaces for each module were outlined and agreed upon, in order to perform shell tests during the early stages of the development cycle. To facilitate the shell tests and general module validation, a Middleware Simulator (MWS) module was created, which is capable of imitating any node within the system. This allows single modules to be thoroughly tested according to its functional and interface specifications.

The primary use of the MWS was to either simulate vessel scenarios by imitating the sensor fusion (SFU) or by replaying recorded data from the sea trials, effectively imitating the entire sensor stack. This enabled each of the modules to reach maturity prior to performing live sea trials, as either parts or the entire system has passed the simulated and recorded data tests.

An instance of middleware is present within all the modules (solid boxes) in

Figure 8.1, the arrows denote whether the given module receives data, through a subscription, from the connecting module.

8.1.2   Electronic outlook

A fundamental component of the autonomy stack is the electronic outlook, as this replaces the core functionality exhibited by the human lookout and other bridge personnel. The responsible people onboard the vessels must gather all possible information from their perceived surroundings, using their senses and the many tools available on the bridge. A well-established description of the current perceived surroundings is crucial for performing adequate situation awareness, risk assessment, application of the COLREGs and similar analyses.

As such, the electronic outlook consolidates all perceived information and provides it to the Sensor Fusion (SFU) module. More specifically, the SFU is fed by information from various sources, such as a camera-based object detection scheme, W-band and X-band radars, lidars, IMU, GNSS, and AIS (additional hardware information is available in Section 1.3).

Traditionally, radars and AIS, combined with the visual outlook of navigators, are used for both open and confined water navigation. In open waters, especially for oceangoing vessels, there is limited interference on the radar and great room for manoeuvrability; therefore, relying on radar equipment to perceive the environment is typically enough for safe navigation.

Transitioning to or operating within confined and inner coastal waters is different. Here, visual aid is crucial to ensure safe and rule-compliant navigation, as it is needed to locate and identify smaller leisure crafts. Small vessels, such as sea kayaks, paddleboarders or smaller power-driven vessels, are not required to carry AIS and may due to their size go undetected by radar.

To correctly apply the given COLREGs rules, it is important to identify the type of vessel (i.e., whether it is power-driven), which is a trivial task for humans. Therefore, to replace human eyesight with the electronic outlook, it is crucial that vessels of all shapes and sizes are detected, and correctly attributed their type, to ensure adequate risk assessment and adherence to the COLREGs.

The proposed SFU module combines the perceived information from a camera-based object detection system, which, over different spectral bands, detects and classifies vessels and buoys [195]–[202], together with the information available from AIS, GNSS and radar [203], [204]. The SFU fuses all perceived information in order to create a consolidated object list of static and dynamic obstacles. In Figure 8.1, the external *sensory information* are grouped as input to the SFU module, with the sensor fusion producing outputs for both the HMI and situation awareness.

8.1.3   Situation awareness

Based on continuously updated estimates and the consolidated object list from the SFU, the Situation Awareness Service (SAS) is responsible for evaluating and reporting the current scenario (or situation) at hand. Using similar techniques as those described in Section 4.2, the SAS module both evaluates the risk of collision and determines the applicable COLREGs. The current version of the situation awareness is based upon straight-line predictions of the target vessels, i.e. the system assumes constant course and speed. Once certain CPA and TCPA values for a given vessel are violated, and the own ship has the give-way obligation, the SAS module forwards the scenario information to the Autonomous Navigation Supervisor (ANS), which serves as the virtual "navigator" [166], [167], [205]. The ANS works along with two other autonomous supervisors, which are described in the following section. The CPA and TCPA information for each target vessel within the vicinity of the own ship is visualised on the HMI, similar to a traditional ECDIS.

8.1.4   The autonomous supervisors

The central element of the autonomy stack consists of the Autonomous Coordination Supervisor (ACS), Autonomous Navigation Supervisor (ANS) and Autonomous Platform Supervisor (APS), which replace the traditional roles employed by the captain, navigator, and chief engineer, respectively [191]–[194]. By covering the functionality employed by the human counterparts, one can ensure that the autonomous system covers and maintains the same level of capabilities.

The main governor is the ACS, as it represents the core logic of the system. Not only is it responsible for accepting route deviations, either autonomously or from the HMI as a decision support tool, it also determines whether the system has reached an emergency state. The ACS is the autonomous captain, but it can at any time be overridden by a human onboard, the Remote Control Center (RCC) or the Shore Control Center (SCC). For the Greenhopper, the ACS is responsible for coordinating the departure sequences and is also responsible for maintaining the nominal route within the Route Server (RUT). The RUT always contains the fixed nominal route, with a "current" route that is continuously updated based on the calculated deviations. For voyages in which no route deviations are required, the current and nominal routes are equal. Based on continuous streams of information from the surrounding modules, the ACS performs the required decision-making. Both the ANS and APS report to the ACS, whenever a navigational decision or an assessment of the machinery is required.

The APS monitors the levels and integrity of all local machinery, relying on the
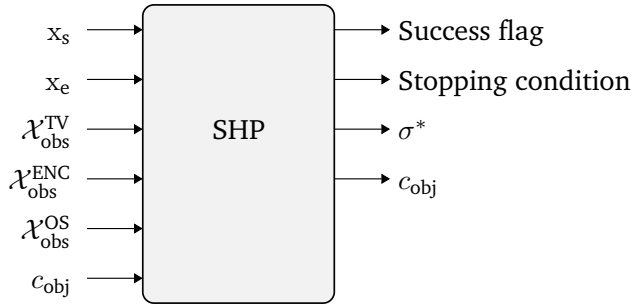
Figure 8.2: Simplified input-output relationship of the SHP module. Given information about the current scenario, i.e. target vessel, environment, and own ship information, the module then computes a deviation or crossing, if one exists, returning the optimal solution.

respective machines' own diagnostic tools to assess its health. The APS continuously reports to the ACS what the current state is such that if needed, the ACS can call for assistance from a human proxy.

As briefly mentioned in Section 8.1.3, together with the SAS module, the ANS is responsible for calling for a route deviation when needed. The ANS essentially facilitates communication between situation awareness and the route planning module (SHP), while also being responsible for reporting the planned manoeuvre to the ACS. The ANS calls for a route deviation when the risk of collision is imminent, as determined by the SAS module and the ANS itself. Furthermore, when the ACS wants to depart, the ANS is called, which queries the route planner to ensure that there is an initial feasible crossing. The ACS is also responsible for providing the planned route to the Voyage Control System (VCS), so that it can be executed.

8.1.5   Short horizon planner

The module in charge of planning the route deviations is the Short Horizon Planner (SHP). The SHP is responsible for achieving both collision and grounding avoidance, whilst ensuring that the generated paths adhere to the COLREGs. Once deemed necessary by the ANS, the scenario information is forwarded from the SAS to the SHP ($\mathcal{X}_{obs}^{TV}$), as well as the current state (x_s) and the constraints of the own ship ($\mathcal{X}_{obs}^{OS}$). As a further input, the SHP receives the nominal route from the RUT, which in the case of the Greenhopper is a single destination waypoint (x_e), but in a general sense could be a sequence of waypoints.

The SHP is designed so that the target vessel information $\mathcal{X}_{obs}^{TV}$ consists of the predicted trajectories for each of the target vessels. Since the SHP simply receives the trajectory information, the module itself is agnostic to the shape of the trajectories.

This allows the autonomy stack to be upgraded with trajectory prediction schemes other than straight lines without requiring changes in the SHP module.

For decision support applications, the SHP is invoked multiple times by the ANS, in order to produce several route suggestions, as the SHP only returns a single deviation per call. To produce different route suggestions, the ANS is able to vary the objective function (c_{obj}) or to alter the safety margins described within ($\mathcal{X}_{\text{obs}}^{\text{TV}}$) and/or ($\mathcal{X}_{\text{obs}}^{\text{ENC}}$). For autonomous operation, the SHP is simply called once, as the optimal route deviation should also be the one executed. Details regarding the SHP input-output is visualised in Figure 8.2.

Due to the selected architecture of the autonomous system, the deviations computed by the SHP are based on static information, as the SAS and ANS provide a snapshot of the current scenario at hand. The importance of considering not only computational speeds, but also stopping conditions and overall predictability of the collision and grounding avoidance scheme while operating under static conditions was previously briefly discussed in Section 5.6. These issues require further consideration, when it comes to transitioning towards practical application.

Module requirements for deployment

Until now, the collision and grounding avoidance algorithms presented in the thesis are based on ideas from sampling-based motion planning (SBMP). Despite their many strengths, there are few weaknesses when it comes to deployment in a real system.

One major concern is the predictability and lack of reproducibility of SBMP algorithms, as they are driven by random samples. When solving the same problem multiple times, SBMP algorithms only guarantee that it converges to the optimal solution in probability. Solving the same problem using a limited number of samples may unfortunately result in a large variation in the performance. For the deployment and commissioning of an autonomous system, such as a MASS, it is crucial that there is a level of consistency in the proposed solutions. As the resolution of the search space is infinitely large when using SBMP algorithms, one cannot quantify when to report or what solution will be reported. Therefore, one should instead consider trading off the continuous nature of the SBMPs in order to solve a simpler problem, which yields a suboptimal solution, but an exact solution.

By moving away from stochastic methods and reducing the problem complexity, one can instead trade-off between optimality of the solution with respect to computational speeds and the ability of report the existence of a solution. As the SHP operates on the basis of static information, it is important that the resulting route deviation is quickly calculated, to ensure its validity with respect to the scenario at

hand. Algorithms with low computational time allows the MASS to act before the validity of the deviation expires, since it can efficiently replan given new information from the SAS module, should the situation change. This also enables the system to deal with a degree of uncertainty in the perceived situations, as new deviations can be rapidly produced in response to the changes. The importance of computational time exists primarily within the confined water, as there is typically greater traffic conditions and a larger degree of uncertainty in the behaviour of others, compared to that of open waters.

For an autonomous harbour bus or ferry, such as the Greenhopper, which in some circumstances has arguably "simple" operating objectives and conditions, it is possible to tailor solutions to the given problem. For particularly collision and grounding avoidance, one can create a tailored implementation that leverages the specific problem information, rather than using methods meant for solving general problems. When the functionality of the SHP is adapted to the Greenhoppers operational conditions, greater performance and predictability is achieved.

Spatio-temporal lattice planner

To meet the desired behaviour of a deterministic and feasibility reporting algorithm in finite time, an alternative collision avoidance scheme is needed.

Leveraging ideas from both sampling-based, but also grid-based, motion planning, a spatio-temporal lattice planner is proposed. Similarly to SBMP, the lattice planner incrementally builds a directed graph of the search space; however, instead of doing so based on random samples, the planner utilises a pre-defined grid.

As with the previous planning problems introduced in Chapter 5, it is assumed that a trajectory of the moving obstacles is given, allowing the restricted or obstacle regions to be represented geometrically through time. Specifically, let $\mathcal{X} \subseteq \mathbb{R}^3$ be the state space with $\mathrm{x} \in \mathcal{X}$ and $\mathrm{x} = [E, N, t]^T$. $\mathcal{X}$ is divided into two subsets, the free space $\mathcal{X}_{\text{free}}$ and the obstacle space $\mathcal{X}_{\text{obs}}$, with $\mathcal{X}_{\text{free}} = \mathcal{X} \backslash \mathcal{X}_{\text{obs}}$. The objective is to find a sequence σ of states that minimises the cost function $c(\sigma)$, while connecting the starting state x_{s} and the end state x_{e}

$$\sigma^* = \underset{\sigma \in \Sigma}{\arg\min} \left\{ c(\sigma) \mid \sigma(0) = \mathrm{x}_{\text{s}}, \ \sigma(1) = \mathrm{x}_{\text{e}}, \ \forall s \in [0, 1], \ \sigma(s) \in \mathcal{X}_{\text{free}} \right\}. \qquad (8.1)$$

As in the general SBMP, the free space $\mathcal{X}_{\text{free}} = \mathcal{X} \backslash \mathcal{X}_{\text{obs}}$ is occupied by constraints within $\mathcal{X}_{\text{obs}}$. Importantly, all states within $\mathcal{X}_{\text{free}}$ are feasible with respect to both the system and environmental constraints. As in Section 5.2, the obstacle subset $\mathcal{X}_{\text{obs}}$ is once again formed as the union over all constraints, namely,

$$\mathcal{X}_{\text{obs}} = \mathcal{X}_{\text{obs}}^{\text{OS}} \cup \mathcal{X}_{\text{obs}}^{\text{ENC}} \cup \mathcal{X}_{\text{obs}}^{\text{TV}}, \qquad \mathcal{X}_{\text{obs}}^{\text{TV}} = \bigcup_{i=1}^{n} \mathcal{X}_{\text{TV},i}(t) \qquad (8.2)$$

with $\mathcal{X}_{\text{obs}}^{\text{OS}}$ containing states that violate own ships manoeuvring constraints, $\mathcal{X}_{\text{obs}}^{\text{ENC}}$ the grounding and buoy collision states, and finally $\mathcal{X}_{\text{obs}}^{\text{TV}}$ the target vessel constraints, which is the union of n vessels, so that all n are considered simultaneously.

The directed graph is built using a deterministic planning algorithm. As in the SBMP, the initial state x_s is equal to the position of the ownship at $t = 0$ in NED, and x_e is equal to the destination at some unknown final time $t = t_f$. Consider a predetermined grid $\mathcal{G}$ with rows G_m,

$$\mathcal{G} = [G_1, \ldots, G_m]^T \in \mathbb{R}^{m \times n}, \quad G_i = [g_{i,1} \ldots, g_{i,n}] \tag{8.3}$$

with each row representing advancement from the starting state towards the destination, and the size (or "width") of each row the available deviations for each step. Each element $g_{i,j} \in \mathcal{G}$ within the grid itself represents a potential waypoint within the deviation, and is described by a location in NED. The grid is refined in order to remove waypoints that violate environmental constraints such that when building the directed graph only feasible points are considered, resulting in the refined grid $\bar{\mathcal{G}}$, described by rows $\bar{\mathcal{G}} = [\bar{G}_1, \ldots, \bar{G}_m]^T$ and elements $\bar{g}_{i,j} \in \bar{\mathcal{G}}$ with $\forall \bar{g}_{i,j} \in \mathcal{X}_{\text{obs}}^{\text{ENC}} = 0$.

Given the updated grid $\bar{\mathcal{G}}$, the directed graph $\mathcal{T}$ is formed starting from the initial state x_s, the graph is built over $m + 1$ iterations, based on the number of rows in the grid $\bar{\mathcal{G}}$. At each iteration, the objective is to connect x_s to every position within each row of $\bar{\mathcal{G}}$, while also removing rows as the algorithm advances.

The method maintains two sets of nodes, one that contains all the current feasible parent nodes $\mathcal{C}_p = \{x_s\}$, which will always contain x_s. Another set that contains all potential child nodes $\mathcal{C}_c = \{x_e\}$, which will always contain the final state x_e. As the algorithm progresses, the two sets are modified by adding or removing grid rows that determine the edges that are to be formed,

$$\begin{aligned} &\mathcal{C}_p = \{x_s\}, \mathcal{C}_c = \{x_e, \bar{G}_k, \bar{G}_{k+1}, \ldots, \bar{G}_m\} &&\text{if } k = 1, \\ &\mathcal{C}_p = \{x_s, \bar{G}_{k-1}\}, \mathcal{C}_c = \{x_e, \bar{G}_k, \bar{G}_{k+1}, \ldots, \bar{G}_m\} &&\text{if } 1 < k < m+1, \\ &\mathcal{C}_p = \{x_s, \bar{G}_{k-1}\}, \mathcal{C}_c = \{x_e\} &&\text{if } k = m+1. \end{aligned} \tag{8.4}$$

Before connecting two given states in $\mathcal{C}_p$ and $\mathcal{C}_c$ and adding them to the graph, the resulting trajectory is evaluated, to ensure feasibility with respect to $\mathcal{X}_{\text{obs}}$.

Remark 8.1. *For certain systems and applications, it may be required to use the system dynamics to ensure the validity of the obstacles checking. This is achieved by solving a two-point boundary value problem between the child and parents states. For the Greenhopper, it is assumed that the vessel is to be stationary at its starting and end states; therefore, a more accurate trajectory is generated by forward simulating its surge dynamics. Detailed information on this approach and Greenhopper system identification is available in Paper F.*

(a) $k = 1$

(b) $k = 2$

(c) $k = 3$

(d) $k = 4$

(e) $k = 5$

(f) $k = 6$
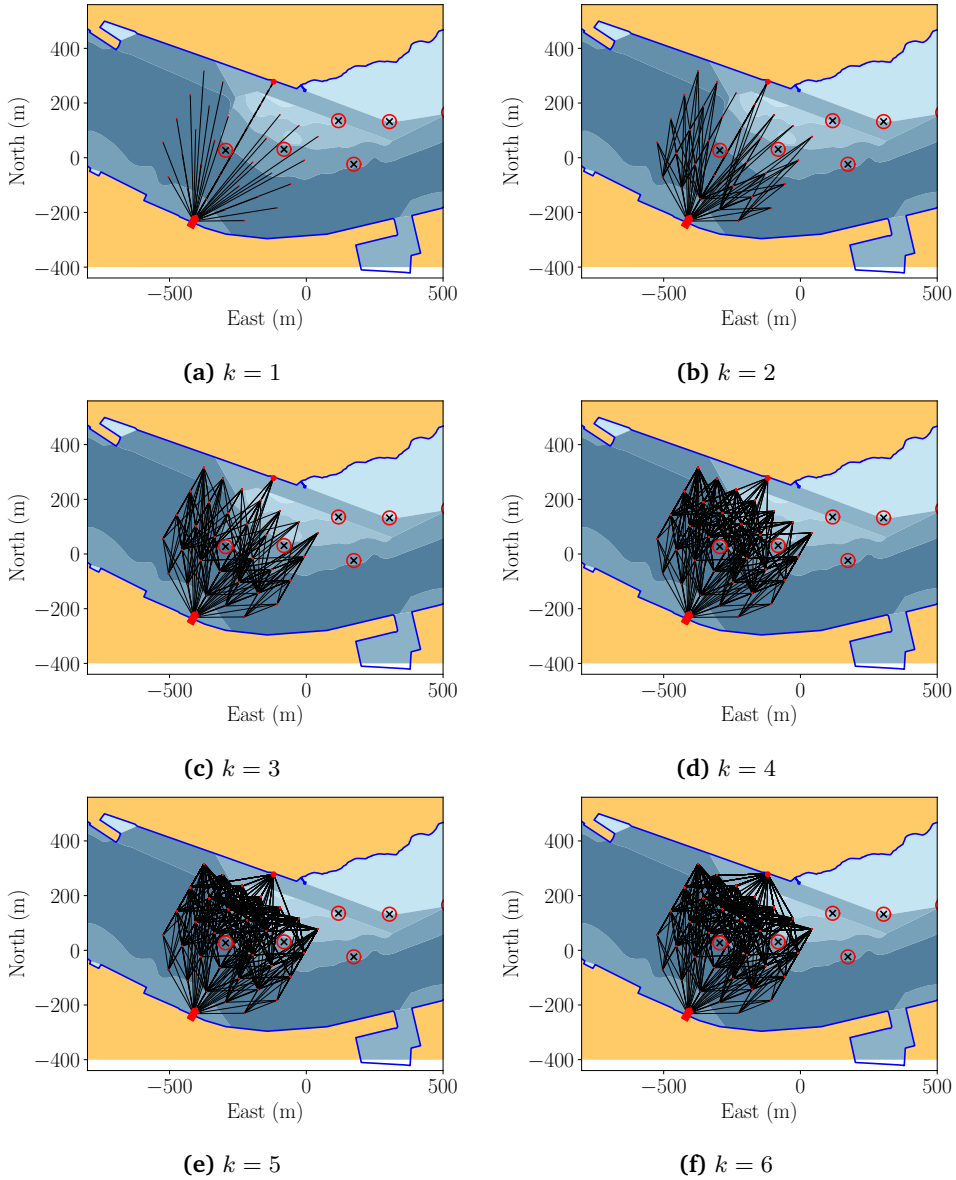
Figure 8.3: Iteratively building the directed graph $\mathcal{T}$ based on the pre-defined and processed grid $\bar{\mathcal{G}}$. States within the grid that violate obstacles constraints, in this case buoys, were removed during the preprocessing step. Each iteration, every state in the currently selected row attempts to form an edge to every other state in the remaining rows. Edges that violates the obstacles and system constraints ($\mathcal{X}_{\text{obs}}$) are disregarded. Feasible points reside within the blue polygon (land and shallow waters), excluding the interior of the red circles (buoys). Deeper waters are visualised with darker colours, however all water within the blue polygon is feasible for own ship in this example.

(a) Lattice built using a 7x5 grid. **(b)** Lattice from an arbitrary x_s.
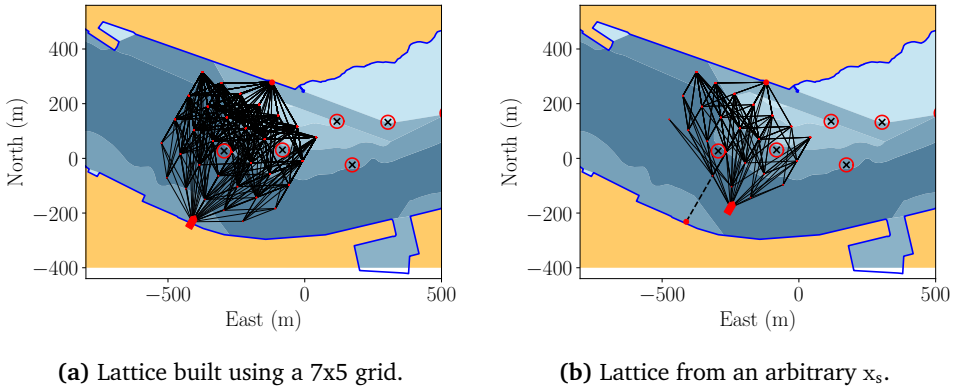
Figure 8.4: The proposed spatio-temporal lattice planner in action, where a directed of graph is generated while subject to the obstacle subset $\mathcal{X}_{\text{obs}}$. Feasible points are within the blue polygon (land and shallow waters), excluding the interior of the red circles (buoys).

Figure 8.3 visualises a step-by-step application of the proposed algorithm. In Figure 8.3a, the set of current parent nodes consists solely of the starting state, i.e., $\mathcal{C}_p = \{x_s\}$, and the set of potential child nodes contains all the states within the grid $\bar{\mathcal{G}}$ and the end state x_e. The edges are then formed between $\mathcal{C}_p$ and all states within $\mathcal{C}_c$, where feasible, to end the first iteration. In the next iteration, detailed in Figure 8.3b, all feasible states in the first row of the grid are removed from the child set and instead added to the parent set, that is, $\mathcal{C}_p = \{x_s, \bar{G}_1\}$ and $\mathcal{C}_c = \{x_e, \bar{G}_2, \ldots, \bar{G}_m\}$. Then, new edges are formed between all the parent and child nodes, further evolving the graph. This cycle repeats until only x_s and x_e are left in their respective set. A complete graph generation cycle for a grid with $m = 5$ is visualised in Figures 8.3a-8.3f.

It should be noted that the proposed planning algorithm is capable of computing paths from arbitrary starting locations, as shown in Figure 8.4b. The proposed algorithm will build a graph based on the selected grid and will then return the directed graph, as well as a list of feasible (obstacle free) edges that connect with the desired end state. Depending on the chosen objective function, a path is then returned by selecting the combination of edges that provide the minimum cost.

As grid points are discarded whenever they are infeasible with respect to the system and obstacles constraints, the overall runtime of the algorithm decreases. This means that based on a chosen grid size, the upper limit of the computational time can be precomputed or assessed based on the complexity of the problem. As the algorithm is capable of exhausting all possible combinations in finite time, the lattice-based approach is efficiently able to report if a solution exists.

(a) Departure requires immediate deviation.

(b) Shortest path to reach destination.

(c) Shortest path to reach destination in the face of a target vessel.

(d) Departure requires an immediate manoeuvre to avoid two target vessels.
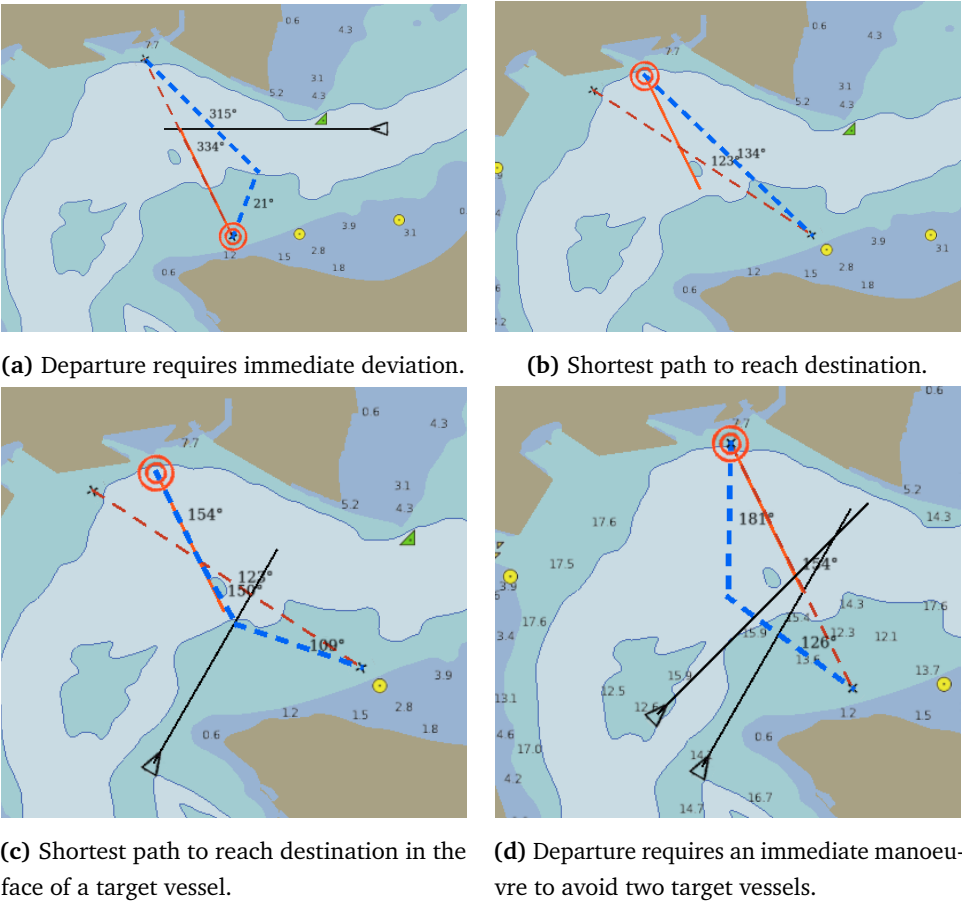
Figure 8.5: Simulation of the entire hardware stack, where the MWS mimics the sensor fusion and acts as a kinematic simulator for both own ship and the target vessels. The own ship is conducting a crossing in confined waters near the Danish Little belt. The figures feature examples of required departure manoeuvres and the initiation of the planning scheme at locations different than the initial waypoint along the nominal route. The red dashed lines indicates the nominal, and blue dashed the proposed route. The triangle symbol are target vessels detected by AIS, with their respective speed vectors.

Table 8.2: Example module interactions and sequences from within the autonomy stack.

Modules	Description
Situation awareness	SFU → {SAS, HMI} → ANS
Pre-departure	ACS → {SAS, ANS} → {SHP, RUT} → ACS
Departure	ACS → VCS
Voyage	{SAS, ANS} → {SHP, RUT} → {ACS, HMI} → VCS
Arrival	ACS → VCS

8.2   Autonomous operation and decision support

After numerous development cycles, the entire autonomy stack reached maturity to carry out software and hardware-in-the-loop testing. Each module is containerised and can be deployed on a single or multiple hardware nodes, as is supported by the middleware. This section details some of the simulation studies, where the entire system is running based on a simulated SFU, i.e. sensor fusion data. The complex interaction between the autonomous supervisors and the collision avoidance module will be described for the various departure and voyage sequences.

8.2.1   Module interconnection and sequences

As is evident from Figure 8.1, the interconnection of the autonomy stack is highly complex. However, the actual operation can be boiled down to a few modules that are continuously interacting. Table 8.2 describes the five most common sequences that are active during the nominal operation of the autonomous system.

Whenever the system is powered on, the situation awareness (SAS) remains active throughout the operation, also while docked. This is important as the SAS module maintains an overview of the surrounding vessels, which is used by the MASS as it prepares for departure.

When the MASS is ready to depart, the region surrounding the crossing or its immediate vicinity is checked for clearance, in order to depart safely. This is achieved by passing the current scenario to the SHP, such that an initial route can be computed. In some cases, there may be no traffic and the route computed by SHP is equal to the nominal one. Once the SHP reports the existence of a route, the ACS provides it to the VCS and the vessel can begin its departure. As the system relies on the response from the SHP in order to depart, its ability to report whether or not a feasible solution exists is crucial. Figure 8.5 details instances where the MASS is ready to depart, and for two of the four cases an immediate deviation is required.

Once departed, the situation awareness and ANS continuously monitor the surroundings, calling the SHP as needed to provide alternative route deviations. The SAS and ANS interactions are based on specified CPA and TCPA limits, as described previously in Section 8.1.3. When the MASS reaches it final destination, the ACS either disables the VCS or activates an auto-docking routine, depending on the given application.

8.2.2   Greenhopper - autonomous collision and grounding avoidance

The following section details simulation results for the Greenhopper, an autonomous harbour bus, from the case study presented in Section 1.3 and Figure 1.5. The

(a) t=10s

(b) t=1m40s

(c) t=2m40s

(d) t=2m47s

(e) t=4m16s

(f) t=5m58s
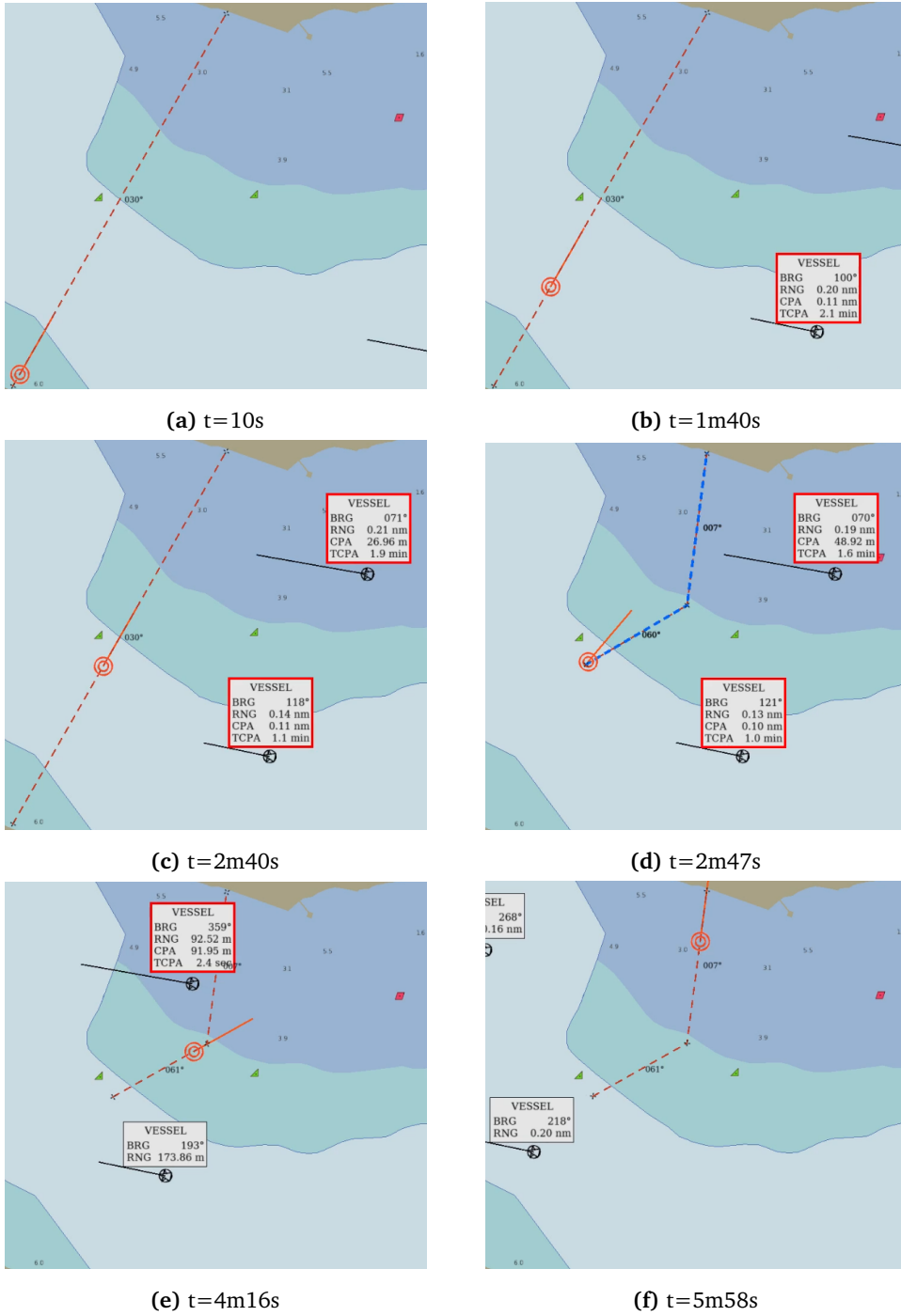
Figure 8.6: Simulated demonstration of the SHP with most of the autonomy stack, with the MWS acting as the SFU. The Greenhopper is departing the southern harbour, following the nominally planned path. A manoeuvre is required while underway, as two other vessels approach from starboard. The SHP deconflict the scenario according the COLREGs.

overall simulation results are visualised in Figure 8.6. As with the other results in this chapter, the simulations are performed using the MWS as a substitute for the SFU and as a kinematic simulator to execute the proposed routes and simulate the target vessels. The SAS and ANS are operating with CPA limit $d_{act} = 100$m and TCPA limit $t_{act} = 100$s, which are both configurable at runtime.

In this example, the Greenhopper is set to depart its southern harbour in Limfjorden, heading slightly north-east. Before departing, the ACS instructs the system to call the SHP, providing it with the information of the current scenario, in order to obtain a clear for departure. As there is no incoming traffic, the Greenhopper departs (Figure 8.6a). After a while, as the voyage takes place, two vessels approach the Greenhopper from the east (Figure 8.6b). At the time of initial observation, the one with the lowest TCPA value is not a threat, as the CPA value is greater than the selected limit. As the scenario unfolds, the Greenhopper and the second target vessel are on an apparent collision course (Figure 8.6c). Once both the TCPA and CPA values for the second target vessel are violated, the SAS and ANS then trigger the SHP for a route deviation. The collision avoidance algorithm proposes a slight deviation towards starboard, in order to correctly comply with COLREGs rule 15 (Figure 8.6d). The proposed route, indicated by the blue dashed lines in Figure 8.6d, is forwarded to the ACS, which then accepts and publishes it to the VCS. Triggering the route deviation and subsequently computing it takes place in less than a tenth of a second, so that once ACS accepts it, it can be executed immediately. The Greenhopper then follows the updated route and is able to safely deconflict the situation, before finally reaching its destination on the northern side of the Limfjorden (Figures 8.6d-8.6f).

All the visualisations in Figure 8.6 are on the HMI, where the circular symbols for the target vessels indicate detections using both AIS and radar.

8.3 Discussion

Developing, testing, and commissioning an autonomy stack for MASS is a complex task. This chapter presented the autonomy stack developed as part of the ShippingLab project, specifically demonstrated on scenarios related to the Greenhopper autonomous harbour bus. The software stack and development cycles were presented, detailing the custom middleware solution. Each module within the stack was presented with its functionality and responsibilities outlined.

The need for robust and predictable collision and grounding avoidance algorithms was discussed, as reproducibility and the ability to report feasibility is crucial, not only from a commissioning point of view but also functionally. Deterministic

and predicable behaviour is important in order to get an automated collision and grounding system approved, as its behaviour must be able to be accounted for and reasoned in any given scenario. By combining the strengths of SBMP with a deterministic search space, the proposed collision avoidance scheme is capable of efficiently computing deviations and is further able to report the existence of a solution. By construction, it is possible to determine the upper computational limit of the algorithms, as it scales by the choice and resolution of the selected grid. The proposed deterministic algorithm was implemented within the SHP and integrated into the remaining stack. Using both software and hardware in the loop testing, the SHP was demonstrated alongside most of the remaining modules. The sequencing and cooperation required for decision support and autonomous navigation, between all modules, was successfully discussed and demonstrated. The proposed planning algorithm barely scratches the surface of deterministic SBMPs, as there exists numerous other techniques in the literature [206]–[209].

The proposed collision and grounding avoidance scheme adopts the assumption that it will receive an adequate prediction of the scenario. This is because the autonomy stack essentially perceives, predicts, plans, and executes. As this is the case, the system acts based upon each prediction of the current scenario, and continuously re-plans based on how the perceived scenario changes. This requires that all modules are capable of producing their respective outputs as quickly as possible, to ensure that the execution can occur while the information is still valid.

It is worth noting that based on the proposed system architecture, each module, starting from the electronic outlook, is required to correctly perceive the situation at hand, in order to correctly apply and adhere to the COLREGs. The collision and grounding avoidance scheme solely relies on the information about target vessel locations and types as given by the situation awareness, which in turn receives it from the sensor fusion and electronic outlook. The simulation studies show that given correct classifications and predictions of the target vessel behaviours, the combined system is capable of safely navigating whilst adhering to the relevant COLREGs. Given instances where the target vessel types are incorrectly classified or their behaviour is inadequately estimated, the resulting actions proposed by the collision avoidance scheme may result in both unsafe behaviour and actions in violation of COLREGs. It is therefore crucial to further investigate the consequences of ill-performing modules within the stack, and attempt to quantify safeguards for ensuring that the perceived situation is as representative as possible. An initial step could be to leverage detection and classification uncertainties, along with the resulting uncertain trajectory predictions, to perform robust decision-making in the face of uncertain information.

Chapter 9

Conclusions and future research

9.1 Conclusions

Motivated by the potential impact of Maritime Autonomous Surface Ships (MASS) technologies on navigational safety and overall efficiency of waterborne transport, this thesis presented research conducted within the realm of informed sampling-based collision and grounding avoidance for autonomous marine crafts. Improved navigational capabilities were achieved through the primary research objectives, which concerned the development of a framework and methods capable of computing route deviations that follow the practises of safe navigation, while also adhering to the COLREGs.

A detailed description and discussion of applicable rules and practises for safe navigation were presented in the context of collision and grounding avoidance. This resulted in the development of novel ship domains for achieving partial COLREGs-compliance, with respect to rules 8 and 13-17, based on custom Lamé curves. The information and assumptions required to obtain the said adherence were discussed, where it was pointed out that the ability to determine not only the type of target vessel, but also its current manoeuvrability, was crucial to correctly apply the COL-REGs for collision avoidance. It was also pointed out that the complexities of the COLREGs are highly dependent on local and circumstantial rules, rather than a single complete set of regulations. Furthermore, the COLREGs uses the application of "good seamanship" as a catch-all clause for all situations not encapsulated by rules for a given situation. This results in additional challenges for materialising a generalised collision and grounding avoidance system, capable of taking local variations and other ambiguities into account.

Sampling-based motion planning (SBMP) proved valuable in conquering the complex nature of the COLREGs, as well as the geometries presented by navigating

within confined and inner coastal waters. Traditionally, SBMPs algorithms are used to solve path planning problems, which assume no prior knowledge of a nominal route, where the desire is to find an optimal path through an unknown environment. In contrast, the immediate objective of collision avoidance is to first avoid collision, and second, at least within the marine context, one also desires to do so with the smallest possible route deviation, as the nominal route encodes the operational safety and desired efficiency conditions. By introducing a novel objective function, it was shown that SBMP is capable of computing paths of minimum deviation from a given nominal. This is especially important for MASS, as the nominal route is carefully planned to take into account numerous safety features and other metrics related to the planned voyage. Using the feasible depth information obtained from the ENC, the proposed algorithms were able to take into account shallow waters while planning route deviations. Armed with the proposed ship domains and the ENC information, the presented SBMP framework yielded route deviations in partial compliance with the COLREGs.

Navigational behaviour and safety were further addressed by introducing data-driven methods to quantify "good seamanship". Using AIS data from inner coastal waters to estimate a probabilistic description of past behaviours enabled the SBMP framework to produce paths that mimicked behavioural traits such as those exhibited by human navigators. It was shown that the proposed objective function allows grounding-aware planning, with the resulting deviations maintaining a safer distance toward the shallow water contours, as human navigators typically would. The probabilistic descriptions were further leveraged in order to generate a custom sampling strategy capable of generating new states, guaranteed to be feasible with respect to the static obstacle conditions.

To increase the performance of SBMP algorithms, the thesis presented advanced sampling strategies capable of increasing the convergence rate, while also decreasing the cost of the solution. By triangulating the geometries described by feasible depth information from within the ENCs, a uniform non-convex sampling strategy allowed directly generating states that were feasible with respect to the manoeuvring restrictions of the vessel. Additionally, two informed sampling strategies were presented, which allowed adaptive reduction of the search space as the cost of the solution improved. One of the two spaces was specifically designed to generate samples within a subset of states that adhered to COLREGs rules 13-15. The second focused on efficiently solving the collision avoidance problem, with the informed sampling strategy honing its search to the neighbourhood around the nominal path. Both sampling strategies showed statistical improvements over their baseline counterparts, both in terms of computational speed and eventual solution cost,

underlining the effectiveness of the use of an informed subset.

During the later stages of technology development and integration of the collision and grounding avoidance scheme, the Short Horizon Planner (SHP), within the autonomy stack, some of the apparent shortcomings with using SBMP were identified. The stochastic nature of the methods, as well as its performance guarantees in probability, are most commonly well suited for problems of high complexity. However, using SBMP also results in varying degrees of solution quality for the same number of samples, as it lacks predictability due to its random sampling. Furthermore, SBMP cannot provide guarantees with respect to reporting feasibility and overall computational time. It was determined that the general functional complexity of the SHP should be reduced, to instead focus on the minimal functionality required to achieve the desired performance and characteristics. Therefore, a deterministic lattice-based algorithm was proposed to generate directed graphs describing the route deviations, which alleviated some of the previously discussed issues. The lattice is calculated on the basis of a predetermined grid, ensuring that continuously solving the same planning problem always yields the same solution. Furthermore, due to the deterministic nature of the algorithm, it is ensured that all solutions are exhausted once it has finished iterating. This allows the updated SHP to sacrifice optimality for the sake of not only reproducibility but also low computational time and guaranteed feasibility reporting within finite time.

The thesis demonstrated novel contributions within methods and algorithms for SBMP, with a specific emphasis on COLREGs-compliant collision and grounding avoidance for MASS. In addition, it presented generalised techniques for using SBMP algorithms for collision avoidance, while also introducing methods to increase its performance. Compared to the existing literature, the thesis proposed techniques to leverage SBMP for collision avoidance, rather than simply path planning. Furthermore, the proposed collision and grounding avoidance framework included feasible depth and dredge information from the ENCs without any compromise, ensuring no loss of generality in terms of navigable area. The thesis presented the development of a collision avoidance module within an autonomy stack for an autonomous harbour bus, discussing the challenges associated with its implementation and surrounding technologies. The overall results show the feasibility of an automated collision and grounding avoidance scheme, given that the remaining autonomy stack is capable of providing the required information regarding the navigation scenario of the own ship.

The research findings have been disseminated through publication or submission to international journals and presented at international conferences. All scientific articles, already published or currently under review, are attached to the thesis.

9.2   Future research

The findings within the thesis have contributed to research on autonomous collision and grounding avoidance for marine crafts; however, there are still a number of challenges to be addressed before the transition to full autonomy can occur.

To maximise the full potential of sampling-based collision and grounding avoidance, emphasis should be placed on researching and developing methods to report feasible solutions, in combination with conditions to terminate SBMP algorithms.

More work is required on the interpretation and implementation of the COLREGs for autonomy to ensure that an eventual MASS acts and adheres to the same set of rules as human navigators. Current state-of-the-art methods continue to focus on creating better methods for situation awareness, in combination with collision avoidance, to increase the adherence to the COLREGs.

Leveraging information, such as shallow water conditions, from the ENCs is crucial to ensuring safe navigation. However, there are numerous other sources of information that can be found within the chart, which human navigators use to not only navigate safely but also navigate according to local rules. Therefore, it is worth quantifying which additional chart information is relevant, how it can be used to increase safety, ensure adherence to "good seamanship", and act predictably alongside human navigators.

In general, there is a lack of common consensus on how to algorithmically quantify "good seamanship", other than that it serves as a tool to deal with situations outside of the COLREGs. Proper interpretation and implementation of good seamanship is necessary to ensure solid decision-making of an eventual fully implemented and commissioned MASS.

The proposed architecture of the autonomy stack was built on "perceiving, predicting, planning, and executing", which placed tight demands on each step of the process. It could be argued that, by sequentially dividing these tasks, the entire problem is forced to operate on static information, limiting the overall ability of the prediction and planning phases. Applying the COLREGs during multiple vessel encounters proves to be particularly challenging when planning based on static information, as the fixed trajectories for each target vessel do not reflect the individual interaction each of targets may have with one another. It may be possible to combine prediction and planning in an iterative procedure to assess the impact of the resulting actions from multiple vessels interacting with each other. Such techniques may be required to solve complicated scenarios, where human navigators typically use their experience and ability to reason what others do based on what is required by the COLREGs.

The proposed areas for future work could potentially be addressed by further exploring the intersection between stochastic and deterministic SBMP algorithms. As it may contain both the effectiveness and robustness required for deploying and commissioning a collision and grounding avoidance scheme for MASS. As mentioned above, complicated multiple vessel scenarios may require an iterative planning procedure that consists of both situation awareness and motion planning, to correctly encapsulate how each vessel interacts. By formulating the problem in terms of game theory, one may be able to model the interactivity between the vessels. Existing work for marine crafts explores the topic of dynamic games, in order to perform game-theoretical collision avoidance for multiple vessel encounters [210]–[212], however, the ability to consider the COLREGs and grounding avoidance simultaneously during complex encounters in confined or inner coastal waters is yet to be explored. Emerging techniques from game-theoretical motion planning for autonomous road vehicles are proving highly effective not only for considering the available actions of other agents, but also the multi-objective nature of the objective functions for autonomous systems [213]–[217]. Current research shows that certain game-theoretic motion planning methods allow one to prioritise the preferences and ordering of the multiple objective functions during multiobjective optimisation [216], [217].

Bibliography

[1] EMSA, *Annual overview of marine casualties and incidents 2021*, 2021.

[2] T. T. Enevoldsen, C. Reinartz, and R. Galeazzi, "COLREGs-Informed RRT* for Collision Avoidance of Marine Crafts," *2021 IEEE International Conference on Robotics and Automation (ICRA)*, 2021, pp. 8083–8089. DOI: `10.1109/ICRA48506.2021.9560909`.

[3] T. T. Enevoldsen and R. Galeazzi, "Grounding-aware RRT* for Path Planning and Safe Navigation of Marine Crafts in Confined Waters," *IFAC-PapersOnLine*, vol. 54, no. 16, pp. 195–201, 2021, 13th IFAC Conference on Control Applications in Marine Systems, Robotics, and Vehicles CAMS 2021. DOI: `https://doi.org/10.1016/j.ifacol.2021.10.093`.

[4] T. T. Enevoldsen, M. Blanke, and R. Galeazzi, "Sampling-based collision and grounding avoidance for marine crafts," *Ocean Engineering*, vol. 261, p. 112 078, 2022. DOI: `https://doi.org/10.1016/j.oceaneng.2022.112078`.

[5] T. T. Enevoldsen and R. Galeazzi, "Informed sampling-based collision avoidance with least deviation from the nominal path," *2022 IEEE/RSJ International Conference on Intelligent Robots and Systems (IROS)*, 2022, pp. 8094–8100. DOI: `10.1109/IROS47612.2022.9982202`.

[6] T. T. Enevoldsen and R. Galeazzi, "Guaranteed Rejection-free Sampling Method Using Past Behaviours for Motion Planning of Autonomous Systems," 2022, Under review. DOI: `https://doi.org/10.48550/arXiv.2109.14687`.

[7] T. T. Enevoldsen, M. Blanke, and R. Galeazzi, "Autonomy for Ferries and Harbour Buses: a Collision Avoidance Perspective," 2023, Under review. DOI: `https://doi.org/10.48550/arXiv.2301.02711`.

[8] F. E. T. Schöller, T. T. Enevoldsen, J. B. Becktor, and P. N. Hansen, "Trajectory Prediction for Marine Vessels using Historical AIS Heatmaps and Long Short-Term Memory Networks," *IFAC-PapersOnLine*, vol. 54, no. 16, pp. 83–89,

2021, 13th IFAC Conference on Control Applications in Marine Systems, Robotics, and Vehicles CAMS 2021. DOI: `https://doi.org/10.1016/j.ifacol.2021.10.077`.

[9] P. N. Hansen, T. T. Enevoldsen, D. Papageorgiou, and M. Blanke, "Autonomous navigation in confined waters - a colregs rule 9 compliant framework," *IFAC-PapersOnLine*, vol. 55, no. 31, pp. 222–228, 2022, 14th IFAC Conference on Control Applications in Marine Systems, Robotics, and Vehicles CAMS 2022. DOI: `https://doi.org/10.1016/j.ifacol.2022.10.435`.

[10] C. Reinartz, T. T. Enevoldsen, R. Galeazzi, and O. Ravn, "A causal model-based planner for the reconfiguration of continuous processes," *2021 European Control Conference (ECC)*, 2021, pp. 1751–1756. DOI: `10.23919/ECC54610.2021.9655016`.

[11] C. Reinartz and T. T. Enevoldsen, "pyTEP: A Python package for interactive simulations of the Tennessee Eastman process," *SoftwareX*, vol. 18, p. 101 053, 2022. DOI: `https://doi.org/10.1016/j.softx.2022.101053`.

[12] United Nations Office of Legal Affairs, *The Second World Ocean Assessment*. United Nations, 2021.

[13] S. Wan, X. Yang, X. Chen, Z. Qu, C. An, B. Zhang, K. Lee, and H. Bi, "Emerging marine pollution from container ship accidents: Risk characteristics, response strategies, and regulation advancements," *Journal of Cleaner Production*, p. 134 266, 2022.

[14] G. C. Ceyhun, "The impact of shipping accidents on marine environment: A study of turkish seas," *European Scientific Journal*, vol. 10, no. 23, 2014.

[15] M. Jin, W. Shi, K. F. Yuen, Y. Xiao, and K. X. Li, "Oil tanker risks on the marine environment: An empirical study and policy implications," *Marine Policy*, vol. 108, p. 103 655, 2019.

[16] IMO, *Convention on the international regulations for preventing collisions at sea, 1972 (COLREGs)*. 1972.

[17] IMO, *International Convention for the Safety of Life at Sea (SOLAS)*, 2011.

[18] L. M. Millefiori, P. Braca, D. Zissis, G. Spiliopoulos, S. Marano, P. K. Willett, and S. Carniel, "Covid-19 impact on global maritime mobility," *Scientific reports*, vol. 11, no. 1, pp. 1–16, 2021.

[19] Ö. Uğurlu, U. Yıldırım, and E. Başar, "Analysis of grounding accidents caused by human error," *Journal of Marine Science and Technology*, vol. 23, no. 5, pp. 748–760, 2015.

[20] J. Chen, Z. Di, J. Shi, Y. Shu, Z. Wan, L. Song, and W. Zhang, "Marine oil spill pollution causes and governance: A case study of sanchi tanker collision and explosion," *Journal of Cleaner Production*, vol. 273, p. 122 978, 2020. DOI: https://doi.org/10.1016/j.jclepro.2020.122978.

[21] ITOPF, *Oil tanker spill statistics 2021*, https://www.itopf.org/fileadmin/uploads/itopf/data/Documents/Company_Lit/Oil_Spill_Stats_2021.pdf (Accessed November 25th, 2022, 2021.

[22] K. Bimbraw, "Autonomous cars: Past, present and future a review of the developments in the last century, the present scenario and the expected future of autonomous vehicle technology," *2015 12th International Conference on Informatics in Control, Automation and Robotics (ICINCO)*, vol. 01, 2015, pp. 191–198.

[23] H. Shokravi, H. Shokravi, N. Bakhary, M. Heidarrezaei, S. S. Rahimian Koloor, and M. Petru, "A review on vehicle classification and potential use of smart vehicle-assisted techniques," *Sensors*, vol. 20, no. 11, p. 3274, 2020.

[24] R. K. Kamalanathsharma, H. A. Rakha, and I. H. Zohdy, "Survey on in-vehicle technology use: Results and findings," *International journal of transportation science and technology*, vol. 4, no. 2, pp. 135–149, 2015.

[25] M. Caccia, "Autonomous surface craft: Prototypes and basic research issues," *2006 14th Mediterranean Conference on Control and Automation*, IEEE, 2006, pp. 1–6.

[26] B. Rivkin, "Unmanned ships: Navigation and more," *Gyroscopy and Navigation*, vol. 12, no. 1, pp. 96–108, 2021.

[27] E. F. Brekke, E. Eide, B. H. Eriksen, E. F. Wilthil, M. Breivik, E. Skjellaug, Ø. K. Helgesen, A. M. Lekkas, A. B. Martinsen, E. H. Thyri, *et al.*, "Milliampere: An autonomous ferry prototype," *Journal of Physics: Conf. Series*, vol. 2311, 2022, p. 012 029.

[28] W. Wang, B. Gheneti, L. A. Mateos, F. Duarte, C. Ratti, and D. Rus, "Roboat: An autonomous surface vehicle for urban waterways," *2019 IEEE/RSJ International Conference on Intelligent Robots and Systems (IROS)*, IEEE, 2019, pp. 6340–6347.

[29] W. Wang, T. Shan, P. Leoni, D. Fernández-Gutiérrez, D. Meyers, C. Ratti, and
      D. Rus, "Roboat II: A novel autonomous surface vessel for urban environ-
      ments," *2020 IEEE/RSJ Int. Conf. on Intelligent Robots and Systems (IROS)*,
      IEEE, 2020, pp. 1740–1747.

[30] L. Johnsen, F. Duarte, C. Ratti, T. Xiaojie, and T. Tian, "Roboat: A fleet of
      autonomous boats for amsterdam," *Landscape Architecture Frontiers*, vol. 7,
      no. 2, pp. 100–110, 2019.

[31] H. Ringbom, "Regulating autonomous ships—concepts, challenges and
      precedents," *Ocean Development & International Law*, vol. 50, no. 2-3,
      pp. 141–169, 2019.

[32] A. Komianos, "The autonomous shipping era. operational, regulatory, and
      quality challenges," *TransNav: International Journal on Marine Navigation
      and Safety of Sea Transportation*, vol. 12, 2018.

[33] M. Kim, T.-H. Joung, B. Jeong, and H.-S. Park, "Autonomous shipping and its
      impact on regulations, technologies, and industries," *Journal of International
      Maritime Safety, Environmental Affairs, and Shipping*, vol. 4, no. 2, pp. 17–25,
      2020.

[34] Det Norske Veritas (DNV), *IMO Maritime Safety Committee (MSC 105)*,
      `https://www.dnv.com/news/imo-maritime-safety-committee-msc-`
      `105--224289` (Accessed November 25th, 2022), Apr. 2022.

[35] Søfartsstyrelsen, *Bekendtgørelse om sejlads m.m. i visse danske farvande (BEK
      nr 656 af 20/05/2020)*, `https://www.retsinformation.dk/eli/lta/`
      `2020/656`, 2020.

[36] Søfartsstyrelsen, *Bekendtgørelse om sejlads på Limfjorden mellem Egholm og
      Kattegat (BEK nr 953 af 18/12/1991)*, `https://www.retsinformation.`
      `dk/eli/lta/1991/953`, 1991.

[37] C. Tam, R. Bucknall, and A. Greig, "Review of collision avoidance and
      path planning methods for ships in close range encounters," *The Journal of
      Navigation*, vol. 62, no. 3, pp. 455–476, 2009.

[38] Y. Huang, L. Chen, P. Chen, R. R. Negenborn, and P. van Gelder, "Ship colli-
      sion avoidance methods: State-of-the-art," *Safety science*, vol. 121, pp. 451–
      473, 2020.

[39] A. Vagale, R. Oucheikh, R. T. Bye, O. L. Osen, and T. I. Fossen, "Path planning
      and collision avoidance for autonomous surface vehicles I: a review," *Journal
      of Marine Science and Technology*, vol. i, no. 0123456789, pp. 2018–2028,
      Jan. 2021. DOI: `10.1007/s00773-020-00787-6`.

[40] A. Vagale, R. T. Bye, R. Oucheikh, O. L. Osen, and T. I. Fossen, "Path planning and collision avoidance for autonomous surface vehicles II: a comparative study of algorithms," *Journal of Marine Science and Technology*, no. 0123456789, Feb. 2021. DOI: 10.1007/s00773-020-00790-x.

[41] S. Campbell, W. Naeem, and G. Irwin, "A review on improving the autonomy of unmanned surface vehicles through intelligent collision avoidance manoeuvres," *Annual Reviews in Control*, vol. 36, no. 2, pp. 267–283, 2012.

[42] C. Tam and R. Bucknall, "Cooperative path planning algorithm for marine surface vessels," *Ocean Engineering*, vol. 57, pp. 25–33, 2013.

[43] M. R. Benjamin and J. A. Curcio, "COLREGS-based navigation of autonomous marine vehicles," *2004 IEEE/OES Autonomous Underwater Vehicles (IEEE Cat. No. 04CH37578)*, IEEE, 2004, pp. 32–39.

[44] M. R. Benjamin, "The interval programming model for multi-objective decision making," 2004.

[45] M. R. Benjamin, J. J. Leonard, J. A. Curcio, and P. M. Newman, "A method for protocol-based collision avoidance between autonomous marine surface craft," *Journal of Field Robotics*, vol. 23, no. 5, pp. 333–346, 2006.

[46] M. R. Benjamin, J. A. Curcio, J. J. Leonard, and P. M. Newman, "Navigation of unmanned marine vehicles in accordance with the rules of the road," *Proceedings 2006 IEEE International Conference on Robotics and Automation, 2006. ICRA 2006.*, IEEE, 2006, pp. 3581–3587.

[47] J. Larson, M. Bruch, and J. Ebken, "Autonomous navigation and obstacle avoidance for unmanned surface vehicles," *Unmanned systems technology VIII*, International Society for Optics and Photonics, vol. 6230, 2006, p. 623 007.

[48] J. Larson, M. Bruch, R. Halterman, J. Rogers, and R. Webster, "Advances in autonomous obstacle avoidance for unmanned surface vehicles," *Association for Unmanned Vehicle Systems International - Unmanned Systems North America Conference 2007*, vol. 1, pp. 484–498, 2007.

[49] Y.-i. Lee and Y.-G. Kim, "A collision avoidance system for autonomous ship using fuzzy relational products and colregs," *International Conference on Intelligent Data Engineering and Automated Learning*, Springer, 2004, pp. 247–252.

[50] L. Perera, J. Carvalho, and C. G. Soares, "Fuzzy logic based decision making system for collision avoidance of ocean navigation under critical collision conditions," *Journal of marine science and technology*, vol. 16, no. 1, pp. 84–99, 2011.

[51] M. Blaich, M. Rosenfelder, M. Schuster, O. Bittel, and J. Reuter, "Extended grid based collision avoidance considering colregs for vessels," *IFAC Proceedings Volumes*, vol. 45, no. 27, pp. 416–421, 2012.

[52] C. Y. Lee, "An algorithm for path connections and its applications," *IRE transactions on electronic computers*, no. 3, pp. 346–365, 1961.

[53] E. M. Goodwin, "A statistical study of ship domains," *The Journal of navigation*, vol. 28, no. 3, pp. 328–344, 1975.

[54] M. Blaich, M. Rosenfelder, M. Schuster, O. Bittel, and J. Reuter, "Fast grid based collision avoidance for vessels using a* search algorithm," *2012 17th International Conference on Methods & Models in Automation & Robotics (MMAR)*, IEEE, 2012, pp. 385–390.

[55] S. Campbell and W. Naeem, "A rule-based heuristic method for colregs-compliant collision avoidance for an unmanned surface vehicle," *IFAC Proceedings Volumes*, vol. 45, no. 27, pp. 386–391, 2012.

[56] S. Campbell, M. Abu-Tair, and W. Naeem, "An automatic colregs-compliant obstacle avoidance system for an unmanned surface vehicle," *Proceedings of the Institution of Mechanical Engineers, Part M: Journal of Engineering for the Maritime Environment*, 2014.

[57] W. Naeem, G. W. Irwin, and A. Yang, "COLREGs-based collision avoidance strategies for unmanned surface vehicles," *Mechatronics*, vol. 22, no. 6, pp. 669–678, 2012.

[58] Y. Singh, S. Sharma, R. Sutton, D. Hatton, and A. Khan, "A constrained A* approach towards optimal path planning for an unmanned surface vehicle in a maritime environment containing dynamic obstacles and ocean currents," *Ocean Engineering*, vol. 169, pp. 187–201, 2018.

[59] A. Lazarowska, "Ship's trajectory planning for collision avoidance at sea based on ant colony optimisation," *Journal of Navigation*, vol. 68, no. 2, pp. 291–307, 2015.

[60] A. Lazarowska, "A Trajectory Base Method for Ship's Safe Path Planning," *Procedia Computer Science*, vol. 96, pp. 1022–1031, 2016.

[61] A. Lazarowska, "Research on algorithms for autonomous navigation of ships," *WMU Journal of Maritime Affairs*, vol. 18, no. 2, pp. 341–358, Jun. 2019.

[62] S. Ni, Z. Liu, Y. Cai, and X. Wang, "Modelling of ship's trajectory planning in collision situations by hybrid genetic algorithm," *Polish Maritime Research*, vol. 25, no. 3, pp. 14–25, 2018.

[63] S. Ni, Z. Liu, and Y. Cai, "Ship manoeuvrability-based simulation for ship navigation in collision situations," *Journal of Marine Science and Engineering*, vol. 7, no. 4, 2019.

[64] M.-C. C. Tsou, "Multi-target collision avoidance route planning under an ECDIS framework," *Ocean Engineering*, vol. 121, pp. 268–278, Jul. 2016. DOI: `10.1016/j.oceaneng.2016.05.040`.

[65] L. Hu, W. Naeem, E. Rajabally, G. Watson, T. Mills, Z. Bhuiyan, and I. Salter, "COLREGs-Compliant Path Planning for Autonomous Surface Vehicles: A Multiobjective Optimization Approach," *IFAC-PapersOnLine*, vol. 50, no. 1, pp. 13 662–13 667, 2017.

[66] L. Hu, W. Naeem, E. Rajabally, G. Watson, T. Mills, Z. Bhuiyan, C. Raeburn, I. Salter, and C. Pekcan, "A Multiobjective Optimization Approach for COLREGs-Compliant Path Planning of Autonomous Surface Vehicles Verified on Networked Bridge Simulators," *IEEE Transactions on Intelligent Transportation Systems*, 2019.

[67] Y. Xue, B. Lee, and D. Han, "Automatic collision avoidance of ships," *Proceedings of the Institution of Mechanical Engineers, Part M: Journal of Engineering for the Maritime Environment*, vol. 223, no. 1, pp. 33–46, 2009.

[68] S.-M. Lee, K.-Y. Kwon, and J. Joongseon, "A fuzzy logic for autonomous navigation of marine vehicles satisfying colreg guidelines," *International Journal of Control, Automation, and Systems*, vol. 2, no. 2, pp. 171–181, 2004.

[69] W. Naeem, S. C. Henrique, and L. Hu, "A Reactive COLREGs-Compliant Navigation Strategy for Autonomous Maritime Navigation," *IFAC-PapersOnLine*, vol. 49, no. 23, pp. 207–213, 2016.

[70] P. Wilson, C. Harris, and X. Hong, "A line of sight counteraction navigation algorithm for ship encounter collision avoidance," *The Journal of Navigation*, vol. 56, no. 1, pp. 111–121, 2003.

[71] Y. Kuwata, M. T. Wolf, D. Zarzhitsky, and T. L. Huntsberger, "Safe maritime navigation with COLREGS using velocity obstacles," *2011 IEEE/RSJ International Conference on Intelligent Robots and Systems*, IEEE, 2011, pp. 4728–4734.

[72] Y. Huang, P. H. van Gelder, and Y. Wen, "Velocity obstacle algorithms for collision prevention at sea," *Ocean Engineering*, vol. 151, no. January, pp. 308–321, 2018. DOI: 10.1016/j.oceaneng.2018.01.001.

[73] Y. Huang, L. Chen, and P. H. van Gelder, "Generalized velocity obstacle algorithm for preventing ship collisions at sea," *Ocean Engineering*, vol. 173, no. November 2018, pp. 142–156, 2019. DOI: 10.1016/j.oceaneng.2018.12.053.

[74] B. H. Eriksen and M. Breivik, "MPC-Based mid-level collision avoidance for ASVs using nonlinear programming," *2017 IEEE Conference on Control Technology and Applications (CCTA)*, Institute of Electrical and Electronics Engineers (IEEE), 2017.

[75] B. H. Eriksen, M. Breivik, E. F. Wilthil, A. L. Flåten, and E. F. Brekke, "The branching-course model predictive control algorithm for maritime collision avoidance," *Journal of Field Robotics*, vol. 36, no. 7, pp. 1222–1249, 2019.

[76] B. H. Eriksen, G. Bitar, M. Breivik, and A. M. Lekkas, "Hybrid collision avoidance for ASVs compliant with COLREGs rules 8 and 13–17," *Frontiers in Robotics and AI*, vol. 7, p. 11, 2020.

[77] T. A. Johansen, T. Perez, and A. Cristofaro, "Ship collision avoidance and COLREGS compliance using simulation-based control behavior selection with predictive hazard assessment," *IEEE transactions on intelligent transportation systems*, vol. 17, no. 12, pp. 3407–3422, 2016.

[78] I. B. Hagen, D. K. M. Kufoalor, E. F. Brekke, and T. A. Johansen, "MPC-based collision avoidance strategy for existing marine vessel guidance systems," *2018 IEEE International Conference on Robotics and Automation (ICRA)*, IEEE, 2018, pp. 7618–7623.

[79] D. K. M. Kufoalor, E. Wilthil, I. B. Hagen, E. F. Brekke, and T. A. Johansen, "Autonomous COLREGs-Compliant Decision Making using Maritime Radar Tracking and Model Predictive Control," *2019 18th European Control Conference (ECC)*, IEEE, 2019, pp. 2536–2542.

[80] D. K. M. Kufoalor, T. A. Johansen, E. F. Brekke, A. Hepsø, and K. Trnka, "Autonomous maritime collision avoidance: Field verification of autonomous surface vehicle behavior in challenging scenarios," *Journal of Field Robotics*, vol. 37, no. 3, pp. 387–403, 2020.

[81] M. Abdelaal, M. Fränzle, and A. Hahn, "Nonlinear Model Predictive Control for trajectory tracking and collision avoidance of underactuated vessels with disturbances," *Ocean Engineering*, vol. 160, no. April, pp. 168–180, 2018. DOI: 10.1016/j.oceaneng.2018.04.026.

[82] S. Garrido, D. Alvarez, and L. E. Moreno, "Marine applications of the fast marching method," *Frontiers in Robotics and AI*, vol. 7, p. 2, 2020.

[83] P. Chen, Y. Huang, E. Papadimitriou, J. Mou, and P. van Gelder, "Global path planning for autonomous ship: A hybrid approach of Fast Marching Square and velocity obstacles methods," *Ocean Engineering*, vol. 214, no. August, p. 107 793, 2020. DOI: 10.1016/j.oceaneng.2020.107793.

[84] G. Tan, J. Zou, J. Zhuang, L. Wan, H. Sun, and Z. Sun, "Fast marching square method based intelligent navigation of the unmanned surface vehicle swarm in restricted waters," *Applied Ocean Research*, vol. 95, p. 102 018, 2020.

[85] P. Svec, B. C. Shah, I. R. Bertaska, J. Alvarez, A. J. Sinisterra, K. Von Ellenrieder, M. Dhanak, and S. K. Gupta, "Dynamics-aware target following for an autonomous surface vehicle operating under COLREGs in civilian traffic," *IEEE International Conference on Intelligent Robots and Systems*, pp. 3871–3878, 2013. DOI: 10.1109/IROS.2013.6696910.

[86] B. C. Shah, P. Švec, I. R. Bertaska, A. J. Sinisterra, W. Klinger, K. von Ellenrieder, M. Dhanak, and S. K. Gupta, "Resolution-adaptive risk-aware trajectory planning for surface vehicles operating in congested civilian traffic," *Autonomous Robots*, vol. 40, no. 7, pp. 1139–1163, Oct. 2016.

[87] K. Bergman, O. Ljungqvist, J. Linder, and D. Axehill, "A COLREGs Compliant Motion Planner for Autonomous Maneuvering of Marine Vessels in Complex Environments," *arXiv:2012.12145*, 2020.

[88] H.-T. L. Chiang and L. Tapia, "COLREG-RRT: An RRT-based COLREGS-compliant motion planner for surface vehicle navigation," *IEEE Robotics and Automation Letters*, vol. 3, no. 3, pp. 2024–2031, 2018.

[89] R. Zaccone, M. Martelli, and M. Figari, "A COLREG-compliant ship collision avoidance algorithm," *2019 18th European Control Conference, ECC 2019*, no. August, pp. 2530–2535, 2019.

[90] R. Zaccone, "COLREG-Compliant Optimal Path Planning for Real-Time Guidance and Control of Autonomous Ships," *Journal of Marine Science and Engineering*, vol. 9, no. 4, 2021. DOI: 10.3390/jmse9040405.

[91] J. Zhang, H. Zhang, J. Liu, D. Wu, and C. G. Soares, "A two-stage path planning algorithm based on rapid-exploring random tree for ships navigating in multi-obstacle water areas considering colregs," *Journal of Marine Science and Engineering*, vol. 10, no. 10, p. 1441, 2022.

[92] P. Silveira, A. Teixeira, and C. G. Soares, "A method to extract the quaternion ship domain parameters from ais data," *Ocean Engineering*, vol. 257, p. 111 568, 2022.

[93] S. Cao, P. Fan, T. Yan, C. Xie, J. Deng, F. Xu, and Y. Shu, "Inland waterway ship path planning based on improved rrt algorithm," *Journal of Marine Science and Engineering*, vol. 10, no. 10, p. 1460, 2022.

[94] C. Liang, X. Zhang, Y. Watanabe, and B. Zhao, "Novel l+ and fo l+ algorithms based on enc data for automatic route planning of ships," *Ocean Engineering*, vol. 235, p. 109 389, 2021.

[95] S. Blindheim and T. A. Johansen, "Electronic navigational charts for visualization, simulation, and autonomous ship control," *IEEE Access*, vol. 10, pp. 3716–3737, 2021.

[96] S. Blindheim and T. A. Johansen, "Particle swarm optimization for dynamic risk-aware path following for autonomous ships," *IFAC-PapersOnLine*, vol. 55, no. 31, pp. 70–77, 2022.

[97] N. P. Reddy, M. K. Zadeh, C. A. Thieme, R. Skjetne, A. J. Sorensen, S. A. Aanondsen, M. Breivik, and E. Eide, "Zero-emission autonomous ferries for urban water transport: Cheaper, cleaner alternative to bridges and manned vessels," *IEEE Electrification Magazine*, vol. 7, no. 4, pp. 32–45, 2019.

[98] G. Bitar, B. H. Eriksen, A. M. Lekkas, and M. Breivik, "Three-phase automatic crossing for a passenger ferry with field trials," *2021 European Control Conference (ECC)*, IEEE, 2021, pp. 2271–2277.

[99] E. H. Thyri, M. Breivik, and A. M. Lekkas, "A path-velocity decomposition approach to collision avoidance for autonomous passenger ferries in confined waters," *IFAC-PapersOnLine*, vol. 53, no. 2, pp. 14 628–14 635, 2020.

[100] E. H. Thyri, E. A. Basso, M. Breivik, K. Y. Pettersen, R. Skjetne, and A. M. Lekkas, "Reactive collision avoidance for asvs based on control barrier functions," *2020 IEEE Conference on Control Technology and Applications (CCTA)*, IEEE, 2020, pp. 380–387.

[101]   E. H. Thyri and M. Breivik, "A domain-based and reactive COLAV method with a partially COLREGs-compliant domain for ASVs operating in confined waters," *Field Robotics*, vol. 2, pp. 637–677, 2022.

[102]   J. de Vries, E. Trevisan, J. van der Toorn, T. Das, B. Brito, and J. Alonso-Mora, "Regulations aware motion planning for autonomous surface vessels in urban canals," *2022 Int. Conf. on Robotics and Automation (ICRA)*, 2022, pp. 3291–3297. DOI: 10.1109/ICRA46639.2022.9811608.

[103]   P. Koschorrek, M. Kosch, M. Nitsch, D. Abel, and D. Jürgens, "Towards semi-autonomous operation of an over-actuated river ferry," *Automatisierungstechnik*, vol. 70, no. 5, pp. 433–443, 2022. DOI: 10.1515/auto-2021-0152.

[104]   M. Kosch, P. Koschorrek, and D. Abel, "A reference trajectory-based approach to safe and efficient trajectory planning for an overactuated river ferry," *IFAC-PapersOnLine*, vol. 55, no. 31, pp. 31–36, 2022.

[105]   X. Yuan, D. Zhang, J. Zhang, C. Wan, and L. Fan, "A two-stage collision avoidance path planning approach for inland ferries under dynamic channel crossing risk conditions," *Available at SSRN 4264717*,

[106]   J. H. Mei and M. R. Arshad, "COLREGs based navigation of riverine Autonomous Surface Vehicle," *2016 IEEE International Conference on Underwater System Technology: Theory and Applications (USYS)*, IEEE, 2016, pp. 145–149.

[107]   H. W. Hjelmeland, B. H. Eriksen, O. J. Mengshoel, and A. M. Lekkas, "Identification of failure modes in the collision avoidance system of an autonomous ferry using adaptive stress testing," *IFAC-PapersOnLine*, vol. 55, no. 31, pp. 470–477, 2022.

[108]   L. E. Kavraki, P. Svestka, J.-C. Latombe, and M. H. Overmars, "Probabilistic roadmaps for path planning in high-dimensional configuration spaces," *IEEE transactions on Robotics and Automation*, vol. 12, no. 4, pp. 566–580, 1996.

[109]   L. E. Kavraki, M. N. Kolountzakis, and J.-C. Latombe, "Analysis of probabilistic roadmaps for path planning," *IEEE Transactions on Robotics and automation*, vol. 14, no. 1, pp. 166–171, 1998.

[110]   R. Geraerts and M. H. Overmars, "A comparative study of probabilistic roadmap planners," *Algorithmic foundations of robotics V*, Springer, 2004, pp. 43–57.

[111]   S. M. LaValle, "Rapidly-exploring random trees : A new tool for path planning," *The annual research report*, 1998.

[112] J. J. Kuffner and S. M. LaValle, "RRT-connect: An efficient approach to single-query path planning," *Proceedings 2000 ICRA. Millennium Conference. IEEE International Conference on Robotics and Automation. Symposia Proceedings (Cat. No. 00CH37065)*, IEEE, vol. 2, 2000, pp. 995–1001.

[113] S. M. LaValle and J. J. Kuffner, "Randomized Kinodynamic Planning," *The International Journal of Robotics Research*, vol. 20, no. 5, pp. 378–400, May 2001.

[114] R. Pepy, A. Lambert, and H. Mounier, "Path Planning using a Dynamic Vehicle Model," 1, vol. 1, IEEE, 2006, pp. 781–786.

[115] S. Karaman and E. Frazzoli, "Incremental sampling-based algorithms for optimal motion planning," *Robotics Science and Systems VI*, vol. 104, no. 2, 2010.

[116] S. Karaman and E. Frazzoli, "Sampling-based algorithms for optimal motion planning," *The international journal of robotics research*, vol. 30, no. 7, pp. 846–894, 2011.

[117] J. D. Gammell and M. P. Strub, "Asymptotically optimal sampling-based motion planning methods," *Annual Review of Control, Robotics, and Autonomous Systems*, vol. 4, pp. 295–318, 2021.

[118] V. Vonásek, J. Faigl, T. Krajník, and L. Přeučil, "RRT-path–a guided rapidly exploring random tree," *Robot Motion and Control 2009*, Springer, 2009, pp. 307–316.

[119] X. Lan and S. Di Cairano, "Continuous curvature path planning for semi-autonomous vehicle maneuvers using RRT," *2015 European control conference (ECC)*, IEEE, 2015, pp. 2360–2365.

[120] H. Tang, Q. Zhu, E. Shang, B. Dai, and C. Hu, "A reference path guided RRT* method for the local path planning of UGVS," *2020 39th Chinese Control Conference (CCC)*, IEEE, 2020, pp. 3904–3909.

[121] Y. Lin, S. Maierhofer, and M. Althoff, "Sampling-based trajectory repairing for autonomous vehicles," *2021 IEEE International Intelligent Transportation Systems Conference (ITSC)*, IEEE, 2021, pp. 572–579.

[122] C. Urmson and R. Simmons, "Approaches for heuristically biasing RRT growth," *Proceedings 2003 IEEE/RSJ International Conference on Intelligent Robots and Systems (IROS 2003)(Cat. No. 03CH37453)*, IEEE, vol. 2, 2003, pp. 1178–1183.

[123] L. G. D. Véras, F. L. Medeiros, and L. N. Guimaráes, "Systematic literature review of sampling process in rapidly-exploring random trees," *IEEE Access*, vol. 7, pp. 50 933–50 953, 2019.

[124] Y. Abbasi-Yadkori, P. Bartlett, V. Gabillon, and A. Malek, "Hit-and-run for sampling and planning in non-convex spaces," *Artificial Intelligence and Statistics*, PMLR, 2017, pp. 888–895.

[125] S. R. Lindemann and S. M. LaValle, "Current issues in sampling-based motion planning," *Robotics research. The eleventh international symposium*, Springer, 2005, pp. 36–54.

[126] M. Kobilarov, "Cross-entropy randomized motion planning," *Robotics: Science and Systems*, vol. 7, 2012, pp. 153–160.

[127] L. Janson, E. Schmerling, and M. Pavone, "Monte carlo motion planning for robot trajectory optimization under uncertainty," *Robotics Research*, Springer, 2018, pp. 343–361.

[128] T. Osa, "Multimodal trajectory optimization for motion planning," *The International Journal of Robotics Research*, vol. 39, no. 8, pp. 983–1001, 2020.

[129] E. Schmerling and M. Pavone, "Evaluating trajectory collision probability through adaptive importance sampling for safe motion planning," *arXiv preprint arXiv:1609.05399*, 2016.

[130] J. D. Gammell, S. S. Srinivasa, and T. D. Barfoot, "Informed RRT*: Optimal sampling-based path planning focused via direct sampling of an admissible ellipsoidal heuristic," *2014 IEEE/RSJ International Conference on Intelligent Robots and Systems*, IEEE, 2014, pp. 2997–3004.

[131] J. D. Gammell, T. D. Barfoot, and S. S. Srinivasa, "Informed sampling for asymptotically optimal path planning," *IEEE Transactions on Robotics*, vol. 34, no. 4, pp. 966–984, 2018.

[132] A. Mandalika, R. Scalise, B. Hou, S. Choudhury, and S. S. Srinivasa, "Guided incremental local densification for accelerated sampling-based motion planning," *arXiv preprint arXiv:2104.05037*, 2021.

[133] S. S. Joshi and T. Panagiotis, "Non-parametric informed exploration for sampling-based motion planning," *2019 International Conference on Robotics and Automation (ICRA)*, IEEE, 2019, pp. 5915–5921.

[134]   T. Kunz, A. Thomaz, and H. Christensen, "Hierarchical rejection sampling for informed kinodynamic planning in high-dimensional spaces," *2016 IEEE International Conference on Robotics and Automation (ICRA)*, IEEE, 2016, pp. 89–96.

[135]   D. Yi, R. Thakker, C. Gulino, O. Salzman, and S. Srinivasa, "Generalizing informed sampling for asymptotically-optimal sampling-based kinodynamic planning via markov chain monte carlo," *2018 IEEE International Conference on Robotics and Automation (ICRA)*, IEEE, 2018, pp. 7063–7070.

[136]   C. Li, C. Wang, J. Wang, Y. Shen, and M. Q.-H. Meng, "Sliding-Window Informed RRT*: A Method for Speeding Up the Optimization and Path Smoothing," *2021 IEEE International Conference on Real-time Computing and Robotics (RCAR)*, IEEE, 2021, pp. 141–146.

[137]   H. Ryu and Y. Park, "Improved informed RRT* using gridmap skeletonization for mobile robot path planning," *International Journal of Precision Engineering and Manufacturing*, vol. 20, no. 11, pp. 2033–2039, 2019.

[138]   J. D. Gammell, S. S. Srinivasa, and T. D. Barfoot, "Batch informed trees (BIT*): Sampling-based optimal planning via the heuristically guided search of implicit random geometric graphs," *2015 IEEE international conference on robotics and automation (ICRA)*, IEEE, 2015, pp. 3067–3074.

[139]   M. P. Strub and J. D. Gammell, "Adaptively Informed Trees (AIT*): Fast asymptotically optimal path planning through adaptive heuristics," *2020 IEEE International Conference on Robotics and Automation (ICRA)*, IEEE, 2020, pp. 3191–3198.

[140]   S. Choudhury, J. D. Gammell, T. D. Barfoot, S. S. Srinivasa, and S. Scherer, "Regionally accelerated batch informed trees (RABIT*): A framework to integrate local information into optimal path planning," *2016 IEEE International Conference on Robotics and Automation (ICRA)*, IEEE, 2016, pp. 4207–4214.

[141]   T. F. Iversen and L.-P. Ellekilde, "Kernel density estimation based self-learning sampling strategy for motion planning of repetitive tasks," *2016 IEEE/RSJ International Conference on Intelligent Robots and Systems (IROS)*, IEEE, 2016, pp. 1380–1387.

[142]   P. Lehner and A. Albu-Schäffer, "Repetition sampling for efficiently planning similar constrained manipulation tasks," *2017 IEEE/RSJ International Conference on Intelligent Robots and Systems (IROS)*, IEEE, 2017, pp. 2851–2856.

[143] P. Lehner and A. Albu-Schäffer, "The repetition roadmap for repetitive constrained motion planning," *IEEE Robotics and Automation Letters*, vol. 3, no. 4, pp. 3884–3891, 2018.

[144] C. Chamzas, A. Shrivastava, and L. E. Kavraki, "Using local experiences for global motion planning," *2019 International Conference on Robotics and Automation (ICRA)*, IEEE, 2019, pp. 8606–8612.

[145] C. Zhang, J. Huh, and D. D. Lee, "Learning implicit sampling distributions for motion planning," *2018 IEEE/RSJ International Conference on Intelligent Robots and Systems (IROS)*, IEEE, 2018, pp. 3654–3661.

[146] O. Arslan and P. Tsiotras, "Machine learning guided exploration for sampling-based motion planning algorithms," *2015 IEEE/RSJ International Conference on Intelligent Robots and Systems (IROS)*, IEEE, 2015, pp. 2646–2652.

[147] B. Ichter, J. Harrison, and M. Pavone, "Learning sampling distributions for robot motion planning," *2018 IEEE International Conference on Robotics and Automation (ICRA)*, IEEE, 2018, pp. 7087–7094.

[148] B. Ichter and M. Pavone, "Robot motion planning in learned latent spaces," *IEEE Robotics and Automation Letters*, vol. 4, no. 3, pp. 2407–2414, 2019.

[149] L. Li, Y. Miao, A. H. Qureshi, and M. C. Yip, "MPC-MPNet: Model-Predictive Motion Planning Networks for Fast, Near-Optimal Planning under Kinodynamic Constraints," *IEEE Robotics and Automation Letters*, vol. 6, no. 3, pp. 4496–4503, 2021.

[150] I. Noreen, A. Khan, and Z. Habib, "Optimal path planning using RRT* based approaches: a survey and future directions," *Int. J. Adv. Comput. Sci. Appl*, vol. 7, no. 11, pp. 97–107, 2016.

[151] B. Paden, M. Čáp, S. Z. Yong, D. Yershov, and E. Frazzoli, "A survey of motion planning and control techniques for self-driving urban vehicles," *IEEE Transactions on intelligent vehicles*, vol. 1, no. 1, pp. 33–55, 2016.

[152] L. Claussmann, M. Revilloud, D. Gruyer, and S. Glaser, "A review of motion planning for highway autonomous driving," *IEEE Transactions on Intelligent Transportation Systems*, vol. 21, no. 5, pp. 1826–1848, 2019.

[153] J. J. Park and B. Kuipers, "Feedback motion planning via non-holonomic RRT* for mobile robots," *IEEE International Conference on Intelligent Robots and Systems*, vol. 2015-Decem, pp. 4035–4040, 2015.

[154] P. Pharpatara, B. Herisse, and Y. Bestaoui, "3-D Trajectory Planning of Aerial Vehicles Using RRT*," *IEEE Transactions on Control Systems Technology*, vol. 25, no. 3, pp. 1116–1123, 2017.

[155] L. Janson, E. Schmerling, A. Clark, and M. Pavone, "Fast marching tree: A fast marching sampling-based method for optimal motion planning in many dimensions," *The International journal of robotics research*, vol. 34, no. 7, pp. 883–921, 2015.

[156] M. P. Strub and J. D. Gammell, "Advanced BIT* (ABIT*): Sampling-based planning with advanced graph-search techniques," *2020 IEEE International Conference on Robotics and Automation (ICRA)*, IEEE, 2020, pp. 130–136.

[157] S. Klemm, J. Oberländer, A. Hermann, A. Roennau, T. Schamm, J. M. Zollner, and R. Dillmann, "RRT*-Connect: Faster, asymptotically optimal motion planning," *2015 IEEE international conference on robotics and biomimetics (ROBIO)*, IEEE, 2015, pp. 1670–1677.

[158] D. Yi, M. A. Goodrich, and K. D. Seppi, "MORRF*: Sampling-based multi-objective motion planning," *Twenty-Fourth International Joint Conference on Artificial Intelligence*, 2015.

[159] M. Otte and E. Frazzoli, "RRT^X: Asymptotically optimal single-query sampling-based motion planning with quick replanning," *The International Journal of Robotics Research*, vol. 35, no. 7, pp. 797–822, 2016.

[160] A. Cockcroft and J. Lameijer, *A Guide to the Collision Avoidance Rules*. Elsevier Science, 2011.

[161] H.-C. Burmeister and M. Constapel, "Autonomous collision avoidance at sea: A survey," *Frontiers in Robotics and AI*, p. 297, 2021.

[162] CSA, *Collision Regulations, C.R.C., c. 1416, Canada Shipping Act (CSA), 2001*, https://laws-lois.justice.gc.ca/PDF/C.R.C.,_c._1416.pdf, 2001.

[163] IMO, *Revised Guidelines for the onboard operational use of shipborne automatic identification systems (AIS)*, 2015.

[164] Søfartsstyrelsen, *Bekendtgørelse om passagerfartøjer udelukkende i fart i havneområder eller på indsøer m.v. (BEK nr 916 af 03/07/2013)*, https://www.retsinformation.dk/eli/lta/2013/916, 2013.

[165] T. Porathe, "Maritime autonomous surface ships (mass) and the colregs: Do we need quantified rules or is "the ordinary practice of seamen" specific enough?," 2019.

[166] D. Papageorgiou, M. Blanke, M. Lützen, M. Bennedsen, J. Mogensen, and S. Hansen, "Parallel automaton representation of marine crafts' COLREGs-based manoeuvering behaviours," *IFAC-PapersOnLine*, vol. 52, no. 21, pp. 103–110, 2019.

[167] P. N. Hansen, D. Papageorgiou, M. Blanke, R. Galeazzi, M. Lützen, J. Mo-
       gensen, M. Bennedsen, and D. Hansen, "COLREGs-based Situation Aware-
       ness for Marine Vessels-a Discrete Event Systems Approach," *IFAC-PapersOnLine*,
       vol. 53, no. 2, pp. 14 501–14 508, 2020. DOI: `10.1016/j.ifacol.2020.12.`
       `1453`.

[168] Y. Fujii and K. Tanaka, "Traffic capacity," *Journal of Navigation*, vol. 24,
       no. 4, pp. 543–552, 1971. DOI: `10.1017/S0373463300022384`.

[169] E. M. Goodwin, "A statistical study of ship domains," *Journal of Navigation*,
       vol. 28, no. 3, pp. 328–344, 1975. DOI: `10.1017/S0373463300041230`.

[170] T. Coldwell, "Marine traffic behaviour in restricted waters," *The Journal of
       Navigation*, vol. 36, no. 3, pp. 430–444, 1983.

[171] M. G. Hansen, T. K. Jensen, T. Lehn-Schiøler, K. Melchild, F. M. Rasmussen,
       and F. Ennemark, "Empirical ship domain based on AIS data," *The Journal
       of Navigation*, vol. 66, no. 6, pp. 931–940, 2013.

[172] R. Smierzchalski and Z. Michalewicz, "Modeling of ship trajectory in collision
       situations by an evolutionary algorithm," *IEEE Transactions on Evolutionary
       Computation*, vol. 4, no. 3, pp. 227–241, 2000.

[173] M. Zhu, R. Skulstad, L. Zhao, H. Zhang, and G. Li, "Mpc-based path plan-
       ning for ship collision avoidance under colregs," *2022 IEEE International
       Conference on Systems, Man, and Cybernetics (SMC)*, 2022, pp. 1930–1935.
       DOI: `10.1109/SMC53654.2022.9945135`.

[174] L.-z. Sang, X.-p. Yan, A. Wall, J. Wang, and Z. Mao, "Cpa calculation method
       based on ais position prediction," *The journal of navigation*, vol. 69, no. 6,
       pp. 1409–1426, 2016.

[175] S. M. LaValle, *Planning algorithms*. Cambridge university press, 2006.

[176] J. L. Bentley, "Multidimensional binary search trees used for associative
       searching," *Communications of the ACM*, vol. 18, no. 9, pp. 509–517, 1975.

[177] P. Indyk and R. Motwani, "Approximate nearest neighbors: Towards remov-
       ing the curse of dimensionality," *Proceedings of the thirtieth annual ACM
       symposium on Theory of computing*, 1998, pp. 604–613.

[178] International Hydrographic Organization (IHO), *S-57 APPENDIX B.1, Annex
       A - Use of the Object Catalogue for ENC*, Edition 4.1.0 - January 2018, Jan.
       2018.

[179] R. Osada, T. Funkhouser, B. Chazelle, and D. Dobkin, "Shape distributions,"
       ACM Transactions on Graphics (TOG), vol. 21, no. 4, pp. 807–832, 2002.

[180] L. P. Chew, "Constrained delaunay triangulations," *Algorithmica*, vol. 4, no. 1, pp. 97–108, 1989.

[181] D. H. Douglas and T. K. Peucker, "Algorithms for the reduction of the number of points required to represent a digitized line or its caricature," *Cartographica: the international journal for geographic information and geovisualization*, vol. 10, no. 2, pp. 112–122, 1973.

[182] L. Devroye, *Non-Uniform Random Variate Generation*. Springer New York, 1986.

[183] T. Odland, *tommyod/KDEpy: Kernel Density Estimation in Python*, Dec. 2018. DOI: 10.5281/zenodo.2392268.

[184] A. Gramacki, *Nonparametric kernel density estimation and its computational aspects*. Springer, 2018.

[185] D. W. Scott, *Multivariate density estimation: theory, practice, and visualization*. John Wiley & Sons, 2015.

[186] B. W. Silverman, "Algorithm as 176: Kernel density estimation using the fast fourier transform," *Journal of the Royal Statistical Society. Series C (Applied Statistics)*, vol. 31, no. 1, pp. 93–99, 1982.

[187] Z. I. Botev, J. F. Grotowski, and D. P. Kroese, "Kernel density estimation via diffusion," *The annals of Statistics*, vol. 38, no. 5, pp. 2916–2957, 2010.

[188] T. A. O'Brien, K. Kashinath, N. R. Cavanaugh, W. D. Collins, and J. P. O'Brien, "A fast and objective multidimensional kernel density estimation method: fastKDE," *Computational Statistics & Data Analysis*, vol. 101, pp. 148–160, 2016.

[189] A. Gramacki and J. Gramacki, "FFT-based fast computation of multivariate kernel density estimators with unconstrained bandwidth matrices," *Journal of Computational and Graphical Statistics*, vol. 26, no. 2, pp. 459–462, 2017.

[190] L. Devroye and L. Gyorfi, *Nonparametric Density Estimation: The L_1 View* (Wiley Interscience Series in Discrete Mathematics). Wiley, 1985.

[191] K. Dittmann, N. Hansen, D. Papageorgiou, S. Jensen, M. Lützen, and M. Blanke, "Autonomous Surface Vessel with Remote Human on the Loop: System Design for STCW Compliance," *Proceedings of 13th IFAC Conference on Control Applications in Marine Systems, Robotics, and Vehicles*, 2021.

[192] K. Dittmann, P. N. Hansen, D. Papageorgiou, and M. Blanke, "Autonomy for ships: A sovereign agents architecture for reliability and safety by design," *IEEE Xplore-Proc. IEEE SysTol*, 2021.

[193] K. Dittmann and M. Blanke, "Risk mitigation by design of autonomous maritime automation systems," *at - Automatisierungstechnik*, vol. 70, no. 5, pp. 469–481, May 2022. DOI: `10.1515/auto-2021-0151`.

[194] K. Dittmann, "Autonomy for ships: System thinking and engineering," *2022 International Conference on Software, Telecommunications and Computer Networks (SoftCOM)*, 2022, pp. 1–6. DOI: `10.23919/SoftCOM55329.2022. 9911446`.

[195] M. Blanke, S. Hansen, J. D. Stets, T. Koester, J. Brøsted, A. L. Maurin, N. Nykvist, J. Bang, and D. M. Authority, "Outlook for navigation–comparing human performance with a robotic solution," *Proc. of ICMASS*, 2018.

[196] F. Schöller, M. Blanke, M. Plenge-Feidenhans'l, and L. Nalpantidis, "Vision-based object tracking in marine environments using features from neural network detections," English, 2020.

[197] J. Becktor, F. Schöller, E. Boukas, M. Blanke, and L. Nalpantidis, "Lipschitz constrained neural networks for robust object detection at sea," *IOP Conference Series: Materials Science and Engineering*, IOP Publishing, vol. 929, 2020, p. 012 023.

[198] F. E. Schöller, M. K. Plenge-Feidenhans, J. D. Stets, and M. Blanke, "Object detection at sea using ensemble methods across spectral ranges," *IFAC-PapersOnLine*, vol. 54, no. 16, pp. 1–6, 2021.

[199] F. E. T. Schöller, L. Nalpantidis, and M. Blanke, "Buoy light pattern classification for autonomous ship navigation using recurrent neural networks," *IEEE Transactions on Intelligent Transportation Systems*, 2022.

[200] J. Becktor, F. E. Schöller, E. Boukas, M. Blanke, and L. Nalpantidis, "Bolstering maritime object detection with synthetic data," *IFAC-PapersOnLine*, vol. 55, no. 31, pp. 64–69, 2022.

[201] J. Becktor, E. Boukas, and L. Nalpantidis, "Re-annotation of training samples for robust maritime object detection," *Machine Learning with Applications*, vol. 10, p. 100 411, 2022. DOI: `https://doi.org/10.1016/j.mlwa.2022. 100411`.

[202] M. K. Plenge-Feidenhans'l and M. Blanke, "Open water detection for autonomous in-harbor navigation using a classification network," 2021, 13th IFAC Conference on Control Applications in Marine Systems, Robotics, and Vehicles CAMS 2021. DOI: `https://doi.org/10.1016/j.ifacol.2021. 10.069`.

[203] D. Dagdilelis, M. Blanke, R. H. Andersen, and R. Galeazzi, "Cyber-resilience for marine navigation by information fusion and change detection," *Ocean Engineering*, vol. 266, p. 112 605, 2022. DOI: `https://doi.org/10.1016/j.oceaneng.2022.112605`.

[204] D. Dagdilelis, M. Blanke, and R. Galeazzi, "Gnss independent position fixing using multiple navigational features registration," *IFAC-PapersOnLine*, vol. 55, no. 31, pp. 243–248, 2022, 14th IFAC Conference on Control Applications in Marine Systems, Robotics, and Vehicles CAMS 2022. DOI: `https://doi.org/10.1016/j.ifacol.2022.10.438`.

[205] D. Papageorgiou, P. N. Hansen, K. Dittmann, and M. Blanke, "Anticipation of ship behaviours in multi-vessel scenarios," *Ocean Engineering*, vol. 266, p. 112 777, 2022. DOI: `https://doi.org/10.1016/j.oceaneng.2022.112777`.

[206] S. M. LaValle, M. S. Branicky, and S. R. Lindemann, "On the relationship between classical grid search and probabilistic roadmaps," *The International Journal of Robotics Research*, vol. 23, no. 7-8, pp. 673–692, 2004.

[207] L. Janson, B. Ichter, and M. Pavone, "Deterministic sampling-based motion planning: Optimality, complexity, and performance," *The International Journal of Robotics Research*, vol. 37, no. 1, pp. 46–61, 2018.

[208] M. Tsao, K. Solovey, and M. Pavone, "Sample complexity of probabilistic roadmaps via ε-nets," *2020 IEEE International Conference on Robotics and Automation (ICRA)*, IEEE, 2020, pp. 2196–2202.

[209] L. Palmieri, L. Bruns, M. Meurer, and K. O. Arras, "Dispertio: Optimal sampling for safe deterministic motion planning," *IEEE Robotics and Automation Letters*, vol. 5, no. 2, pp. 362–368, 2019.

[210] "The dynamic game models of safe navigation," *TransNav, International Journal on Marine Navigation and Safety od Sea Transportation*, vol. 1, no. 1, 2007.

[211] J. Lisowski, "Review of ship collision avoidance guidance algorithms using remote sensing and game control," *Remote Sensing*, vol. 14, no. 19, p. 4928, 2022.

[212] Y. Tu, Y. Xiong, and J. Mou, "Decision-making method for multi-ship collision avoidance based on improved extensive game model," *Maritime Technology and Research*, vol. 4, no. 4, Manuscript–Manuscript, 2022.

[213] M. Wang, N. Mehr, A. Gaidon, and M. Schwager, "Game-Theoretic Planning for Risk-Aware Interactive Agents," *2020 IEEE/RSJ International Conference on Intelligent Robots and Systems (IROS)*, Las Vegas, NV, USA (Virtual): IEEE, Oct. 2020, pp. 6998–7005.

[214] S. Le Cleac'h, M. Schwager, and Z. Manchester, "LUCIDGames: Online Unscented Inverse Dynamic Games for Adaptive Trajectory Prediction and Planning," *IEEE Robotics and Automation Letters*, vol. 6, no. 3, pp. 5485–5492, 2021.

[215] S. Le Cleac'h, M. Schwager, and Z. Manchester, "ALGAMES: A Fast Augmented Lagrangian Solver for Constrained Dynamic Games," *Autonomous Robots*, 2021.

[216] A. Zanardi, G. Zardini, S. Srinivasan, S. Bolognani, A. Censi, F. Dörfler, and E. Frazzoli, "Posetal games: Efficiency, existence, and refinement of equilibria in games with prioritized metrics," *IEEE Robotics and Automation Letters*, vol. 7, no. 2, pp. 1292–1299, 2021.

[217] A. Zanardi, E. Mion, M. Bruschetta, S. Bolognani, A. Censi, and E. Frazzoli, "Urban driving games with lexicographic preferences and socially efficient nash equilibria," *IEEE Robotics and Automation Letters*, vol. 6, no. 3, pp. 4978–4985, 2021.

Corrections

Paper A

In Section A.2.4, while defining the CPA and TCPA, the velocity vectors are defined incorrectly, as follows

Let $\mathbf{v}_{OS} = [V_{OS}\sin\psi_{OS}, V_{OS}\cos\psi_{OS}]^T$ and $\mathbf{v}_{TV} = [V_{TV}\sin\psi_{TV}, V_{TV}\cos\psi_{TV}]^T$

the $\sin$ and $\cos$ should be swapped, such that

Let $\mathbf{v}_{OS} = [V_{OS}\cos\psi_{OS}, V_{OS}\sin\psi_{OS}]^T$ and $\mathbf{v}_{TV} = [V_{TV}\cos\psi_{TV}, V_{TV}\sin\psi_{TV}]^T$

Paper C

In Equation C.33 and C.34, while defining the CPA and TCPA, the velocity vectors are defined incorrectly, as follows

$$\mathbf{v}_{OS} = [U_{OS}\sin(\psi_{OS}), U_{OS}\cos(\psi_{OS})]^T$$
$$\mathbf{v}_{TV} = [U_{TV}\sin(\psi_{TV}), U_{TV}\cos(\psi_{TV})]^T$$

the $\sin$ and $\cos$ should be swapped, such that

$$\mathbf{v}_{OS} = [U_{OS}\cos(\psi_{OS}), U_{OS}\sin(\psi_{OS})]^T$$
$$\mathbf{v}_{TV} = [U_{TV}\cos(\psi_{TV}), U_{TV}\sin(\psi_{TV})]^T$$

The cost function for path length in Equation C.12 is given by

$$c_l(\mathcal{P}^d) = \sum_{i=1}^{m} \|P_i^d - P_{i-1}^d\|_2, \quad \forall P_i^d \in \mathcal{P}^d.$$

where the correct range is $m-1$, instead of simply m

$$c_l(\mathcal{P}^d) = \sum_{i=1}^{m-1} \|P_i^d - P_{i-1}^d\|_2, \quad \forall P_i^d \in \mathcal{P}^d.$$

The sum for computing the cross-track error in Equation C.19, given by

$$c_e(\mathcal{P}^d) = \sum_{i=1}^{m-1} e_{P_i^d}, \quad \forall P_i^d \in \mathcal{P}^d$$

as $\mathcal{P}^d$ excludes both P_s^d and P_e^d, and $P_s^d = P_0$ and $P_e^d = P_{m-1}$, should be corrected to

$$c_e(\mathcal{P}^d) = \sum_{i=1}^{m-2} e_{P_i^d}, \quad \forall P_i^d \in \mathcal{P}^d.$$

Paper D

The cost function for path length in Equation D.2 is given by

$$c_l(\sigma) = \sum_{i=1}^{n} \|\mathbf{x}_i - \mathbf{x}_{i-1}\|_2, \quad \forall \mathbf{x}_i \in \sigma.$$

where the correct range is $n-1$, instead of simply n

$$c_l(\sigma) = \sum_{i=1}^{n-1} \|\mathbf{x}_i - \mathbf{x}_{i-1}\|_2, \quad \forall \mathbf{x}_i \in \sigma.$$

Paper A

COLREGs-Informed RRT* for Collision Avoidance of Marine Crafts

Thomas Thuesen Enevoldsen[1*], Christopher Reinartz[1] and Roberto Galeazzi[1]

[1]Automation and Control Group, Department of Electrical Engineering, Technical University of Denmark, DK-2800 Kgs. Lyngby, Denmark {tthen,ccrein,rg}@elektro.dtu.dk

Abstract:
The paper proposes novel sampling strategies to compute the optimal path alteration of a surface vessel sailing in close quarters. Such strategy directly encodes the rules for safe navigation at sea, by exploiting the concept of minimal ship domain to determine the compliant region where the path deviation is to be generated. The sampling strategy is integrated within the optimal rapidly-exploring random tree algorithm, which minimizes the length of the path deviation. Further, the feasibility of the path with respect to the steering characteristics of own ship is verified by ensuring that the position of the new waypoints respects the minimum turning radius of the vessel. The proposed sampling strategy brings a significant performance improvement both in terms of optimal cost, computational speed and convergence rate.

A.1   Introduction

The transport sector is witnessing an increasing interest in the adoption of autonomous systems' technologies, driven by the expectation of e.g. improving the intermodal logistic chain and solving the last mile problem [A1], [A2]. The deployment of autonomous means of transport such as busses, trucks and ships strongly depends on the development of two key technologies: Situation awareness and collision avoidance. Despite the technological needs are common across the different transport domains, the technologies are not easily portable due to the specificity of the operational environment and regulations that dictate how vehicles must operate. The pathway towards full autonomous operations is convoluted since social, economic and normative barriers need to be addressed alongside the technical challenges [A3], [A4]. However, the intermediate adoption of technologies providing partly autonomous capabilities integrated within decision support systems seems in clear sight, as already shown by the advanced driving assistance systems in the automotive industry. A similar focus is present in the maritime cluster that expects Advanced Navigation Assistance Systems (ANAS) to be one of the first byproducts of the autonomous ship development. Advanced Navigation Assistance Systems (ANAS) will encompass both situation awareness and collision avoidance systems; however the decision making process will remain rooted within the ship navigator. The introduction of ANAS in merchant vessels is expected to increase the operational safety, thereby reducing the likelihood of incidents caused by human error, which is still one of the main factors [A5].

   This paper addresses the design of the short horizon planner for collision avoidance. The essence of collision avoidance for marine vessels revolves around finding a feasible path deviation from the nominal planned route to avoid potential collision and grounding situations, whilst adhering to the International Regulations for Preventing Collisions at Sea (COLREGs). The paper proposes novel sampling strategies for the optimal rapidly-exploring random tree (RRT*) algorithm, which directly encodes the COLREGs by defining a compliant region of the configuration space where feasible paths should be searched for.

A.1.1   Literature review

RRT-based algorithms have been widely adopted by the robotics community since it was first proposed in [A6], [A7]. To address the lack of optimality of the found path, [A8], [A9] proposed RRT*, which allows the inclusion of optimization metrics to improve the quality of the obtained solutions as the number of samples goes to infinity, thus ensuring asymptotic optimality. To further improve the performance of

RRT* [A10] proposed Informed-RRT*, which constrains the search for the optimal solution in an elliptical region of the configuration space once a feasible path is found.

RRT-based algorithms have also been applied for the design of collision avoidance schemes for marine vessels. For explanatory details regarding specific COLREGs, see Section A.2.3. In [A11] a non-holonomic RRT (RRT* [A12], [A13]) is combined with an aggressive goal-seeking strategy to generate a path that complies with COLREGs rules 14-15. Compliance is achieved by describing the target vessels as virtual obstacles, which extends their collision boundaries, and forces the tree to grow around a given target vessel. [A14], [A15] implemented an RRT* algorithm that produces a tree of waypoints optimized with respect to distance, curvature and repulsion from obstacles. Later in [A16] an extension is made to include the COLREGs, where the RRT* algorithm will reject non COLREGs compliant samples.

Research on collision avoidance for autonomous ships has been extensive in recent years, and [A17] provides a broad survey of the developed algorithms. [A18], [A19] proposed a multi-objective approach for the generation of COLREGs compliant paths using the human element of *good seamanship*, which was assessed based on expert knowledge. [A20] proposed a collision avoidance scheme that is compliant with COLREGs rules 8 and 14, with the scheme generating waypoints adhering to the vessel dynamics whilst considering both static and dynamic objects. [A21] detailed a modified version of the Artificial Potential Fields algorithm, which generates COLREGs compliant paths (adhering to rules 13, 14 and 15), whilst considering a multi-vessel encounter with static obstacles. Model Predictive Control (MPC) has also been adopted for the design of collision avoidance schemes. [A22] showed an implementation addressing both static and dynamic obstacles, which minimizes the deviation from the nominal course. Later, [A23] presented the branching-course MPC that favours trajectories that are compliant with rules 14 and 15, whilst adhering to rules 8, 13 and 17. [A24] and [A25] presented a detailed account of how to represent the COLREGs in an autonomous setting, and proposed a multi-objective optimization method within a behaviour-based control framework to obtain compliant traversal. Various variants of popular search-based algorithms have also been investigated in the marine setting: [A26] used the A* algorithm to compute a collision free path in the presence of ocean currents; [A27] investigated a heuristic rule-based A* (R-RA*) algorithm to develop a real time COLREGs compliant path planner, which was validated on a bridge simulator [A28]. Other collision avoidance schemes include approaches using genetic algorithms [A29], [A30], Ant Colony Optimization (ACO) [A31], [A32] and lattice-based methods [A33].

A.1.2   Novelty and contribution

The paper proposes two new sampling strategies for the RRT* algorithm to naturally translate the COLREGs into geometrical regions of the configuration space, where feasible and collision free paths have to be generated. Exploiting the concept of minimal ship domain, half-annulus and elliptical half-annulus regions are proposed as search areas for the path alteration, and corresponding sampling schemes are derived to ensure uniform coverage of such regions. This implicitly defines a-priori forbidden zones that RRT* cannot explore because of breaching the COLREGs. The paper shows that the proposed sampling strategies significantly improve the performance of the RRT* algorithm with respect to the metrics of mean time to discover a feasible path, computational speed to find the optimal solution and convergence to the optimal cost, when compared to implementations adopting reference sampling strategies and rejection sampling [A9], [A10], [A15].

A.2   Preliminaries

A.2.1   Vessel and control scheme assumptions

This study focuses on path planning for merchant vessels, such as ferries, ro-ro vessels and container feeders, whose maneuvering capability is described by the minimum turning radius R_{min}. The considered collision scenarios are assumed to occur during open water passage with single vessel encounters. In such situations, human navigators avoid collision by minimizing the path alteration and trying to avoid speed variations. Therefore, it is further assumed that both own ship and target vessel will proceed with constant speed throughout the collision scenario. Moreover, the steering dynamics of own ship is controlled through an autopilot or track pilot, which receives a sequence of waypoints $W_i = (N_i, E_i, R_i)$, where N_i is the North position, E_i is the East position, and R_i is the radius of acceptance, which are feasible with respect to the manoeuvring capabilities (i.e minimal turning radius). Given the radius of acceptance R_i it is possible to compute the turning radius $\bar{R}_i$ required to transition between two consecutive legs of the path, i.e.

$$\bar{R}_i = R_i \tan\left(\frac{\phi}{2}\right), \quad \phi = (\alpha - \beta + \pi) \mod 2\pi \tag{A.1}$$

where α and β describe the path tangential angles of the two legs. Consecutive waypoints must be positioned such that $\bar{R}_i \geq R_{min}$.
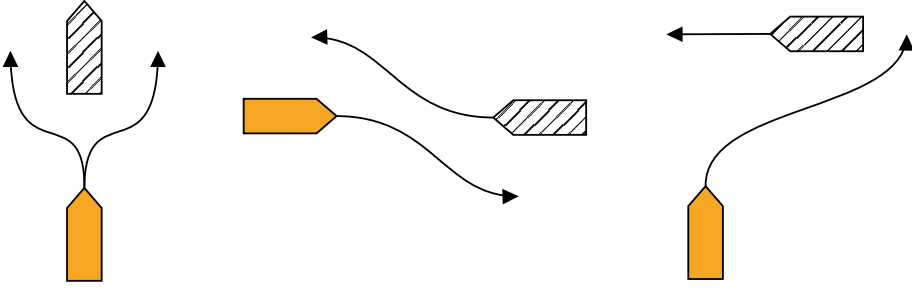
Figure A.1: Visualization of the encounters described by COLREGs rules 13-15, i.e. overtaking, head-on and crossing scenarios. The solid coloured vessel is in a give-way situation.

A.2.2   Target vessel representation

Using AIS (Automatic Identification System) data from vessels sailing in Southern Danish waters [A34] estimated the minimum ship domain in which a navigator feels comfortable. Such comfort zone can be described by an ellipse with major axis $a_{sd} = 8L$ and minor axis $b_{sd} = 3.2L$, where L is the ship length. The minimum ship domain can be utilized within the short horizon planner to ensure the generation of a collision free path between own ship and the target vessels.

At time $t = \bar{t}$, a target vessel violates the comfort zone of own ship if the following inequality is true

$$
\frac{\left(\Delta E(\bar{t}) \sin \psi(\bar{t}) + \Delta N(\bar{t}) \cos \psi(\bar{t})\right)^2}{\left(\frac{a_{sd}}{2}\right)^2} +
$$
$$
\frac{\left(\Delta E(\bar{t}) \cos \psi(\bar{t}) - \Delta N(\bar{t}) \sin \psi(\bar{t})\right)^2}{\left(\frac{b_{sd}}{2}\right)^2} \leq 1 \tag{A.2}
$$

where $\Delta E(\bar{t}) = E_{OS}(\bar{t}) - E_{TV}(\bar{t})$ and $\Delta N(\bar{t}) = N_{OS}(\bar{t}) - N_{TV}(\bar{t})$ are the difference in East and North directions of own ship and the target vessel, and $\psi(\bar{t})$ is the heading of the target vessel.

Last, it is assumed that position, speed and heading of the target vessel are available through e.g. AIS or RADAR.

A.2.3   COLREGs overview

The following is a brief overview of the International Regulations for Preventing Collisions at Sea (COLREGs, [A35]), which an advanced navigation assistance system must abide by. The listed rules describe the most commonly occurring collision risk scenarios for two vessels, and only apply if both vessels are power-driven. A graphical representation of rules 13-15 is provided in Fig. A.1.
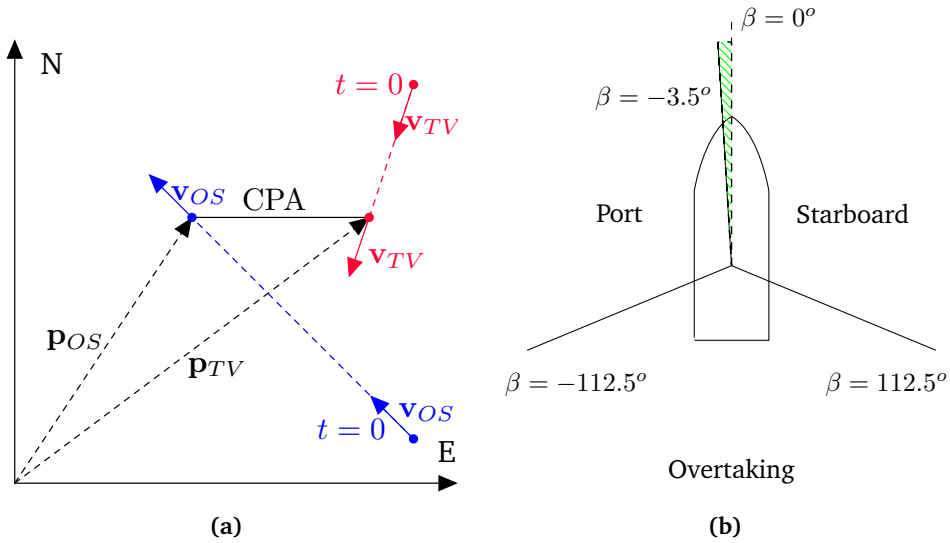
Figure A.2: (a) Vector definitions for the derivation of CPA and TCPA for two vessels with constant speed and heading. (b) Angles used to determine the relative position between own ship and the given target vessel. The gridded area indicates uncertainty associated with the head-on situation, see [A36].

Rule 13, Overtaking: The vessel being overtaken must maintain current course and speed, whereas the other may overtake on either side.

Rule 14, Head-on: Both vessels must perform a manoeuvre such that they pass one-another on their port sides.

Rule 15, Crossing: A vessel must give-way to another vessel, if the second vessel approaches from starboard side. The vessel that has the right of way must keep the current course and speed.

Rules 16-17: Specify "good behaviour" of a given vessel, depending on whether it is the stand-on or give-way vessel. Rule 16 dictates that the give-way vessel should take early action and remain a safe distance from the stand-on vessel. Rule 17 urges a vessel in the stand-on situation to remain so, and not attempt to avoid collision unless it is clear that the give-way vessel is not abiding by the COLREGs.

A.2.4   CPA and TCPA

The Closest Point of Approach (CPA) and Time to Closest Point of Approach (TCPA) are two metrics used by master mariners in order to navigate a vessel in a safe manner, where CPA together with the relative bearing is a determining factor for whether or not a COLREGs situation is developing, and an evasive manoeuvre must

be performed.

Let $\mathbf{p}_{OS} = [N_{OS}, E_{OS}]^T$ and $\mathbf{p}_{TV} = [N_{TV}, E_{TV}]^T$ be the position of own ship and target vessel in the North-East inertial frame.

Let $\mathbf{v}_{OS} = [V_{OS} \sin \psi_{OS}, V_{OS} \cos \psi_{OS}]^T$ and $\mathbf{v}_{TV} = [V_{TV} \sin \psi_{TV}, V_{TV} \cos \psi_{TV}]^T$ be the own ship and target vessel velocity vectors in the same frame, where $V_{(\cdot)}$ is the vessel's speed and $\psi_{(\cdot)}$ is the vessel's heading. Knowing the positions and velocities of both vessels at the current time, TCPA is defined as

$$\text{TCPA} \triangleq -\frac{(\Delta\mathbf{p}(0))^T \, \Delta\mathbf{v}}{(\Delta\mathbf{v})^T \, \Delta\mathbf{v}} \tag{A.3}$$

with $\Delta\mathbf{v} = \mathbf{v}_{OS} - \mathbf{v}_{TV}$, $\Delta\mathbf{p}(0) = \mathbf{p}_{TV}(0) - \mathbf{p}_{OS}(0)$. Assuming constant speed for both vessels, their respective positions at time TCPA is computed as

$$\mathbf{p}_{OS}(\text{TCPA}) = \mathbf{p}_{OS}(0) + \mathbf{v}_{OS} \cdot \text{TCPA} \tag{A.4}$$

$$\mathbf{p}_{TV}(\text{TCPA}) = \mathbf{p}_{TV}(0) + \mathbf{v}_{TV} \cdot \text{TCPA} \tag{A.5}$$

The CPA is then defined as follows

$$\text{CPA} \triangleq \left\| \Delta\mathbf{p}(\text{TCPA}) - \frac{(\Delta\mathbf{p}(0))^T \, \Delta\mathbf{v}}{(\Delta\mathbf{v})^T \, \Delta\mathbf{v}} \Delta\mathbf{v} \right\| \tag{A.6}$$

which provides a metric of how close the two vessels will be at $t = \text{TCPA}$. A graphical interpretation of this derivation is provided in Fig. A.2a.

A.3 Sampling the COLREGs compliant subset

A.3.1 Defining the COLREGs compliant subset

To improve the sampling performance of RRT* the COLREGs compliant sampling space is built. First, the current COLREGs scenario must be identified; this can be achieved by using a limit on the minimum allowed CPA along with the relative bearing between the vessels. If $\text{CPA} < d_{act}$, where d_{act} is a specified distance, then at $t = \text{TCPA}$ the two considered vessels will enter too close quarters and either collide or pose a collision risk. The relative bearing is the determining factor for which vessel is in the stand-on or give-way situation. Fig. A.2b details the various relative angles, which provides information regarding own ships location compared the target vessel. If OS is located on the port-side of the TV, then OS is the give-way vessel, and must therefore perform a COLREGs compliant manoeuvre to mitigate the risk of collision. This manoeuvre is initiated when $\text{TCPA} < t_{act}$ where t_{act} is a specified time. Both d_{act} and t_{act} strongly depend on the vessel type, and typically increase in size as the vessel size increases.
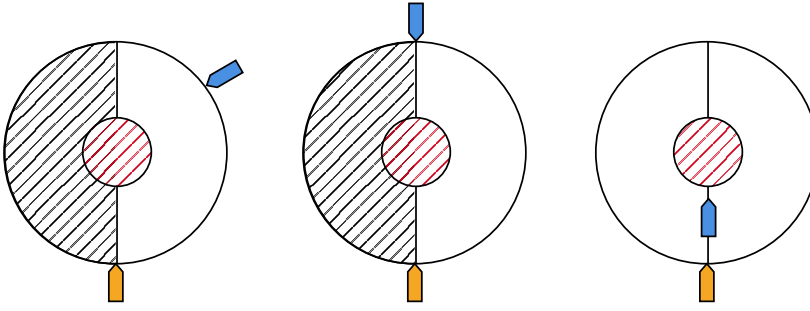
Figure A.3: Three COLREGs compliant subsets, given the different encounter types. The outer-circle radius is defined as the the limit t_{act}, with the radius of the inner circle being d_{act}.

The single vessel encounters for rules 13-15 (Fig. A.1), can be represented in terms of two circles, as shown in Fig. A.3, with the radius of the inner circle determined by d_{act} and the outer radius by t_{act}. Navigating within the inner circle violates the CPA limit, and the outer circle represents the area (given the time span) where action is required. The plain areas represent points in time which are COLREGs compliant with respect to the identified situation, assuming that the stand-on vessel maintains constant course and speed. The sampling space can be represented as a half-annulus for all three scenarios, with the overtaking scenario having the freedom to be represented as an annulus. By limiting sampling to this space, it is ensured that all points are valid with the respect to the COLREGs, rendering COLREGs specific rejection sampling unnecessary.

The notion of this COLREGs compliant subspace can be further extended by including ideas from the sampling techniques presented in [A10], namely the Informed-RRT*. The authors argued that the probability of improving the overall cost of the found solution is low, whilst continuing to sample in the original sampling space since it contains an abundance of points that do not improve the solution. The strategy of using the COLREGs compliant subset is extended such that once an initial solution is obtained using the half-annulus sampling space, a second space is introduced. This second space is the elliptical half-annulus, which has dimensions similar to the informed subset introduced in [A10]. A notable difference is that the informed subset uniformly samples an entire ellipse, whereas the COLREGs compliant subset consists of an elliptical half-annulus. The length of the ellipse is equal to the current cost of the best solution c_{best} and the width is equal to $\sqrt{c_{best}^2 - c_{min}^2}$, where c_{min} is the straight line distance between the start and end nodes.

A.3.2   Uniform sampling of the half-annulus subset

In order to uniformly sample the annulus, we apply the inversion method for non-uniform random variate generation [A37, Chapter 2]. Let X be a random variable with probability density function (PDF)

$$f(x) \triangleq \underbrace{\frac{A_{\text{inner}}}{A_{\text{circle}}}}_{c_i} + 2 \underbrace{\frac{A_{\text{outer}}}{A_{\text{circle}}}}_{c_o} x \qquad \text{(A.7)}$$

where $A_{\text{inner}} = \pi r_{min}^2$, $A_{\text{outer}} = \pi \left(r_{max}^2 - r_{min}^2 \right)$ and $A_{\text{circle}} = \pi r_{\text{max}}^2$, with inner radius r_{min} and an outer radius r_{max}. The cumulative distribution function (CDF) is then defined as,

$$F(x) \triangleq c_i x + c_o x^2 \qquad \text{(A.8)}$$

and its inverse can be found by solving the equality $F\left(F^{-1}\left(u\right)\right) = u$ for $F^{-1}(u)$ where $u \sim \mathcal{U}(0,1)$ is a realization of the uniform distribution. In the original set of parameters $F^{-1}(u)$ reads

$$F^{-1}(u) = \frac{-r_{min}^2}{2\left(r_{max}^2 - r_{min}^2\right)} + \sqrt{\left(\frac{r_{min}^2}{2\left(r_{max}^2 - r_{min}^2\right)}\right)^2 + \frac{r_{max}^2}{r_{max}^2 - r_{min}^2}u} \qquad \text{(A.9)}$$

Using the inverse CDF for sampling the radius, then a random point in the North-East plane within the annulus is given by

$$N = r\cos\theta, \quad E = r\sin\theta \qquad \text{(A.10)}$$

where $\theta \sim \mathcal{U}(0, 2\pi)$ is uniformly distributed, and

$$r = r_{\text{min}} + F^{-1}(u)(r_{\text{max}} - r_{\text{min}}). \qquad \text{(A.11)}$$

The sampling is restricted to the half-annulus by limiting the range of θ.

A.3.3   Uniform sampling of a concentric elliptical annulus

Similar to the annulus, it is possible to uniformly sample a concentric elliptical annulus avoiding rejection sampling.

Let r_{min} be the radius of the inner circle, θ the polar angle measured from the major axis of the ellipse, and $r_{max}(\theta)$ the radius of the ellipse

$$r_{max}\left(\theta\right) = \frac{ab}{\sqrt{\left(b\cos\theta\right)^2 + \left(a\sin\theta\right)^2}} \qquad \text{(A.12)}$$

with a and b the major and minor axes. To achieve uniform sampling within the concentric elliptical annulus, the likelihood of sampling θ should be higher where

$r_{max}(\theta) - r_{min}$ is large. This is equivalent to say that the PDF of θ should be

$$f(\theta)d\theta = \frac{dA}{A} \tag{A.13}$$

where dA is the differential area corresponding to the differential angle $d\theta$, and A is the total area of the concentric elliptical annulus.

Given an angle θ, the differential area dA is given by

$$dA = \frac{1}{2}\left(r_{max}^2(\theta) - r_{min}^2\right)d\theta \tag{A.14}$$

and the total area is computed as

$$A = \pi(ab - r_{min}^2) \tag{A.15}$$

i.e. the area of the ellipse subtracted the area of the inner circle. Substituting (A.12) into (A.14) the PDF of the random variable θ reads

$$f(\theta)d\theta = \frac{1}{2A}\left(\frac{(ab)^2}{(b\cos\theta)^2 + (a\sin\theta)^2} - r_{min}^2\right)d\theta \tag{A.16}$$

and the resulting CDF is

$$F(\theta) = \frac{ab\tan^{-1}\left(\frac{a\tan\theta}{b}\right) - \theta r_{min}^2}{2A}. \tag{A.17}$$

Obtaining a closed form solution of the inverse CDF for the concentric elliptical annulus is infeasible since

$$\frac{ab\tan^{-1}\left(\frac{a\tan\theta}{b}\right) - \theta r_{min}^2}{2A} = u \tag{A.18}$$

has no exact solution for θ. Using a numerical approximation, such as Newton-Raphson, the value of θ can be approximated. Given a realization u of the uniform distribution $\mathcal{U}$, the approximation is computed as

$$\theta_{k+1} = \theta_k + \frac{f(\theta_k)}{f'(\theta_k)} \tag{A.19}$$

where

$$f(\theta_k) = \frac{ab\tan^{-1}\left(\frac{a\tan\theta_k}{b}\right) - \theta_k r_{min}^2}{2A} - u \tag{A.20}$$

$$f'(\theta_k) = \frac{1}{2A}\left(\frac{(ab)^2}{(b\cos\theta_k)^2 + (a\sin\theta_k)^2} - r_{min}^2\right). \tag{A.21}$$

Due to the singularity of $\tan(\cdot)$ at $\pm\pi/2$, the uniform distribution is defined in the closed interval $[0, 0.24\bar{9}]$. The radius length is sampled in similar fashion as for the annulus.

A.3.4 Theoretical sampling performance improvements

Directly sampling a reduced valid subspace leads to a performance improvement proportional to the the ratio of the areas of the original and the reduced subspaces, assuming equal sampling speed. This can be expressed as

$$\alpha = \frac{A_{orig}}{A_{valid}} \tag{A.22}$$

where α is the relative performance improvement. Based on this, directly sampling an annulus with inner radius r_{min} and outer radius r_{max} instead of a square with side-length $2r_{max}$ leads to a performance improvement of

$$\alpha_{\text{annulus}} = \frac{A_{\text{square}}}{A_{\text{annulus}}} = \frac{4}{\pi \left(1 - (r_{min}/r_{max})^2 \right)} \tag{A.23}$$

considering that $A_{\text{square}} = 4r_{max}^2$ and $A_{\text{annulus}} = \pi(r_{max}^2 - r_{min}^2)$. The lower bound is obtained for $r_{min} = 0$, leading to a circle within a square, such that $\alpha_{min} = 4/\pi$. It follows that for a half-annulus, this lower bound doubles. For the Informed-RRT*, the performance gain obtained by directly sampling the elliptical half-annulus, instead of the regular informed ellipse, becomes

$$\alpha_{\text{ell. ann.}} = \frac{A_{\text{ell.}}}{A_{\text{ell. ann.}}} = \frac{c_{best} \sqrt{c_{best}^2 - 4r_{max}^2}}{c_{best} \sqrt{c_{best}^2 - 4r_{max}^2} - 4r_{min}^2} \tag{A.24}$$

given the area of the elliptical annulus in (A.15).

The relative performance gain obtained by sampling an elliptical annulus instead of an ellipse thus depends on the inner radius of the annulus and current best cost c_{best}. Fig. A.4 demonstrates the concentration of samples in the subspace of interest for the collision avoidance case.

A.3.5 Selecting the half-annulus or elliptical half-annulus

As described in Section A.3.1, once an initial solution is obtained, the algorithm switches to sampling the elliptical half-annulus, if it promises performance improvement. For some solution costs c_{best}, the area of the elliptical half-annulus may be larger than the half-annulus. A switching condition can be computed based on the area ratio. Let A_{he} and A_{sc} be the areas of the half ellipse and outer semi-circle, respectively. The elliptical half-annulus will be sampled, rather than the half-annulus, if

$$\frac{A_{he}}{A_{sc}} < 1 \Leftrightarrow c_{best} \sqrt{c_{best}^2 - c_{min}^2} < r_{max}^2. \tag{A.25}$$
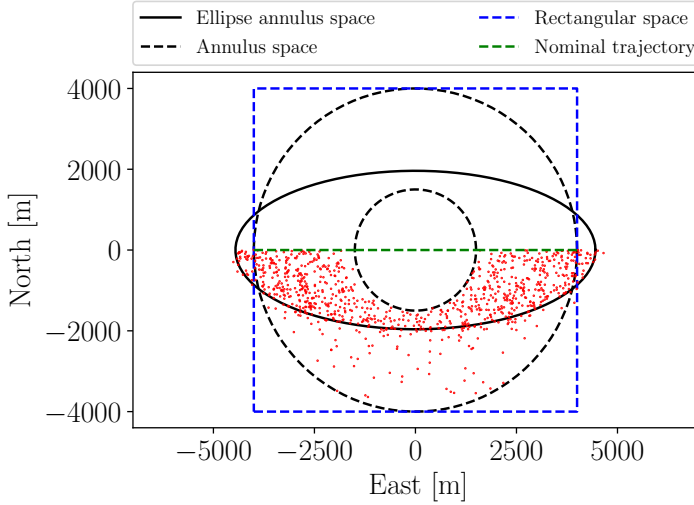
Figure A.4: The distribution $n = 1000$ samples, where the half-annulus sampling space is decreased into the elliptical half-annulus once an initial feasible path is obtained.

By squaring (A.25) and solving the associated 4th order polynomial for c_{best}, the following condition γ is obtained,

$$\gamma = \sqrt{\frac{c_{min}^2}{2} + \sqrt{\left(\frac{c_{min}^2}{2}\right)^2 + r_{max}^4}} \tag{A.26}$$

which is the resulting switching condition for sampling the elliptical half-annulus when $c_{best} < \gamma$.

A.4   COLREGs-Informed RRT*

The underlying planning algorithm consists of a marine-oriented RRT*, which is configured to sample in the COLREGs compliant subset, thus increasing sampling quality and avoiding rejection sampling due to breaching the COLREGs.

Algorithm A.1 (adopted from [A10]) describes the main structure of the marine-oriented RRT* procedure, where the core RRT* components are based on the work presented by [A9]. The method grows a tree $\mathcal{T} = (V, E)$, where V and E represent the sets of nodes and edges, respectively. A given node z represents a North-East position of the vessel at time t, with the edges containing relevant cost information. The underlying RRT* method is modified such that nodes resemble waypoints which are compliant with the underlying track-control scheme and the maneuvering capabilities of the vessel. The method Feasible($z_{nearest}, z_{new}, x_{new}$) is responsible for ensuring validity of the sampled points and the trajectory between

---

Algorithm A.1: RRT* (Modified sampling)

    Given: z_{start}, z_{goal}

1   $V \leftarrow \{z_{start}\}, \quad E \leftarrow \emptyset, \quad \mathcal{T} = (V, E);$

2   **for** i $= 1 \ldots N$ **do**

3      $c_{best} \leftarrow \min_{z_{soln} \in Z_{soln}} \{\texttt{Cost}(z_{soln})\};$

4      $z_{rand} \leftarrow \texttt{Sample}(z_{start}, z_{goal}, c_{best});$

5      $z_{nearest} \leftarrow \texttt{NearestNode}(\mathcal{T}, z_{rand});$

6      $(z_{new}, x_{new}) \leftarrow \texttt{ExtendTowards}(z_{nearest}, z_{rand});$

7   **if** $\texttt{Feasible}(z_{nearest}, z_{new}, x_{new})$ **then**

8          $\mathcal{T} \leftarrow \texttt{InsertNode}(\mathcal{T}, z_{new});$

9          $Z_{near} \leftarrow \texttt{Near}(\mathcal{T}, z_{new}, r);$

10         $z_{min} \leftarrow z_{nearest};$

11         $c_{min} \leftarrow \texttt{Cost}(z_{min}) + \texttt{Line}(z_{min}, z_{new});$

12   **for** $\forall z_{near} \in Z_{near}$ **do**

13             $c_{new} \leftarrow \texttt{Cost}(z_{near}) + \texttt{Line}(z_{near}, z_{new});$

14   **if** $c_{new} < c_{min}$ **then**

15   **if** $\texttt{Feasible}(z_{near}, z_{new}, x_{new})$ **then**

16                   $z_{min} \leftarrow z_{near};$

17                   $c_{min} \leftarrow c_{new};$

18         $E \leftarrow E \cup \{z_{min}, z_{new}\};$

19   **for** $\forall z_{near} \in Z_{near}$ **do**

20             $c_{near} \leftarrow \texttt{Cost}(z_{near});$

21             $c_{new} \leftarrow \texttt{Cost}(z_{new}) + \texttt{Line}(z_{new}, z_{near});$

22   **if** $c_{new} < c_{near}$ **then**

23   **if** $\texttt{Feasible}(z_{new}, z_{near}, x_{near})$ **then**

24                   $z_{parent} \leftarrow \texttt{Parent}(z_{near});$

25                   $E \leftarrow E \backslash \{z_{parent}, z_{near}\};$

26                   $E \leftarrow E \cup \{z_{new}, z_{near}\};$

27   **if** $\texttt{InGoalRegion}(z_{new})$ **then**

28             $Z_{soln} \leftarrow Z_{soln} \cup \{z_{new}\}$

29   **return** $\mathcal{T};$

---

two nodes with respect to vessel capabilities (e.g. the turning radius (A.1)), static obstacles and dynamic obstacles. The red lines (Lines 3, 4 and 28) indicate the modifications required for sampling the proposed COLREGs compliant subsets. Until an initial solution is obtained, the sampling ($\texttt{Sample}(z_{start}, z_{goal}, c_{best})$) is solely performed using the proposed method in Section A.3.2, i.e the half-annulus. Once an initial solution is obtained, the cost is compared to the threshold (A.26), which then initiates the sampling routine described in Section A.3.3, if sampling the elliptical half-annulus provides more valuable samples.
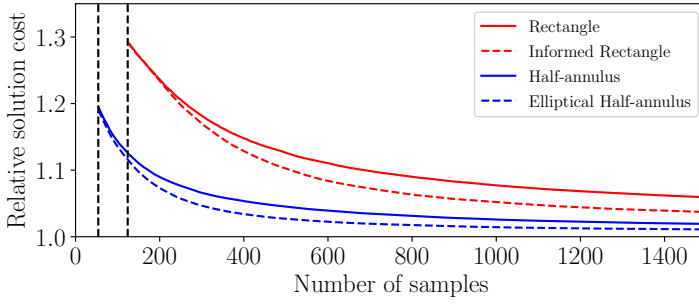
(a) Relative solution cost (c_{best}/c_{min}). The mean number of samples required to find an initial solution, using the half-annulus and rectangular spaces, is 54 and 124 respectively.
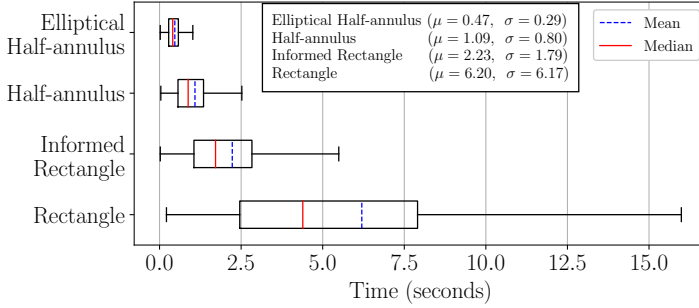
(b) Time required to be within 5% of the optimal solution. The μ and σ values indicate the mean and standard deviation for the computational time in seconds.

Figure A.5: Comparison between the Rectangular space ([A9], [A15]), Informed Rectangular space ([A10]) and the two proposed sampling spaces. Each comparison is done over 2500 trials, with the only algorithmic modifications occurring within Line 4 in Algorithm A.1, and the utilization of rejection sampling for COLREGs compliance in the two former sampling methods.

A.5   Results

The proposed COLREGs compliant sampling stagies presented in Section A.3 are implemented to yield a marine-oriented RRT* algorithm. Fig. A.6 shows a single vessel encounter, where own ship is the give-way vessel in a crossing scenario. The computed path deviation ensures a reaction to the approaching target vessel in ample time, and therefore adheres to Rule 16. Furthermore, the deviation from the nominal trajectory is both COLREGs compliant (w.r.t. Rule 15) and collision free. This is guaranteed by design for both crossing and head-on scenarios for any initial configuration of own ship and target vessel for which TCPA $> t_{act}$. In an overtaking
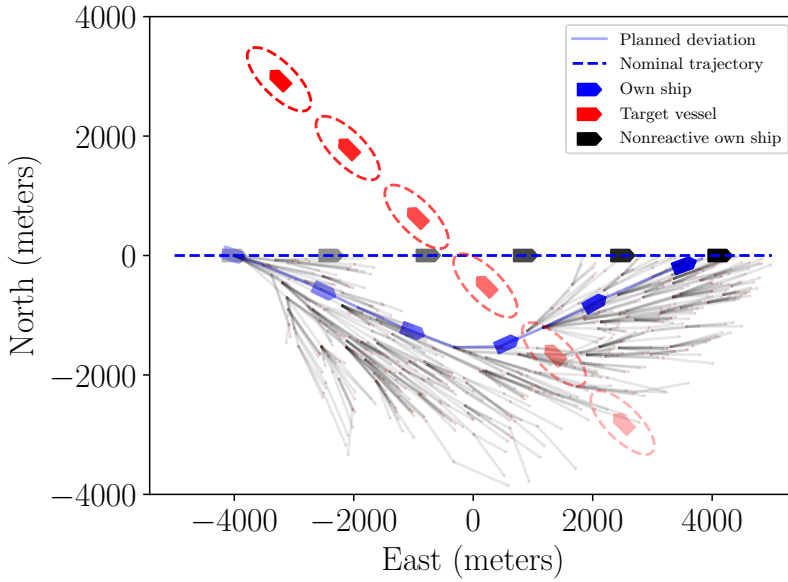
Figure A.6: Proposed path deviation to a starboard crossing computed by the COLREGs-Informed RRT*

scenario the computed path is still guaranteed to be COLREGs compliant; however the ability to find a collision free path depends on the difference in forward speed between own ship and target vessel. This is due the chosen definition of the goal region for the RRT* algorithm.

The performance of the two proposed sampling schemes is compared to the baseline RRT* [A9], [A15] and Informed-RRT* [A10] algorithms, which use rectangular sampling spaces and rejection sampling to adhere to the COLREGs. The methods are evaluated in terms of the obtained solution cost after n samples, number of iterations required to obtain an initial feasible solution, and overall execution speed.

As pointed out by the theoretical analysis in Section A.3.4, an increased performance is obtained by sampling directly in the COLREGs compliant subspace. Sampling in the half-annulus, compared to the rectangular space, obtains an initial path in a shorter amount of time (proportional to the area difference). Fig. A.5a shows the relative solution cost, as well as the average amount of samples required to find an initial solution. The proposed COLREGs compliant subspaces achieve a higher sampling density in the relevant regions and thus find an initial solution with fewer iterations. Fig. A.5b compares the computational speed of RRT* for different sampling strategies, and it is evident the clear computational advantage offered by the proposed sampling methods.

A.6   Conclusions

The paper presented the concept of COLREGs compliant sampling spaces for use within the RRT* algorithm to generate collision free path alterations for vessels in close quarters. The proposed sampling spaces, i.e. the half-annulus and elliptical half-annulus, directly encode the COLREGs rules 13-15; hence the RRT* algorithm searches for path deviations that are guaranteed to adhere the rules of safe navigation. This results in a significant enhancement of the path planner performance when compared to reference sampling strategies with respect to the metrics of mean time to discover a feasible path, computational speed to find the optimal solution and convergence to the optimal cost. This improvement is due to the specialization of the sampling space, which both increases the probability of gaining value for each sample and removes the need of rejection sampling. These high-gain sampling strategies could prove valuable when extending the implementation to include additional complexities, such as system dynamics, since it will result in fewer solutions to boundary-value problems.

A.7   References

[A1]   L. Ranieri, S. Digiesi, B. Silvestri, and M. Roccotelli, "A review of last mile logistics innovations in an externalities cost reduction vision," *Sustainability*, vol. 10, no. 3, p. 782, 2018.

[A2]   C. M. d. Oliveira, R. Albergaria De Mello Bandeira, G. Vasconcelos Goes, D. N. Schmitz Gonçalves, and M. D. A. D'Agosto, "Sustainable vehicles-based alternatives in last mile distribution of urban freight transport: A systematic literature review," *Sustainability*, vol. 9, no. 8, p. 1324, 2017.

[A3]   A. Komianos, "The autonomous shipping era. operational, regulatory, and quality challenges," *TransNav: International Journal on Marine Navigation and Safety of Sea Transportation*, vol. 12, 2018.

[A4]   M. Kim, T.-H. Joung, B. Jeong, and H.-S. Park, "Autonomous shipping and its impact on regulations, technologies, and industries," *Journal of International Maritime Safety, Environmental Affairs, and Shipping*, vol. 4, no. 2, pp. 17–25, 2020.

[A5]   EMSA, *Annual overview of marine casualties and incidents 2019*, 2019.

[A6]   S. M. LaValle, "Rapidly-exploring random trees: A new tool for path planning," 1998.

[A7]   S. M. LaValle and J. J. Kuffner, "Randomized Kinodynamic Planning," *The International Journal of Robotics Research*, vol. 20, no. 5, pp. 378–400, May 2001.

[A8]   S. Karaman and E. Frazzoli, "Incremental sampling-based algorithms for optimal motion planning," *Robotics Science and Systems VI*, vol. 104, no. 2, 2010.

[A9]   S. Karaman and E. Frazzoli, "Sampling-based algorithms for optimal motion planning," *The international journal of robotics research*, vol. 30, no. 7, pp. 846–894, 2011.

[A10] J. D. Gammell, S. S. Srinivasa, and T. D. Barfoot, "Informed RRT*: Optimal sampling-based path planning focused via direct sampling of an admissible ellipsoidal heuristic," *IEEE International Conference on Intelligent Robots and Systems*, pp. 2997–3004, 2014.

[A11] H. T. L. Chiang and L. Tapia, "COLREG-RRT: An RRT-Based COLREGS-Compliant Motion Planner for Surface Vehicle Navigation," *IEEE Robotics and Automation Letters*, vol. 3, no. 3, pp. 2024–2031, 2018.

[A12] J. J. Park and B. Kuipers, "Feedback motion planning via non-holonomic RRT* for mobile robots," *IEEE International Conference on Intelligent Robots and Systems*, vol. 2015-Decem, pp. 4035–4040, 2015.

[A13] P. Pharpatara, B. Herisse, and Y. Bestaoui, "3-D Trajectory Planning of Aerial Vehicles Using RRT*," *IEEE Transactions on Control Systems Technology*, vol. 25, no. 3, pp. 1116–1123, 2017.

[A14] R. Zaccone and M. Martelli, "A random sampling based algorithm for ship path planning with obstacles," *Proceedings of the International Ship Control Systems Symposium (iSCSS)*, vol. 2, 2018, p. 4.

[A15] R. Zaccone and M. Martelli, "A collision avoidance algorithm for ship guidance applications," *Journal of Marine Engineering and Technology*, vol. 19, no. sup1, pp. 62–75, 2020.

[A16] R. Zaccone, M. Martelli, and M. Figari, "A COLREG-compliant ship collision avoidance algorithm," *2019 18th European Control Conference, ECC 2019*, no. August, pp. 2530–2535, 2019.

[A17] Y. Huang, L. Chen, P. Chen, R. R. Negenborn, and P. van Gelder, "Ship collision avoidance methods: State-of-the-art," *Safety science*, vol. 121, pp. 451–473, 2020.

[A18]   L. Hu, W. Naeem, E. Rajabally, G. Watson, T. Mills, Z. Bhuiyan, and I. Salter, "COLREGs-compliant path planning for autonomous surface vehicles: A multiobjective optimization approach," *IFAC-PapersOnLine*, vol. 50, no. 1, pp. 13 662–13 667, 2017.

[A19]   L. Hu, W. Naeem, E. Rajabally, G. Watson, T. Mills, Z. Bhuiyan, C. Raeburn, I. Salter, and C. Pekcan, "A multiobjective optimization approach for COLREGs-compliant path planning of autonomous surface vehicles verified on networked bridge simulators," *IEEE Transactions on Intelligent Transportation Systems*, 2019.

[A20]   W. Naeem, G. W. Irwin, and A. Yang, "COLREGs-based collision avoidance strategies for unmanned surface vehicles," *Mechatronics*, vol. 22, no. 6, pp. 669–678, 2012.

[A21]   W. Naeem, S. C. Henrique, and L. Hu, "A reactive COLREGs-compliant navigation strategy for autonomous maritime navigation," *IFAC-PapersOnLine*, vol. 49, no. 23, pp. 207–213, 2016.

[A22]   B. H. Eriksen and M. Breivik, "MPC-based mid-level collision avoidance for ASVs using nonlinear programming," *2017 IEEE Conference on Control Technology and Applications (CCTA)*, Institute of Electrical and Electronics Engineers (IEEE), 2017.

[A23]   B. H. Eriksen, M. Breivik, E. F. Wilthil, A. L. Flåten, and E. F. Brekke, "The branching-course model predictive control algorithm for maritime collision avoidance," *Journal of Field Robotics*, vol. 36, no. 7, pp. 1222–1249, 2019.

[A24]   M. R. Benjamin and J. A. Curcio, "Colregs-based navigation of autonomous marine vehicles," *2004 IEEE/OES Autonomous Underwater Vehicles (IEEE Cat. No. 04CH37578)*, IEEE, 2004, pp. 32–39.

[A25]   M. R. Benjamin, J. A. Curcio, J. J. Leonard, and P. M. Newman, "Navigation of unmanned marine vehicles in accordance with the rules of the road," *Proceedings 2006 IEEE International Conference on Robotics and Automation, 2006. ICRA 2006.*, IEEE, 2006, pp. 3581–3587.

[A26]   Y. Singh, S. Sharma, R. Sutton, D. Hatton, and A. Khan, "A constrained A* approach towards optimal path planning for an unmanned surface vehicle in a maritime environment containing dynamic obstacles and ocean currents," *Ocean Engineering*, vol. 169, pp. 187–201, 2018.

[A27]   S. Campbell and W. Naeem, "A rule-based heuristic method for COLREGS-compliant collision avoidance for an unmanned surface vehicle," *IFAC Proceedings Volumes*, vol. 45, no. 27, pp. 386–391, 2012.

[A28] S. Campbell, M. Abu-Tair, and W. Naeem, "An automatic COLREGs-compliant obstacle avoidance system for an unmanned surface vehicle," *Proceedings of the Institution of Mechanical Engineers, Part M: Journal of Engineering for the Maritime Environment*, 2014.

[A29] S. Ni, Z. Liu, Y. Cai, and X. Wang, "Modelling of ship's trajectory planning in collision situations by hybrid genetic algorithm," *Polish Maritime Research*, vol. 25, no. 3, pp. 14–25, 2018.

[A30] S. Ni, Z. Liu, and Y. Cai, "Ship manoeuvrability-based simulation for ship navigation in collision situations," *Journal of Marine Science and Engineering*, vol. 7, no. 4, 2019.

[A31] A. Lazarowska, "Ship's trajectory planning for collision avoidance at sea based on ant colony optimisation," *Journal of Navigation*, vol. 68, no. 2, pp. 291–307, 2015.

[A32] A. Lazarowska, "Research on algorithms for autonomous navigation of ships," *WMU Journal of Maritime Affairs*, vol. 18, no. 2, pp. 341–358, Jun. 2019.

[A33] B. C. Shah, P. Švec, I. R. Bertaska, A. J. Sinisterra, W. Klinger, K. von Ellenrieder, M. Dhanak, and S. K. Gupta, "Resolution-adaptive risk-aware trajectory planning for surface vehicles operating in congested civilian traffic," *Autonomous Robots*, vol. 40, no. 7, pp. 1139–1163, Oct. 2016.

[A34] M. G. Hansen, T. K. Jensen, T. Lehn-Schiøler, K. Melchild, F. M. Rasmussen, and F. Ennemark, "Empirical ship domain based on ais data," *The Journal of Navigation*, vol. 66, no. 6, pp. 931–940, 2013.

[A35] IMO, *Convention on the international regulations for preventing collisions at sea, 1972 (COLREGs)*. 1972.

[A36] D. Papageorgiou, M. Blanke, M. Lützen, M. Bennedsen, J. Mogensen, and S. Hansen, "Parallel automaton representation of marine crafts' COLREGs-based manoeuvering behaviours," *IFAC-PapersOnLine*, vol. 52, no. 21, pp. 103–110, 2019.

[A37] L. Devroye, *Non-Uniform Random Variate Generation*. Springer New York, 1986.

Paper B

Grounding-aware RRT* for Path Planning and Safe Navigation of Marine Crafts in Confined Waters

Thomas T. Enevoldsen[1*] and Roberto Galeazzi[1]

[1]Automation and Control Group, Department of Electrical Engineering, Technical University of Denmark, DK-2800 Kgs. Lyngby, Denmark {tthen,ccrein,rg}@elektro.dtu.dk

Abstract:
The paper presents a path planning algorithm based on RRT* that addresses the risk of grounding during evasive manoeuvres to avoid collision. The planner achieves this objective by integrating a collective navigation experience with the systematic use of water depth information from the electronic navigational chart. Multivariate kernel density estimation is applied to historical AIS data to generate a probabilistic model describing seafarer's best practices while sailing in confined waters. This knowledge is then encoded into the RRT* cost function to penalize path deviations that would lead own ship to sail in shallow waters. Depth contours satisfying the own ship draught define the actual navigable area, and triangulation of this non-convex region is adopted to enable uniform sampling. This ensures the optimal path deviation.

B.1   Introduction

According to a report by the European Maritime Safety Agency (EMSA), incidents rooted within human error, such as collision, contact and grounding, account for 44% of the total, with specifically grounding accounting for 13% [B1]. Uğurlu *et al.* [B2] investigated grounding incidents caused by human error, and found that poor usage of the available equipment and poor assessment of the situation are key triggers. Decision support systems for collision and grounding avoidance can significantly improve the safety of navigation, by providing the human navigator with path alterations that are optimal with respect to the collision scenario and surrounding environment.

Navigation in confined waters is challenging since collision avoidance must be weighed against the risk of grounding, possibly overestimated by navigators in search for more comfortable, deeper waters. Nonetheless, the collective navigation experience of seafarers across years of sailing may enable the creation of "good seamanship" models to inform the collision and grounding avoidance algorithms about best sailing practices. This paper researches a method to harvest such collective navigation experience and encode it into a probabilistic model describing seafarers' sailing behaviour in confined waters. Further, the paper specializes the RRT* path planning algorithm by integrating this probabilistic model with water depths information retrieved from the electronic navigational chart (ENC) to compute optimal path deviations to deconflict collision scenarios.

B.1.1   Related work

Methods for quantifying and including relevant environmental information for safe navigation and collision avoidance within confined waters has been widely investigated. The review by Huang *et al.* [B3] provides a broad insight into the typical components required for collision avoidance methods, with a distinction between motion prediction, conflict detection and resolution. Vagale *et al.* [B4], [B5] presented a detailed review of the path planning aspect of collision avoidance, discussing the potential advantages and challenges for autonomous surface vessels, as well as presenting various planning schemes.

Chen *et al.* [B6] used a binary occupancy grid along with the Fast Marching Method, and Singh *et al.* [B7] similarly with the A* algorithm. Bitar *et al.* [B8] detailed a two-stage trajectory planner, where the initial step uses a discretized polygonal representation of the configuration space, such that a hybrid A* algorithm can compute an initial dynamically feasible trajectory. Xue *et al.* [B9] generated potential functions from arbitrary polygons, as well as satellite images, for use with

an Artificial Potential Fields algorithm. Both Candeloro *et al.* [B10] and Niu *et al.* [B11] combine the use of Voronoi diagrams with real spatial data. Martinsen *et al.* [B12] detailed the use of Constrained Delaunay Triangulation on land contours, to obtain an adjacency graph for trajectory refinement. Tsou [B13] formed obstacles and Predicted Areas of Danger (PAD) by utilizing information from the Electronic Chart Display and Information System (ECDIS) and AIS, in order to plan using a genetic algorithm. Reed and Schmidt [B14] and Otterholm [B15] both detailed the use S-57 charts in the context of collision avoidance, and presented various approximations for the obstacles.

Sampling-based planning strategies are prime-candidates for computing both feasible and optimal paths within the space such as those defined by the non-convex depth contours. Since its inception, the Rapidly-exploring Random Trees (RRT) algorithm [B16] has played an important role in sampling-based strategies, with Karaman and Frazzoli [B17] introducing the asymptotically optimal RRT*. Within sampling-based collision avoidance schemes for marine crafts, Chiang and Tapia [B18] detailed the use of a non-holonomic RRT, modelling the land masses as arbitrary polygons. Zaccone [B19] presented a COLREGs compliant RRT*, which minimized path length, curvature and repulsion from objects. Enevoldsen *et al.* [B20] presented the COLREGs-Informed RRT*, which directly samples COLREGs compliant trajectories for single vessel encounters in open-waters.

B.1.2   Novelty and contribution

This paper proposes a novel marine-oriented RRT* path planning algorithm for collision and grounding avoidance of vessels sailing in confined waters. Current sampling-based algorithms adopted within the marine domain, such as RRT*, consider simplified or artificial representations of the environment. In contrast this contribution operates directly on environment information (e.g. depth contours) extracted from the real electronic navigational chart. We introduce the concept of *collective navigation experience* to describe the best practices of seafarers while sailing in a given restricted sea region. We propose to use multivariate kernel density estimation on historical AIS data to generate probabilistic models that describe the seafarers' behaviour in steering vessels of different draught. We define the planning region by extracting from the ENC depth contours satisfying the vessel's draught requirements, and we propose triangulation of such non-convex polygons as a mean to achieve uniform sampling of the space. This ensures optimality of the sought path deviation. The probabilistic model is exploited in the RRT* cost function to sway the path planner towards deconflicting path alterations that favor comfortable
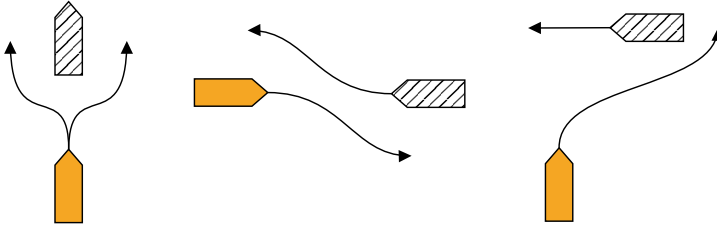
Figure B.1: Encounters described by COLREGs rules 13-15, i.e. overtaking, head-on and crossing scenarios. The solid coloured vessel is in a give-way situation.

navigation, as seen from the eyes of human navigator, while still exploring the whole navigable area as described by the ENC.

B.2   Preliminaries

B.2.1   Vessel assumptions

Own ship

This study concerns path planning for large vessels with maneuvering restrictions due to their draught and minimum required turning radius, such as ro-ro vessels, container feeders, bulk carriers, etc. It is assumed that a track control system is responsible to steer the vessel based on a sequence of waypoints $W_i = (N_i, E_i, R_i)$, where N_i is the North position, E_i is the East position, and R_i is the radius of acceptance. The manoeuvring capabilities (e.g. minimal turning radius) of own ship are accounted for when generating a feasible waypoint sequence.

Target vessels

Target vessels are characterized by means of a comfort zone described by an ellipse whose dimensions are related to the ship length L, with $8L$ and $3.2L$ defining major and minor axis, respectively [B21].

B.2.2   COLREGs description and compliance

Any collision avoidance system must adhere to the "rules-of-the-road", namely the COLREGs. The most frequently considered rules are Rules 13-15, which deal with overtaking, head-on and crossing scenarios, respectively. The rules are defined for single-vessel encounters, assuming both vessels are power-driven. Figure B.1 visualizes the before-mentioned rules, where the vessel in give-away situation must yield for the stand-on vessel. For Rules 14 and 15, the give-way vessel must pass

on the starboard side of the stand-on vessel, whereas both a port and starboard passing for Rule 13 is valid. The relative bearing between own ship and target vessel determines the collision scenario at hand. For further details regarding the relevant COLREGs, interpretation of the relative bearing, and assessment of the collision scenario see [B20].

B.2.3 Electronic navigational charts

The electronic chart display and information system is a compliant, digital alternative to paper nautical charts. The ECDIS serves the navigator with important information, typically contained within the conventional paper charts, as well as information from RADAR and AIS. The Electronic Navigational Charts (ENC) must conform to the S-57 standard in order to be used with the ECDIS. Within the S-57 charts various information layers exist, containing data about land and depth contours, buoys identifiers and placement, recommended navigational tracks, dredges, restricted areas, etc. The information contained within the ENC is fundamental for navigating in confined waters, since it directly encodes geographical areas which are feasible with respect to the draught of a given vessel. Therefore, the information layer of the ENC utilized for this particular study is that one containing the depth contours, namely `DEPARE`. For visualization purposes the land masses contained within `LNDARE` are also extracted. Through software, all depth contours intersecting with a geofilter are selected and subsequently cropped (Fig. B.2a), resulting in a collection of polygons described by their geodetic coordinates, minimum and maximum water depths. Figure B.2b visualizes the cropped depth contours with minimum water depth greater than 6m (white areas are waters shallower than 6m).

B.3 Collective navigation experience

B.3.1 Multivariate kernel density estimation

Kernel density estimation (KDE) belongs to the family of non-parametric methods for estimating an unknown probability density function based on a finite data sample.

Let $\mathbf{X}_i = (X_{i1}, X_{i2}, \ldots, X_{ip})^\top$, $i = 1, 2, \ldots, n$, be a sequence of independent and identically distributed p-variate random variables drawn from an unknown density f. Then, the general form of the p-dimensional multivariate kernel density estimator is [B22]

$$\hat{f}(\mathbf{x}, \mathbf{H}) = \frac{1}{n} \sum_{i=1}^{n} |\mathbf{H}|^{-1/2} K(\mathbf{H}^{-1/2}(\mathbf{x} - \mathbf{X}_i)) \tag{B.1}$$

(a) Geofiltered (black)

(b) Cropped contours

(c) Triangulated feasible depths
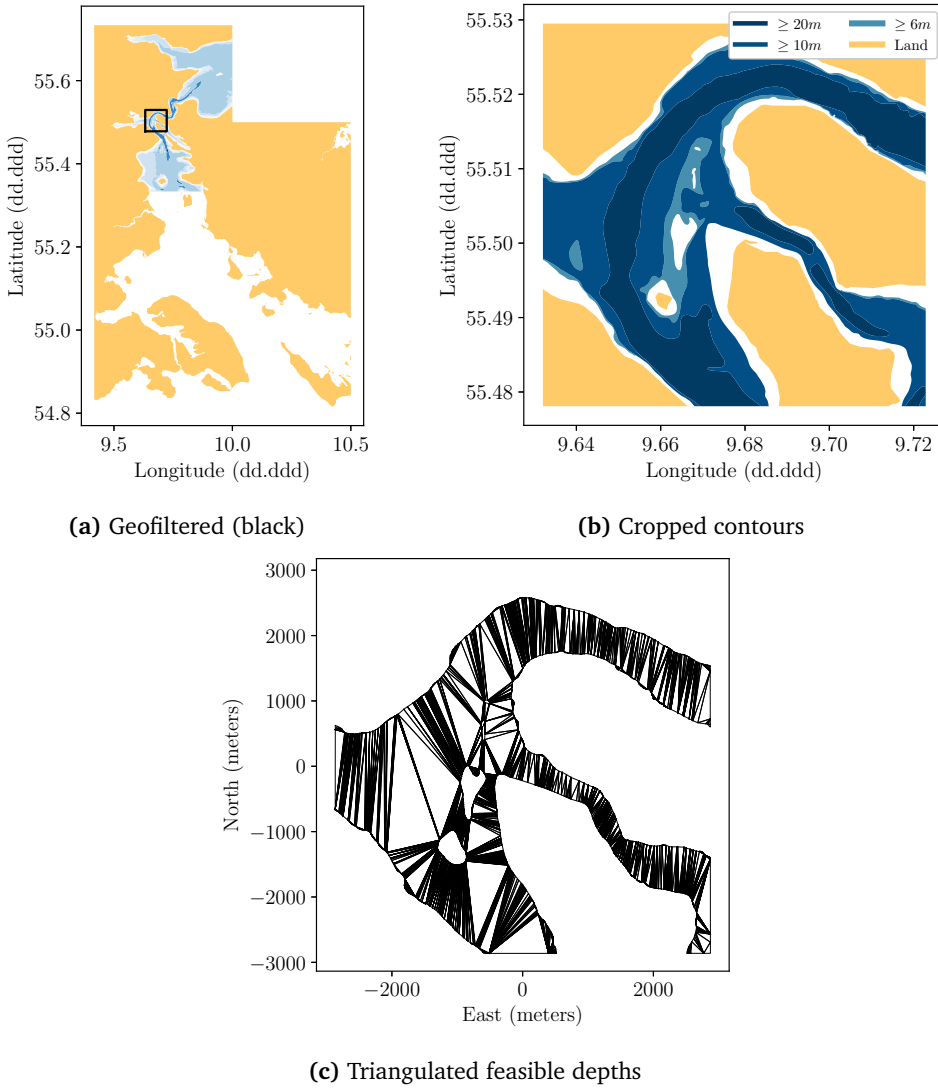
Figure B.2: Extracting data from the S-57 ENC using a pre-defined geofilter (black square in Fig. B.2a), and subsequently manipulating the polygons in order to extract contours with a specified minimum water depth (Fig. B.2b).

where $\mathbf{H} = \mathbf{H}^\top > 0$ is the non-random $p \times p$ bandwidth matrix, and $K(\cdot)$ is the unscaled kernel.

The bandwidth matrix and the kernel determines the degree of smoothness of the estimated density, which in fact inherits all the smoothness properties of the underlying kernel. Probability density functions are generally adopted as kernel functions. This implies that the area under the kernel must be equal to one, and that

the kernel function is always positive. A commonly adopted kernel is the multivariate normal density

$$K(\mathbf{z}) = \frac{1}{\sqrt{(2\pi)^p}} \exp\left(-\frac{1}{2}\mathbf{z}^\top \mathbf{z}\right) \tag{B.2}$$

The bandwidth matrix $\mathbf{H}$ determines both the amount and orientation of the smoothing. In the most general case of an unconstrained bandwidth, there are $n(n+1)/2$ parameters to be determined in order to achieve the desired level of smoothing. Due to the complexity of solving the unconstrained case, it is common to constrain the bandwidth matrix such that $\mathbf{H} = h^2\mathbf{I}_p$ with $h > 0$ or $\mathbf{H} = \mathrm{diag}\{h_1^2, h_2^2 \dots, h_p^2\}$ with $h_i > 0$. In these cases there is a wide array of methods that can be applied to estimate the values of the parameters h_i from the available data [B22, Chapter 4]. Estimation problems addressing large data sets with high dimensionality show a computational complexity as high as $O(n^2)$, if a naive evaluation of the kernel function $K(\cdot)$ is performed. Several methods have been developed to accelerate the computation of the kernel functions [B23], and one of the most effective applies the Fast Fourier Transform (FFT) [B24], [B25].

B.3.2 Automatic Identification System (AIS)

The overall collection of historical AIS data is represented as the set $\mathcal{A}$, whose elements are messages $\boldsymbol{m}_i$

$$\boldsymbol{m}_i = \begin{bmatrix} \mathrm{MMSI}_i & t_i & \mathrm{SOG}_i & D_i & \lambda_i & \phi_i \end{bmatrix} \tag{B.3}$$

containing the following data entries: the Maritime Mobile Service Identity MMSI_i, the timestamp t_i, the speed-over-ground SOG_i, the vessel draught D_i, the vessel position in geodetic coordinates (latitude λ_i and longitude ϕ_i). The generation of the collective navigation experience for a specific geographical region is based on a subset of $\mathcal{A}$, which contains data pertaining to vessels sailing in such region. Let introduce the geodetic region of interest $\mathcal{R} = \{(\lambda_i, \phi_i) \mid \lambda_{min} \leq \lambda_i \leq \lambda_{max} \wedge \phi_{min} \leq \phi_i \leq \phi_{max}\}$, and the speed range of interest $\mathcal{V} = \{\mathrm{SOG}_i \mid \mathrm{SOG}_{min} < \mathrm{SOG}_i < \mathrm{SOG}_{max}\}$. Then the set containing the data relevant to the estimation of the collective navigation experience for vessels with draught larger than or equal to a given draught $\bar{D}$ is defined as

$$\mathcal{N}_{\bar{D}} \triangleq \left\{\boldsymbol{m}_i \in \mathcal{A} \mid (\lambda_i, \phi_i) \in \mathcal{R} \wedge \mathrm{SOG}_i \in \mathcal{V} \wedge D_i \geq \bar{D}\right\} \tag{B.4}$$

The set $\mathcal{V}$ guarantees that only AIS messages from marine vessels are considered, leaving out from the set $\mathcal{N}_{\bar{D}}$ data referring to drifting buoys and fast moving rescue vehicles.
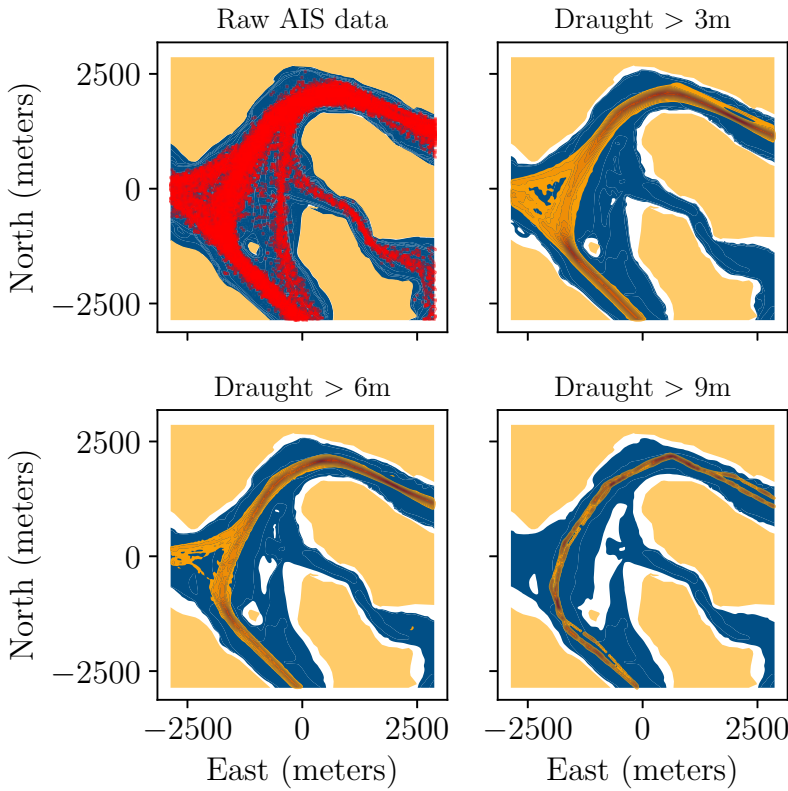
Figure B.3: Various KDEs within the Little Belt area of Denmark, for different draughts and depths.

B.3.3   Learning navigators' best practices in confined waters

Navigating within confined waters presents a plethora of new variables for navigators to consider, including the trade-off between voyage duration and safe passage. Safe navigation in complex waters is heavily dependant on the traffic within said waters, and the constraints presented by shallow waters. These trade-offs occurring within Danish waters have been documented through a national database of AIS messages. By computing multivariate KDEs using the past positions of vessels within the region of interest, the collective navigation experience can be quantified in a probabilistic sense.

The top left corner of Fig. B.3 shows an example of AIS data for the region of interest $\mathcal{R} = \{(\lambda_i, \phi_i) \mid 55.48° \leq \lambda_i \leq 55.53° \wedge 9.64° \leq \phi_i \leq 9.72°\}$, corresponding to the Little Belt area in Denmark. The data refers to vessels navigating in the speed range of interest $\mathcal{V} = \{\mathrm{SOG}_i \mid 0.5\mathrm{kn} < \mathrm{SOG}_i < 50\mathrm{kn}\}$. Different KDEs can then be estimated by creating the set $\mathcal{N}_{\bar{D}}$ for different values of $\bar{D}$. For the

estimation process we utilized the multivariate normal density as kernel function, and the constrained bandwidth model $\mathbf{H} = h^2 \mathbf{I}_p$ where h was hand-tuned. The actual estimation of the kernel density was performed leveraging the Python toolbox KDEpy [B26]; specifically the FFT-based KDE scheme was utilized for its superior computational speed on the large AIS data set. Figure B.3 details the resulting KDEs estimated on three sets $\mathcal{N}_{\bar{D}}$ for increasing value of $\bar{D}$, and the underlying Electronic Navigational Chart (ENC) data corresponds to waters whose minimal depth is greater than the specified draught. By excluding parts of the data set based on draught restrictions, the overall encoded behaviour from previous navigators changes. An important thing to note in this particular study-case is that, despite there is a direct northbound path, the majority of density moves North-West, before continuing North-East. This indicates that through past experiences, the navigators deem the passage directed North less safe, due to the heavily restricted waters, compared to prolonging the journey and increasing the overall safety margin. This shows that the probabilistic representation contains valuable information regarding the safe navigation of confined water areas. As observed, past navigators consistently practice navigational safety, which is evident within the historical data, where the majority of the density maintains a safe distance from shallow waters and other waters which are associated with higher navigational risks.

B.4 Grounding-aware RRT*

B.4.1 Problem definition

The generalized optimal planning problem considered in this paper is defined in a similar fashion to [B27]. Let $\mathcal{X} \subseteq \mathbb{R}^n$ be the state space, which is divided into two subsets, X_{free} and X_{obs}, with $X_{\text{free}} = \mathcal{X} \backslash X_{\text{obs}}$. The states within X_{free} contain all states that are feasible with respect to maneuvering constraints, COLREGs compliance, collision and grounding. Let $\mathbf{x}_{\text{start}} \in X_{\text{free}}$ be the initial state at $t = 0$ and $\mathbf{x}_{\text{goal}} \in X_{\text{free}}$ be the desired final state. Let $\sigma : [0, 1] \mapsto \mathcal{X}$ be a sequence of states constituting a found path and Σ be the set of all nontrivial and feasible paths. The objective is then to find the optimal path σ^*, which minimizes a cost function while connecting $\mathbf{x}_{\text{start}}$ to $\mathbf{x}_{\text{goal}}$ through X_{free},

$$\sigma^* = \underset{\sigma \in \Sigma}{\arg \min} \left\{ c(\sigma) \mid \sigma(0) = \mathbf{x}_{\text{start}} , \, \sigma(1) = \mathbf{x}_{\text{goal}} , \, \forall s \in [0, 1], \, \sigma(s) \in X_{\text{free}} \right\}. \quad \text{(B.5)}$$

We propose a cost function that trades off between two performance indexes: the path length and the grounding risk. The latter is defined as the complementary of the normalized kernel density estimate, and represents the discomfort of fellow navigators when manoeuvring vessels too close to shallow waters. The cost function

---

Algorithm B.1: RRT*

    Given : x_{start}, x_{goal}

1 $V \leftarrow \{x_{start}\}, \quad E \leftarrow \emptyset, \quad \mathcal{T} = (V, E)$;

2 **for** i $= 1 \ldots N$ **do**

3      $x_{rand} \leftarrow$ `Sample`(x_{goal});

4      $x_{nearest} \leftarrow$ `NearestNode`($\mathcal{T}$, x_{rand});

5      $x_{new} \leftarrow$ `ExtendTowards`($x_{nearest}$, x_{rand});

6   **if** `Feasible`($x_{nearest}$, x_{new}) **then**

7          $X_{near} \leftarrow$ `Near`($\mathcal{T}$, x_{new}, r);

8          $x_{min} \leftarrow$ `BestParent`(X_{near}, $x_{nearest}$, x_{new});

9          $\mathcal{T} \leftarrow$ `InsertNode`($\mathcal{T}$, x_{new});

10         $\mathcal{T} \leftarrow$ `ReWire`($\mathcal{T}$, X_{near}, x_{min}, x_{new});

11 **return** $\mathcal{T}$;

---

reads as

$$c(\sigma) = w_1(1 - \bar{F}(\sigma)) + w_2 l(\sigma) \tag{B.6}$$

with scalar weights w_i, the over all path length $l(\sigma)$, and

$$\bar{F}(\sigma) = \hat{f}(\sigma, \mathbf{H}) / \max \left(\hat{f}(\mathbf{X}, \mathbf{H}) \right) \tag{B.7}$$

is the normalized kernel density along the path σ.

Remark B.1. *The simple structure of the cost function* (B.6) *aims at emphasizing the role of the collective navigation experience encoded in the estimated kernel density towards the generation of the path deviation during a potential collision scenario. However, the RRT* offers a general framework where the cost function can include an arbitrary number of performance indexes focusing on e.g., speed loss, energy consumption, fuel consumption, etc.*

B.4.2   RRT*

The underlying RRT* algorithm is a marine-oriented variant of the general algorithm presented by Karaman and Frazzoli [B17]. Algorithm B.1 describes the main structure of the general RRT* planner. The routine consists of growing a tree $\mathcal{T} = (V, E)$, where V and E represent the sets of nodes and edges, respectively. A given node x represents a particular state at time t, containing the North-East position of the vessel, with the connecting edges containing cost and constraint information. The algorithm is modified to incorporate the cost function (B.6). `Feasible`($x_{nearest}$, x_{new}) ensures that only feasible nodes are added to the tree, and therefore rejects node

sequences that are either non-COLREGs compliant, outside the bounds of X_{free} or violates the remaining constraints (such as the minimum turning radius). Due to availability of depth contours within the ENC, which directly encode a draught dependant representation of X_{free}, the proposed sampling strategy is tailored in order to leverage the non-convex polygons that describe the navigable regions. The following section, details the proposed uniform sampling scheme of general non-convex depth contours.

B.4.3 Sampling non-convex depth contours

The depth contours extracted from the ENC are represented by arbitrary non-convex polygons. To achieve the uniform sampling of this space, thereby ensuring optimality of the sought path, the Constrained Delaunay Triangulation (CDT) [B28] is applied to decompose the non-convex polygon into a finite set of triangles. CDT guarantees that all the obtained triangles are contained within the perimeter of the polygon. Figure B.2c shows CDT applied to the polygon data obtained from the depth contours in Fig. B.2b. The uniform sampling of the obtained triangles is a two-step procedure: first there is the uniform selection of a triangle, weighted by area; then the uniform sampling of the selected triangle takes place. Given any triangle composed by vertices (A, B, C), a uniformly sampled point P within the triangle is then described by

$$P = \left(1 - \sqrt{r_1}\right) A + \sqrt{r_1}\left(1 - r_2\right) B + \sqrt{r_1}r_2 C \tag{B.8}$$

where $r_1 \sim \mathcal{U}(0, 1)$ and $r_2 \sim \mathcal{U}(0, 1)$ [B29].The polygon geometries contained within the ENC are represented at a very a high resolution. Hence it is recommended to simplify the polygons using a line simplification method, such as the Douglas-Peucker algorithm [B30].

Remark B.2. *The standard RRT* algorithm performs sampling in a rectangular region surrounding the space where the path needs to be planned. For navigation in confined waters, the sampling of such space is highly inefficient with respect to finding the optimal path. This is because many samples are likely to fall in correspondence of land masses and shallow waters. Rejection sampling is therefore applied to retain only the valuable samples. On the contrary, sampling the triangular regions within the perimeter of the depth contours is highly efficient since all the samples in such region contributes to improve the found solution.*
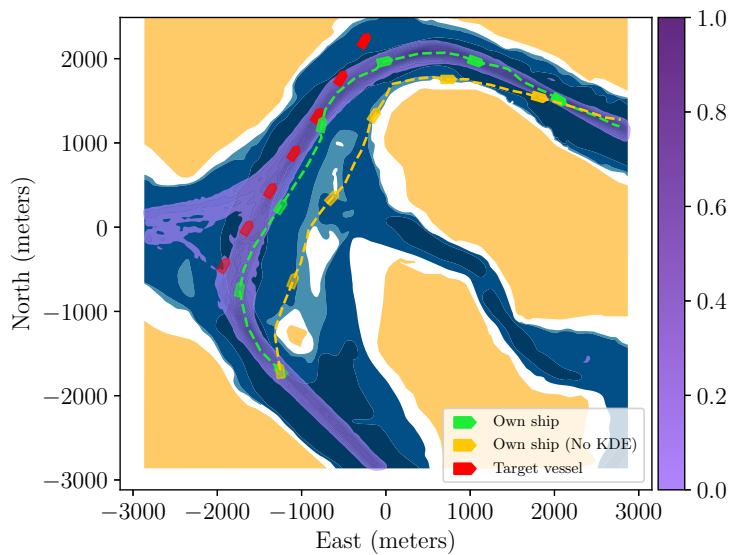
(a) Overtaking scenario in the waters around Skærbæk, Fænø and Middelfart, at the Little Belt area in Denmark.
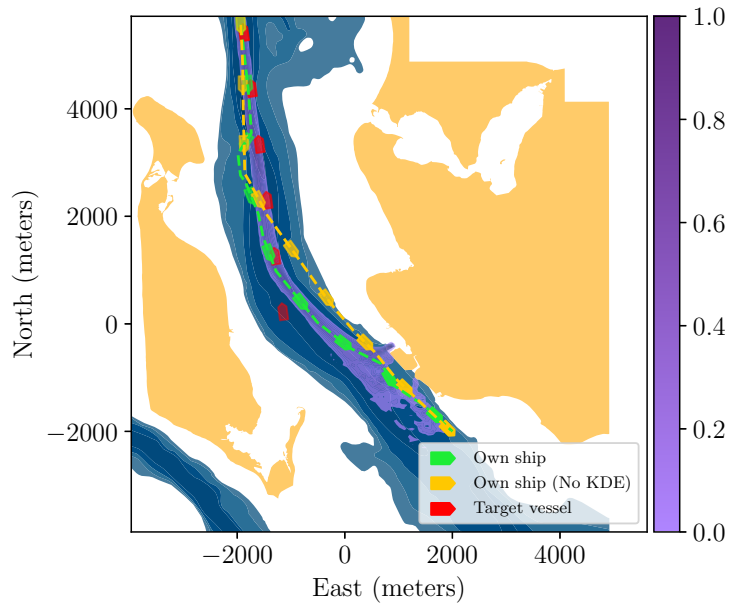
(b) Head-on scenario in the waters between Agersø and Stignæs, at the Great Belt area in Denmark.

Figure B.4: Two scenarios for single-vessel encounters in confined water. The visualized depth contours are waters deeper than 6m and indicate the feasible area for own ship to traverse; white areas indicate shallow waters.

B.5   Results

The grounding-aware RRT* planner is evaluated on two confined water scenarios. Each scenario includes a single-vessel encounter, where own ship must perform an evasive manoeuvre to avoid collision. The planning scheme receives the position of own ship as the starting configuration, and selects a point along the nominal trajectory as the goal configuration. The resulting trajectories for both scenarios are visualized in Fig. B.4. Two different deviations, with differing objectives, were computed for each scenario. For the first objective, the weights of the cost function (B.6) were selected to emphasise the value provided by the learned behaviour from the AIS data, and for the second the weights were selected to only consider the minimization of the path elongation (i.e. $w_1 = 0$).

In the first scenario, Fig. B.4a, own ship is travelling northbound through the Little Belt area when it encounters a target vessel also northbound, but travelling at a lower speed. The encounter with the target vessel is identified as an overtaking scenario, using the relative bearing. The second scenario, Fig. B.4b, features own ship heading South down a narrow channel at the Great Belt area. The grounding-aware RRT* planner is initiated due to an incoming target vessel that, based on the relative bearings, is identified as a head-on encounter. This implies that own ship must yield.

In both study-cases, the grounding-aware RRT* path planner computes a COL-REGs compliant path alteration, which ensures both the collision avoidance and the safe navigation across confined waters. The computed path alterations clearly show how the planner negotiates between the collective navigation experience embodied by the KDE and the water depth information provided by the ENC. The former attracts the path of own ship to traverse waters that have been heavily navigated in the past by other vessels of equal draught; the latter pushes the path to cross deep enough waters closer to shore to ensure that the comfort zone of the target vessel is never violated during the evasive manoeuvre. The combined effect is a path deviation that concomitantly achieves collision and grounding avoidance while safeguarding the navigation comfort of both own ship and target vessel. The two additionally computed deviations which seek to minimize the path length, also provide COLREGs complaint path alterations, however both disregard the risks associated with traversing possibly too shallow waters. This results in a more risky passage due to both potential grounding risks and the limited space for maneuvers given additional incoming vessels.

The paper proposed using triangulation of the depth contours for computing valid samples in scenarios with confined waters. Its performance is compared against
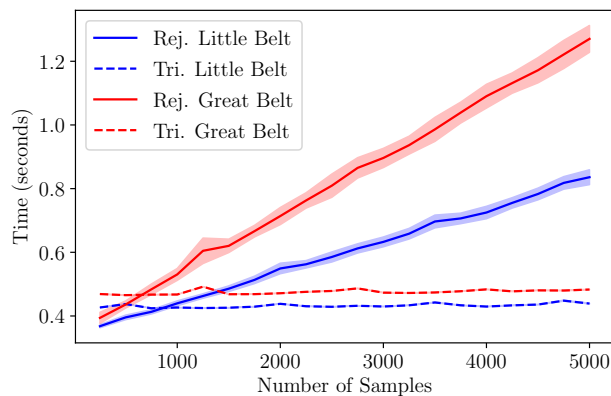
Figure B.5: Performance comparison between the rejection sampling scheme (Rej.) and the proposed scheme which samples the triangulated depth contours (Tri.). The area ratio between the rectangular region and the depth contours for the rejection sampling method is approximately 0.2677 and 0.4065 for the Great Belt and Little Belt, respectively. The transparent bands indicate the 3σ confidence interval.

a standard sampling approach based on a rectangular region and rejection sampling. The comparison is performed using Monte Carlo simulations. Figure B.5 illustrates the computational time in seconds as the number of valid samples increases: it is evident that the proposed triangulation scheme outperforms the baseline rejection sampler. Additionally, the performance related to configuring the sampling spaces is provided in Table B.1.

For both scenarios, the triangulation scheme is initially at a disadvantage, since on average it takes longer to extract the contours and compute the triangles, compared to simply extracting the depth contours as required by the rejection sampler. It should be noted, that due to variations in the polygonal data between the two scenarios, the preprocessing duration differs between the two presented scenarios. However, once the configuration of the sampling spaces is finalized, the proposed triangulation based sampling scheme significantly outperforms the rejection sampling scheme at higher sample quantities. The ability to rapidly compute valid samples is key

Table B.1: Statistical performances in seconds related to the configuration of sampling spaces for the Great Belt (GB) and Little Belt (LB) scenarios.

Scheme	GB(μ)	GB (σ)	LB (μ)	LB (σ)
Rejection	0.3501	0.0087	0.3469	0.0063
Triangulation	0.4730	0.0115	0.4299	0.0108

for optimal sampling-based algorithms and the speed in which they converge to the respective optimal solution [B20], [B27]. Noteworthy that the performance of the rejection sampling heavily depends on the area ratio between the surface inside the depth contours and the total surface within the bounding box. As the area ratio decreases, the probability of successfully computing a valid sample also decreases, leading to slower sampling performance. This is clearly shown in Fig. B.5 where an area ratio difference of about 14% between the Great Belt and Little Belt study-cases produces a change of about 40% in computational time. This issue is mitigated by utilizing the computed triangulation, since it directly represents the valid sampling space, guaranteeing that any computed sample is valid, resulting in no wasted sampling effort.

B.6   Conclusion

The paper presented a grounding-aware RRT* path planning algorithm for collision avoidance in confined waters. The proposed algorithm combines the navigation experience of seafarers with the water depth information available through the ENC, to achieve optimal path alterations that trade off between comfortable navigation (not too close to shallow waters) and feasible navigation (crossing navigable areas for the current draught). The paper proposed the use of multivariate kernel density estimation on historical AIS data to generate a probabilistic model that describes the best sailing practices of seafarers in a given restricted sea region. This model is then used as cost factor in the performance index of a COLREGs compliant RRT* collision avoidance scheme. This enables the planner to compute safe path deviations, which are aware of both collision and grounding risks. Furthermore, compared to existing marine-oriented RRT* implementations, the presented scheme directly utilizes the complex geometries present within the chart data. Through triangulation the sampling scheme has increased probability of improving the computed solution. The augmented planning scheme was successfully demonstrated in simulation for two separate confined water collision scenarios, where the results clearly show the value provided by taking advantage of the prior navigational experiences.

B.7   References

[B1]   EMSA, *Annual overview of marine casualties and incidents 2020*, 2020.

[B2]   Ö. Uğurlu, U. Yıldırım, and E. Başar, "Analysis of grounding accidents caused by human error," *Journal of Marine Science and Technology*, vol. 23, no. 5, pp. 748–760, 2015.

[B3]   Y. Huang, L. Chen, P. Chen, R. R. Negenborn, and P. van Gelder, "Ship collision avoidance methods: State-of-the-art," *Safety science*, vol. 121, pp. 451–473, 2020.

[B4]   A. Vagale, R. T. Bye, R. Oucheikh, O. L. Osen, and T. I. Fossen, "Path planning and collision avoidance for autonomous surface vehicles II: a comparative study of algorithms," *Journal of Marine Science and Technology*, no. 0123456789, Feb. 2021. DOI: 10.1007/s00773-020-00790-x.

[B5]   A. Vagale, R. Oucheikh, R. T. Bye, O. L. Osen, and T. I. Fossen, "Path planning and collision avoidance for autonomous surface vehicles I: a review," *Journal of Marine Science and Technology*, vol. i, no. 0123456789, pp. 2018–2028, Jan. 2021. DOI: 10.1007/s00773-020-00787-6.

[B6]   P. Chen, Y. Huang, E. Papadimitriou, J. Mou, and P. van Gelder, "Global path planning for autonomous ship: A hybrid approach of fast marching square and velocity obstacles methods," *Ocean Engineering*, 2020.

[B7]   Y. Singh, S. Sharma, R. Sutton, D. Hatton, and A. Khan, "A constrained A* approach towards optimal path planning for an unmanned surface vehicle in a maritime environment containing dynamic obstacles and ocean currents," *Ocean Engineering*, vol. 169, pp. 187–201, 2018.

[B8]   G. Bitar, A. B. Martinsen, A. M. Lekkas, and M. Breivik, "Two-Stage Optimized Trajectory Planning for ASVs Under Polygonal Obstacle Constraints: Theory and Experiments," *IEEE Access*, vol. 8, pp. 199 953–199 969, 2020.

[B9]   Y. Xue, D. Clelland, B. Lee, and D. Han, "Automatic simulation of ship navigation," *Ocean Engineering*, vol. 38, no. 17-18, pp. 2290–2305, 2011.

[B10]   M. Candeloro, A. M. Lekkas, and A. J. Sørensen, "A voronoi-diagram-based dynamic path-planning system for underactuated marine vessels," *Control Engineering Practice*, vol. 61, pp. 41–54, 2017.

[B11]   H. Niu, Y. Lu, A. Savvaris, and A. Tsourdos, "An energy-efficient path planning algorithm for unmanned surface vehicles," *Ocean Engineering*, vol. 161, pp. 308–321, 2018.

[B12]   A. B. Martinsen, A. M. Lekkas, and S. Gros, "Optimal model-based trajectory planning with static polygonal constraints," *arXiv preprint arXiv:2010.14428*, 2020.

[B13]   M.-C. Tsou, "Multi-target collision avoidance route planning under an ECDIS framework," *Ocean Engineering*, vol. 121, pp. 268–278, 2016.

[B14]   S. Reed and V. E. Schmidt, "Providing nautical chart awareness to autonomous surface vessel operations," *OCEANS 2016*, IEEE, 2016.

[B15] O. S. Otterholm, "Extracting mapped hazards from electronic navigational charts for ASV collision avoidance," M.S. thesis, NTNU, 2019.

[B16] S. M. LaValle, "Rapidly-exploring random trees: A new tool for path planning," 1998.

[B17] S. Karaman and E. Frazzoli, "Sampling-based algorithms for optimal motion planning," *The international journal of robotics research*, vol. 30, no. 7, pp. 846–894, 2011.

[B18] H. T. L. Chiang and L. Tapia, "COLREG-RRT: An RRT-Based COLREGS-Compliant Motion Planner for Surface Vehicle Navigation," *IEEE Robotics and Automation Letters*, vol. 3, no. 3, pp. 2024–2031, 2018.

[B19] R. Zaccone, "COLREG-Compliant Optimal Path Planning for Real-Time Guidance and Control of Autonomous Ships," *Journal of Marine Science and Engineering*, vol. 9, no. 4, 2021. DOI: 10.3390/jmse9040405.

[B20] T. T. Enevoldsen, C. Reinartz, and R. Galeazzi, "COLREGs-Informed RRT* for Collision Avoidance of Marine Crafts," *2021 International Conference on Robotics and Automation (ICRA)*, IEEE, 2021.

[B21] M. G. Hansen, T. K. Jensen, T. Lehn-Schiøler, K. Melchild, F. M. Rasmussen, and F. Ennemark, "Empirical ship domain based on AIS data," *The Journal of Navigation*, vol. 66, no. 6, pp. 931–940, 2013.

[B22] A. Gramacki, *Nonparametric kernel density estimation and its computational aspects*. Springer, 2018.

[B23] V. C. Raykar, R. Duraiswami, and L. H. Zhao, "Fast computation of kernel estimators," *Journal of Computational and Graphical Statistics*, vol. 19, no. 1, pp. 205–220, 2010.

[B24] B. W. Silverman, "Algorithm as 176: Kernel density estimation using the fast fourier transform," *Journal of the Royal Statistical Society. Series C (Applied Statistics)*, vol. 31, no. 1, pp. 93–99, 1982.

[B25] A. Gramacki and J. Gramacki, "FFT-based fast computation of multivariate kernel density estimators with unconstrained bandwidth matrices," *Journal of Computational and Graphical Statistics*, vol. 26, no. 2, pp. 459–462, 2017.

[B26] T. Odland, *tommyod/KDEpy: Kernel Density Estimation in Python*, version v0.9.10, Dec. 2018. DOI: 10.5281/zenodo.2392268.

[B27] J. D. Gammell, S. S. Srinivasa, and T. D. Barfoot, "Informed RRT*: Optimal sampling-based path planning focused via direct sampling of an admissible ellipsoidal heuristic," *IEEE International Conference on Intelligent Robots and Systems*, pp. 2997–3004, 2014.

[B28]   L. P. Chew, "Constrained delaunay triangulations," *Algorithmica*, vol. 4, no. 1, pp. 97–108, 1989.

[B29]   R. Osada, T. Funkhouser, B. Chazelle, and D. Dobkin, "Shape distributions," *ACM Transactions on Graphics (TOG)*, vol. 21, no. 4, pp. 807–832, 2002.

[B30]   D. H. Douglas and T. K. Peucker, "Algorithms for the reduction of the number of points required to represent a digitized line or its caricature," *Cartographica: the international journal for geographic information and geovisualization*, vol. 10, no. 2, pp. 112–122, 1973.

Paper C

Sampling-based Collision and Grounding Avoidance for Marine Crafts

Thomas T. Enevoldsen[1*], Mogens Blanke[1] and Roberto Galeazzi[1]

[1]Automation and Control Group, Department of Electrical and Photonics Engineering, Technical University of Denmark, DK-2800 Kgs. Lyngby, Denmark, Contact: {tthen,mobl,roga}@dtu.dk

Abstract:

Collisions and groundings account for a great deal of fiscal losses and human risks in the statistics of marine accidents related to ocean going vessels. With highly automated vessels offering a high degree of situational awareness, algorithms can anticipate developments and suggest timely actions to avoid or deconflict critical events, in accordance to safe navigational practices and in compliance with the Convention on the International Regulations for Preventing Collisions at Sea (COLREGs). To avoid such accidents related to navigation, this article proposes a Short Horizon Planner (SHP) for decision support or automated route deviations, as a means to mitigate prevailing risks. The planner adopts a sampling-based planning framework that uses the concepts of cross-track error and speed loss during a steady turn, together with sampling spaces directly extracted from the electronic navigational chart to compute optimal and COLREGs compliant paths with the least deviation from the ship's nominal route. COLREGs compliance (rules 8, 13-17) is achieved through an elliptical-like representations of the given COLREGs, which rejects samples based on modified ship domains. High fidelity simulations show properties of the method and the information made available to human- or automated execution of route alterations.

C.1   Introduction
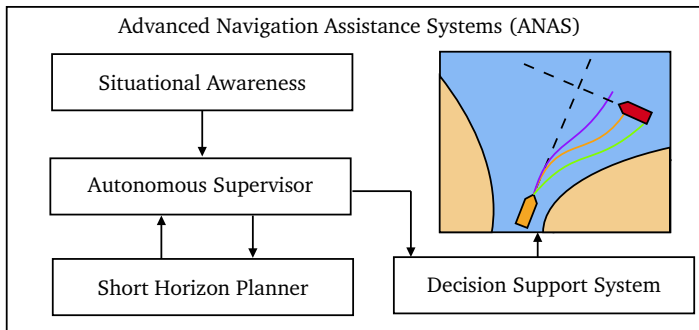
Figure C.1: Crucial components for an ANAS.

Despite the continuous technological advancement of integrated bridge systems, comprising of Electronic Chart Display and Information Systems (ECDIS) and Automatic Radar Plotting Aid (ARPA) radar systems, to ensure the safe passage of marine vessels, collisions and groundings still account for a large part of fiscal losses and human risks in the statistics of marine accidents, and human error remains a root cause [C1]. In Uğurlu *et al.* [C2] it was pointed out that poor use of the available equipment and poor assessment of the situation are key triggers for grounding events. Recent developments within situational awareness and collision avoidance systems in the pursuit of the autonomous ship could provide the necessary means for significantly improving the safety of navigation. Although fully autonomous ships are not yet in clear sight, mainly due to regulatory and commercial barriers [C3], [C4], by-products of ship autonomy could be retrofitted into the existing fleet and integrated into new buildings, in the form of Advanced Navigation Assistance Systems (ANAS), following a development path similar to that of the automotive industry.

The autonomous ship architecture presented in Dittmann *et al.* [C5], [C6], where functions currently performed by human personnel are matched to cyber-agents, suggests that future ANAS could comprise the following subsystems (see Fig. C.1)

- *Situational Awareness System* devoted to the monitoring and interpretation of own ship surroundings

- *Autonomous Supervisor* devoted to the monitoring and assessment of own ship

- *Short Horizon Planner* devoted to the computation of alternative routes to avoid collisions and groundings

- *Decision Support System* devoted to the provision and visualisation of operational insight on an ECDIS-like system to support decision making

The ANAS could therefore assist the navigator with maintaining a solid overview of the unfolding navigation scenarios, as well as proposing potential evasive manoeuvres in the event of a risk of collision or grounding.

C.1.1 Short horizon planner

This paper focuses on the design and framework of a *Short Horizon Planner* (SHP) for marine vessels, such as merchant and ro-ro vessels, that is capable of deconflicting collision scenarios that arise during the voyage in open or confined waters, while avoiding risk of grounding. Larger marine crafts have a look-ahead time, depending on their size, in the range of minutes. If risk of collision should occur, a COLREGs compliant evasive manoeuvre must to be planned to avoid that a situation becomes critical. The role of the SHP is to plan a suitable deviation from the nominal route given the current perceived scenario, provided by an onboard situational awareness system [C7], [C8]. As all encounters dynamically evolve over time, the SHP, together with the situational awareness system and an autonomous supervisor [C9], operate in a closed-loop. The SHP is evoked whenever a situation develops such that a deviation is required. The combined system continues to deconflict until all conflicts have been resolved.

The SHP uses a standard route description consisting of waypoints, track segments and speed along legs to specify deviations from a nominal route, and hence adheres to standards for electronic display and voyage control systems. This description allows the planning problem to be dealt with at a geometrical level and be executed using a standard autopilot or by manual control of heading and shaft speed. The SHP will compute optimal and compliant path alterations based on relevant metrics and suggest route alterations to avoid navigational risks. A navigator may decide which path alteration is desired or the output of the SHP could be executed automatically in case of fully autonomous operation.

C.1.2 Problem definition

Marine vessels perform sea passages based on nominal optimal routes that should be followed to make the port of call within the given time schedule and meeting the passage requirements in terms of fuel and energy efficiency. However, such a nominal route defines an ideal voyage, inconsiderate of varying traffic conditions and conflicts with target vessels that may arise. Conventionally, a skilled navigator

must assess the situation and propose route deviations such that the given situation is dealt with in an optimal manner. If partially or fully autonomous operations are envisaged, then such deviations must be computed by the collision avoidance system and reported to the human navigator for consideration or executed directly.

The problem addressed in this paper is the following.

Problem C.1. *Consider own ship $\mathcal{S}$ following its nominal optimal route $\mathcal{P}^w$ consisting of a finite set of connected waypoints, possibly traversing areas with shallow waters and static obstacles. Further, consider a finite set of target vessels $\mathcal{T}_i$, encountering own ship at a-priori unknown locations along $\mathcal{P}^w$. It is desired to automatically compute the optimal path alterations $\mathcal{P}^d$ that minimise deviations from the nominal optimal route while ensuring collision and grounding avoidance in compliance with safe navigation practises. The path deviation $\mathcal{P}^d$ starts and ends at arbitrary positions along the nominal optimal route in a close neighbourhood of the waypoints in the vicinity of the collision scenario, and it includes supplemental waypoints such that collision is deconflicted, as well as obstacles and shallow water areas are safely avoided.*

Figure C.2 exemplifies a deviation in response to two target vessels, where additional waypoints are inserted into the nominal route, such that a given collision risk is deconflicted.

C.1.3   Related work

Exhaustive reviews of the state-of-the-art in collision avoidance have recently appeared in Huang *et al.* [C10] and Vagale *et al.* [C11], [C12], where methods and algorithms have been presented, analysed, and compared.

The challenge of developing collision avoidance systems fully compliant with the International Regulations for Preventing Collisions at Sea (COLREGs, [C13]) was first addressed by Campbell *et al.* [C14] and Tam and Bucknall [C15], which argued that one of the notable shortcomings of such systems is the inability to deal with complex multi vessel encounters, due to the requirement of human-like decision-making.

Campbell and Naeem [C16] presented the heuristic rule-based A* (R-RA*) algorithm integrated together with a decision-making framework, which determines the current COLREGs situation using the relative bearing. COLREGs compliance to rules 13-15 is enforced at the output of the algorithm when the optimal path is delivered. This work was extended in Campbell *et al.* [C17] by including target vessel detection, as well as hardware-in-the-loop testing.

Collision avoidance systems based on swarm intelligence algorithms (Ant Colony Optimisation and Genetic Algorithms) were proposed in Lazarowska [C18], [C19],
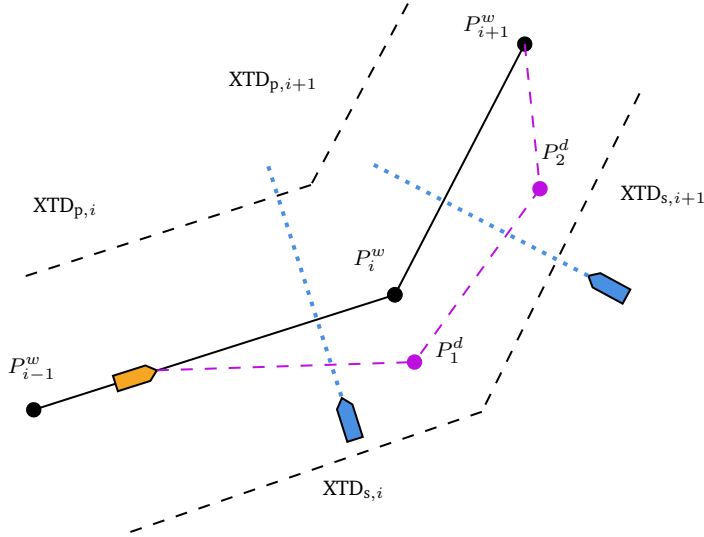
Figure C.2: An illustration of a computed deviation to a nominal path, as provided by the collision and grounding avoidance scheme. The example deviation is computed in response to two crossing encounters (blue dotted lines). The dashed black lines indicate the port and starboard side cross-track distances. The nominal route, consisting of waypoints P_{i-1}^w, P_i^w and P_{i+1}^w, is augmented such that the middle waypoint P_i^w is replaced by the computed deviation $\{P_1^d, P_2^d\}$ (purple dashed lines).

Ni *et al.* [C20], [C21], and Tsou [C22]. COLREGs compliance is achieved to a different degree for the rules 8, 13-15 by adopting the concepts of ship domain, distance to the closest point of approach and predicted area of danger.

Naeem *et al.* [C23] adopted the Artificial Potential Field to design a COLREGs compliant reactive planner adhering to rules 13-15, whilst considering a multi-vessel encounter with both static and dynamic obstacles. The velocity obstacle method and its generalised extension was investigated in Huang *et al.* [C24], [C25] and COLREGs compliance, rules 14 and 15, was achieved by disallowing port side manoeuvres.

Eriksen and Breivik [C26] showed an implementation that addresses both static and dynamic obstacles, which minimises the deviation from the nominal course. Later, Eriksen *et al.* [C27] presented the branching-course model predictive control (MPC) method that favours trajectories that comply with rules 14 and 15, whilst adhering to rules 8, 13 and 17. Johansen *et al.* [C28] and Hagen *et al.* [C29] presented MPC-based schemes, where the computed trajectories are penalised based on the degree of COLREGs compliance of the current trajectory. The COLREGs, rules 8 and 13-16, are enforced by considering the relative bearing of own ship and the given target vessel, as well as their respective velocities. Later in Kufoalor *et al.*

[C30] the previously proposed scheme is extended to include uncertainties such as those that occur when using real radar information. Kufoalor *et al.* [C31] presented exhaustive field verification of the previously described works. Eriksen *et al.* [C27] combined the branching-course Model Predictive Control (MPC) collision avoidance scheme with an elliptical COLREGs penalty function, which is defined based on the ship domain. The same implementation is utilised in later work, Eriksen *et al.* [C32], for a hybrid MPC-variant combining various levels of collision avoidance, adhering towards COLREGs rules 8 and 13-17. Abdelaal *et al.* [C33] proposed a COLREGs compliant nonlinear MPC trajectory tracking and collision avoidance scheme, which obeys COLREGs rules 13-15 by introducing a soft constraint on the yaw rate, favouring starboard manoeuvres.

The Fast Marching Method was adopted in Chen *et al.* [C34] and Garrido *et al.* [C35] for the design of global path planning and collision avoidance scheme in the presence of environmental disturbances; however COLREGs compliance was not enforced. Lattice-based COLREGs compliant planning schemes were proposed in Svec *et al.* [C36], Shah *et al.* [C37], and Bergman *et al.* [C38], where the adherence to rules 13-15 is enforced in the trajectory design phase.

Chiang and Tapia [C39] proposed an non-holonomic rapidly-exploring random tree (RRT) planning scheme, which produced dynamically feasible and COLREGs compliant paths for rules 14 and 15. Compliance is enforced by representing the area surrounding the target vessel as virtual obstacles. The computed deviations are suboptimal due to the choice of algorithm. In Zaccone *et al.* [C40] and Zaccone [C41] the authors proposed a COLREGs compliant collision avoidance scheme based on the asymptotic optimal RRT, namely RRT*, where the solution is optimised with respect to path length, curvature and repulsive forces from obstacles. The authors utilise a vector representation of the COLREGs to enforce rules 13-15. Enevoldsen *et al.* [C42] presented a specialised informed sampling scheme for single vessel encounters, which ensured that the computed samples fall within the COLREGs compliant region. The method complies with rules 13-15 and was demonstrated using RRT*. Enevoldsen and Galeazzi [C43] presented a data-driven grounding-aware cost function, as well as a uniform triangulation-based sampling strategy for confined waters. The former contribution showed the importance of grounding awareness while planning in confined waters, in order to ensure safe navigation.

C.1.4   Novelty and contribution

This paper presents a *Short Horizon Planner* for collision and grounding avoidance of large merchant vessels exploiting a sampling-based path planning framework. The proposed framework leverages key concepts from track control for marine vessels,

such as the minimum turning radius, the cross-track error and the speed loss during steady turns, in combination with sampling spaces directly encoding information about shallow waters to compute optimal path alterations that

- Minimise the deviation from the nominal optimal route

- Minimise the speed loss throughout the path alteration

- Minimise the overall path elongation with respect to the nominal optimal route

- Achieve collision avoidance in compliance with a subset of the COLREGs

- Safely navigate within confined waters and areas with shallow waters

The proposed sampling strategy and the remaining framework is demonstrated using the asymptotic optimal sampling-based planning algorithm RRT*.

The inclusion of elements from track control as planning constraints (minimum turning radius) and performance indexes (cross-track error and speed loss) ensures that the computed path alteration deviates the least possible from the nominal optimal route, thereby reducing the negative impact on metrics adopted to assess the overall passage (time, fuel consumption, energy efficiency, etc.). COLREGs compliance for rules 8, 13-17 is achieved by introducing comfort zones as super and asymmetric ellipses around the target vessels, and applying rejection sampling to discard potential waypoints that violate these comfort zones. Further, the proposed SHP addresses collision scenarios with single and multiple vessel encounters based on the same framework.

C.2 Preliminaries

C.2.1 Situational awareness

The backbone to enable autonomous operation or advanced navigational assistance is a well-functioning system that provides situational awareness. Proper situational awareness is a fundamental requirement for collision and grounding avoidance, since an automatic system must operate alongside human navigators, and must therefore interpret scenarios and perform decision making to at least the same level as existing navigators. Such systems for situational awareness are an open research question, where developments have shown that a degree of situational awareness can be achieved by combining information from radar, Automatic identification system (AIS), electro-optical sensors, global navigation satellite system (GNSS) and other inputs.

Detection, classification and behaviour prediction of objects at sea is crucial for planning adequate maneuvers. Trajectory prediction schemes, both data-driven [C44], [C45] and model-based [C37], [C46], are well-investigated within the state-of-the-art. Correctly identifying and applying a given COLREGs rule to deconflict a collision scenario is also a requirement for autonomous operation or decision support. These kinds of system are also investigated in the literature, such as by using discrete-event systems [C7], [C47], state-machines [C32] or fuzzy logic [C48].

These assumptions are contained within the *Situational Awareness* and *Autonomous Supervisor* blocks presented in Section C.1 and in Fig. C.1. The planning phase is initiated once a collision risk is imminent, based on Closest Point of Approach (CPA) and Time to Closest Point of Approach (TCPA) limits (see Appendix C.9 for more details). Navigators use these limits to determine when there is risk of collision and when to take action. For larger crafts, the time to act (t_{act}) is on the order of 15-20 minutes; however, this greatly depends on the given vessel and its manoeuvrability. For details regarding situational awareness using CPA and TCPA limits see Hansen *et al.* [C7] and Papageorgiou *et al.* [C47].

C.2.1.1   Target vessels

Situational awareness is assumed to be available to own ship, from a planning perspective. This involves assuming that any vessels present in close proximity to own ship are correctly detected and classified, and that the future trajectories of a given target vessel are available through a prediction scheme. Furthermore, for demonstration purposes, it is assumed that if multiple target vessels are present, they do not interact with each other. The minimum required trajectory prediction, that is, a straight-line prediction, can be obtained through standard equipment such as an ARPA radar. The proposed framework is capable of leveraging any advanced deterministic trajectory prediction scheme that produces a time-series output. Including advanced schemes that provide interaction-aware trajectory predictions.

Remark C.1. *The quality of the deviation from the SHP heavily depends on the quality and accuracy of the perceived situation, due to its dependency on a situational awareness system. However, since the planning scheme works in a closed-loop with the situational awareness, as described in Section C.1.1, the quality of the calculated deviations increases as the quality of the assessed scenario improves.*

The considered target vessel are assumed to be a similar size, as the one considered as own ship, and must therefore respect the same water depth restrictions.

Table C.1: Parameter subset of *Luna Maersk*, see [C52] for a full list of parameters.

Parameter	Symbol	Value
Length between perpendiculars	L_{PP}	230m
Beam	B_s	32m
Draught (Light loading condition)	D_s	8.5m
Nominal ship speed	U_0	25kn

Finally, based on Hansen *et al.* [C49] a minimum elliptical comfort zones is to be respected, which is scaled by the ship length corresponding to the given target vessel.

C.2.1.2   Own ship assumptions

The own ship is a medium-to-large merchant vessel (e.g. container vessel, ro-ro, ferry, etc.) with propulsion and steering positioned astern of the hull. Such types of vessels are limited in their ability to manoeuvre: the large inertia inhibits sudden changes in course and speed; the limited actuation prevents pure sideways motion and station keeping.

Due to the size of the considered vessels, as well as encouraged by Rule 8 of COLREGs (see Section C.2.4 or Cockcroft and Lameijer [C50]), own ship only accepts course alterations in order to deconflict a given scenario at hand. It is assumed that speed changes either take place prior to deviating or not at all. Furthermore, the vessel has minimum turning radius equal to two times its ship length, at full rudder angle [C51, Chapter 9].

In particular the study cases presented in Section C.2.2 utilises ship parameters and operational profiles of *Luna Maersk*, whose detailed manoeuvring model based on full-scale measurements was introduced in Blanke and Jensen [C52]. Table C.1 shows the relevant ship data for the SHP.

C.2.2   Case study

The proposed collision and grounding avoidance framework will be demonstrated on multiple scenarios from within the Danish waters. More specifically, the chosen case study occurs enroute between the Danish cities Fredericia and Copenhagen. Fig. C.3 details the location of the nominal route with respect to the rest of Denmark, as well as a highlighted section containing the geometries encountered throughout.

The vessel of choice for own ship is the previously defined vessel *Luna Maersk*, which can safely travel in waters 10 metres or deeper, with a nominal cruising speed of 25kn, as described in Section C.2.1.2.
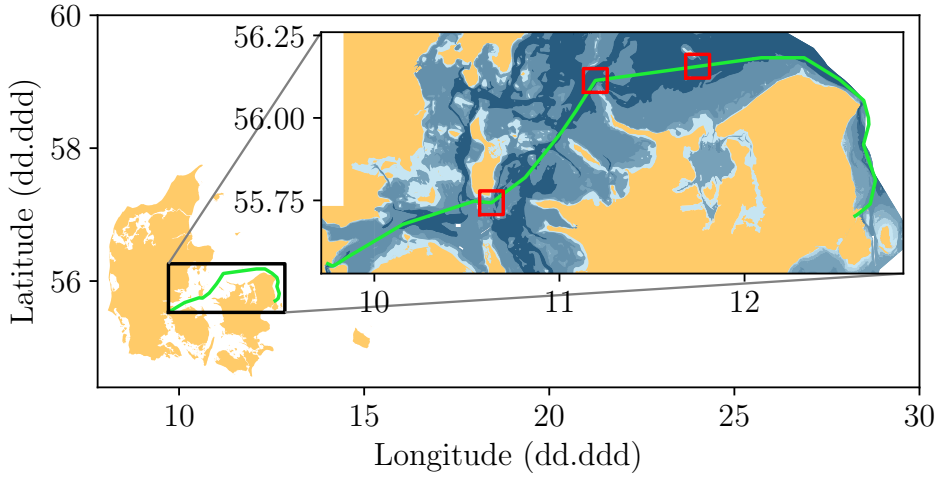
Figure C.3: Visualisation of the Danish shipping route between Fredericia and Copenhagen. The nominally planned route is visualised in green. The red regions indicate the geographical locations of the chosen case-studies, detailed in Section C.7.

C.2.3   Track control system

Merchant vessels are usually equipped with a track control system that maintains the ship on a pre-planned route under various operational conditions and within the ship manoeuvrability constraints (rate of turn in open and confined waters as specified in the Safety Management System of the ship's owner). The nominal route is described as a sequence of waypoints $\mathcal{P}^w = \{P_1^w, P_2^w, \ldots, P_n^w\}$ connected by great circle segments. Each waypoint is defined as

$$P_i^w \triangleq \{\lambda, \phi, R_t, \chi, U\} \tag{C.1}$$

where λ is latitude, ϕ is the longitude, R_t is the turning radius, χ is the desired course angle, and U is the desired forward speed. In the guidance literature the desired course angle is also known as the path tangential angle.

The track control system switches from the current waypoint P_i^w to the next one P_{i+1}^w when the distance from the current ship position to the waypoint's geographical location is smaller than the radius of acceptance R_a. The intersection between the circle of acceptance centred at P_i^w and the great circle segment $\overline{P_{i-1}^w P_i^w}$ defines the point where the ship begins to turn; however since the manoeuvring does not occur instantaneously the actual turning manoeuvre starts one ship length before at the wheel over point (WOP).

The nominal route has three associated quantities related to safety and track following performance: The cross-track limit (XTL), the cross-track distance (XTD),
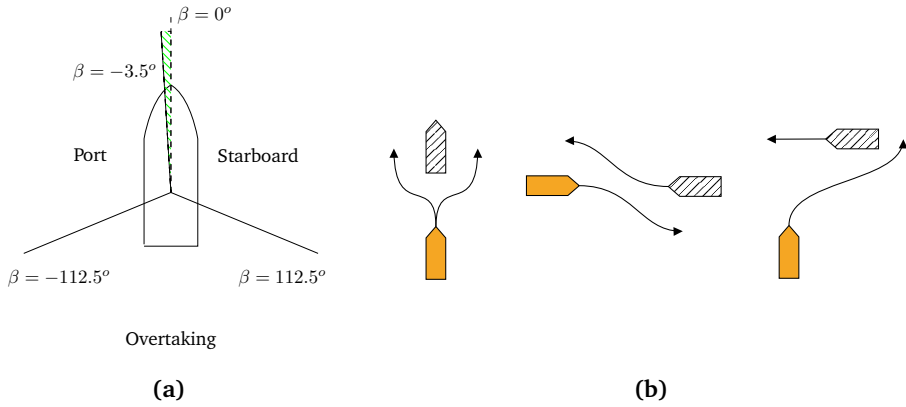
Figure C.4: (a) Angles used to determine the relative position between own ship and the given target vessel. The gridded area indicates uncertainty associated with the head-on situation, see Papageorgiou *et al.* [C47]. (b) Encounters described by COLREGs rules 13-15, i.e. overtaking, head-on and crossing scenarios. The solid coloured vessel is in a give-way situation.

and the cross-track error (XTE). XTL is defined as the smallest safety corridor along the entire navigational path. XTD is the maximum orthogonal deviation from each individual leg of the navigational path. XTE is the actual deviation of the vessel from the planned route; an alarm triggers when XTE is greater than XTL. The track control system steers the vessel along the nominal route, and try to ensure that XTE is smaller than XTL.

C.2.4   Prerequisites for safe navigation and COLREGs compliance

Adhering to the COLREGs is a fundamental requirement for any autonomous surface vessel, or for any system that proposes route deviations. COLREGs compliance is one of the first steps towards applying practices of safe navigation.

Systems for determining a given COLREGs scenario were detailed in Section C.2.1, however to apply safe navigational practices, parts of such a system must also be considered when computing route deviations. Navigators use the Closest Point of Approach (CPA) and Time to Closest Point of Approach (TCPA) metrics in order to determine if a collision scenario or potential conflict will occur and also when it will occur, respectively. If there is a violation of the CPA, the navigator then identifies which COLREGs scenario applies. Traditionally, a given COLREGs scenario is identified based on which ship lanterns are visible to the human navigator, this analogous to using the relative bearing (Fig. C.4a) between the own ship and the given target vessel to apply the appropriate COLREGs rule. Section C.2.4.1 presents

Table C.2: Common COLREGs used in collision and grounding avoidance. Rules are paraphrased from [C13] and [C50]

Rules	Explanation
Rule 8	Action to avoid collision: The give-way vessel must perform its alterations in such a way that the change in behaviour is easily observable to other vessels. The rule also recommends that, if possible, fewer and larger course change(s) is preferred over speed changes and smaller more frequent course adjustments.
Rule 13	Overtaking scenario: The vessel being overtaken must maintain its course and speed, whereas the overtaking vessel may overtake on either side of the stand-on vessel.
Rule 14	Head-on scenario: Both vessels must perform a manoeuvre such that they pass one-another on their respective port sides.
Rule 15	Crossing scenario: A vessel must give-way to another vessel, if the second vessel approaches from starboard side. The vessel that has the right of way must keep the current course and speed.
Rule 16	Give-way vessel behaviour: The give-way vessel should take early action and remain a safe distance from the stand-on vessel.
Rule 17	Stand-on vessel behaviour: The stand-on vessel is urged to maintain constant course and speed, and not attempt to avoid collision unless it is clear that the give-way vessel is not abiding by the COLREGs.

the most commonly applied COLREGs rules for collision and grounding avoidance, and Appendix C.9 details the derivation and computation of CPA and TCPA.

C.2.4.1   Common COLREGs

The following is a brief overview of the International Regulations for Preventing Collisions at Sea (COLREGs, [C13]), which any autonomous vessel or decision support system must abide by. The selected rules, rules 8 and 13-17, describe the most common collision risk scenarios, defined between two vessels, and only apply if both vessels are power-driven. The rules are described in Table C.2, with further details available in Cockcroft and Lameijer [C50]. A graphical representation of rules 13-15 is provided in Fig. C.4b, these rules represent the three most common conflicts and are typically considered the bare minimum required rules necessary for

COLREGs compliance. Rules 8 and 16-17 specify "good behaviour" or best practices of a given vessel, depending on whether it is deemed the stand-on or give-way vessel.

C.3   Optimal sampling-based collision and grounding avoidance for marine vessels

The following section introduces the formalities related to the optimal sampling-based collision and grounding avoidance problem for marine vessels. The optimal collision and grounding avoidance problem differs from the typical optimal path planning, due to the existence of the initial optimally computed nominal path. The nominal path (or route) is in the marine case computed prior to initiating the voyage and is optimised with respect to criteria such as weather routing, port call times, tide information, etc. The nominal route is computed in such a way that the surrounding water is spacious enough to allow for deconfliction using appropriate route deviations, should a collision scenario arise.

The generalised optimal sampling-based collision and grounding avoidance problem considered in this article is presented as a modified version of the optimal sampling-based planning problem presented by Gammell *et al.* [C53].

Let $\mathcal{X} \subseteq \mathbb{R}^n$ be the state space, which is divided into two subsets, $\mathcal{X}_{\text{free}}$ and $\mathcal{X}_{\text{obs}}$, with $\mathcal{X}_{\text{free}} = \mathcal{X} \backslash \mathcal{X}_{\text{obs}}$. The subset $\mathcal{X}_{\text{obs}}$ consists of the union over all constraints imposed by the current navigational problem at hand, namely

$$\mathcal{X}_{\text{obs}} = \mathcal{X}_{\text{obs}}^{\text{OS}} \cup \mathcal{X}_{\text{obs}}^{\text{ENC}} \cup \mathcal{X}_{\text{obs}}^{\text{TV}} \tag{C.2}$$

where $\mathcal{X}_{\text{obs}}^{\text{OS}}$ contains all states that violate the manoeuvring constraints imposed by the geometric properties of own ship and the track control scheme, $\mathcal{X}_{\text{obs}}^{\text{ENC}}$ represents the states that violate the restrictions imposed by the contours of the ENC and draught of own ship, and finally $\mathcal{X}_{\text{obs}}^{\text{TV}}$, given by

$$\mathcal{X}_{\text{obs}}^{\text{TV}} = \bigcup_{i=1}^{m} \mathcal{X}_{\text{TV},i}(t) \tag{C.3}$$

which represents the temporal constraints of the m considered target vessels. Collision avoidance and COLREGs compliance is encoded within the temporal contents of a given $\mathcal{X}_{\text{TV},i}(t)$, which at each time step describes a domain that represents states in violation. By considering the union of all target vessels, the optimisation problem takes into account all target vessels simultaneously. Details regarding $\mathcal{X}_{\text{obs}}^{\text{OS}}$ and $\mathcal{X}_{\text{obs}}^{\text{ENC}}$ can be found in Enevoldsen *et al.* [C42] and Enevoldsen and Galeazzi [C43] respectively.

Consequently, the states within $\mathcal{X}_{\text{free}}$ then contains all states that are feasible, both temporally and geometrically, with respect to manoeuvring constraints, COLREGs compliance, collision and grounding.

Let $\mathcal{P}^w : [0, 1] \mapsto \mathcal{X}$ be the nominal sequence of waypoints, and $\mathcal{P}^d : [0, 1] \mapsto \mathcal{X}$ be a sequence of waypoints for a given route deviation and Σ the set of all nontrivial and feasible deviations. Let $P_s \in \mathcal{X}_{\text{free}}$ be the initial waypoint at $t = T$ along the nominal route, and $P_e \in \mathcal{X}_{\text{free}}$ be the waypoint that denotes the reentry point to the nominal route. Coupled with P_s are the initial velocity and heading of own ship, which is used as initial conditions. The objective is then to find the optimal route deviation $\mathcal{P}^{d*}$, which minimises a cost function $c(\mathcal{P}^d)$ while connecting P_s to P_e through $\mathcal{X}_{\text{free}}$,

$$\mathcal{P}^{d*} = \operatorname*{arg\,min}_{\mathcal{P}^d \in \Sigma} \left\{ c(\mathcal{P}^d) \mid \mathcal{P}^d(0) = P_s,\, \mathcal{P}^d(1) = P_e,\, \forall s \in [0, 1],\, \mathcal{P}^d(s) \in \mathcal{X}_{\text{free}} \right\}.$$

(C.4)

The most widespread algorithm for solving the optimal sampling-based motion planning problem is RRT* [C54], however alternatives exist such as Batch Informed Trees (BIT*) [C55] and Fast Marching Trees (FMT*) [C56], for a deeper overview of the current state-of-the-art within optimal sampling-based motion planning see [C57]. A sampling-based motion planner consists of the following: A sampling scheme, cost function, constraints and finally the optimiser. Choice of constraints and cost functions will be introduced in Section C.4 and C.5 respectively, generation of the sampling scheme is detailed in Section C.6, and finally a short description of the chosen optimiser, RRT*, is provided in Section C.3.1.

C.3.1   Rapidly-exploring random tree algorithms

One of the most important contributions to sampling-based motion planning, was the introduction of the Rapidly-exploring Random Tree (RRT) algorithm by Lavalle [C58]. Compared to previous algorithms, RRT is capable of exploring the state space rapidly and thereby verify and obtain any existing feasible solution to the problem at hand. RRT guarantees that as the number of samples approaches infinity, a path from the starting node is mapped to every feasible point within the space, meaning that the algorithm is capable of finding the feasible solution if it exists. Therefore, due to the nature of the algorithm, there are no guarantees for optimality. Later, Karaman and Frazzoli [C54] proposed the RRT*, which introduced new components to the algorithms, for selecting the parent and child vertices. The new capabilities of RRT* were shown to guarantee asymptotic optimality as the number of samples tend towards infinity. There exists a vast amount of extensions and performance enhancements to sampling-based motion planners, such as RRT*, as demonstrated

by Véras *et al.* [C59] and their exhaustive review on the subject. However, these additions are beyond the scope of the content presented in the article.

For general algorithmic details about the RRT* algorithm see Karaman and Frazzoli [C54]. Detailed descriptions of marine-oriented implementations of RRT* are provided in Zaccone [C41] and Enevoldsen *et al.* [C42].

C.4 Enforcing COLREGs compliance

COLREGs compliance can be included in the collision avoidance framework as either a cost term or a constraint. When considering the COLREGs as a constraint, a time-varying region of the state space is typically considered a no-go zone. Such as the predicted area of danger (PAD) approach [C60], bias in the ship domain [C19], time-varying occupancy grid for A* [C16], a vectorial approach to rejecting non-compliant samples [C40] and virtual obstacle barriers [C39]. However, in some circumstances modelling the given COLREGs scenario as a constraint can lead to lack of convergence or be infeasible for a given algorithm. As an alternative, Eriksen *et al.* [C32] and Naeem *et al.* [C23] modelled the respective scenarios as potential functions, for use with MPC or Artificial Potential Fields.

Elliptical descriptions of both comfort zones and dynamic obstacles are common within the collision avoidance literature, due to their nice properties for collision checking. For marine vessels, elliptical regions have been used to specify comfort zones, often depending on ship length [C49]. The following section proposes an ellipse-like rejection sampling approach for adhering towards COLREGs rules 13-15.

C.4.1 Ellipse-like COLREGs formulation

The following section places an emphasis on adherence to rules 13-15, which are considered the rules that cover the three most basic encounter types for single vessel encounters. The adherence towards rules 8 and 16 is included in the various descriptions for rules 13-15, however rule 17 will not be discussed, since for all case studies in the article own ship will be the give-way vessel.

The following section describes rules 13-15 as different ellipse-like expressions such that non-compliant samples produced by the collision avoidance scheme can be adequately rejected, thereby enforcing the COLREGs.

The proposed regions are described as shapes centred at the origin of the north-east-down (NED) system, facing $0°$ northbound. At each time instant t, the i-th target vessel is represented by some position and heading in the NED frame

$$\text{TV}_i = \{N_i(t), E_i(t), \psi_i(t)\} \tag{C.5}$$

(a) Overtaking (Rule 13)   **(b)** Head-on (Rule 14)   **(c)** Crossing (Rule 15)
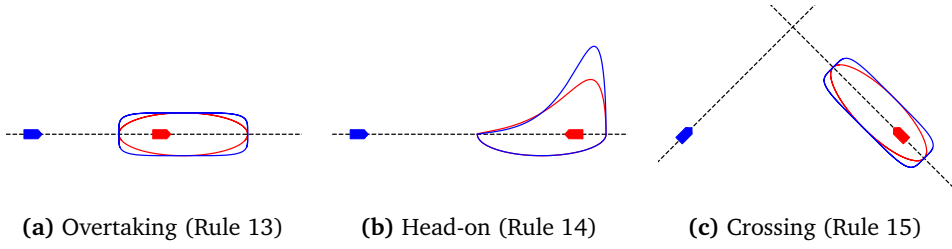
Figure C.5: Various ellipse-like representations of COLREGs rules 13-15. (a) and (c) represents the overtaking and crossing scenarios, respectively, as super ellipses (blue $p = 5$, red $p = 2$). (b) represents the head-on scenario as a combination of a regular ellipse and a transformed ellipse with $g(\bar{N}(t), c) = e^{c\bar{N}(t)}$. Using the offsets in Eq. (C.7), the target vessel can be placed arbitrarily within the ellipse. COLREGs compliance for all three encounter types is achieved by rejecting samples that fall within the elliptical regions.

therefore, to check for constraint violations, a given state is checked with respect to the system placed at the origin at $0°$. This can be achieved by the following transformation

$$\begin{bmatrix} \bar{E}(t) \\ \bar{N}(t) \end{bmatrix} = \begin{bmatrix} \cos(\psi_{\text{TV},i}(t)) & \sin(\psi_{\text{TV},i}(t)) \\ -\sin(\psi_{\text{TV},i}(t)) & \cos(\psi_{\text{TV},i}(t)) \end{bmatrix} \begin{bmatrix} \Delta E(t) \\ \Delta N(t) \end{bmatrix} \tag{C.6}$$

which transforms a given point with respect to the placement of an i-th target vessel within the North-East-Down (NED) frame, where the reverse translation is given by

$$\Delta E(t) = E_{\text{OS}}(t) - E_{\text{TV},i}(t) + E_{\text{offset}}$$
$$\Delta N(t) = N_{\text{OS}}(t) - N_{\text{TV},i}(t) + N_{\text{offset}} \tag{C.7}$$

where N_{offset} and E_{offset} are offsets along the north and east axis respectively. Allowing one to bias the target vessel off-centre, to accommodate safety needs in a given application.

C.4.1.1 Crossing and overtaking

Compliance with crossing and overtaking scenarios can be achieved by using a super ellipse (Lamé curve), given by

$$h_{\text{OT, GW},p} \triangleq \left| \frac{\bar{E}(t)}{a} \right|^p + \left| \frac{\bar{N}(t)}{b} \right|^p \leq 1 \tag{C.8}$$

where a and b are some scalar values determined based on the target vessels length.

A super ellipse differs from the ordinary ellipse by its exponent p, for $p > 2$ the area covered by the ellipse increases, whilst maintaining its specified major and minor axes lengths. This particular approximation is favourable compared to an

n-sided polygon, due to the ease of checking whether or not a point falls within it. In the overtaking scenario (Fig. C.5a), the super ellipse ensures that an overtaking manoeuvre is initiated from a safe distance at the rear, whilst also ensuring an adequate distance to the target vessel when returning to the nominal trajectory. This particular formulation allows the own ship to pass safely both on the port and starboard sides of the target vessel, such that both options are available given potential restrictions posed from confined waters. For crossing scenarios (Fig. C.5c), the super ellipse ensures that the own ship performs a manoeuvre towards starboard in order to correctly deconflict the crossing scenario. A manoeuvre towards the port side is only performed if own ship is capable of maintaining a sufficient safety distance towards the target vessel at hand. The offset parameters in Eq. (C.7) provides adjustment of the target vessel location within the shape, since a greater clearance, such as in the rear, may be required in some circumstances.

C.4.1.2   Head-on

Compared to the overtaking and crossing scenarios, expressing the constraints for the head-on scenario requires additional terms. Rule 14 states that both vessels must give-way with manoeuvres towards starboard, and therefore the elliptical expression must both reject manoeuvres towards portside, but also reject manoeuvres that initiate too late.

This is achieved by creating an asymmetric ship domain, consisting of two half ellipses, governed by the following modified equation of an ellipse

$$h_{\text{HO},c} \triangleq \left(\frac{\bar{E}(t)}{a}\right)^2 g_c\left(\bar{N}(t)\right) + \left(\frac{\bar{N}(t)}{b}\right)^2 \leq 1 \tag{C.9}$$

where a and b are scalar values determined based on the target vessels length. The expression $g\left(\bar{N}(t)\right)$ transforms the shape of the ellipse along the major axis, depending on the magnitude of the scalar c. The transform is given by

$$g_{c>0}\left(\bar{N}(t)\right) = e^{c\bar{N}(t)}, \quad c \geq 0. \tag{C.10}$$

If the scalar is strictly greater than 0, then the transform extends the domain along the major axis in both directions. The asymmetric ship domain is then constructed by combining the following two half ellipses, where for positive east and negative east values, the following ship domain is described

$$h_{\text{HO}}(t) = \begin{cases} \left(\frac{\bar{E}(t)}{a}\right)^2 e^{c\bar{N}(t)} + \left(\frac{\bar{N}(t)}{b}\right)^2 \leq 1 & \text{if } \bar{E}(t) \geq 0 \\ \left(\frac{\bar{E}(t)}{a}\right)^2 + \left(\frac{\bar{N}(t)}{b}\right)^2 \leq 1, & \text{if } \bar{E}(t) < 0 \end{cases} \tag{C.11}$$

then if waypoint $P(t) = (N(t), E(t)) \in h_{\text{HO}}$, the sample is rejected due to being non-compliant with rule 14. Fig. C.5b visualises the two half ellipses, and how the ship domain is biased to reject deviations to the port side. Combining the two shapes is necessary in order to obtain a formulation similar to the proposed super ellipses from Section C.4.1.1.

C.4.2   Rule 8 & 16 compliance

The COLREGs, in particular rule 8, state that when a vessel alters its course, it must be visible to the naked eye. Furthermore, it is stated that course alterations should consist of a few large changes, rather than multiple smaller changes. Since the planning phase begins at the TCPA limit, ample time prior to TCPA, the required deviation typically consists of a course alteration of a few degrees. Despite this, since the TCPA is on the order of minutes, a change of a few degrees is clearly visible to the surrounding navigators. Planning in advance and in combination with the proposed elliptical regions also enforces rule 16, since early action is taken and adequate safety distance is maintained.

C.5   Marine-oriented cost functions

As detailed earlier in the article, the particular vessels that are considered are those with an underlying track control scheme. An important performance index is then to compute a deviation such that it minimally deviates from the nominal route, which can be achieved by including a minimisation term for the cross-track error of the proposed deviation. One may encounter issues if only penalising the cross-track error, since this may force the deviation to tightly follow the nominal route, which most often is infeasible for larger crafts. Therefore, minimisation of cross-track error is balanced by also considering the path elongation simultaneously.

Another import factor to consider is the loss of speed due to waypoints having smaller turning radii than usually planned. This gives rise to consider the combination of speed loss during turns, path deviation and path elongation, and the resulting impact on the overall route. when reaching the final destination.

C.5.1   Path elongation (path length)

Minimisation of the Euclidian path length is one of the most common performance indices, for any given system. When deviating from the nominal path, one wishes to minimise the amount of path elongation, since an increased path length also impacts
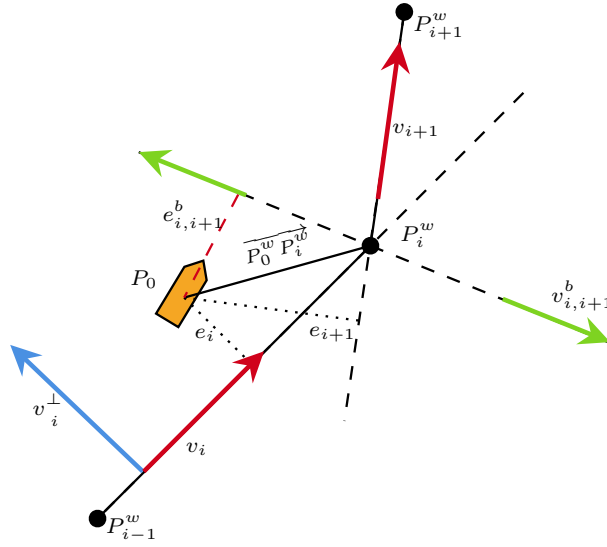
Figure C.6: Vector quantities relating to computing the cross-track error (CTE) for a given leg. The bisecting vector in the middle provides a condition for whether or not the CTE should be computed with respect to leg v_i or v_{i+1}.

the overall travel time and fuel and energy spent. Given a m-dimensional list of waypoints $\mathcal{P}^d$ which represent the proposed deviation, the resulting path length for $\mathcal{P}^d$ is then given by

$$c_l(\mathcal{P}^d) = \sum_{i=1}^{m} \|P_i^d - P_{i-1}^d\|_2, \quad \forall P_i^d \in \mathcal{P}^d. \tag{C.12}$$

C.5.2 Cross-track error

Simply minimising the path length works well during cruising scenarios in open waters, where the route deviation re-enters the same leg as it began from. However, in confined water or at critical points throughout the voyage, the route deviation might take place along multiple legs. By leveraging ideas from the track control paradigm, it is possible to generate a metric which optimally selects a given leg to minimize towards.

A path segment $\overline{P_{i-1}^w P_i^w}$ is defined by two waypoints and the desired course angle $\chi_{P_i^w}$ of the incoming waypoint P_i^w. Let $\boldsymbol{P}_{i-1}^w$ and $\boldsymbol{P}_i^w$ the position vectors of the waypoints P_{i-1}^w and P_i^w expressed in the NED frame, then the directional vector for the path segment $\overline{P_{i-1}^w P_i^w}$, $\boldsymbol{v}_i$, is defined as

$$\boldsymbol{v}_i = (\cos(\psi_i), \sin(\psi_i)) \tag{C.13}$$

and its perpendicular reads

$$\boldsymbol{v}_i^{\perp} = \left(-\sin\left(\psi_i\right), \cos\left(\psi_i\right)\right). \tag{C.14}$$

The cross-track error between the current position of own ship, $\boldsymbol{P}_0$, and the given path segment $\overline{P_{i-1}^w P_i^w}$ is given by

$$\boldsymbol{e}_i = \boldsymbol{P}_0 \boldsymbol{P}_i^{\boldsymbol{w}} \cdot \boldsymbol{v}_i^{\perp}. \tag{C.15}$$

The complexity in minimising cross-track error, compared to path length, lies in determining if the error should be computed towards the path segment $\overline{P_{i-1}^w P_i^w}$ or $\overline{P_i^w P_{i+1}^w}$. This is solved by utilising the bisecting line between the two legs, and is described as follows

$$\boldsymbol{v}_{i,i+1}^b = \frac{(\boldsymbol{v}_{i+1} + \boldsymbol{v}_i)}{\|\boldsymbol{v}_{i+1} + \boldsymbol{v}_i\|}. \tag{C.16}$$

By computing and checking the signed distance to the bisection line $\boldsymbol{v}_{i,i+1}^b$

$$\boldsymbol{e}_{i,i+1}^b = \overrightarrow{\boldsymbol{P}_0 \boldsymbol{P}_i^{\boldsymbol{w}}} \cdot \left(\boldsymbol{v}_{i,i+1}^b\right)^{\perp} \tag{C.17}$$

it possible determine whether the cross-track error should be computed for $\boldsymbol{P}_i$ or for $\boldsymbol{P}_{i+1}$. The cross-track error for P_i^d along the proposed deviation $\mathcal{P}^d$ is then

$$e_{P_i^d} = \begin{cases} \boldsymbol{P}_i^d \boldsymbol{P}_i^{\boldsymbol{w}} \cdot \boldsymbol{v}_i^{\perp} & \text{if } e_{i,i+1}^b \leq 0 \\ \boldsymbol{P}_i^d \boldsymbol{P}_{i+1}^{\boldsymbol{w}} \cdot \boldsymbol{v}_{i+1}^{\perp}, & \text{if } e_{i,i+1}^b > 0 \end{cases} \tag{C.18}$$

with the computation of cross-track error along the entire deviation, $\mathcal{P}^d$ (excluding P_s^d and P_e^d), computed as

$$c_e(\mathcal{P}^d) = \sum_{i=1}^{m-1} e_{P_i^d}, \quad \forall P_i^d \in \mathcal{P}^d. \tag{C.19}$$

C.5.3   Speed loss

Speed loss during a turn is governed by the surge dynamics [C61]–[C63]. With propulsion provided by the forward force balancing hull resistance, the forward speed dynamics in calm water reads (main terms only):

$$m_x \dot{U} = -X(U) + X_{prop} + (m + X_{vr})vr + X_{rud}. \tag{C.20}$$

The hull resistance $X(U)$, propeller thrust X_{prop}, and relation between turn rate and rudder angle are tabular functions that are known for own ship. Furthermore, for manoeuvres with small turning rate the steady-state added resistance due to

Table C.3: Nomenclature for *Luna Maersk* surge dynamics. Parameter values are available in [C52].

Parameter	Symbol
Ship's mass	m
Ship's mass plus added mass in surge	m_x
Sway velocity in body coordinates	v
Turn rate in body coordinates	r
Net propeller X force on hull (reduced by thrust deduction)	X_{prop}
Hull resistance	$X(U)$
Added mass for fictive acceleration vr	X_{vr}
Drag (X) force from rudder	X_{rud}
Ship resistance in calm water	$X_{|u|u}$
Side slip angle	β_s
Turning radius	R

rudder deflection X_{rud} is small compared to the term governed by the centripetal acceleration vr.

When turning at a waypoint P_i specified by its turning radius R, the turn rate is $r = \frac{U}{R}$. The sway velocity through water v is not generally available, but v can be found as function of forward speed U and sideslip angle β_s [C64]

$$v = -U \sin \beta_s \approx -U\beta_s. \tag{C.21}$$

The sideslip angle is not measured; however, there are approximations that relate β_s with the ship's length between perpendiculars L_{PP} and the turning radius R. Molland and Turnock [C65] reported that for single-screw vessels the following approximation for β_s in degrees is valid

$$\beta_s = 22.5 \frac{L_{PP}}{R}. \tag{C.22}$$

Inserting Eqs. (C.21)-(C.22) into Eq. (C.20) and considering the kinematic relation between turn rate and forward speed in a steady turn, the surge dynamics then reads

$$m_x \dot{U} = -X(U) + X_{prop} - (m + X_{vr}) \frac{U^2 L_{PP}}{R^2} \beta_s. \tag{C.23}$$

Assuming a constant propulsion force in the forward direction X_{prop}, and a quadratic relation for $X(U) = X_{|u|u} U^2$, then the steady-state value of the forward speed U during the turn is given by

$$U_{turn} = \sqrt{\frac{X_{prop}}{X_{|u|u} + 0.39(m + X_{vr})\frac{L_{pp}}{R^2}}} \tag{C.24}$$

where β_s has been converted from degrees to radians.

The propulsion force along a given leg of the nominal route can be computed using the forward speed $U_{P_{i-1}}$ associated with the waypoint P_{i-1}

$$X_{prop} = X_{|u|u}U_{P_{i-1}}^2 \tag{C.25}$$

Replacing X_{prop} in Eq. (C.24) with Eq. (C.25) the steady-state forward speed during the turn reads

$$U_{turn} = \sqrt{\frac{X_{|u|u}U_{P_{i-1}}^2}{X_{|u|u} + 0.39(m + X_{vr})\frac{L_{pp}}{R^2}}} \tag{C.26}$$

The speed loss is then defined as the difference between the forward speed at waypoint P_{i-1} and the steady-state forward speed during the turn U_{turn}

$$U_{loss} \triangleq U_{P_{i-1}} - U_{\text{turn}}$$

$$= U_{P_{i-1}} - \sqrt{\frac{X_{|u|u}U_{P_{i-1}}^2}{X_{|u|u} + 0.39(m + X_{vr})\frac{L_{pp}}{R^2}}} \tag{C.27}$$

Given a route deviation $\mathcal{P}^d$ consisting of m waypoints P_i^d, the turning radius R_i is a function of the desired course angles $\chi_{P_i^d}$ and $\chi_{P_{i+1}^d}$. Therefore, the total speed loss along $\mathcal{P}^d$ is defined as

$$c_s(\chi) \triangleq \sum_{i=1}^{m-1} U_{loss}\left(R(\chi_{P_i^d}, \chi_{P_{i+1}^d})\right)^2 \quad \forall P_i^d \in \mathcal{P}^d \tag{C.28}$$

Remark C.2. *The sway velocity v appearing in the term $(m + X_{vr})vr$ can also be obtained through the steady-state analysis of the steering dynamics. This gives a linear relation between the sway velocity and turn rate, i.e. $v = c_{vr}r$ where c_{vr} is a constant parameter function of hydrodynamic derivatives and ship dimensions. Such parameter is also ship dependent, as the used approximation for the sideslip angle.*

C.5.4 Cost summary

Given the computed deviation $\mathcal{P}^d$ and the desired course angles χ, the overall cost for such a path is given by

$$c(\mathcal{P}^d) = w_l c_l(\mathcal{P}^d) + w_e c_e(\mathcal{P}^d) + w_s c_s(\chi) \tag{C.29}$$

where w_l, w_e and w_s are scalar weights.

The overall cost can be further extended by including additional cost factors evaluating other key factors related to an ocean passage such as fuel and energy consumption, since for long voyages these may have a significant impact. Furthermore, a model of the time loss that considers both the path elongation and the speed

(a) Rectangular approximation

(b) Eroded and dilated contours

(c) Triangulated space
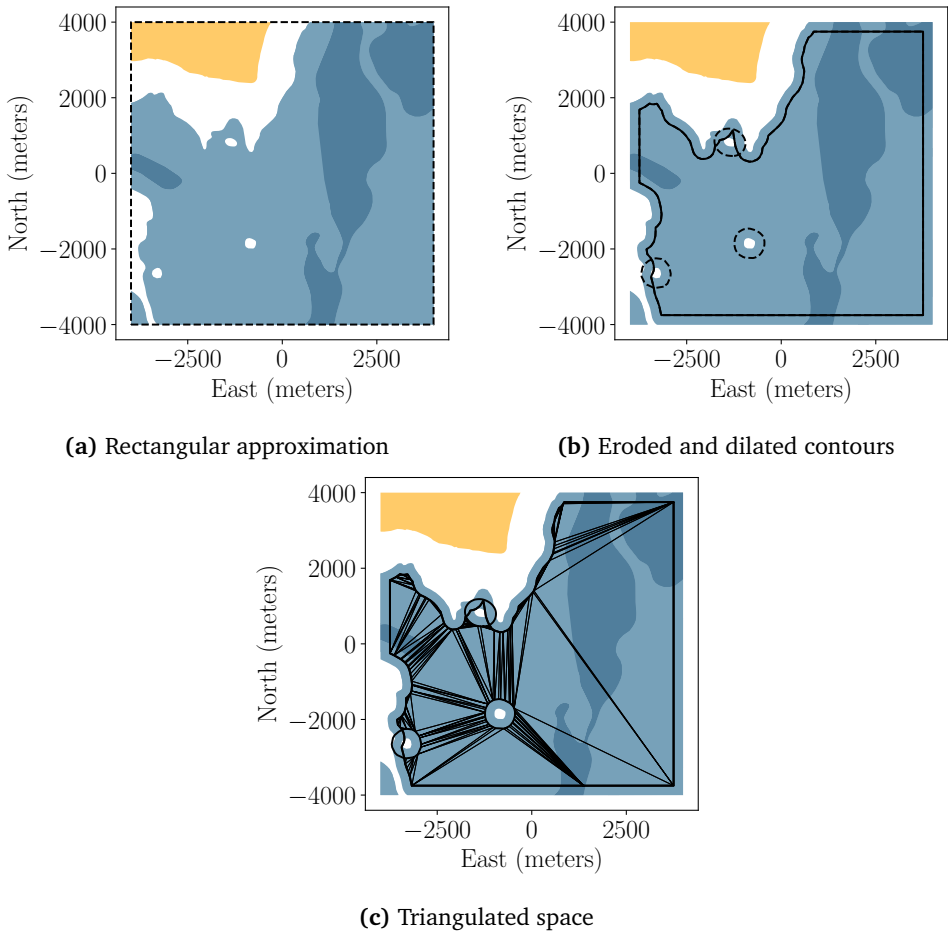
Figure C.7: Visualisation of real depth contours, where blue regions are feasible water depths, white indicate shallow waters and yellow the landmasses. (a) Represents the common rectangular approximation for sampling spaces and (c) the proposed triangulated contours. (b) By eroding the boundary contour (solid) and dilating holes (dashed) based on some safety margin, it is possible to encode safety distance directly into the the sampling space.

loss could also be included to minimise the impact of the proposed deviation(s) on the eventual port call. Examples of various other cost terms used in sampling-based planning include minimising the curvature or repulsive forces from obstacles and vessel [C41] or adding grounding awareness by including a probabilistic description of past behaviours in the area [C43].

C.6   Open and confined water sampling schemes

A large part of the effectiveness of a sampling-based motion planner is based on efficiently producing valuable samples. In order to maintain the optimality properties, a given sampling scheme must be able to uniformly sample the free space, in such a way that points that may improve the current best solution are always included. In most applications a rectangular shaped approximation is used to uniformly generate samples within the space. The rectangular approximation is useful for sampling in open waters, and can produce uniform samples in the North-East system as follows

$$N \sim \mathcal{U}(N_{\min}, N_{\max}), \quad E \sim \mathcal{U}(E_{\min}, E_{\max}), \tag{C.30}$$

where $\mathcal{U}$ produces uniformly distributed samples between its limits. However, such an approximation can be very poor, especially in circumstances where the area ratio between feasible water depths and the area of the sampling region is low [C43]. Furthermore, when dealing with confined waters, the generated samples must also be accepted/rejected depending on whether or not they fall within feasible water depths.

Therefore, it is proposed to directly sample the depth contours, rather than to uniformly sample a rectangle, and then reject samples that are infeasible. Since the feasible depth contours are shaped as arbitrary non-convex polygons, uniform sampling can be achieved through triangulation. By triangulating the non-convex contours, each triangle then represents a subregion that can be sampled uniformly. Constrained Delaunay Triangulation (CDT) [C66] is applied to generate a finite set of triangles. A property of CDT is that all triangles are guaranteed to be contained within the perimeter of the original non-convex polygon.

Once the set of triangles has been computed, uniformly generating points within the set is achieved using a two-step procedure: Uniformly selecting a triangle from the set, weighted by its area; then uniformly generating a North-East sample within the selected triangle.

Given an arbitrary triangle composed by the following vertices (A, B, C), a uniformly sampled point P within the triangle is then described by

$$P = (1 - \sqrt{r_1}) A + \sqrt{r_1} (1 - r_2) B + \sqrt{r_1} r_2 C \tag{C.31}$$

where $r_1 \sim \mathcal{U}(0, 1)$ and $r_2 \sim \mathcal{U}(0, 1)$ [C67].

Remark C.3. *The polygonal geometries from within a real ENC are typically represented at a very high resolution. Therefore, the triangulation procedure may results in a large set of very small triangles. For computational reasons it is recommended to simplify the polygons using a line simplification method, e.g. by using the Douglas-Peucker*

algorithm [C68]. Note that by simplifying the polygons one can no longer guarantee
that the polygon represents exactly the same boundary, meaning that a simplification
may cause the polygon contours to fall within shallow waters.

C.6.1   Sampling spaces for grounding avoidance

An interesting note is that measures for grounding avoidance can be considered
directly in the formulation of the sampling space, simply by eroding or dilating the
contour lines. By doing so, the generated sampling space will uniformly sample
the area that maintains a certain safety distance from the contours lines. Fig. C.7b
shows the erosion and dilation procedure being applied to real ENC contours, and
by instead triangulating these polygons (Fig. C.7c) a sampling space which respects
a certain safety margin is generated.

Grounding avoidance can also be considered by formulating the sampling space
such that one only samples points that fall within the XTD limits of the nominal
route. This may result in conservative deviations, however, it does guarantee that
the proposed deviations conform with the requirements specified for the nominal
route.

C.7   Results

The following section details the simulation results obtained from applying the
proposed collision and grounding avoidance framework on the case studies presented
in Section C.2.2. The case study is divided into three local areas, with each area
having a varying degree of restrictions due confined waters and the underlying
complexity of the nominal route. Fig. C.8 summarises the results, where each of the
three areas is divided into two scenarios, successfully demonstrating the ability of
the framework to compute safe and compliant route deviations when subjected to
single and multiple vessel encounters.

More specifically, the results in Fig. C.8a, C.8b, C.8d, and C.8e highlights a
crucial component of the proposed framework, namely the ability to consider a
multi-leg nominal route. Such multi-leg problems are rarely considered within the
state-of-the-art for this particular class of algorithms, and if so, are often dealt with as
conventional path planning problems, where typically the entire path is re-planned
using path length as a metric [C40], [C41]. However, such a drastic re-plan may be
infeasible for larger crafts, due to inherent navigational restrictions and poor safety
guarantees.

The nominal route plays an important role for navigational safety, as it is part
of the design process before departure. Disregarding its existence when computing

(a) Crossing scenario

(b) Overtaking scenario

(c) Head-on scenario

(d) Crossing and head-on scenario

(e) Overtaking and crossing scenario

(f) Head-on and crossing scenario
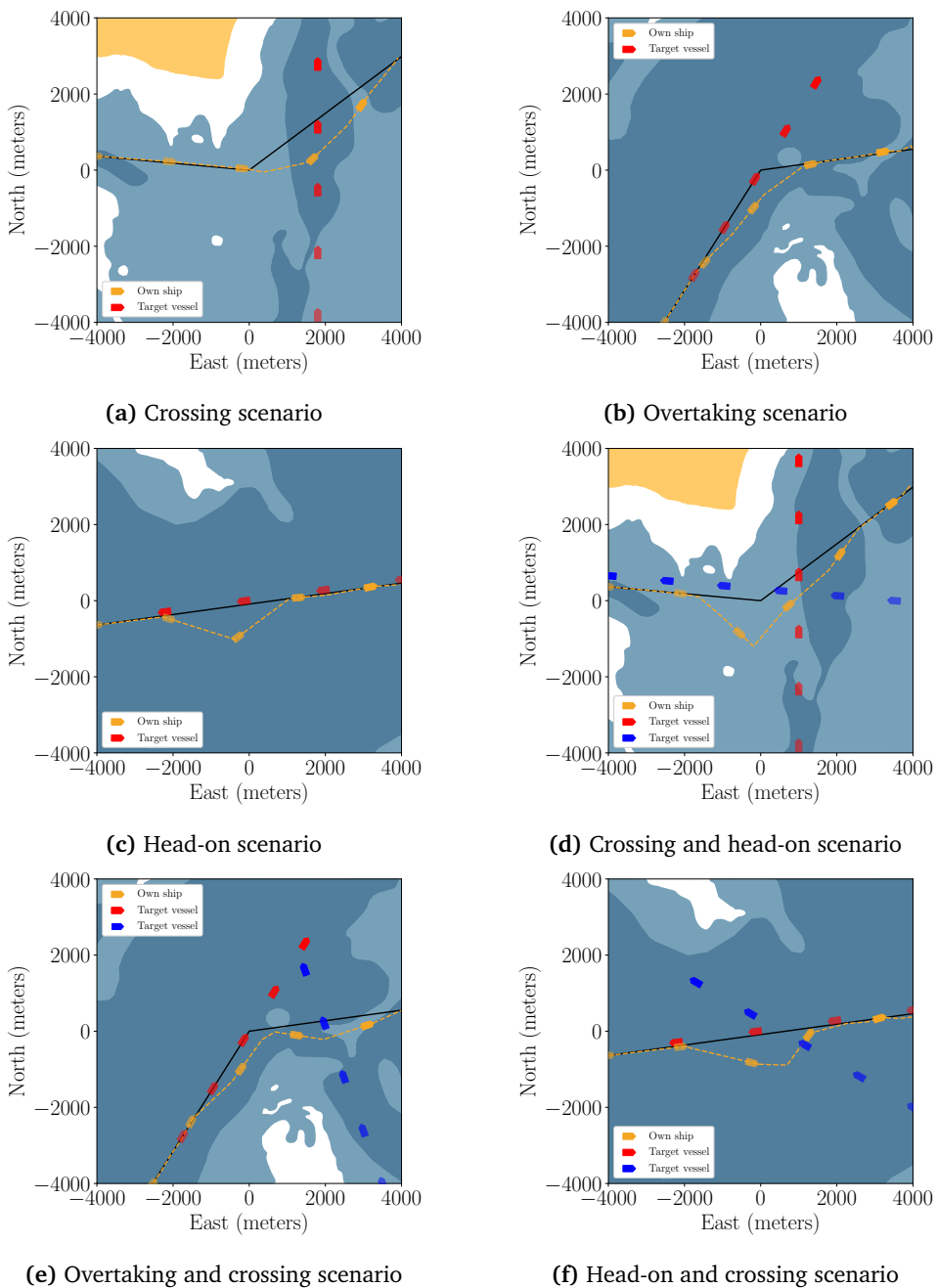
Figure C.8: Results demonstrating the proposed frameworks ability to deal with single and multi vessel encounters, along single and multiple legs, where each of the scenarios utilize a combination of the proposed cost terms. The scenarios presented in (a),(b),(d) and (e) highlight the frameworks ability to compute deviations that respect the existence of a nominal trajectory.
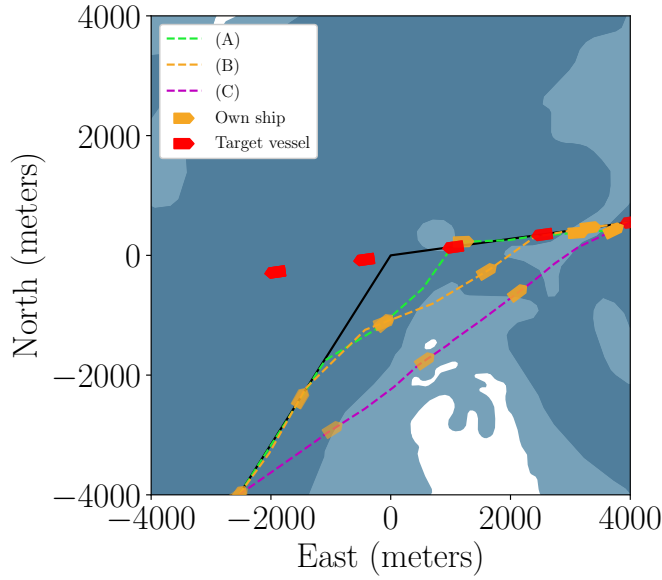
Figure C.9: Three proposed route deviations using different optimisation criteria. (A) Neglecting path elongation $c(\mathcal{P}^d) = w_e c_e + w_s c_s$, (B) Neglecting speed loss $c(\mathcal{P}^d) = w_l c_l + w_e c_e$, and (C) Neglecting cross-track error $c(\mathcal{P}^d) = w_l c_l + w_s c_s$.

a deviation introduces potential risks associated with both navigational comfort and safety. The results in Figs. C.8a, C.8b, C.8d, and C.8e show that the proposed framework accounts for the nominal route $\mathcal{P}^w$, and the cross-track error cost term $c_e(\mathcal{P}^d)$ ensures that the proposed deviations remain within its vicinity.

Figures C.8c and C.8f show the suggested path alterations for a scenario of lower navigation complexity where single and multiple vessel encounters occur along a single straight leg of the nominal path. Despite its reduced complexity, this scenario is very relevant for ocean going vessels, since a vast majority of the nominal passage is characterised by long straight path segments.

As detailed in Section C.1, an important use case for such a collision and grounding avoidance framework is as a decision support system to the navigator. The results in Fig. C.9 compare the path alterations generated using three different performance measures. One neglects path elongation (A), speed loss (B) and cross-track error (C). Suggested route deviations are shown on a graphical interface overlaid on an ENC, together with positional information for own ship and the target vessels. The navigator then selects the preferred deviation.

When the cost terms are selectively enabled and disabled, the importance of each individual term becomes evident. From the simple single-vessel encounter considered in Fig. C.9, it is clear that by disregarding the cost term related to the

cross-track error the SHP produces a highly unsafe trajectory, as the algorithm no longer considers the existence of the nominal route and instead minimises the path length between the initial and reentry point. This highlights the importance of considering the nominal route when computing a deviation, in order to maintain a safety close to that of the nominal route.

The results demonstrate the ability of the proposed framework to compute safe and COLREGs compliant route deviations. Using the sampling-based approach, the high-resolution nature of the depth contours present within the ENCs can be directly considered as part of the collision avoidance problem. The adopted cost terms ensure that the proposed alterations respect the nominal route, by including cross-track error as a performance index.

Currently, the framework constrains the computed deviation based on shallow water restrictions and the COLREGs. Additional constraints can be included to further comply with constraints of own vessel or of the voyage control system, such as limits to turn rate or routes with legs of insufficient length.

Deconflicting a collision situation by reducing speed is often an efficient means of avoiding changing course at a later time. This paper focuses on the course alteration part of collision avoidance and considers the possible change of speed as a separate problem.

C.8   Conclusions

The paper presented a novel framework to design a *Short Horizon Planner* for collision and grounding avoidance of ocean going vessels. The SHP builds on two main components: The availability of a nominal optimal route which must be considered when computing path alterations; the definition of sampling spaces that directly encode the navigation information available in the ENC. The former drove the design of the cost function by including the two key terms related to cross-track error and speed loss during steady turns. The latter enabled the planner to design optimal path deviations that are implicitly grounding aware, since shallow-water regions are not part of the sampling space.

Simulation scenarios of single and multi vessel encounters along single and multi-leg nominal paths have demonstrated the ability of the SHP to deconflict complex collision scenarios in open and confined waters. Moreover, the effect of the different cost terms has been analysed, and the importance of the cross-track error cost in ensuring a path alteration with the least nominal route deviation has been pointed out.

The proposed framework for the design of the SHP is very flexible to the intro-

duction of additional cost terms in the performance index (e.g. fuel consumption, energy efficiency, time loss); additional manoeuvring constraints (e.g. minimum distance between waypoints); different descriptors of the traversable water areas (e.g. probabilistic descriptors as in Enevoldsen and Galeazzi [C43]). This flexibility makes the proposed SHP largely adaptable to different types of ship operational profiles, as well as to preferences of the navigator who would like to use it as decision support tool.

CRediT authorship contribution statement

Thomas T. Enevoldsen: Conceptualization, Methodology, Software, Validation, Investigation, Writing - Original Draft. **Mogens Blanke**: Conceptualization, Writing - Review & Editing, Supervision, Funding acquisition. **Roberto Galeazzi**: Conceptualization, Writing - Review & Editing, Supervision, Funding acquisition.

Acknowledgements

C.9   A. CPA and TCPA

The Closest Point of Approach (CPA) and Time to Closest Point of Approach (TCPA) are two important quantities used by master mariners in order to navigate a vessel in a safe manner, where CPA together with the relative bearing is a determining factor for whether or not a COLREGs situation is developing, and an evasive manoeuvre must be performed.

Let

$$\mathbf{p}_{OS} = [N_{OS}, E_{OS}]^T, \quad \mathbf{p}_{TV} = [N_{TV}, E_{TV}]^T \tag{C.32}$$

be the position of own ship and target vessel in the North-East inertial frame respectively. Let

$$\mathbf{v}_{OS} = [U_{OS}\sin(\psi_{OS}), U_{OS}\cos(\psi_{OS})]^T \tag{C.33}$$

$$\mathbf{v}_{TV} = [U_{TV}\sin(\psi_{TV}), U_{TV}\cos(\psi_{TV})]^T \tag{C.34}$$

be the own ship and target vessel velocity vectors in the same frame, where $U_{(.)}$ is the vessel's speed and $\psi_{(.)}$ is the vessel's heading.

Knowing the positions and forward velocities of both vessels at the current time, TCPA is defined as

$$\text{TCPA} \triangleq -\frac{(\Delta \mathbf{p}(0))^T \Delta \mathbf{v}}{(\Delta \mathbf{v})^T \Delta \mathbf{v}} \tag{C.35}$$

with $\Delta \mathbf{v} = \mathbf{v}_{OS} - \mathbf{v}_{TV}$, $\Delta \mathbf{p}(0) = \mathbf{p}_{TV}(0) - \mathbf{p}_{OS}(0)$. Assuming both vessels maintain constant speed, their respective positions at time TCPA is computed as

$$\mathbf{p}_{OS}(\text{TCPA}) = \mathbf{p}_{OS}(0) + \mathbf{v}_{OS} \cdot \text{TCPA} \tag{C.36}$$

$$\mathbf{p}_{TV}(\text{TCPA}) = \mathbf{p}_{TV}(0) + \mathbf{v}_{TV} \cdot \text{TCPA} \tag{C.37}$$

The CPA is then defined as follows

$$\text{CPA} \triangleq \left\| \Delta \mathbf{p}(\text{TCPA}) - \frac{(\Delta \mathbf{p}(0))^T \Delta \mathbf{v}}{(\Delta \mathbf{v})^T \Delta \mathbf{v}} \Delta \mathbf{v} \right\| \tag{C.38}$$

which provides a metric of how close the two vessels will be at $t = \text{TCPA}$. A graphical interpretation of this derivation is provided in Fig. C.10.
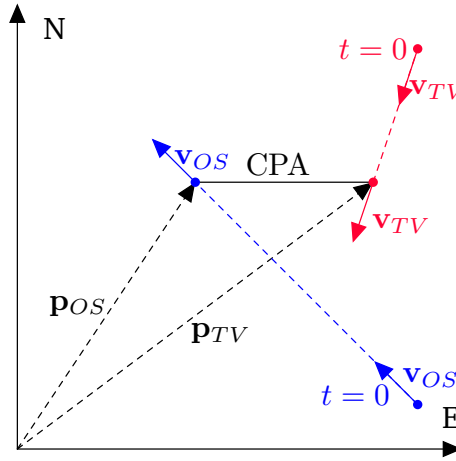
Figure C.10: Vector definitions for the derivation of CPA and TCPA for two vessels with constant speed and heading.

C.10   References

[C1]   EMSA, *Annual overview of marine casualties and incidents 2020*, 2020.

[C2]   Ö. Uğurlu, U. Yıldırım, and E. Başar, "Analysis of grounding accidents caused by human error," *Journal of Marine Science and Technology*, vol. 23, no. 5, pp. 748–760, 2015.

[C3]   A. Komianos, "The autonomous shipping era. operational, regulatory, and quality challenges," *TransNav: International Journal on Marine Navigation and Safety of Sea Transportation*, vol. 12, 2018.

[C4]   M. Kim, T.-H. Joung, B. Jeong, and H.-S. Park, "Autonomous shipping and its impact on regulations, technologies, and industries," *Journal of International Maritime Safety, Environmental Affairs, and Shipping*, vol. 4, no. 2, pp. 17–25, 2020.

[C5]   K. Dittmann, N. Hansen, D. Papageorgiou, S. Jensen, M. Lützen, and M. Blanke, "Autonomous Surface Vessel with Remote Human on the Loop: System Design for STCW Compliance," *Proceedings of 13th IFAC Conference on Control Applications in Marine Systems, Robotics, and Vehicles*, 2021.

[C6]   K. Dittmann, P. N. Hansen, D. Papageorgiou, and M. Blanke, "Autonomy for ships: A sovereign agents architecture for reliability and safety by design," *IEEE Xplore-Proc. IEEE SysTol*, 2021.

[C7]   P. N. Hansen, D. Papageorgiou, M. Blanke, R. Galeazzi, M. Lützen, J. Mogensen, M. Bennedsen, and D. Hansen, "COLREGs-based Situation Awareness for Marine Vessels-a Discrete Event Systems Approach," *IFAC-PapersOnLine*, vol. 53, no. 2, pp. 14 501–14 508, 2020. DOI: 10.1016/j.ifacol.2020.12.1453.

[C8]   D. Papageorgiou, P. Hansen, and M. Blanke, "Anticipation of ship behaviours in multi-vessel scenarios," *Ocean Engineering*, 2022, re-submitted.

[C9]   K. Dittmann and M. Blanke, "Risk mitigation by design of autonomous maritime automation systems," *at - Automatisierungstechnik*, vol. 70, no. 5, pp. 469–481, May 2022. DOI: 10.1515/auto-2021-0151.

[C10] Y. Huang, L. Chen, P. Chen, R. R. Negenborn, and P. van Gelder, "Ship collision avoidance methods: State-of-the-art," *Safety science*, vol. 121, pp. 451–473, 2020.

[C11]   A. Vagale, R. T. Bye, R. Oucheikh, O. L. Osen, and T. I. Fossen, "Path planning and collision avoidance for autonomous surface vehicles II: a comparative study of algorithms," *Journal of Marine Science and Technology*, no. 0123456789, Feb. 2021. DOI: 10.1007/s00773-020-00790-x.

[C12]   A. Vagale, R. Oucheikh, R. T. Bye, O. L. Osen, and T. I. Fossen, "Path planning and collision avoidance for autonomous surface vehicles I: a review," *Journal of Marine Science and Technology*, vol. i, no. 0123456789, pp. 2018–2028, Jan. 2021. DOI: 10.1007/s00773-020-00787-6.

[C13]   IMO, *Convention on the international regulations for preventing collisions at sea, 1972 (COLREGs)*. 1972.

[C14]   S. Campbell, W. Naeem, and G. Irwin, "A review on improving the autonomy of unmanned surface vehicles through intelligent collision avoidance manoeuvres," *Annual Reviews in Control*, vol. 36, no. 2, pp. 267–283, 2012.

[C15]   C. Tam and R. Bucknall, "Cooperative path planning algorithm for marine surface vessels," *Ocean Engineering*, vol. 57, pp. 25–33, 2013.

[C16]   S. Campbell and W. Naeem, "A rule-based heuristic method for COLREGS-compliant collision avoidance for an unmanned surface vehicle," *IFAC Proceedings Volumes*, vol. 45, no. 27, pp. 386–391, 2012.

[C17]   S. Campbell, M. Abu-Tair, and W. Naeem, "An automatic COLREGs-compliant obstacle avoidance system for an unmanned surface vehicle," *Proceedings of the Institution of Mechanical Engineers, Part M: Journal of Engineering for the Maritime Environment*, 2014.

[C18]   A. Lazarowska, "Ship's trajectory planning for collision avoidance at sea based on ant colony optimisation," *Journal of Navigation*, vol. 68, no. 2, pp. 291–307, 2015.

[C19]   A. Lazarowska, "Research on algorithms for autonomous navigation of ships," *WMU Journal of Maritime Affairs*, vol. 18, no. 2, pp. 341–358, Jun. 2019.

[C20]   S. Ni, Z. Liu, Y. Cai, and X. Wang, "Modelling of ship's trajectory planning in collision situations by hybrid genetic algorithm," *Polish Maritime Research*, vol. 25, no. 3, pp. 14–25, 2018.

[C21]   S. Ni, Z. Liu, and Y. Cai, "Ship manoeuvrability-based simulation for ship navigation in collision situations," *Journal of Marine Science and Engineering*, vol. 7, no. 4, 2019.

[C22] M.-C. C. Tsou, "Multi-target collision avoidance route planning under an ECDIS framework," *Ocean Engineering*, vol. 121, pp. 268–278, Jul. 2016. DOI: 10.1016/j.oceaneng.2016.05.040.

[C23] W. Naeem, S. C. Henrique, and L. Hu, "A reactive COLREGs-compliant navigation strategy for autonomous maritime navigation," *IFAC-PapersOnLine*, vol. 49, no. 23, pp. 207–213, 2016.

[C24] Y. Huang, P. H. van Gelder, and Y. Wen, "Velocity obstacle algorithms for collision prevention at sea," *Ocean Engineering*, vol. 151, no. January, pp. 308–321, 2018. DOI: 10.1016/j.oceaneng.2018.01.001.

[C25] Y. Huang, L. Chen, and P. H. van Gelder, "Generalized velocity obstacle algorithm for preventing ship collisions at sea," *Ocean Engineering*, vol. 173, no. November 2018, pp. 142–156, 2019. DOI: 10.1016/j.oceaneng.2018.12.053.

[C26] B. H. Eriksen and M. Breivik, "Mpc-based mid-level collision avoidance for asvs using nonlinear programming," *2017 IEEE Conference on Control Technology and Applications (CCTA)*, 2017, pp. 766–772. DOI: 10.1109/CCTA.2017.8062554.

[C27] B. H. Eriksen, M. Breivik, E. F. Wilthil, A. L. Flåten, and E. F. Brekke, "The branching-course model predictive control algorithm for maritime collision avoidance," *Journal of Field Robotics*, vol. 36, no. 7, pp. 1222–1249, 2019.

[C28] T. A. Johansen, T. Perez, and A. Cristofaro, "Ship collision avoidance and COLREGS compliance using simulation-based control behavior selection with predictive hazard assessment," *IEEE transactions on intelligent transportation systems*, vol. 17, no. 12, pp. 3407–3422, 2016.

[C29] I. B. Hagen, D. K. M. Kufoalor, E. F. Brekke, and T. A. Johansen, "MPC-based collision avoidance strategy for existing marine vessel guidance systems," *2018 IEEE International Conference on Robotics and Automation (ICRA)*, IEEE, 2018, pp. 7618–7623.

[C30] D. K. M. Kufoalor, E. Wilthil, I. B. Hagen, E. F. Brekke, and T. A. Johansen, "Autonomous colregs-compliant decision making using maritime radar tracking and model predictive control," *2019 18th European Control Conference (ECC)*, IEEE, 2019, pp. 2536–2542.

[C31] D. K. M. Kufoalor, T. A. Johansen, E. F. Brekke, A. Hepsø, and K. Trnka, "Autonomous maritime collision avoidance: Field verification of autonomous surface vehicle behavior in challenging scenarios," *Journal of Field Robotics*, vol. 37, no. 3, pp. 387–403, 2020.

[C32] B. H. Eriksen, G. Bitar, M. Breivik, and A. M. Lekkas, "Hybrid collision avoidance for ASVs compliant with COLREGs rules 8 and 13–17," *Frontiers in Robotics and AI*, vol. 7, p. 11, 2020.

[C33] M. Abdelaal, M. Fränzle, and A. Hahn, "Nonlinear Model Predictive Control for trajectory tracking and collision avoidance of underactuated vessels with disturbances," *Ocean Engineering*, vol. 160, no. April, pp. 168–180, 2018. DOI: 10.1016/j.oceaneng.2018.04.026.

[C34] P. Chen, Y. Huang, E. Papadimitriou, J. Mou, and P. van Gelder, "Global path planning for autonomous ship: A hybrid approach of Fast Marching Square and velocity obstacles methods," *Ocean Engineering*, vol. 214, no. August, p. 107 793, 2020. DOI: 10.1016/j.oceaneng.2020.107793.

[C35] S. Garrido, D. Alvarez, and L. E. Moreno, "Marine applications of the fast marching method," *Frontiers in Robotics and AI*, vol. 7, p. 2, 2020.

[C36] P. Svec, B. C. Shah, I. R. Bertaska, J. Alvarez, A. J. Sinisterra, K. Von Ellenrieder, M. Dhanak, and S. K. Gupta, "Dynamics-aware target following for an autonomous surface vehicle operating under COLREGs in civilian traffic," *IEEE International Conference on Intelligent Robots and Systems*, pp. 3871–3878, 2013. DOI: 10.1109/IROS.2013.6696910.

[C37] B. C. Shah, P. Švec, I. R. Bertaska, A. J. Sinisterra, W. Klinger, K. von Ellenrieder, M. Dhanak, and S. K. Gupta, "Resolution-adaptive risk-aware trajectory planning for surface vehicles operating in congested civilian traffic," *Autonomous Robots*, vol. 40, no. 7, pp. 1139–1163, Oct. 2016.

[C38] K. Bergman, O. Ljungqvist, J. Linder, and D. Axehill, "A COLREGs Compliant Motion Planner for Autonomous Maneuvering of Marine Vessels in Complex Environments," *arXiv:2012.12145*, 2020.

[C39] H. T. L. Chiang and L. Tapia, "COLREG-RRT: An RRT-Based COLREGS-Compliant Motion Planner for Surface Vehicle Navigation," *IEEE Robotics and Automation Letters*, vol. 3, no. 3, pp. 2024–2031, 2018.

[C40] R. Zaccone, M. Martelli, and M. Figari, "A COLREG-compliant ship collision avoidance algorithm," *2019 18th European Control Conference, ECC 2019*, no. August, pp. 2530–2535, 2019.

[C41] R. Zaccone, "COLREG-Compliant Optimal Path Planning for Real-Time Guidance and Control of Autonomous Ships," *Journal of Marine Science and Engineering*, vol. 9, no. 4, 2021. DOI: 10.3390/jmse9040405.

[C42]   T. T. Enevoldsen, C. Reinartz, and R. Galeazzi, "COLREGs-Informed RRT* for Collision Avoidance of Marine Crafts," *2021 IEEE International Conference on Robotics and Automation (ICRA)*, 2021, pp. 8083–8089. DOI: `10.1109/ICRA48506.2021.9560909`.

[C43]   T. T. Enevoldsen and R. Galeazzi, "Grounding-aware RRT* for Path Planning and Safe Navigation of Marine Crafts in Confined Waters," *IFAC-PapersOnLine*, vol. 54, no. 16, pp. 195–201, 2021, 13th IFAC Conference on Control Applications in Marine Systems, Robotics, and Vehicles CAMS 2021. DOI: `https://doi.org/10.1016/j.ifacol.2021.10.093`.

[C44]   S. Hexeberg, A. L. Flåten, E. F. Brekke, *et al.*, "Ais-based vessel trajectory prediction," *2017 20th International Conference on Information Fusion (Fusion)*, IEEE, 2017, pp. 1–8.

[C45]   F. E. T. Schöller, T. T. Enevoldsen, J. B. Becktor, and N. Hansen, "Trajectory prediction for marine vessels using historical ais heatmaps and long short-term memory networks," *Proceedings of 13th IFAC Conference on Control Applications in Marine Systems, Robotics, and Vehicles*, 2021.

[C46]   S. Lefèvre, D. Vasquez, and C. Laugier, "A survey on motion prediction and risk assessment for intelligent vehicles," *ROBOMECH journal*, vol. 1, no. 1, pp. 1–14, 2014.

[C47]   D. Papageorgiou, M. Blanke, M. Lützen, M. Bennedsen, J. Mogensen, and S. Hansen, "Parallel automaton representation of marine crafts' COLREGs-based manoeuvering behaviours," *IFAC-PapersOnLine*, vol. 52, no. 21, pp. 103–110, 2019.

[C48]   L. Perera, J. Carvalho, and C. G. Soares, "Fuzzy logic based decision making system for collision avoidance of ocean navigation under critical collision conditions," *Journal of marine science and technology*, vol. 16, no. 1, pp. 84–99, 2011.

[C49]   M. G. Hansen, T. K. Jensen, T. Lehn-Schiøler, K. Melchild, F. M. Rasmussen, and F. Ennemark, "Empirical ship domain based on AIS data," *The Journal of Navigation*, vol. 66, no. 6, pp. 931–940, 2013.

[C50]   A. N. Cockcroft and J. N. F. Lameijer, *Guide to the collision avoidance rules*. Elsevier, 2003.

[C51]   E. Lewis, S. of Naval Architects, and M. E. (U.S.), *Principles of Naval Architecture: Motions in waves and controllability*. Society of Naval Architects and Marine Engineers, 1988.

[C52]   M. Blanke and A. G. Jensen, "Dynamic properties of a container vessel with low metacentric height," *Transactions of the Institute of Measurement and Control*, vol. 19, no. 2, pp. 78–93, 1997.

[C53]   J. D. Gammell, S. S. Srinivasa, and T. D. Barfoot, "Informed RRT*: Optimal sampling-based path planning focused via direct sampling of an admissible ellipsoidal heuristic," *IEEE International Conference on Intelligent Robots and Systems*, pp. 2997–3004, 2014.

[C54]   S. Karaman and E. Frazzoli, "Sampling-based algorithms for optimal motion planning," *The international journal of robotics research*, vol. 30, no. 7, pp. 846–894, 2011.

[C55]   J. D. Gammell, S. S. Srinivasa, and T. D. Barfoot, "Batch informed trees (BIT*): Sampling-based optimal planning via the heuristically guided search of implicit random geometric graphs," *2015 IEEE international conference on robotics and automation (ICRA)*, IEEE, 2015, pp. 3067–3074.

[C56]   L. Janson, E. Schmerling, A. Clark, and M. Pavone, "Fast marching tree: A fast marching sampling-based method for optimal motion planning in many dimensions," *The International journal of robotics research*, vol. 34, no. 7, pp. 883–921, 2015.

[C57]   J. D. Gammell and M. P. Strub, "Asymptotically optimal sampling-based motion planning methods," *Annual Review of Control, Robotics, and Autonomous Systems*, vol. 4, pp. 295–318, 2021.

[C58]   S. M. Lavalle, "Rapidly-exploring random trees: A new tool for path planning," Tech. Rep., 1998.

[C59]   L. G. D. Véras, F. L. Medeiros, and L. N. Guimaráes, "Systematic literature review of sampling process in rapidly-exploring random trees," *IEEE Access*, vol. 7, pp. 50 933–50 953, 2019.

[C60]   J. Larson, M. Bruch, and J. Ebken, "Autonomous navigation and obstacle avoidance for unmanned surface vehicles," *Unmanned systems technology VIII*, International Society for Optics and Photonics, vol. 6230, 2006, p. 623 007.

[C61]   M. Abkowitz, *Lectures on Ship Hydrodynamics: Steering and Maneuvrability* (Hydrodynamisk og aerodynamisk Laboratorium; report; series Hy). Hydro- og Aerodynamisk Laboratorium, Hydrodynamics Department, 1964.

[C62]   M. Blanke, *Ship propulsion losses related to automatic steering and prime mover control*. Technical University of Denmark, 1981.

[C63] Z. Chuang and S. Steen, "Speed loss due to seakeeping and maneuvering in zigzag motion," *Ocean engineering*, vol. 48, pp. 38–46, 2012.

[C64] T. I. Fossen, *Handbook of marine craft hydrodynamics and motion control*. John Wiley & Sons, 2011.

[C65] A. F. Molland and S. R. Turnock, "8 - manoeuvring," *Marine Rudders and Control Surfaces*, A. F. Molland and S. R. Turnock, Eds., Oxford: Butterworth-Heinemann, 2007, pp. 333–343. DOI: https://doi.org/10.1016/B978-075066944-3/50011-1.

[C66] L. P. Chew, "Constrained delaunay triangulations," *Algorithmica*, vol. 4, no. 1, pp. 97–108, 1989.

[C67] R. Osada, T. Funkhouser, B. Chazelle, and D. Dobkin, "Shape distributions," *ACM Transactions on Graphics (TOG)*, vol. 21, no. 4, pp. 807–832, 2002.

[C68] D. H. Douglas and T. K. Peucker, "Algorithms for the reduction of the number of points required to represent a digitized line or its caricature," *Cartographica: the international journal for geographic information and geovisualization*, vol. 10, no. 2, pp. 112–122, 1973.

Paper D

Informed Sampling-based Collision Avoidance with Least Deviation from the Nominal Path

Thomas T. Enevoldsen[1*] and Roberto Galeazzi[1]

[1]Automation and Control Group, Department of Electrical and Photonics Engineering, Technical University of Denmark, DK-2800 Kgs. Lyngby, Denmark {tthen,roga}@dtu.dk

Abstract:
This paper addresses local path re-planning for n-dimensional systems by introducing an informed sampling scheme and cost function to achieve collision avoidance with minimum deviation from an (optimal) nominal path. The proposed informed subset consists of the union of ellipsoids along the specified nominal path, such that the subset efficiently encapsulates all points along the nominal path. The cost function penalizes large deviations from the nominal path, thereby ensuring current safety in the face of potential collisions while retaining most of the overall efficiency of the nominal path. The proposed method is demonstrated on scenarios related to the navigation of autonomous marine crafts.

D.1   Introduction

The collision avoidance system is a crucial component for the safe motion control of autonomous systems seeking widespread adoption across different industrial sectors, such as collective mobility, precision farming, intermodal logistics, smart manufacturing. In all these industrial processes the operations carried out by or with the support of autonomous systems are characterized by some combination of metrics of efficiency – e.g., minimum time, minimum energy, minimum distance –, and safety. The efficient execution of such operations implies the adherence to an (optimal) nominal path by the autonomous bus [D1], [D2], autonomous ship [D3] or autonomous robot [D4]. At the mission planning stage it is hard to account for the dynamically changing local environments. Hence, there is the need for a path planner that computes optimal local deviations from the nominal path to ensure current safety while retaining most of the overall efficiency of nominal path, whenever a collision may disrupt the ongoing operation.

Sampling-based motion planners are highly efficient at addressing complex planning problems with multiple constraints, such as those posed by collision avoidance and autonomous navigation tasks. Mechanisms and techniques for computing paths that minimize path length using sampling-based methods are widespread in current literature [D5], [D6], with one of the most influential methods being the Informed RRT* [D7], which reduces the sampling space to an informed subset, contained within an ellipsoid, once an initial path is obtained. The informed set guarantees that it contains any point that can improve the solution, whilst increasing the probability that the solution cost is decreased by sampling within the subset. However, these methods typically seek to minimize path length, where for collision avoidance one may instead wish to efficiently compute paths with minimal deviation from a nominal.

This paper focuses on local path re-planning for n-dimensional systems which have an (optimal) nominal path to achieve collision avoidance in dynamic environments, and it makes the following contributions. First, we propose an extension to the concept of the informed subset to allow for convergence towards solutions with minimum path deviation. This is achieved by introducing a cost function, which allows the underlying algorithm to minimize with respect to the nominal path. The extension involves forming multiple overlapping informed subsets along the nominal path, which results in an informed set composed of the union of multiple ellipsoidal subsets (Fig. D.1). Last, a switching condition and additional sampling biasing are proposed to allow for rapid convergence towards the nominal path.

(a) $N = 250$, $c_d(\sigma) = 895$

(b) $N = 500$, $c_d(\sigma) = 285$

(c) $N = 750$, $c_d(\sigma) = 229$

(d) $N = 1000$, $c_d(\sigma) = 206$
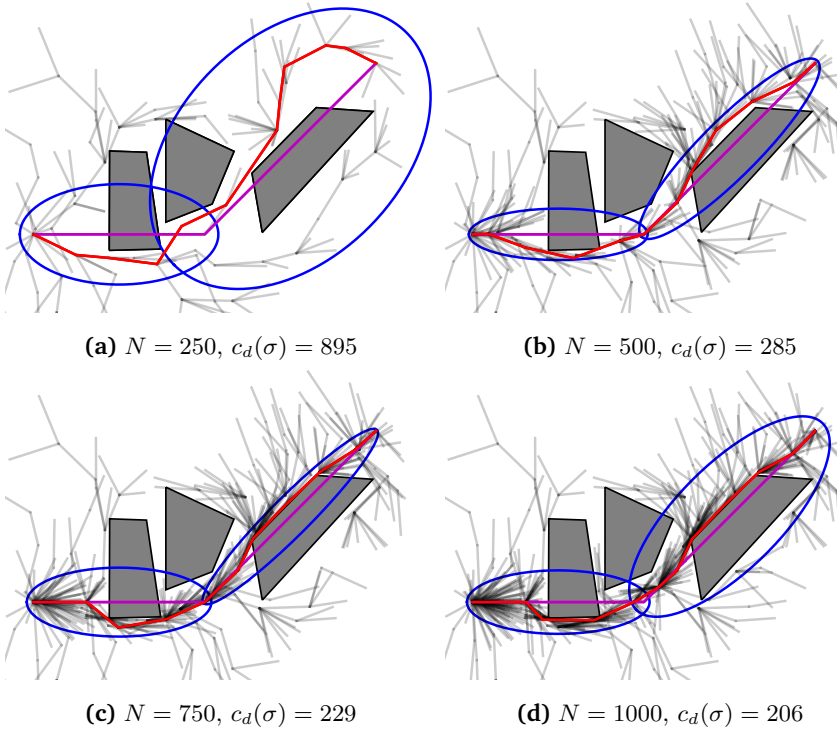
Figure D.1: Informed sampling strategy for computing the minimum path deviation, where an ellipsoidal subset is formed along each segment of the nominal trajectory. The nominal trajectory (magenta) is obstructed by some obstacles, and therefore the planned path (red) is computed to circumvent these whilst minimizing the deviation from the nominal path.

D.1.1 Related work

Optimal Sampling-based Motion Planning (SBMP) came to fruition when [D8] introduced RRT* and PRM*, which are asymptotically optimal in probability [D6]. To improve the convergence rate and performance of RRT*, [D7], [D9] proposed the Informed RRT*, which reduces the sampling space to an ellipsoidal subset once an initial solution is found. This increases the probability that each subsequent sample has a greater likelihood of improving the current best found solution. The concept of the informed subset then became an integral part of other SBMP algorithms [D10]–[D12].

Current research aims at extending the capabilities of the informed subset to further accelerate convergence to certain classes of solutions. Recently, [D13] identifies smaller informed sets within the informed set itself, using the notion of a beacon, and thereby honing the search. In [D14] the authors also propose a method for identifying subregions within the informed set. [D15] specializes an informed

sampling scheme that decreases the size of the search space to produce paths that abide by the maritime rules-of-the-road. [D16] slides an informed subset along the found path, computing local solutions of minimum path length. The work by [D17] utilizes a pre-computed gridmap in order to find an initial solution quickly, such that the informed subset [D7] can be applied sooner. [D18] proposes a scheme for sampling generalized informed sets using Markov Chain Monte Carlo, allowing for arbitrarily shaped non-convex informed sets. [D19] proposes to inform the planning algorithm about the manipulation task of mobile manipulators, i.e. a sequence of poses the end-effector must reach, by introducing it as success criterion when computing the movement of the mobile base. [D6] details a general overview of the state-of-the-art in optimal SBMP.

Within the fields of self-driving cars and autonomous marine systems, SBMP has gotten a foothold. [D20] and [D21] survey the application of various motion planning techniques for autonomous vehicles, providing insight into the use of SBMP for driving in urban environments and highways, respectively. [D22] proposes a method for repairing existing trajectories, where infeasible parts of the nominal trajectory are repaired to compute feasible deviations. [D23] discretizes the nominal trajectory and places guide points in locations that are infeasible with the nominal, and thereby biases the sampling. [D24] uses an estimated nominal path, such as from a Voronoi graph, to guide the RRT exploration through cluttered environments. [D25] explores a sampling-based scheme that compute paths, which are similar in curvature to the nominal path. Whereas within the realm of discrete planning, algorithms such as lifelong planning A* [D26] and D*-lite [D27] concern efficient re-planning.

In the maritime domain, SBMP algorithms are favoured due to the existence of both the complex constraints and environments. [D28] investigates using a non-holonomic RRT for collision avoidance. [D3], [D29] and [D30] utilize RRT* for collision avoidance, taking various other metrics into account, such as minimizing nominal path deviation, speed loss, curvature and grounding risk.

The reviewed literature emphasizes two main aspects: The informed set is a powerful and effective concept to channel the sampling effort of SBMP algorithms and achieve faster convergence to the optimal path; SBMP algorithms have been used to plan between the start and goal states for designing both nominal paths and path alterations along a single straight segment of a nominal path. This paper advances the application of informed SBMP algorithms to collision avoidance along multi-segment paths by introducing an extended informed set and a cost function that penalizes deviations from the nominal path.

D.2 Preliminaries

The general formulation of the optimal sampling-based motion planning problem is now presented, as well as the formalization of the informed subset as proposed by [D7].

D.2.1 Optimal sampling-based motion planning

Let $\mathcal{X} \subseteq \mathbb{R}^n$ be the state space, with $\mathbf{x}$ denoting the state. The state space is composed of two subsets: the free space X_{free}, and the obstacles X_{obs}, where $X_{\text{free}} = \mathcal{X} \backslash X_{\text{obs}}$. The states contained within X_{free} are all states that are feasible with respect to the constraints posed by the system and the environment. Let $\mathbf{x}_{\text{start}} \in X_{\text{free}}$ be the initial state at some time $t = 0$ and $\mathbf{x}_{\text{end}} \in X_{\text{free}}$ the desired final state at some time $t = T$. Let $\sigma : [0,1] \mapsto X_{\text{free}}$ be a sequence of states that constitutes a found path, and Σ be the set of all feasible and nontrivial paths. The objective is then to find the optimal path σ^*, which minimizes a cost function $c(\cdot)$, while connecting $\mathbf{x}_{\text{start}}$ to $\mathbf{x}_{\text{end}}$ through states $\mathbf{x}_i \in X_{\text{free}}$,

$$\sigma^* = \underset{\sigma \in \Sigma}{\arg \min} \left\{ c(\sigma) \mid \sigma(0) = \mathbf{x}_{\text{start}}, \, \sigma(1) = \mathbf{x}_{\text{end}}, \forall s \in [0,1], \, \sigma(s) \in X_{\text{free}} \right\}. \quad \text{(D.1)}$$

The most commonly adopted cost function is the Euclidean path length, which gives rise to the shortest path problem. Given a path σ consisting of n states, the Euclidean path length is given by

$$c_l(\sigma) = \sum_{i=1}^{n} \|\mathbf{x}_i - \mathbf{x}_{i-1}\|_2, \quad \forall \, \mathbf{x}_i \in \sigma. \quad \text{(D.2)}$$

The cost function is additive, i.e. given a sequence of n states and some index k the following equality holds true

$$c((\mathbf{x}_0, \dots, \mathbf{x}_n)) = c((\mathbf{x}_0, \dots, \mathbf{x}_k)) + c((\mathbf{x}_k, \dots, \mathbf{x}_n)) \quad \text{(D.3)}$$

Therefore, whenever a new node or edge is added, the cost to go from the root to the nearest node, together with the cost from the nearest node to the new node, is computed as

$$c(\sigma) = c((\mathbf{x}_{\text{start}}, \dots, \mathbf{x}_{\text{nearest}})) + c((\mathbf{x}_{\text{nearest}}, \mathbf{x}_{\text{new}})) \quad \text{(D.4)}$$

as required by the underlying SBMP [D8].

D.2.2 Informed sampling

The concept of an informed sampling space was introduced by [D7] with the Informed RRT*. It was shown that the reduction of the sampling region to an informed
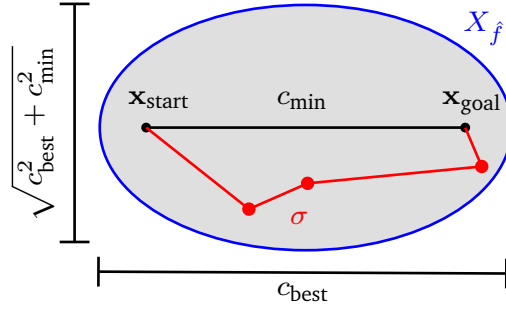
Figure D.2: The informed subset as proposed by [D7], the sampling region is reduced to an ellipsoid, and thereby increasing the probability that the sampled states improve the found path.

subset increased the probability that each subsequent sample would improve the current best found solution. In the case of [D7], [D9] an informed subset for the euclidean distance was formulated as an ellipsoid, and was given by

$$X_{\hat{f}} = \{\mathbf{x} \in \mathcal{X} \mid \|\mathbf{x}_{\text{start}} - \mathbf{x}\|_2 + \|\mathbf{x} - \mathbf{x}_{\text{end}}\|_2 \leq c_{\text{best}}\} \tag{D.5}$$

with $\mathbf{x}_{\text{start}}$ and $\mathbf{x}_{\text{end}}$ representing the start and end states of a given path, and c_{best} the path length of the current best found path. Once an initial path is obtained, one can form an informed subset that is scaled based on the the minimum possible path c_{min} and c_{best}, as shown in Fig. D.2. The informed subset, which is a prolate hyperspheroid, represents all possible points that can improve the current solution cost, and allows one to sample these particular points directly. Generating samples within the ellipsoid can be done analytically, as described in [D7].

Typically, the initial sampling scheme consists of uniformly sampling the state space, which is commonly achieved by uniformly sampling a n-dimensional hyper-rectangle $\mathbf{x}_{\text{rand}} \sim \mathcal{U}(X_{\text{rect}})$. In order to ensure that it is favourable to switch to a given informed set, its Lebesgue measure is typically compared to that of the original sampling space

$$\lambda\left(X_{\hat{f}}\right) < \lambda(X_{\text{rect}}) \tag{D.6}$$

where the Lebesgue measure of the ellipsoid is given by [D9]

$$\lambda\left(X_{\hat{f}}\right) = \frac{c_{\text{best}}(c_{\text{best}}^2 - c_{\text{min}}^2)^{\frac{n-1}{2}}}{2^n} \frac{\pi^{\frac{n}{2}}}{\Gamma\left(\frac{n}{2} + 1\right)} \tag{D.7}$$

with c_{best} and c_{min} as shown in Fig. D.2. Further details regarding the informed subset can be found in [D7] and [D9].

D.3   Informed sampling for collision avoidance with least path deviation

The novel contribution of the paper is now introduced by formalizing the cost function for computing paths with minimum deviation, the associated informed space, a proposed sampling bias and the switching condition.

D.3.1   Cost function for minimum path deviation

Let σ^{nom} be the nominal path, i.e. the sequence of m states $\mathbf{x}_i^{\mathrm{nom}} \in \mathcal{X}$ that connect $\mathbf{x}_{\mathrm{start}}$ and $\mathbf{x}_{\mathrm{end}}$. It is assumed that two consecutive states, $\mathbf{x}_i^{\mathrm{nom}}$ and $\mathbf{x}_{i+1}^{\mathrm{nom}}$ belonging to σ^{nom}, are connected by piece-wise linear segments. Let σ^{dev} be the computed path deviation from the state $\mathbf{x}_{\mathrm{start}} \in \sigma^{\mathrm{nom}}$ to the end state $\mathbf{x}_{\mathrm{end}} \in \sigma^{\mathrm{nom}}$, i.e.

$$\sigma^{\mathrm{dev}} = \left(\mathbf{x}_k^{\mathrm{dev}}\right)_{k=1}^N \tag{D.8}$$

where $\mathbf{x}_1^{\mathrm{dev}} = \mathbf{x}_{\mathrm{start}}$ and $\mathbf{x}_N^{\mathrm{dev}} = \mathbf{x}_{\mathrm{end}}$.

The cost function that penalizes deviations from the nominal path is defined as the distance of each state in the path σ^{dev} to the closest point in the nominal path σ^{nom}, as follows

$$c_d(\sigma^{\mathrm{dev}}) \triangleq \sum_{k=1}^N \min \left\|\sigma^{\mathrm{nom}} - \mathbf{x}_k^{\mathrm{dev}}\right\|_2, \quad \forall \mathbf{x}_k \in \sigma^{\mathrm{dev}} \tag{D.9}$$

which yields solutions that tend towards the nominal path. However, depending on the length of each segment in σ^{nom} and the underlying steering function, minimizing the proposed cost function may result in corner cutting behaviour at the transition between two nominal path segments.

For a tighter fit in the corners, both the nominal and found path can be linearly interpolated, such that the deviation is computed with a resolution ϵ between each state in the path σ^{dev} towards the interpolated nominal. As the nominal path remains fixed, one can efficiently compute the distance towards it using e.g. a k-d tree. Depending on the tightness required for a given application, one can adjust ϵ accordingly or entirely skip interpolating.

The cost of the deviation tends towards the global minimum as the resolution of the nominal and deviation is increased,

$$\lim_{\epsilon \to 0} c_d(\sigma^{\mathrm{dev}}) = c_d(\sigma^*) \tag{D.10}$$

where both σ^{dev} and σ^{nom} are linearly interpolated with resolution ϵ. Similarly, for the obstacle free case

$$\lim_{\epsilon \to 0} \sigma^{\mathrm{dev}} = \sigma^* = \sigma^{\mathrm{nom}} \tag{D.11}$$

(a) $n = 80$ **(b)** $n = 180$ **(c)** $n = 400$
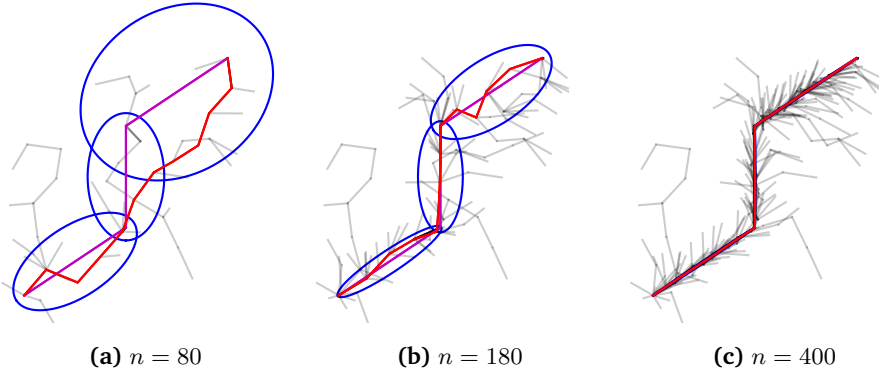
Figure D.3: Without obstacles, the informed subsets (blue) computes a path (red) that converges to the nominal (magenta).

the deviation converges to the global minimum (σ^{nom}), which is demonstrated in Fig. D.3.

Remark D.1. *The proposed motion planner can be extended to account for multiple objectives, potentially conflicting, by expanding the cost function* (D.9) *with additional terms properly weighted. For instance, if path length should also be in focus, then the following cost function will trade off between path deviation $c_d(\cdot)$ and total path length $c_l(\cdot)$ through the weight $\omega \in [0, 1)$*

$$c(\sigma^{dev}) = (1 - \omega)c_d(\sigma^{dev}) + \omega c_l(\sigma^{dev}). \tag{D.12}$$

D.3.2 Informed sampling for minimizing path deviation

Given the nominal path σ^{nom} consisting of m states, the proposed informed subset consists of the union of $m - 1$ ellipsoids along each nominal path segment, that is

$$X_{\hat{F}} = \bigcup_{i=1}^{m-1} X_{\hat{f},i} \tag{D.13}$$

where

$$X_{\hat{f},i} = \{\mathbf{x} \in \mathcal{X} \mid \|\mathbf{x}_i^{\text{nom}} - \mathbf{x}\|_2 + \|\mathbf{x} - \mathbf{x}_{i+1}^{\text{nom}}\|_2 \leq c_{\text{best},i}\}. \tag{D.14}$$

When $m = 2$ the method defaults to the informed subset from [D7]. An important guarantee posed by the informed subset in [D7] is that the encompassing ellipsoid guarantees to include all possible points that may improve the current best found solution. It is therefore important that the union of ellipsoids is constructed such that the same guarantee is maintained.

To ensure that the entire path always falls within the joined ellipsoids, the computation of $c_{\text{best},i}$ must share states with the neighbouring ellipsoids. Given the nominal path σ^{nom} there are $m-2$ states $\mathbf{x}_i^{\text{nom}}$ connecting $\mathbf{x}_{\text{start}}$ to $\mathbf{x}_{\text{end}}$ through σ^{nom}. Let $\mathcal{N}$ be the finite sequence of common states that are defined as the nearest states in the current path deviation σ^{dev} to each of the $m-2$ nominal states $\mathbf{x}_i^{\text{nom}}$, i.e.

$$\mathcal{N} = ((\mathbf{x}^*, k)_j)_{j=1}^{m-2} \tag{D.15}$$

where

$$\mathbf{x}^* = \arg\min_{\mathbf{x}^{\text{dev}} \in \sigma^{\text{dev}}} \left\| \mathbf{x}^{\text{dev}} - \mathbf{x}_i^{\text{nom}} \right\|_2, \quad \forall i = 2, \ldots, m-1 \tag{D.16}$$

and k is the index identifying the position of the state $\mathbf{x}^*$ in the path deviation σ^{dev}. The corresponding $c_{\text{best},i}$ for each ellipsoid is then computed for $m > 2$,

$$\mathcal{C}_{best} = \left(c_{\text{best},i} = c_l(\rho_i) \quad \forall i = 1, \ldots, m-1 \right) \tag{D.17}$$

where

$$\rho_i = \begin{cases} \left(\mathbf{x}_{\text{start}}, \mathbf{x}_2^{\text{dev}}, \ldots, \mathbf{x}_i^*, \mathbf{x}_{i+1}^{\text{nom}} \right) & \text{if } i = 1 \\ \left(\mathbf{x}_i^{\text{nom}}, \mathbf{x}_{i-1}^*, \mathbf{x}_{k_{i-1}+1}^{\text{dev}}, \ldots, \mathbf{x}_i^*, \mathbf{x}_{i+1}^{\text{nom}} \right) & \text{if } 1 < i < m-1 \\ \left(\mathbf{x}_i^{\text{nom}}, \mathbf{x}_{i-1}^*, \mathbf{x}_{k_{i-1}+1}^{\text{dev}}, \ldots, \mathbf{x}_{N-1}^{\text{dev}}, \mathbf{x}_{\text{end}} \right) & \text{if } i = m-1 \end{cases} \tag{D.18}$$

is the piece-wise continuous part of the current path deviation σ^{dev} contained within an ellipsoid, and connected with the closest corresponding state along the nominal trajectory, as shown in Fig. D.4.

Given $X_{\hat{F}}$ and $\mathcal{C}_{\text{best}}$, one can guarantee, by construction, that the current deviation σ^{dev} and all points capable of improving said deviation, are contained within $X_{\hat{F}}$. As a given ρ_i has a state in common with each neighbouring ellipsoid through the node $\mathbf{x}_i^*$, therefore the combined path σ^{dev} is also guaranteed to exist within the union of ellipsoids. The proposed subset maintains this property as the deviation converges to the minimum.

Once the sequence of ellipsoids has been constructed, one can sample them using the technique described by [D9], where a given ellipsoid is selected and subsequently uniformly sampled based on its relative measure. Samples are rejected in proportion to their membership of a given ellipsoid, in order maintain uniformity.

D.3.3   Sample biasing

Sample biasing is a very common technique for improving the performance of SBMP algorithms [D5], [D6], [D31]. Most implementations utilize a goal biasing strategy,
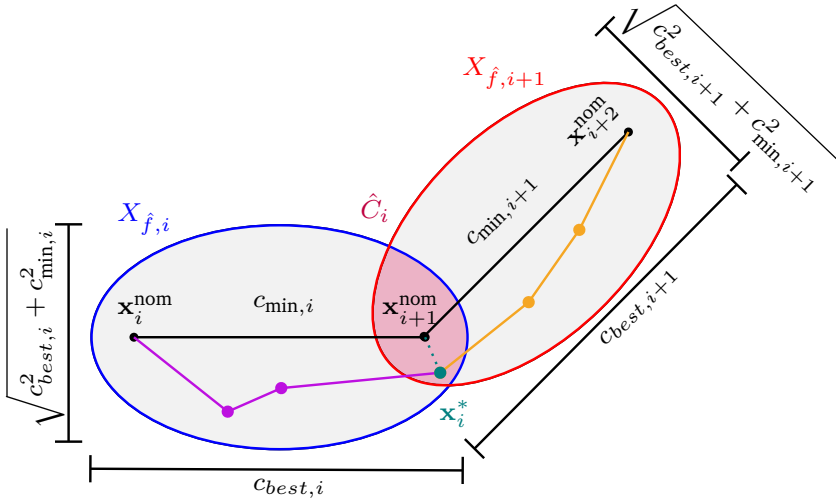
Figure D.4: The proposed informed subset for minimizing path deviations, given a nominal path consisting of m states and $m-1$ piece-wise linear segments. The informed subset is composed of the union of $m-1$ ellipsoids.

in order to ensure that $\mathbf{x}_{\text{start}}$ and $\mathbf{x}_{\text{end}}$ connect [D32]. The bias is introduced by checking if the parameter $0 \le \delta \le 1$ is smaller than the uniformly distributed random variable $u \sim \mathcal{U}(0,1)$, and choosing either the goal state or a sample from the space $\mathcal{U}(X_{\text{rect}})$ as the random sample. This idea is extended to sampling all (except $\mathbf{x}_{\text{start}}$) states belonging to the nominal path σ^{nom}, such that

$$\mathbf{x}_{\text{rand}} = \begin{cases} \mathcal{U}\left(X_{\text{space}}\right), & \text{if } \delta < u \\ \mathcal{U}\left(\left(\mathbf{x}_1^{\text{nom}}, \ldots, \mathbf{x}_m^{\text{nom}}\right)\right), & \text{otherwise} \end{cases} \tag{D.19}$$

where X_{space} is the current sampling space (e.g. X_{rect} or $X_{\hat{F}}$).

D.3.4   Switching condition

Given certain circumstances, sampling the informed set may be disadvantageous, compared to simply sampling the original space, since the informed set is generated based on the current best solution cost [D13], [D15]. With a high cost, the volume of the informed set may be larger than that of the original space. It is therefore natural, and also important, to compute a switching condition, which will determine whether or not the informed set provides sufficient value.

As with (D.6), one can compare the Lebesgue measure of X_{rect} and the proposed informed subset

$$\lambda\left(X_{\hat{F}}\right) < \lambda\left(X_{\text{rect}}\right) \tag{D.20}$$

with the measure of (D.13) given by

$$\lambda \left(X_{\hat{F}} \right) = \sum_{i=1}^{m-1} \lambda \left(X_{\hat{f},i} \right) - \sum_{i=1}^{m-2} \lambda(C_i) \tag{D.21}$$

where $C_i = X_{\hat{f},i} \cap X_{\hat{f},i+1}$. However, computing the exact intersection measure, especially for higher dimensions, is non-trivial. Instead an estimate of the intersection $\hat{C}_i$ is used.

$$\lambda \left(\hat{X}_{\hat{F}} \right) = \sum_{i=1}^{m-1} \lambda \left(X_{\hat{f},i} \right) - \sum_{i=1}^{m-2} \lambda \left(\hat{C}_i \right) \tag{D.22}$$

One of the simplest estimates is simply setting $\hat{C}_i = 0$, with the result that the estimated measure of the informed set contains twice as much intersection volume. For small $X_{\hat{f},i}$ compared to X_{rect} the over-representation of the intersections play a small role in the switching condition. However, if one wants to leverage the informed subset as soon as possible, a better estimate of $\hat{C}_i$ is required. If one disregards the required computational time, estimating $\hat{C}_i$ can be achieved using a Monte Carlo or hypervoxel based method. The main issue is adequately selecting the number of random samples or size of the hypervoxels, and thereby making a trade off between accuracy and computational effort.

Remark D.2. *If the proposed informed sampling scheme remains inactive, either due to a poor choice of heuristic or due to restrictions posed by the problem at hand, the default option is to simply uniformly sample X_{rect}, which results in planning performance equal to the underlying SBMP algorithm.*

D.4   Results and discussion

The proposed method is tested on three different planning scenarios to achieve collision avoidance of an autonomous surface vessel.

For autonomous marine crafts, the nominal route is computed prior to vessel departure according to some specifications and is optimized with respect to many important criteria, such arrival time, safety, weather, grounding risk, etc. In the event of potential collision with other vessels, the planner should compute a path deviation that achieves safe and compliant navigation of own ship. However, it is desired that the path alteration remains as close to the nominal path as possible, to ensure the minimum impact on the overall journey performance parameters (arrival time, fuel consumption, etc.), and to avoid endangering the vessel if navigates in coastal waters (see [D3] and [D30]).

Each simulation case study uses the same baseline SBMP algorithm, RRT*, with its basic parameters unchanged throughout all experiments. The baseline algorithm

(a) Narrow dredged passage

(b) Inner coastal waters

(c) Fjord navigation
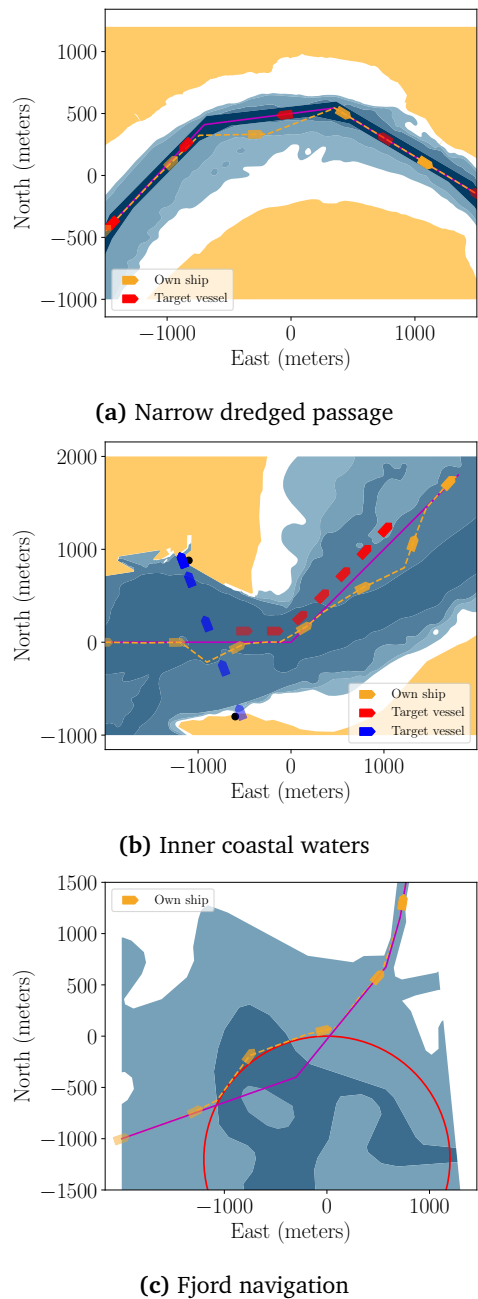
Figure D.5: Three collision avoidance scenarios for an autonomous marine vessel, where the nominal path consists of multiple segments. The feasible water depths for the own ship are indicated by the blue polygons, whereas white areas are shallow waters for said ship. The nominal trajectory is shown in magenta. Own ship is marked by the yellow markers and trajectory.
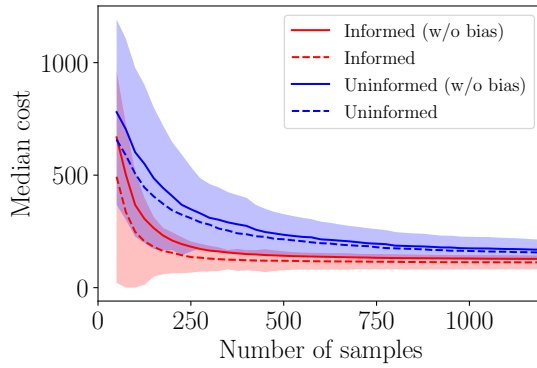
(a) Narrow dredged passage
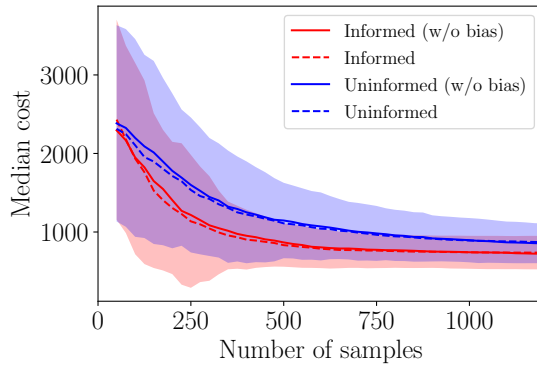
(b) Inner coastal waters
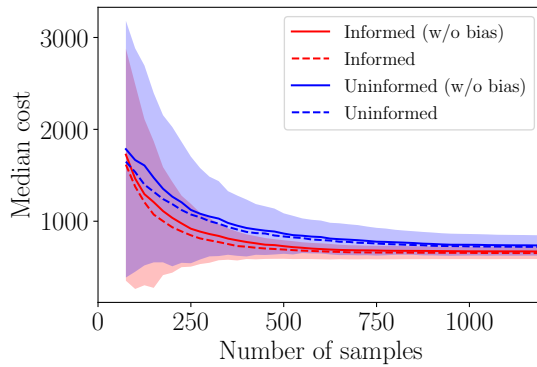
(c) Fjord navigation

Figure D.6: Median costs (250 runs) for each of the scenarios for the autonomous marine craft. The shaded region is the non-parametric 95% confidence interval, and is computed based on the informed and uninformed (with no bias) schemes. The proposed informed scheme converges faster than the uninformed, and is capable of achieving an overall lower solution cost.
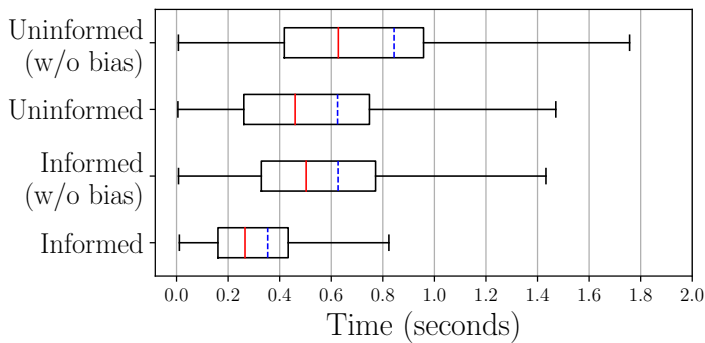
(a) Narrow dredged passage
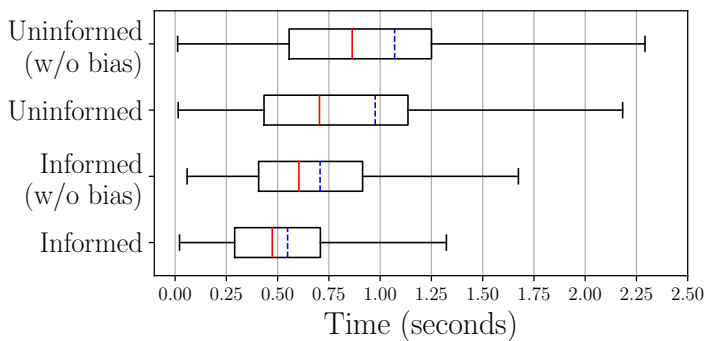
(b) Inner coastal waters
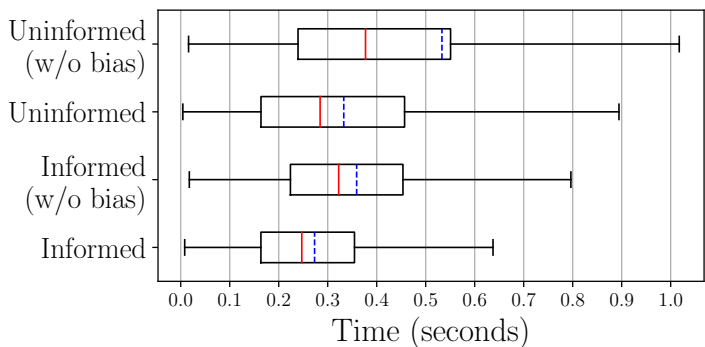
(c) Fjord navigation

Figure D.7: Time required to reach 3σ of the cost, where σ is the non-parametric standard deviation computed based on the experiments in Fig. D.6. The computational time for each of the four algorithmic variations is evaluated over 1000 trials on the three specified scenarios. The proposed informed method outperforms the uninformed counterpart for all three scenarios, performing a factor of 1.8 (D.7a), 2.3 (D.7b) and 1.5 (D.7c) times better, when comparing median computational times.

is referred to as the uninformed method. This section contains a comparison study between the proposed informed scheme and the uninformed one, with and without the sampling bias. Each simulation assumes $\hat{C}_i = 0$ for the estimate of the Lebesgue measure of $\hat{X}_{\hat{F}}$ and the cost function (D.9) to achieve the least path deviation. The target vessels are moving along piecewise linear trajectories with arbitrary but known constant speed and heading, as provided, e.g., by the radar. Furthermore, the static obstacles in the environment are represented as polygons and circles, and the target vessels as moving elliptical obstacles. Lastly, the maritime rules-of-the-road (COLREGs rules 13-15) and maneuvering restrictions are enforced as in [D3].

D.4.1 Case study I - Narrow passages

In confined waters, the navigation within narrow passages is a common occurrence. Here, vessels can be severely constrained by the environment and have limited room to manoeuvre with respect to one another. Therefore the nominal path is planned to minimize the grounding risk. Fig. D.5a shows a potential head-on collision scenario, where own ship must deviate. Due to the narrow passage, remaining as close to the nominal as possible is highly important. The proposed method is capable of computing a path that avoids collision while tightly following the nominal path.

D.4.2 Case study II - Inner coastal waters

As one leaves the open seas and enters the inner coastal waters, both the traffic scenarios and environmental constraints may change drastically. Here, new obstacles such as active ferries, stationary vessels, etc., must be avoided, all while ensuring a safe distance is kept from shallow waters. Fig. D.5b details a scenario in which own ship is travelling through inner coastal waters and must yield for a starboard crossing ferry, as well as overtake a slower vessel. It is demonstrated that the proposed method is able to minimize multiple deviations from the nominal path, such that both collision scenarios are dealt with, whilst maintaining a minimal path deviation.

D.4.3 Case study III - Fjord navigation

In some circumstances, the traversable area changes very rapidly, such as the scenario within a fjord depicted in Fig. D.5c. Here own ship is trying to leave the fjord, when its nominal path is obstructed by a fishing boat in action. Since the exit of the fjord is so narrow, it is crucial that the planned deviation remains close and converges to the nominal path. The planned deviation successfully avoids the active fishing region and safely converges to the nominal path.

D.4.4   Analysis and observations

The three autonomous ship scenarios demonstrate the proposed schemes ability to effectively compute paths that minimize the deviation from the nominal. Fig. D.6 demonstrates the informed sets ability to converge to the minimum, and in general an overall lower cost, within a shorter amount of samples compared to the uninformed solution. The results also highlights the impact of the proposed sampling bias, where the bias accelerates the convergence for the informed case. Importantly, a comparison where both the informed and uninformed scheme utilizes the bias was carried out, in order to show that the informed subset is the main contributor to the convergence rate. Fig. D.7 details the computational times for each of the three proposed scenarios. The informed scheme is able to obtain solutions at a greater rate, despite the additional computational complexity of the proposed informed sampling routine. Overall, the proposed scheme generates solutions at 1.5-2.3 times the rate of the uninformed method while also consistently having the smallest standard deviation, although a suboptimal heuristic for the Lebesgue measure (i.e. $\hat{C}_i = 0$) is used. It is also worth noting that the difference in performance decreases as the area ratio $A_r = \lambda(X_{\text{free,static}})/\lambda(X_{\text{space}})$ increases, where $X_{\text{free,static}}$ is the free space accounting only for the static obstacles. This is reflected by the increased overlap of the confidence intervals for Case study II ($A_r = 63.3\%$, Figs. D.6b-D.7b) and Case study III ($A_r = 80.2\%$, Figs. D.6c-D.7c). For comparison the area ratio of Case study I is $A_r = 26.5\%$.

As the minimal deviation converges to the nominal, the overall path length may increase, compared to simply minimizing the path length. This can be observed in Fig. D.1, where the informed set initially decreases in volume (Fig. D.1a-D.1c) as the path improves towards the nominal, however as the path fully converges to the minimum cost (Fig. D.1d), the volume of the ellipsoids increase. This is due to the construction of $X_{\hat{F}}$, since each ellipsoid is scaled based on the "local" path length with respect to a given nominal segment. As the path finds a tighter fit around the obstacles (minimizing the deviation), the overall path length increases. However, despite the increase or decrease in volume, the informed subset still guarantees that no solution that may improve the current best found cost is omitted.

D.5   Conclusions

In this paper, the collision avoidance for n-dimensional systems having an (optimal) nominal path is addressed by introducing a cost function and informed sampling space for computing solutions with minimum deviation from such a nominal path. Furthermore, the need for a heuristic to estimate the volume spanned by the subset

is discussed, with the paper proposing a computationally cheap metric, at the price of a conservative switching condition. The extension to the informed subset allows the scheme to focus its sampling effort in the neighbourhood surrounding the nominal path, resulting in an accelerated convergence to paths that minimally deviate from the nominal. The proposed method is demonstrated on three case studies related to an autonomous marine craft, where the simulated scenarios showed that the proposed method effectively converges to the minimum deviation, at a rate faster than the baseline uninformed method, with the sampling bias further improving the convergence rate of both the informed and uninformed methods. This performance increase is obtained despite using a suboptimal switching condition in the form of the conservative estimate of the Lebesgue measure.

D.6   References

[D1]   M. Werling, J. Ziegler, S. Kammel, and S. Thrun, "Optimal trajectory generation for dynamic street scenarios in a frenet frame," *2010 IEEE International Conference on Robotics and Automation*, IEEE, 2010, pp. 987–993.

[D2]   R. Oliveira, P. F. Lima, G. C. Pereira, J. Mårtensson, and B. Wahlberg, "Path planning for autonomous bus driving in highly constrained environments," *2019 IEEE Intelligent Transportation Systems Conference (ITSC)*, IEEE, 2019, pp. 2743–2749.

[D3]   T. T. Enevoldsen, M. Blanke, and R. Galeazzi, "Sampling-based collision and grounding avoidance for marine crafts," *Ocean Engineering*, 2022.

[D4]   A. Tsoularis and C. Kambhampati, "Avoiding moving obstacles by deviation from a mobile robot's nominal path," *The International Journal of Robotics Research*, vol. 18, no. 5, pp. 454–465, 1999.

[D5]   L. G. D. Véras, F. L. Medeiros, and L. N. Guimaráes, "Systematic literature review of sampling process in rapidly-exploring random trees," *IEEE Access*, vol. 7, pp. 50 933–50 953, 2019.

[D6]   J. D. Gammell and M. P. Strub, "Asymptotically optimal sampling-based motion planning methods," *Annual Review of Control, Robotics, and Autonomous Systems*, vol. 4, pp. 295–318, 2021.

[D7]   J. D. Gammell, S. S. Srinivasa, and T. D. Barfoot, "Informed RRT*: Optimal sampling-based path planning focused via direct sampling of an admissible ellipsoidal heuristic," *2014 IEEE/RSJ International Conference on Intelligent Robots and Systems*, IEEE, 2014, pp. 2997–3004.

[D8]   S. Karaman and E. Frazzoli, "Sampling-based algorithms for optimal motion planning," *The international journal of robotics research*, vol. 30, no. 7, pp. 846–894, 2011.

[D9]   J. D. Gammell, T. D. Barfoot, and S. S. Srinivasa, "Informed sampling for asymptotically optimal path planning," *IEEE Transactions on Robotics*, vol. 34, no. 4, pp. 966–984, 2018.

[D10]   J. D. Gammell, S. S. Srinivasa, and T. D. Barfoot, "Batch informed trees (BIT*): Sampling-based optimal planning via the heuristically guided search of implicit random geometric graphs," *2015 IEEE international conference on robotics and automation (ICRA)*, IEEE, 2015, pp. 3067–3074.

[D11]   M. P. Strub and J. D. Gammell, "Adaptively Informed Trees (AIT*): Fast asymptotically optimal path planning through adaptive heuristics," *2020 IEEE International Conference on Robotics and Automation (ICRA)*, IEEE, 2020, pp. 3191–3198.

[D12]   S. Choudhury, J. D. Gammell, T. D. Barfoot, S. S. Srinivasa, and S. Scherer, "Regionally accelerated batch informed trees (RABIT*): A framework to integrate local information into optimal path planning," *2016 IEEE International Conference on Robotics and Automation (ICRA)*, IEEE, 2016, pp. 4207–4214.

[D13]   A. Mandalika, R. Scalise, B. Hou, S. Choudhury, and S. S. Srinivasa, "Guided incremental local densification for accelerated sampling-based motion planning," *arXiv preprint arXiv:2104.05037*, 2021.

[D14]   S. S. Joshi and T. Panagiotis, "Non-parametric informed exploration for sampling-based motion planning," *2019 International Conference on Robotics and Automation (ICRA)*, IEEE, 2019, pp. 5915–5921.

[D15]   T. T. Enevoldsen, C. Reinartz, and R. Galeazzi, "COLREGs-Informed RRT* for Collision Avoidance of Marine Crafts," *2021 IEEE International Conference on Robotics and Automation (ICRA)*, 2021, pp. 8083–8089. DOI: 10.1109/ICRA48506.2021.9560909.

[D16]   C. Li, C. Wang, J. Wang, Y. Shen, and M. Q.-H. Meng, "Sliding-Window Informed RRT*: A Method for Speeding Up the Optimization and Path Smoothing," *2021 IEEE International Conference on Real-time Computing and Robotics (RCAR)*, IEEE, 2021, pp. 141–146.

[D17]   H. Ryu and Y. Park, "Improved informed RRT* using gridmap skeletonization for mobile robot path planning," *International Journal of Precision Engineering and Manufacturing*, vol. 20, no. 11, pp. 2033–2039, 2019.

[D18] D. Yi, R. Thakker, C. Gulino, O. Salzman, and S. Srinivasa, "Generalizing informed sampling for asymptotically-optimal sampling-based kinodynamic planning via markov chain monte carlo," *2018 IEEE International Conference on Robotics and Automation (ICRA)*, IEEE, 2018, pp. 7063–7070.

[D19] J. Sustarevas, D. Kanoulas, and S. Julier, "Task-consistent path planning for mobile 3d printing," *2021 IEEE/RSJ International Conference on Intelligent Robots and Systems (IROS)*, IEEE, 2021, pp. 2143–2150.

[D20] B. Paden, M. Čáp, S. Z. Yong, D. Yershov, and E. Frazzoli, "A survey of motion planning and control techniques for self-driving urban vehicles," *IEEE Transactions on intelligent vehicles*, vol. 1, no. 1, pp. 33–55, 2016.

[D21] L. Claussmann, M. Revilloud, D. Gruyer, and S. Glaser, "A review of motion planning for highway autonomous driving," *IEEE Transactions on Intelligent Transportation Systems*, vol. 21, no. 5, pp. 1826–1848, 2019.

[D22] Y. Lin, S. Maierhofer, and M. Althoff, "Sampling-based trajectory repairing for autonomous vehicles," *2021 IEEE International Intelligent Transportation Systems Conference (ITSC)*, IEEE, 2021, pp. 572–579.

[D23] H. Tang, Q. Zhu, E. Shang, B. Dai, and C. Hu, "A reference path guided RRT* method for the local path planning of UGVS," *2020 39th Chinese Control Conference (CCC)*, IEEE, 2020, pp. 3904–3909.

[D24] V. Vonásek, J. Faigl, T. Krajník, and L. Přeučil, "RRT-path–a guided rapidly exploring random tree," *Robot Motion and Control 2009*, Springer, 2009, pp. 307–316.

[D25] X. Lan and S. Di Cairano, "Continuous curvature path planning for semi-autonomous vehicle maneuvers using RRT," *2015 European control conference (ECC)*, IEEE, 2015, pp. 2360–2365.

[D26] S. Koenig, M. Likhachev, and D. Furcy, "Lifelong planning A*," *Artificial Intelligence*, vol. 155, no. 1-2, pp. 93–146, 2004.

[D27] S. Koenig and M. Likhachev, "D* lite," *Aaai/iaai*, vol. 15, pp. 476–483, 2002.

[D28] H.-T. L. Chiang and L. Tapia, "COLREG-RRT: An RRT-based COLREGS-compliant motion planner for surface vehicle navigation," *IEEE Robotics and Automation Letters*, vol. 3, no. 3, pp. 2024–2031, 2018.

[D29] R. Zaccone and M. Martelli, "A collision avoidance algorithm for ship guidance applications," *Journal of Marine Engineering & Technology*, vol. 19, no. sup1, pp. 62–75, 2020.

[D30]   T. T. Enevoldsen and R. Galeazzi, "Grounding-aware RRT* for path planning and safe navigation of marine crafts in confined waters," *IFAC-PapersOnLine*, vol. 54, no. 16, pp. 195–201, 2021.

[D31]   C. Urmson and R. Simmons, "Approaches for heuristically biasing RRT growth," *Proceedings 2003 IEEE/RSJ International Conference on Intelligent Robots and Systems (IROS 2003) (Cat. No. 03CH37453)*, IEEE, vol. 2, 2003, pp. 1178–1183.

[D32]   S. M. LaValle and J. J. Kuffner, "Randomized Kinodynamic Planning," *The International Journal of Robotics Research*, vol. 20, no. 5, pp. 378–400, May 2001.

Paper E

Guaranteed Rejection-free Sampling Method Using Past Behaviours for Motion Planning of Autonomous Systems

Thomas T. Enevoldsen[1*] and Roberto Galeazzi[1]

[1]Automation and Control Group, Department of Electrical and Photonics Engineering, Technical University of Denmark, DK-2800 Kgs. Lyngby, Denmark {tthen,roga}@dtu.dk

Abstract:
The paper presents a novel learning-based sampling strategy that guarantees rejection-free sampling of the free space under both biased and approximately uniform conditions, leveraging multivariate kernel densities. Historical data from past states of a given autonomous system is leveraged to estimate a non-parametric probabilistic description of the domain, which in turn also describes the free space where feasible solutions of the motion planning problem are likely to be found. The tuning parameters of the kernel density estimator, the bandwidth and the kernel, are then used to alter the description of the free space so that no sampled states can fall outside the originally defined space. The proposed method is demonstrated in two real-life case studies: An autonomous surface vessel (2D) and an autonomous drone (3D). Two planning problems are solved, showing that the proposed approximately uniform sampling scheme is capable of guaranteeing rejection-free sampling of the considered workspace. Furthermore, the planning effectiveness of the proposed method is statistically validated using Monte Carlo simulations.

E.1   Introduction

The interest in adopting autonomous robotic systems is steadily increasing in several industrial sectors, especially after witnessing the positive impact that robotization has had in large companies to perform mundane, repetitive and dangerous tasks. Small and medium companies see a growth potential in the integration of cobots into the manufacturing process; however, they are also concerned about the challenges associated with frequent changes on the production line. In addition, the transport sector is making the first experiments with the introduction of autonomous vehicles for logistics and urban mobility; however, there are open questions about the flexibility of such systems in the face of changes in the operational environment. If autonomous systems had the ability to leverage past experiences accumulated through the successful execution of tasks to plan the execution of similar tasks in a partly new environment, then the barriers to their actual adoption could be lowered. Furthermore, by leveraging past experiences, autonomous systems can plan in such a way that actions are predictable to humans. For autonomous systems such as cars and marine crafts, this will be of utmost importance, as humans are interacting with these systems on both roads and oceans, respectively.

Learning-based motion planners could provide a solution to transfer these experiences. Past states of the autonomous system collected during the completion of a task or experiences of other agents could be used to hone the search for new solutions to the given motion planning problem, within the region containing the past experiences, as long as the task or objective does not change significantly. When alterations in the task or systems workspace occur, the past states could be used to drive the exploration of previously unaccounted regions of the workspace in the vicinity of that encoded within the past experience. Sampling-based motion planning (SBMP) is proven to conquer complex motion planning tasks, where the given robotic system is highly constrained by its dynamics and working environment. Given the probabilistic nature of the historical data and the SBMP, investigating how to integrate such experiences in the sampling procedure seems like a natural extension.

E.1.1   Novelty and Contribution

This paper proposes a novel learning-based sampling strategy for motion planning of autonomous systems. The method takes advantage of past experiences from prior motions to efficiently find new solutions to the motion planning problem in the presence of changes of the workspace. To achieve this, kernel density estimation with a finite support kernel is adopted to generate a non-parametric probabilistic

description of regions of the free space where feasible solutions of the motion planning problem are likely to be found, in the neighbourhood of past data. The bandwidth of the multivariate probability density function is exploited to redefine the free space by enlarging obstacle regions. The sampling of the KDE in this new restricted space ensures that the generated samples always fall within the original free space. The paper also shows how the estimated kernel density can be exploited to obtain weights for performing importance sampling in the neighbourhood of past motions, for both biased and approximately uniform sampling of the free space, allowing the motion planner to both improve the current solution, but also explore nearby regions to the estimated one in relation to a new planning problem. Both sampling strategies are guaranteed to be rejection-free by construction.

The presented sampling strategy is verified in two case studies that address motion planning for an autonomous ship sailing in coastal waters and for an aerial drone performing a complex inspection task in a confined space.

E.1.2   Related work

Since the introduction of Probabilistic Roadmaps (PRM) [E1]–[E3] and Rapidly-exploring Random Trees (RRT) [E4]–[E6], Sampling-based Motion Planning (SBMP) has had a strong grasp on the motion and path planning space. This class of algorithms has a set of key advantages over traditional grid-based algorithms, primarily due to its ability to deal with systems of greater complexity with less computational burden. State-of-the-art optimal sampling-based motion planners include RRT* and PRM* [E7], Batch Informed Trees (BIT*) [E8], Fast Marching Trees (FMT*) [E9] and additional variants of the aforementioned algorithms [E10]–[E15]. By uniformly sampling the state space, the previously mentioned SBMPs maintain their probabilistic guarantees and are asymptotically optimal.

However, the choice of sampling technique plays an important role in the convergence speed. The primary objective of alternative sampling schemes is to increase the probability of sampling states which can improve the current solution, compared to wasting sampling effort on states which provide no value. An extensive review of sampling techniques utilised in conjunction with RRT and its variants was performed by [E16]. The authors categorised the following sampling objectives: Goal-biased, obstacle-biased, region-based, path-biased, passage-biased, search space reduction and biasing through sampling distributions. Furthermore, [E17] provided an updated overview of the current state of SBMP.

The uniform sampling strategy is applicable to all problems and also guarantees that a solution, if it exists, is found. However, for certain problems, the uniform sampling strategy tends to sample states that are infeasible due to collision or

system constraints. As an alternative, [E18] investigated planning using knowledge of the free space to form a non-convex region, which was then sampled directly using a hit-and-run sampling scheme. [E19] showed that uniform sampling a triangulated representation of a non-convex environment provided a significant increase in sampling value, as the obstacle-to-free space ratio increases, compared to the baseline uniform sampler. Leveraging prior knowledge of the problem is often referred to as importance sampling [E20], which is a class of non-uniform sampling, more specifically, a priori non-uniform sampling. The key idea is that utilising knowledge of the problem will allow for a more rapid convergence to a solution. The application of importance sampling is a general topic within the motion planning literature [E21]–[E23].

Search space reduction was popularised by [E24], which proposed the Informed-RRT*, a method for reducing the search space as the current best found solution improves. This is achieved by uniformly sampling a n-dimensional hyperspheroid, which corresponds to bounding the search space by n-dimensional symmetric ellipses scaled by the current best path length. This concept was further iterated by [E25], who proposed a system that incrementally densifies the internal states of the bounding n-dimensional hyperspheroid. [E26] proposed an informed uniform sampling strategy that directly encodes the maritime rules-of-the-road (known as the COLREGs) by sampling an elliptical half-annulus. [E27] proposed an alternative informed sampling scheme for kinodynamic planning, since the elliptical informed subset is not suitable for systems with kinodynamic constraints. The authors propose a hierarchical rejection sampler which can sample the relevant informed set without explicitly parameterizing it. [E28] proposed sampling routines for generating samples in a generalised informed set, primarily using Markov Chain Monte Carlo. The authors show asymptotic optimality for generally shaped informed spaces.

Recently, a growing interest in exploring learning methods to drive the sampling strategy has emerged. [E29] proposed a self-learning sampling scheme, where an initial uniform distribution is updated with experiences from previous paths. The update occurs by augmenting the uniform distribution with the new data and using kernel density estimation to bias the uniform search space. [E30], [E31] propose a similar idea, however, using Gaussian Mixture Models (GMMs) to bias the sampling towards regions with previous solutions. [E32] created a bank of local samplers by decomposing the work space into smaller regions; these local samplers are then customised to a specific problem based on prior knowledge of the task. The authors argue that the data for local samplers have high complexity and therefore represent the local space with GMMs. [E33] proposed using a variant of GMM called Infinite GMMs, which allows the authors to learn typical GMM tuning parameters based

on the expert data. [E34] demonstrated the use of a GMM sampling bias routine for automated parking, where the underlying data is generated from past parking scenarios carried out by experts. [E35] proposed modelling a rejection sampling technique using Markov Decision Processes, so that an offline policy can be modelled for environments that are similar.

For probabilistic roadmaps, [E36] propose using expansive configuration spaces, where the algorithm attempts to only sample areas of the configuration space of most relevance to the query at hand. [E37] combines sampling-based and optimisation-based planning, while approximating the configuration space. [E38] utilises estimates of observed samples from the obstacle-free space to generate new samples.

A two-stage approach is proposed by [E39], where each sample is classified as collision-free or not. Kernel density estimation is used to create a collection of collision free samples, which then generates new samples with a greater probability of also being collision free. The second stage evaluates the potential of the newly generated sample, to determine whether or not it is capable of providing value. [E40] further iterates on this by restricting the search space to the L^2 informed subset (as proposed by [E24]), while leveraging the information captured by the classifier.

[E41] presented a conditional variational autoencoder, which is trained on past robot experiences. Non-uniform samples biased towards the past experiences are generated using the latent layer, narrowing the search for new paths to the area previously explored. Non-uniform and uniform sampling schemes are combined to retain the optimality guarantees of the given SBMP algorithm. The work was later extended into multiple networks capable of solving the entire SBMP problem [E42]. [E43] proposed Neural RRT*, where a Convolutional Neural Network (CNN) is trained with previously successful paths, and then used to generate biased samples in the neighbourhood of the provided input data. [E44] proposes an imitation learning-based kinodynamic motion planner, where deep neural networks are combined with Model Predictive Control. The method is trained on historical data, to compute paths that directly adhere to the kinodynamic constraints of the given system.

E.2 Preliminaries

E.2.1 The Workspace

Consider some autonomous (robotic) system, for example, an unmanned aerial vehicle (UAV) or an autonomous surface vehicle (ASV), that operates in some workspace $\mathcal{W}$ that is a subset of the Euclidean space $\mathbb{R}^n$. Let $\mathcal{A}$ be some instance of

the aforementioned autonomous system, then $\mathbf{x}_i$ is an instance of coordinates that determines the current state of the system. Obstacles present in the workspace of the autonomous system can also be mapped in the space $\mathcal{W}$. Let $\mathcal{O}$ be an obstacle in the workspace $\mathcal{W}$, then the obstacle in the workspace $\mathcal{W}_{\mathrm{obs}} \subseteq \mathcal{W}$, is defined as $\mathcal{W}_{\mathrm{obs}} \triangleq \{\mathbf{x} \in \mathcal{W} | \mathcal{A}(\mathbf{x}) \cap \mathcal{O} \neq \emptyset\}$, i.e. the set of all states in which the autonomous system collides with the obstacle. The complementary set of the obstacle space is called the free space, that is $\mathcal{W}_{\mathrm{free}} = \mathcal{W} \setminus \mathcal{W}_{\mathrm{obs}}$.

E.2.2   Sampling-based Motion Planning

The proposed method intended use is for computing low-cost feasible solutions in connection with the solution of the optimal sampling-based motion planning problem, defined similarly to [E24].

Consider the state space $\mathcal{X}$, consisting of two subsets, namely $\mathcal{X}_{\mathrm{free}}$ and $\mathcal{X}_{\mathrm{obs}}$, with $\mathcal{X}_{\mathrm{free}} = \mathcal{X} \setminus \mathcal{X}_{\mathrm{obs}}$. The space $\mathcal{X}_{\mathrm{free}}$ contains all states that are feasible with respect to the given system and its operating environment. Let $\mathbf{x}_{\mathrm{start}} \in \mathcal{X}_{\mathrm{free}}$ be the initial state at the initial time $t = t_0$ and $\mathbf{x}_{\mathrm{goal}} \in \mathcal{X}_{\mathrm{free}}$ be the desired final state.

Let $\sigma : [0,1] \mapsto \mathcal{X}$ be a sequence of states that constitute a found path, and Σ be the set of all feasible and non-trivial paths. The objective is to compute the optimal path σ^*, which minimises a cost function $c(\cdot)$ while connecting $\mathbf{x}_{\mathrm{start}}$ to $\mathbf{x}_{\mathrm{goal}}$ through $\mathcal{X}_{\mathrm{free}}$, i.e.,

$$\sigma^* = \arg\min_{\sigma \in \Sigma} \left\{ c(\sigma) \mid \sigma(0) = \mathbf{x}_{\mathrm{start}} , \, \sigma(1) = \mathbf{x}_{\mathrm{goal}} , \forall s \in [0,1], \, \sigma(s) \in \mathcal{X}_{\mathrm{free}} \right\} . \quad \text{(E.1)}$$

For the remainder of the paper, it is assumed that the above-mentioned state space quantities are equal to their workspace counterparts, i.e. $\mathcal{W} = \mathcal{X}$, $\mathcal{W}_{\mathrm{free}} = \mathcal{X}_{\mathrm{free}}$ and $\mathcal{W}_{\mathrm{obs}} = \mathcal{X}_{\mathrm{obs}}$.

E.2.3   Uniform Sampling Strategies

Several sampling techniques exist to obtain new nodes for the exploration of a given state space. *Uniform random sampling* is the simplest strategy to achieve uniform exploration of the space and is based on the random selection of values for each degree of freedom present in the state $x \in \mathcal{X}$. Deterministic methods also exist, where sampling is driven by a *low-dispersion objective* or a *low-discrepancy objective*. The former leads to the use of a grid whose resolution changes so that samples are placed to minimise the size of the uncovered areas. The latter addresses the shortcomings that arise from having grids that are aligned with the coordinate axes of the space. Among these sampling strategies, we find the Halton sequence (and its variants) and lattices.
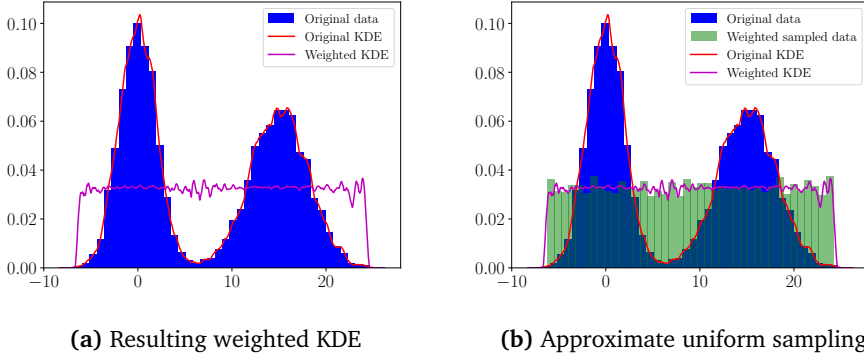
(a) Resulting weighted KDE

(b) Approximate uniform sampling

Figure E.1: One dimensional resampling of the weighted KDE, such that uniform samples of the KDE domain are generated.

E.3   Guaranteed rejection-free sampling of non-parametric spaces

Consider the autonomous system $\mathcal{A}$ performing tasks in the free space $\mathcal{W}_{\text{free}}$ over an arbitrary large time horizon T. In the event of changes of the free space due to e.g., the introduction of new obstacles or operational boundaries, it is of interest to produce new motion plans by leveraging the information carried by the historical paths σ_i traversed by $\mathcal{A}$ over the period T. We propose to leverage the available data from past experiences in order to compute a non-parametric probabilistic representation of the free space that describes the space in which new solutions may exist. Such a non-parametric description can be utilized twofold. Directly sampling the non-parametric distribution provides a biased sampling strategy, aiding in the computation of motion plans similar to those encoded within the data. The non-parametric distribution can also be used to approximately uniformly explore nearby regions of the free space to that traversed by the paths σ_i, yet remaining within the defined free space.

E.3.1   Kernel density estimation

Multivariate kernel density estimation (KDE) is a non-parametric method to estimate an unknown multivariate probability density function $f(\mathbf{x})$ based on a finite data set containing realisations of the multivariate random variable described by $f(\mathbf{x})$. Specifically, the kernel density estimator operates on a set of n data vectors each of which is an identically distributed p-variate random variable drawn from the same and unknown distribution $f(\mathbf{x})$.

Let $X = \{\mathbf{x}_i \in \mathbb{R}^p | \mathbf{x}_i \sim f, \, i = 1, \ldots, n\}$ be the available data set; then the general form of the p-variate kernel density estimator is given by [E45]

$$\hat{f}_X(\mathbf{x}, \mathbf{H}) = \frac{1}{n} \sum_{i=1}^{n} |\mathbf{H}|^{-1/2} K(\mathbf{H}^{-1/2}(\mathbf{x} - \mathbf{x}_i)) \tag{E.2}$$

where $\mathbf{x}_i = [x_{i1}, x_{i2}, \ldots, x_{ip}]^\top \in X$, $\mathbf{x} = [x_1, x_2, \ldots, x_p]^\top \in \mathbb{R}^p$ is an arbitrary element, $\mathbf{H} = \mathbf{H}^\top > 0$ is the non-random $p \times p$ bandwidth matrix, and $K(\cdot)$ is the kernel function.

The kernel and the bandwidth are the tuning parameters; however, as the size of the data set increases, the importance of choosing the bandwidth outweighs the particular choice of the kernel [E46, Section 6.2.3]. In the case of 1D KDEs, if the underlying distribution is unimodal or exhibits normal features, then Silverman's rule or Scott's rule [E47] can be applied to compute the bandwidth. For 1D instances where the data has multiple modes, the Improved Sheather-Jones algorithm serves as a plug-in bandwidth selector [E48]. When multivariate kernel density estimation is performed, such rule-based approaches do not apply. However, data-driven methods exist to compute optimal kernel functions and bandwidth matrices, as shown in [E49], [E50].

E.3.2   Generating samples from $\hat{f}$

The generation of samples from parametric distributions is achieved through inverse transform sampling, in order to uniformly create samples belonging to the corresponding probability density function. Performing such an inversion of a KDE poses several challenges. However, by construction, a KDE $\hat{f}_X(\mathbf{x}, \mathbf{H})$ consists of a mixture of the kernel function $K(\cdot)$. This means that the KDE itself can be reconstructed by sampling the data used to generate it, biased by the chosen kernel function and its parameters.

One can generate m samples from the estimated PDF $\hat{f}_X(\mathbf{x}, \mathbf{H})$, given the data set $X = \{\mathbf{x}_1, \mathbf{x}_2, \ldots, \mathbf{x}_n\}$ used to compute the estimate $\hat{f}$, generate m indices $(k_1, k_2, \ldots, k_m)$ from the discrete uniform density $U(1, 2, \ldots, n)$ in order to uniformly select data from the original data set. Each selected point is then biased by a sample $\mathbf{t}_i$ generated from the chosen scaled multivariate kernel [E46], [E51]

$$\mathbf{s}_i = \mathbf{x}_{k_i} + \mathbf{t}_i, \quad i = 1, \ldots, m. \tag{E.3}$$

This procedure naturally leads to generating samples that are biased towards regions of higher density, and as the number of sampled points m tends toward infinity, the samples represent a densified estimate of the non-parametric distribution of past states.
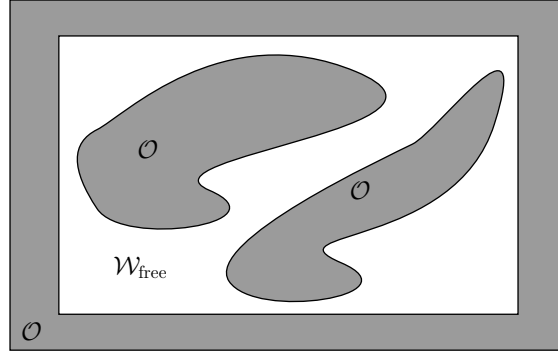
Figure E.2: Example of closed and bounded free space $\mathcal{W}_{\text{free}}$.

For sampling-based motion planning, it may instead be desired that the generated samples are uniformly distributed over the domain of the KDE. This can be achieved by computing the densities for each data point in the set X,

$$\omega_i = \hat{f}_X(\mathbf{x}_i, \mathbf{H}), \quad i = 1, \ldots, j \tag{E.4}$$

and using the reciprocal $1/\omega_i$ to weight the selection of the indices $(k_1, k_2, \ldots, k_m)$. Fig. E.1 shows a one-dimensional implementation of such procedure, where Fig. E.1a illustrates the estimated KDE and the computation of the weights, while Fig. E.1b shows the reweighted sampling of the KDE domain compared to the original KDE.

Remark E.1. *There are complexities in generating the kernel sample $\mathbf{t}_i$, depending on the chosen kernel function. The most common case is a KDE using the Gaussian kernel, where sampling occurs by selecting the data points as described above and subsequently biasing each sample by a zero-mean p-variate normal distribution with the covariance described in terms of the bandwidth.*

Remark E.2. *To ensure that the given sampling-based motion planner maintains its asymptotic optimality, the proposed method should be combined with uniform sampling of the entire space [E41]. This results in λm samples drawn from the proposed scheme and $(1 - \lambda)m$ samples from a uniform sampler, where $0 < \lambda < 1$ is a tuning parameter based on the available data set and the problem at hand.*

E.3.3 Guaranteed Rejection-free Sampling Scheme

Consider the autonomous system $\mathcal{A}$ operating in space $\mathcal{W} \subseteq \mathbb{R}^p$ in the presence of a set of obstacles $\mathcal{O}_0$. Then the free space is defined as

$$\mathcal{W}^0_{\text{free}} = \{\mathbf{x} \in \mathcal{W} \mid \mathcal{A}(\mathbf{x}) \cap \mathcal{O}_0 = \emptyset\}. \tag{E.5}$$

Depending on the configuration of the obstacles, the free space $\mathcal{W}_{\text{free}}^0$ can be either an open and unbounded set, or a closed and bounded. Fig. E.2 shows an exemplification of the latter. The following theorem is valid in both cases.

Theorem E.1. *Let X be the set of states $\mathbf{x}_i \in \mathcal{W}_{\text{free}}^0$ that an agent $\mathcal{A}$ has assumed during a time period $T = [t_0, t_1] \in \mathbb{R}$, $t_1 > t_0 \geq 0$, and $f(\mathbf{x})$ the unknown spatial distribution of such states over the free space $\mathcal{W}_{\text{free}}^0$. Assume that at time $t_2 > t_1$ the free space $\mathcal{W}_{\text{free}}^0$ changes to $\mathcal{W}_{\text{free}}^1$, where $\mathcal{W}_{\text{free}}^1 \cap \mathcal{W}_{\text{free}}^0 \neq \emptyset$. Then the rejection-free sampling of $\mathcal{W}_{\text{free}}^1$ is guaranteed through the sampling of $\hat{f}_X(\mathbf{x}, \mathbf{H})$ on the set $\bar{X} = \{\mathbf{x} \in \mathcal{W}_{\text{free}}^2 \cap X\} \subseteq X$, where $\hat{f}_X(\mathbf{x}, \mathbf{H})$ is a kernel density estimator of $f(\mathbf{x})$ with finite support kernel, and $\mathcal{W}_{\text{free}}^2 \subset \mathcal{W}_{\text{free}}^1$.*

Proof. Given the set X, the p-variate KDE with finite support kernel $K(\cdot)$ (e.g., the box or Epanechnikov's kernel), and bandwidth matrix $\mathbf{H}$ [E46, Section 6.2.3]

$$\hat{f}_X : \mathcal{W}_{\text{free}}^0 \longrightarrow E \tag{E.6}$$

is an estimator of the unknown spatial distribution $f(\mathbf{x})$, which maps elements of the free space to density values, where

$$E = \{e \in \mathbb{R}_+ | 0 \leq e \leq 1\}. \tag{E.7}$$

$\hat{f}_X$ is a biased non-parametric probabilistic description of $\mathcal{W}_{\text{free}}^0$, whose sampling allows to plan the motion of the agent $\mathcal{A}$ within the free space $\mathcal{W}_{\text{free}}^0$.

At an arbitrary time instant $t_2 > t_1$ the free space partly changes such that $\mathcal{W}_{\text{free}}^1 \cap \mathcal{W}_{\text{free}}^0 \neq \emptyset$, i.e.,

$$\mathcal{W}_{\text{free}}^1 = \{\mathbf{x} \in \mathcal{W} \,|\, \mathcal{A}(\mathbf{x}) \cap \mathcal{O}_1 = \emptyset\} \tag{E.8}$$

where $\mathcal{O}_1$ is the new set of obstacles. Let $\mathcal{B} = \{\mathbf{x} \in \mathbb{R}^p \,|\, \|\mathbf{x}\| \leq \varrho\}$ be a ball of radius ϱ, where $\varrho = (\lambda_{\min}(\mu_2(K)\mathbf{I}_p))^{-1}\|\mathbf{H}^{1/2}\|_q$, $\mu_2(K)\mathbf{I}_p$ is the second order moment of the selected kernel function $K(\cdot)$ [E52, Section 3.6], and $\lambda_{\min}$ is its smallest eigenvalue. The new free space $\mathcal{W}_{\text{free}}^2$ is defined by enlarging the obstacle regions $\mathcal{O}_1$, i.e.,

$$\mathcal{O}_2 = \mathcal{O}_1 \oplus \mathcal{B} \tag{E.9}$$

$$\mathcal{W}_{\text{free}}^2 = \{\mathbf{x} \in \mathcal{W} \,|\, \mathcal{A}(\mathbf{x}) \cap \mathcal{O}_2 = \emptyset\}. \tag{E.10}$$

and by construction $\mathcal{W}_{\text{free}}^2 \subset \mathcal{W}_{\text{free}}^1$.

The sampling of $\hat{f}_X(\mathbf{x}, \mathbf{H})$ on the set $\bar{X} = X \cap \mathcal{W}_{\text{free}}^2$ achieves the rejection-free sampling of $\mathcal{W}_{\text{free}}^1$. To guarantee that all samples fall within $\mathcal{W}_{\text{free}}^1$ the chosen kernel $K(\cdot)$ must have finite support, otherwise the use of the kernel $K(\cdot)$ on data points belonging to $\bar{X}$ could generate samples falling outside $\mathcal{W}_{\text{free}}^1$. $\qquad \square$

Remark E.3. *To obtain the approximately uniform sampling of $(\bar{X} \oplus \mathcal{B}) \subset \mathcal{W}_{\text{free}}^1$ the p-variate KDE $\hat{f}_X$ should be reweighted. This can be achieved through two approaches: (i) the estimation of a new KDE based on the data set $\bar{X}$; (ii) the truncation and normalization of the original KDE. Following the latter, $\hat{f}_X(\mathbf{x}, \mathbf{H})$ is first truncated by zeroing the densities that falls outside $\mathcal{W}_{\text{free}}^2$, and then normalized to ensure that the resulting function still qualifies as a density, i.e.,*

$$\bar{f}_{\bar{X}}(\mathbf{x}, \mathbf{H}) = \begin{cases} \hat{f}_X(\mathbf{x}, \mathbf{H}), & \forall \mathbf{x} \in \bar{X} = X \cap \mathcal{W}_{\text{free}}^2 \\ 0, & \text{otherwise} \end{cases} \tag{E.11}$$

$$\hat{f}_{\bar{X}}(\mathbf{x}, \mathbf{H}) = \frac{\bar{f}_{\bar{X}}(\mathbf{x}, \mathbf{H})}{\rho} \tag{E.12}$$

where

$$\rho = \int_{\mathbb{R}^p} \bar{f}_{\bar{X}}(\mathbf{s}, \mathbf{H}) \, \mathrm{d}\,\mathbf{s}. \tag{E.13}$$

E.3.4   Toy Example

The following section presents a toy example to provide a detailed demonstration of how the proposed method is applied to a given problem.

Using two bivariate normally distributed random variables $X_1 \sim \mathcal{N}(\mu_1, \Sigma_1)$ and $X_2 \sim \mathcal{N}(\mu_2, \Sigma_2)$ with parameters $\mu_1 = \mathbf{0}$, $\Sigma_1 = \text{diag}([10, 20])$, $\mu_2 = \begin{bmatrix} 20 & 10 \end{bmatrix}^T$ and $\Sigma_2 = \text{diag}([45, 35])$, some historical data, in this case 1500 samples, is generated, such that a collection of data points

$$X = [(x_1, y_1), (x_2, y_2), \dots, (x_n, y_n)]^\top \tag{E.14}$$

is created. This particular data set is created such that it represents past states that at some point were feasible with respect to the nominal space $\mathcal{W}_{\text{free}}^0$. However, at the current time instant, a boundary limitation has been imposed described by the following polygon P

$$P = [(-10, -10), (22, 3), (30, 27), (-12, 30), (-20, 0)]$$

which now represents the new free space $\mathcal{W}_{\text{free}}^1$. Fig. E.3a visualises the historical data and nominal space, whereas Fig. E.3b visualises the imposed boundary $\mathcal{W}_{\text{free}}^1$ and its impact on the historical data. An unbounded KDE is computed based on the data set X using the bandwidth matrix $\mathbf{H} = 2\mathbf{I}$ and the finite support Epanechnikov kernel. Fig. E.3c shows a visualisation of such KDE. To guarantee that sampling of the new free space $\mathcal{W}_{\text{free}}^1$ occurs completely rejection-free, a final space is introduced. This space is an erosion (or shrinkage) of the polygonal boundary, resulting in

(a) X and $\mathcal{W}^0_{\text{free}}$ **(b)** Imposing $\mathcal{W}^1_{\text{free}}$ on X **(c)** KDE based on data X

(d) Erosion to create $\mathcal{W}^2_{\text{free}}$ **(e)** Truncation of KDE   **(f)** Imposing $\mathcal{W}^2_{\text{free}}$ on X ($\bar{X}$)

(g) Sampling $\hat{f}_{\bar{X}}$ directly   **(h)** Sampling weighted $\hat{f}_{\bar{X}}$
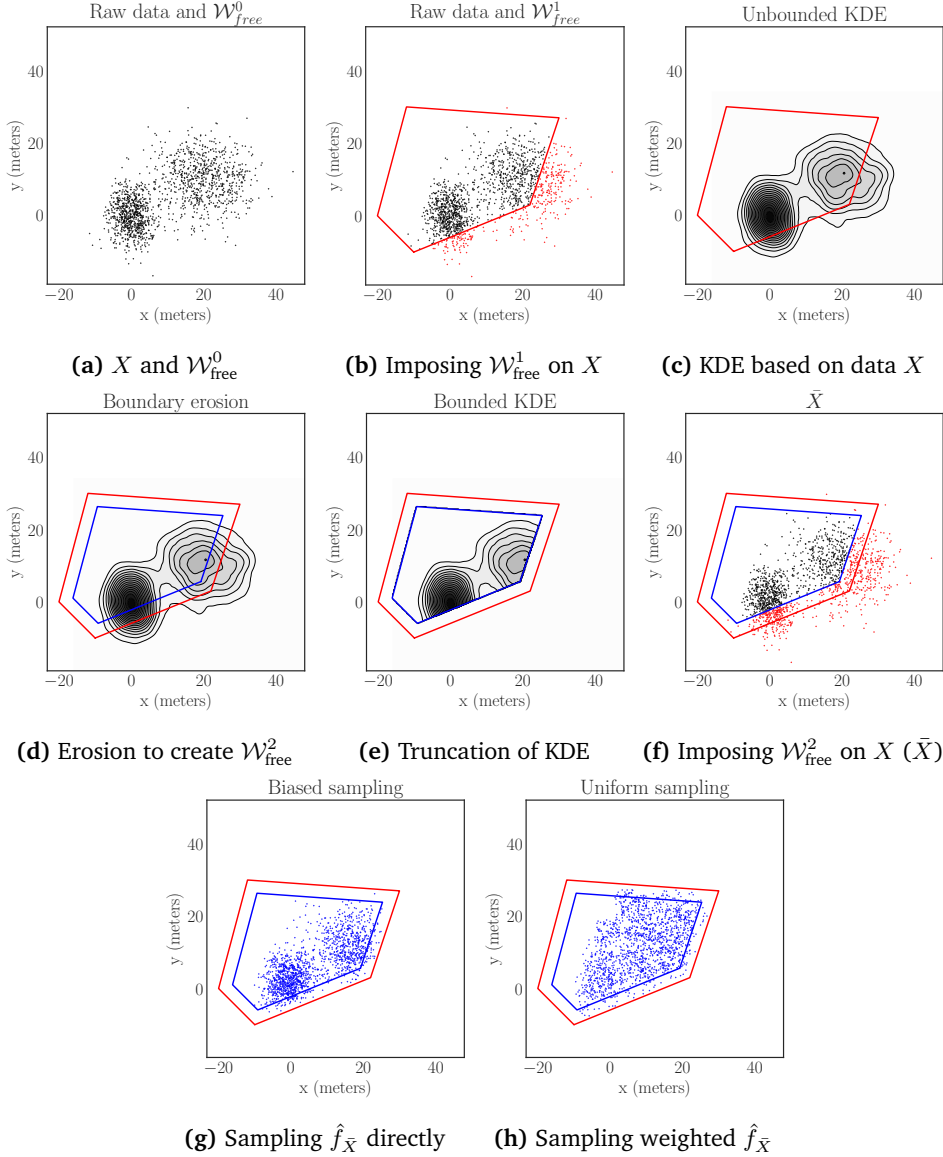
Figure E.3: Visual representation of each step of the proposed method, as described in Section E.3. Once the space $\mathcal{W}^2_{\text{free}}$ (inner blue polygon) has been generated based on the selected bandwidth and the corresponding bounded KDE, one guarantees the ability to sample the $\mathcal{W}^1_{\text{free}}$ space without rejection sampling, within the domain covered by the historical data. Fig. E.3g and Fig. E.3h demonstrates the ability to generate rejection-free samples in both a biased and approximately uniform manner.

the space $\mathcal{W}^2_{\text{free}}$, as shown in Fig. E.3d. The amount of erosion is related to the bandwidth matrix $\mathbf{H}$ through the radius ϱ. The computed KDE is truncated to $\mathcal{W}^2_{\text{free}}$ and normalised, resulting in the KDE presented in Fig. E.3e. By reducing the original data set X to only encompass points which fall within $\mathcal{W}^2_{free}$, $\bar{X}$, the KDE can be sampled in either of the two ways presented in Section E.3.2. Fig. E.3f shows the subset $\bar{X}$, which will be utilised such that no rejection sampling is required. Finally, $\bar{X}$ and the resulting KDE are used to generate samples. Fig. E.3g and Fig. E.3h demonstrate the sampling schemes ability to generate biased samples as well as an approximate uniform coverage of an extended region within $\mathcal{W}^1_{free}$ surrounding the original data set X.

E.4 Case Studies

The following case studies are performed on raw data, without any sort of pre-processing or augmentation. This allows the effectiveness of the proposed method to be demonstrated. However, in practise, one may potentially gain further increased performance from procedures such as upsampling.

All KDEs were computed using KDEpy [E55], an FFT-based KDE package for Python. The proposed rejection-free sampling method is compared to the simplest and most versatile method, namely uniform sampling. The planning problem is solved using RRT* [E7], but the sampling strategy is general and can therefore be used with other sampling-based motion planners. During each simulation in the comparison study, the various planner parameters remain constant; the only change is the sampling scheme. Both case studies are divided into two subproblems: (i) finding a feasible solution, and (ii) finding a solution at a lesser cost than some threshold.

E.4.1 Autonomous Surface Vessel Sailing in Confined Waters

The development of autonomous ships has been in focus in recent years, where it is desired to bring highly automated capabilities to vessels such as harbour buses, small island ferries, or even larger vessels such as container feeders. A key component towards the achievement of autonomous marine navigation is collision and grounding (i.e., sailing in waters shallower than the clearance) avoidance. Therefore, a tailored sampling space for such a system could be designed to directly sample regions where the given vessel would typically operate, without sampling states that may cause grounding. Formulating a data-driven sampling space for this particular application is made possible by a significant amount of available GPS data, since modern standards dictate that certain classes of vessels must broadcast their posi-
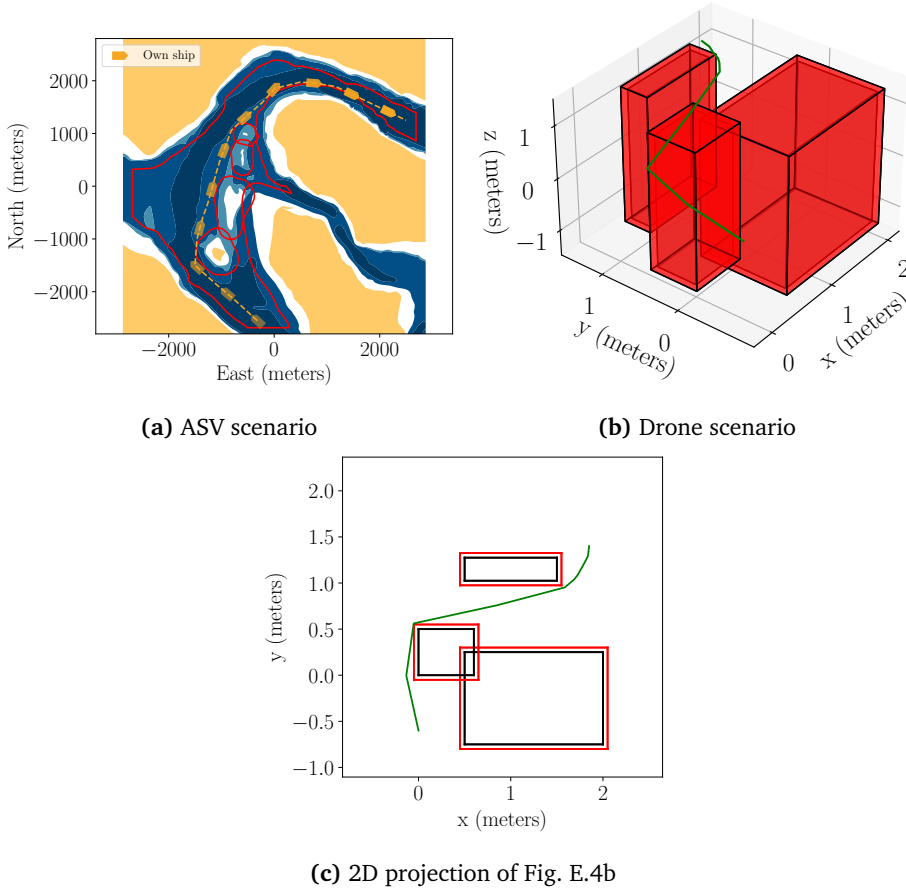
(a) ASV scenario

(b) Drone scenario

(c) 2D projection of Fig. E.4b

Figure E.4: Outcome of the motion planner for the ASV and drone case studies. Fig. E.4a shows a path where the vessel maintains the specified safety distance to shallow waters. The proposed method ensures that only safe samples are generated, thereby increasing the efficiency of computing low cost solutions, as evident in Table E.3 and Fig. E.6. Details regarding safe sampling-based motion planning for ASVs can be found in [E19], [E53]. Fig. E.4b details a similar scenario, but instead for the drone. This particular case study mimics an inspection task, and therefore the drone must also maintain some safety distance from the obstacles (see [E54] for more details). Note that due to limitations with the 3D engine used for plotting, the location of the data points within the figure may be deceptive, see therefore instead the 2D projection in Fig. E.4c.

(a) X and $\mathcal{W}_{\text{free}}^0$

(b) Imposing $\mathcal{W}_{\text{free}}^1$ on X

(c) KDE based on data X

(d) Erosion and dilation to create $\mathcal{W}_{\text{free}}^2$

(e) Sampling $\hat{f}_{\bar{X}}$ directly

(f) Sampling weighted $\hat{f}_{\bar{X}}$
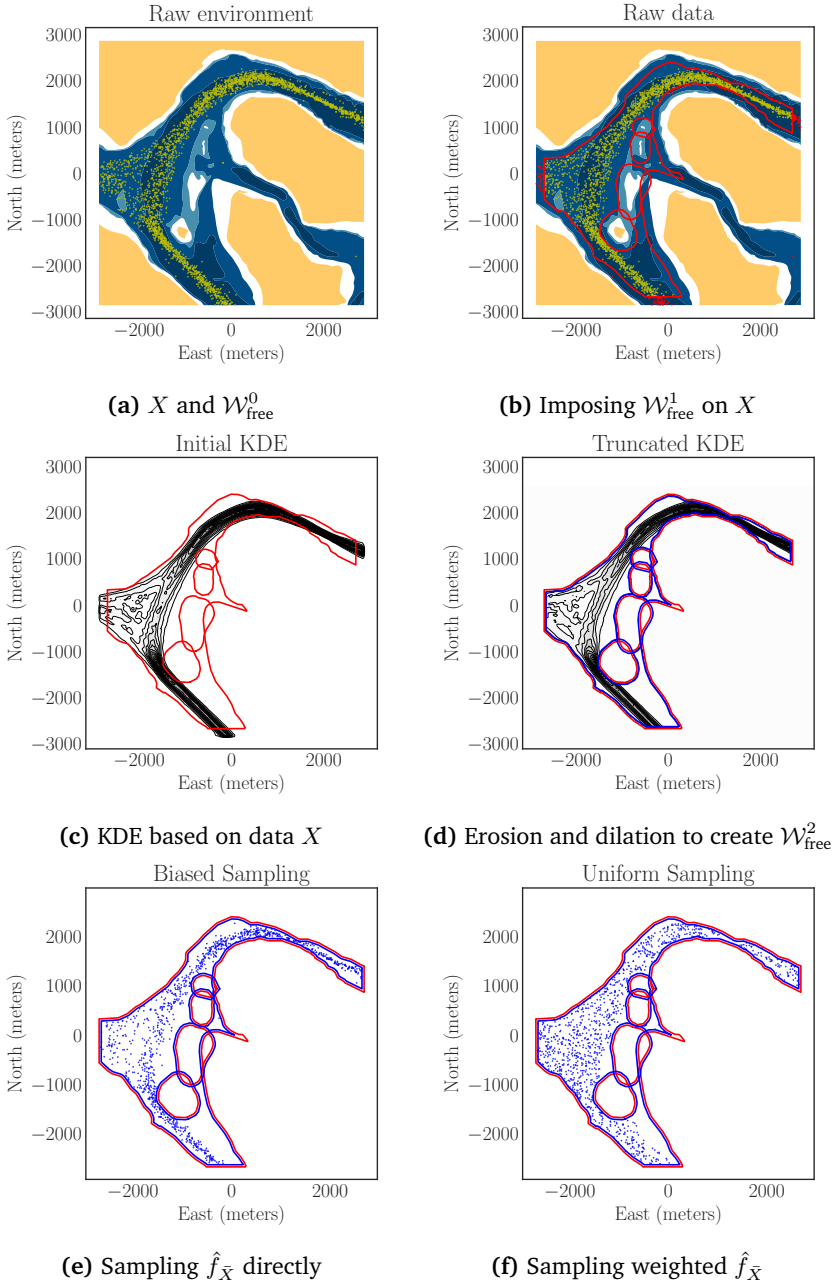
Figure E.5: Application of the proposed method detailed in Section E.3, where the generated sampling schemes are created based on real historical data from vessels passing through the Little belt area of Denmark, such that the resulting samples ensure feasibility with respect to the available water depth. The white regions in Fig. E.5a and E.5b are infeasible regions for the chosen vessel. For more details regarding this particular case study and associated data, see [E19].

(a) Number of samples

(b) Computational time
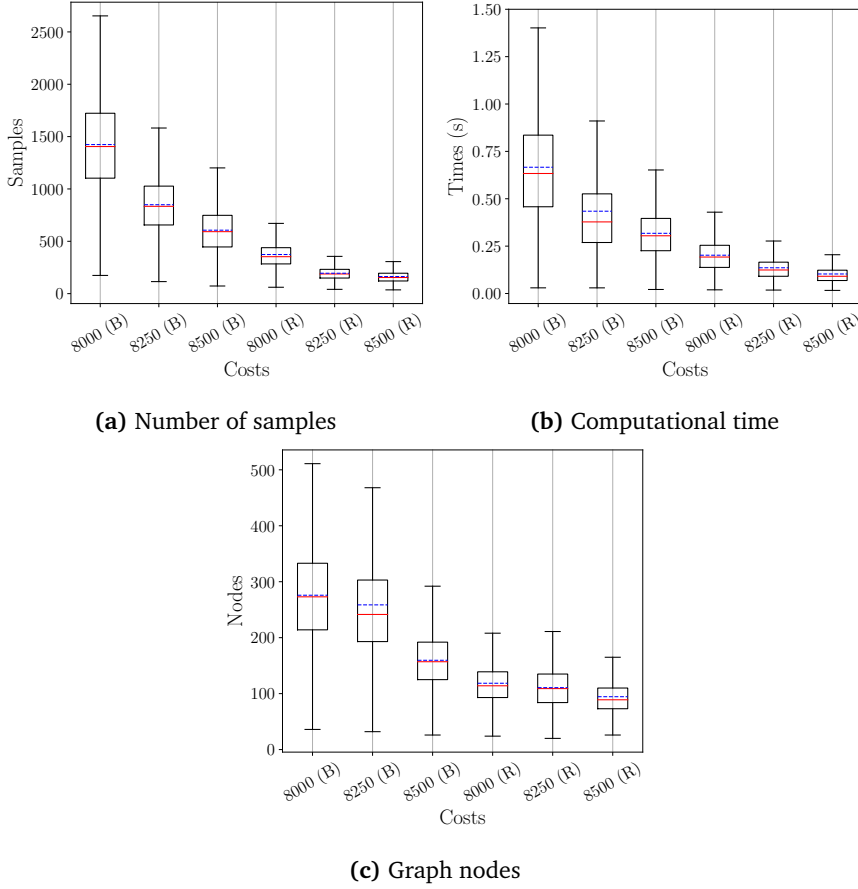
(c) Graph nodes

Figure E.6: Comparison between the required number of samples, computational time and graph nodes required to achieve the specified solution cost ($c = 8000$, $c = 8250$ and $c = 8500$) for both the baseline sampling scheme (B) and proposed rejection-free sampling method (R), when solving the planning problem for the ASV (Fig. E.4a). The blue line indicates the mean and solid red the median. Each method has been simulated 10,000 times, further statistical results can be found in Table E.3.

Table E.1: Computing obstacle-free samples (from $\mathcal{W}_{\text{free}}^1$) 10,000 times (Fig. E.4a). Comparison between the baseline (B) and proposed approach (R), where the percentage ($\Delta\%$) is computed as $(R - B)/B$, where lower numbers are better. Mean (μ), median $\bar{\mu}$ and standard deviation (σ).

	Samples			Times		
	B	R	$\Delta\%$	B	R	$\Delta\%$
μ	9552.722	2500.000	-73.83%	0.423	0.116	-72.63%
$\bar{\mu}$	9551.000	2500.000	-73.83%	0.422	0.116	-72.55%
σ	164.550	0	-100.00%	0.009	0.001	-93.02%

Table E.2: Statistics related to computing feasible solutions to the planning problem related to the ASV 10,000 times (Fig. E.4a). Comparison between the baseline (B) and proposed approach (R), where the percentage ($\Delta\%$) is computed as $(R - B)/B$, where lower numbers are better. Mean (μ), median ($\bar{\mu}$) and standard deviation (σ).

	Samples			Times			Nodes			Cost		
	B	R	$\Delta\%$	B	R	$\Delta\%$	B	R	$\Delta\%$	B	R	$\Delta\%$
μ	318.832	156.470	-50.92%	0.085	0.093	10.07%	53.346	88.325	65.57%	9011.607	8363.973	-7.19%
$\bar{\mu}$	288.000	147.000	-48.96%	0.076	0.082	8.90%	50.000	83.000	66.00%	9001.567	8335.714	-7.40%
σ	155.558	60.195	-61.30%	0.044	0.055	23.86%	19.066	31.671	66.11%	437.860	238.787	-45.47%

tions at all times. The presented case study (Fig. E.5) considers a vessel restricted by shallow waters, which, according to good and safe navigation practise, also wants to maintain a safe distance from shallow water [E53]. The case study uses real ships' position and chart data from the Little Belt area in Denmark (for additional details regarding this particular case study and data see [E19]). Fig. E.5a shows the feasible contours $\mathcal{W}_{\text{free}}^0$ and the past ships' position data X, and Fig. E.5b details the imposed safety distance, both on the data and contours ($\mathcal{W}_{\text{free}}^1$). Fig. E.5c shows the estimated KDE based on the data set X using the box kernel and $\mathbf{H} = 25\mathbf{I}$. Given the selected bandwidth, the boundary polygon is eroded and the obstacles are dilated, as detailed in Fig. E.5d, in order to generate the final space $\mathcal{W}_{\text{free}}^2$. Once obtained, the data set can be reduced by imposing $\mathcal{W}_{\text{free}}^2$ on X, giving $\bar{X}$, and then using it for guaranteed rejection-free sampling of $\mathcal{W}_{\text{free}}^1$.

Given the reduced data set $\bar{X}$ and the truncated KDE, samples can be generated directly from the estimated distribution. However, this results in samples that are biased towards the original dataset, which for motion planning applications may be undesirable. Therefore, samples are weighted by the inverse of their probability

Table E.3: Solutions to the ASV (10,000 times) planning problem (Fig. E.4a), comparing the baseline (B) and proposed approach (R), the planner was terminated once the solution cost c was less than 8500, 8250, and 8000. The percentage ($\Delta\%$) is computed as $(R - B)/B$, where lower numbers are better. Mean (μ), median ($\bar{\mu}$) and standard deviation (σ).

	Samples			Times			Nodes			Cost		
	B	R	$\Delta\%$	B	R	$\Delta\%$	B	R	$\Delta\%$	B	R	$\Delta\%$
						$c = 8500$						
μ	606.060	163.559	-73.01%	0.202	0.103	-49.01%	110.715	94.495	-14.65%	8406.989	8301.497	-1.25%
$\bar{\mu}$	592.000	154.000	-73.99%	0.192	0.091	-52.75%	109.000	89.000	-18.35%	8443.666	8324.918	-1.41%
σ	234.630	63.259	-73.04%	0.091	0.075	-17.76%	38.008	35.274	-7.19%	122.027	153.021	25.40%
						$c = 8250$						
μ	849.348	194.905	-77.05%	0.318	0.136	-57.24%	159.592	118.532	-25.73%	8185.689	8179.320	-0.08%
$\bar{\mu}$	834.000	188.000	-77.46%	0.305	0.124	-59.25%	157.000	114.000	-27.39%	8213.833	8204.987	-0.11%
σ	286.791	72.240	-74.81%	0.134	0.116	-13.30%	51.661	43.497	-15.80%	92.511	83.872	-9.34%
						$c = 8000$						
μ	1423.857	373.699	-73.75%	0.666	0.434	-34.82%	275.855	258.625	-6.25%	7948.200	7979.359	0.39%
$\bar{\mu}$	1405.000	353.000	-74.88%	0.633	0.378	-40.34%	273.000	241.500	-11.54%	7978.459	7987.719	0.12%
σ	478.265	139.103	-70.92%	0.301	0.264	-12.27%	93.382	102.636	9.91%	81.168	39.102	-51.83%

density to generate approximately uniform samples of the domain described by the truncated KDE. The biased sampling and approximately uniform sampling is shown in Fig. E.5e and E.5f respectively, where the only difference is how samples are generated from the KDE.

Monte Carlo simulations were used to investigate the performance of the proposed method for generating approximately uniform samples from the KDE. All the following results were generated from solving the planning problem detailed in Fig. E.4a, where the baseline sampling scheme is simply a rectangular approximation of the planning region.

Table E.1 details 10,000 trials, where the two sampling schemes were tasked with generating 2500 feasible samples. As expected, since the proposed method directly samples the free space in a rejection-free manner, each trial spends exactly 2500 samples in order to generate the required 2500 feasible samples. The performance of the baseline sampler is highly correlated with the area ratio between the actual free space and its approximation. In general, the traditional uniform sampler results in a constant factor, relative to the area ratio, in terms of increased run time [E19], [E38]. These results highlight the sampling efficiency to be gained from specialising the scheme to the particular problem at hand, as the strength of the method becomes more apparent when the baseline sampler is a poor approximation of the free space.

Table E.2 contains the results of 10,000 trials in which the baseline and the proposed method are tasked with simply computing a feasible solution. On average,

the proposed approach is 10% slower at finding an initial solution; however, the achieved solution cost is 7% lower. The results show that the graph density (number of nodes) for the proposed method is 65% higher for this particular case study, which explains why the overall run time is increased.

The true strength of the proposed method is captured when one wishes to find paths within the space of past behaviours, which are lower cost than some desired cost. Table E.3 shows 10,000 trials for both methods, where both planners solve the problem in Fig. E.4a until the reported solution cost is lower than 8500, 8250 and 8000. Fig. E.6 visualises the table data, where it is clear that to obtain a specific solution cost, the rejection-free method excels. The proposed method for all three cost scenarios outperform every baseline, whilst also significantly reducing the amount of standard deviation in the resulting solution. As previously detailed, using the proposed method allows one to successfully capture the underlying navigational behaviour of past vessels. The sampling scheme guarantees that any generated sample is approximately uniform in the domain of the KDE, which describes the past behaviours of other vessels, and always falls within the defined free space. The approach allows one to include design specifications directly in the formulation of the sampling space, which in this case translate to maintaining a certain safety distance towards the shallow waters.

E.4.2   Navigating Autonomous Drones in challenging environments

Drones are widely adopted in various industries, proving their worth in many highly automated or autonomous tasks. Their ability to move freely in 3D provides significant value when it comes to performing inspection, monitoring, and surveying tasks, as well as providing the ability to interact and reach places infeasible for humans. This particular case study was chosen to demonstrate the applicability of the proposed methods to higher-dimensional problems. This case study uses data from a real drone that has previously inspected a marine vessel, specifically ballast tank inspection [E54]. The motion planning problem is then to compute a path for a new inspection task. Fig. E.7 details the steps of the proposed method. Given some inspection data collected in $\mathcal{W}_{\text{free}}^0$, the problem changes to contain new obstacles and a safety distance requirement, which generates $\mathcal{W}_{\text{free}}^1$ (Fig. E.7a and Fig. E.7b). Next, the bandwidth matrix $\mathbf{H} = 0.18\mathbf{I}$ and Epanechnikov kernel is selected and the KDE is computed and evaluated (Fig. E.7c), where then the space $\mathcal{W}_{\text{free}}^1$ is dilated by the bandwidth, generating $\mathcal{W}_{\text{free}}^2$ (Fig. E.7d). By imposing $\mathcal{W}_{\text{free}}^2$ on X, one can generate biased or approximately uniform samples as desired (Fig. E.7e and Fig. E.7f).

Compared to the ASV case study, when looking for a feasible solution to the drone scenario, the proposed method significantly outperforms the baseline. Table
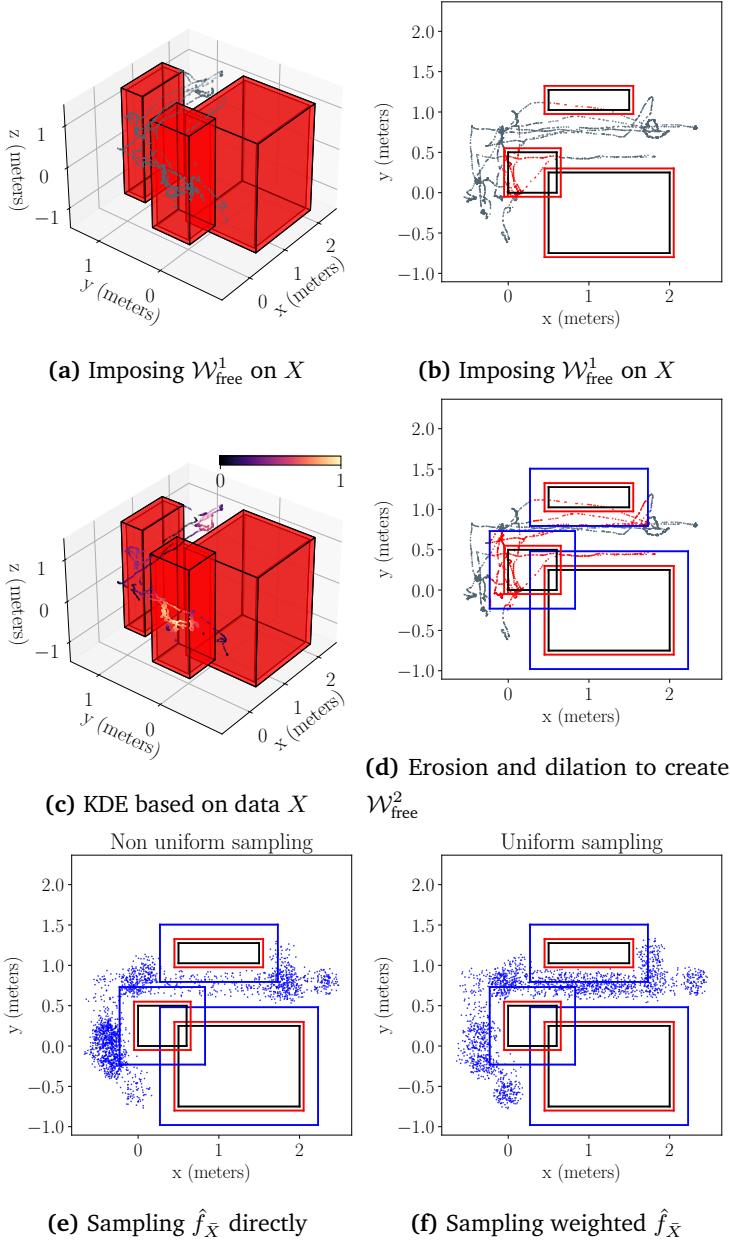
(a) Imposing $\mathcal{W}_{\text{free}}^1$ on X

(b) Imposing $\mathcal{W}_{\text{free}}^1$ on X

(c) KDE based on data X

(d) Erosion and dilation to create $\mathcal{W}_{\text{free}}^2$

(e) Sampling $\hat{f}_{\bar{X}}$ directly

(f) Sampling weighted $\hat{f}_{\bar{X}}$

Figure E.7: Application of the proposed sampling method from Section E.3, with real life data from a drone inspecting a confined space [E54]. The resulting space ensures that the drone is able to maintain an adequate safety distance from the updated obstacle space. Fig. E.7b and E.7d-E.7f are the 2D projections to the xy-plane of the space shown in Fig. E.7a, for $z = 0$. Fig. E.7c is a 3D visualisation of the untruncated KDE; the colour of each data point indicates the probability density. Note that due to limitations with the 3D engine used for plotting, the location of the data points in Fig. E.7a and Fig. E.7c may be deceptive.
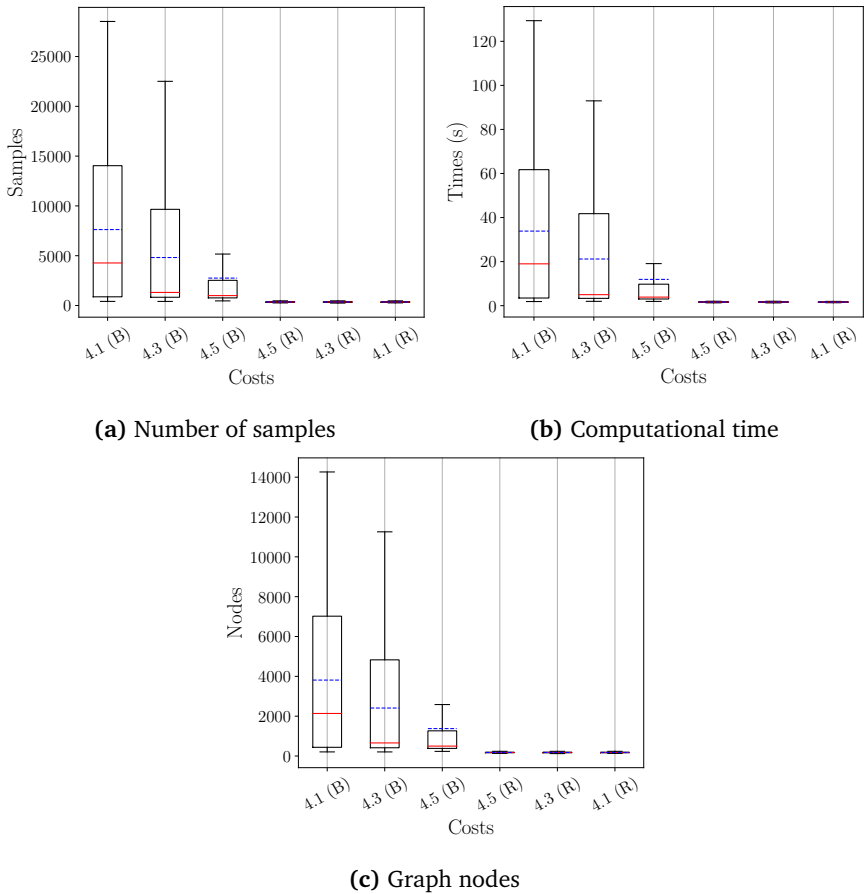
(a) Number of samples

(b) Computational time

(c) Graph nodes

Figure E.8: Comparison between the required number of samples, computational time and graph nodes required to achieve the specified solution cost ($c = 4.1$, $c = 4.3$ and $c = 4.5$) for both the baseline sampling scheme (B) and proposed rejection-free sampling method (R), when solving the drone planning problem in Fig. E.4b and Fig. E.4c. The blue line indicates the mean and solid red the median. Each method has been simulated 500 times, further statistical results can be found in Table E.5.

Table E.4: Statistics related to computing feasible solutions to the drone planning problem 10,000 times (Fig. E.4b). Comparison between the baseline (B) and proposed approach (R), where the percentage ($\Delta\%$) is computed as $(R - B)/B$, where lower numbers are better. Mean (μ), median ($\bar{\mu}$) and standard deviation (σ).

	Samples			Times			Nodes			Cost		
	B	R	$\Delta\%$	B	R	$\Delta\%$	B	R	$\Delta\%$	B	R	$\Delta\%$
μ	1001.151	355.098	-64.35%	4.018	1.701	-57.66%	502.026	178.974	-64.35%	4.268	3.670	-14.02%
$\bar{\mu}$	871.000	351.000	-59.45%	3.555	1.691	-52.44%	436.500	177.000	-59.45%	4.194	3.664	-12.63%
σ	457.672	44.332	-90.31%	1.636	0.163	-90.01%	228.824	22.174	-90.31%	0.402	0.048	-88.15%

Table E.5: Drone planning problem results (500 simulations), Fig. E.4b and Fig. E.4c, the planner was terminated once the cost c was less than 4.5, 4.3, and 4.1. Comparison between the baseline (B) and the proposed approach (R), where the percentage ($\Delta\%$) is computed as $(R - B)/B$, where lower numbers are better. Mean (μ), median ($\bar{\mu}$) and standard deviation (σ).

	Samples			Times			Nodes			Cost		
	B	R	$\Delta\%$	B	R	$\Delta\%$	B	R	$\Delta\%$	B	R	$\Delta\%$
						$c = 4.5$						
μ	2750.836	355.300	-87.08%	11.933	1.630	-86.34%	1376.764	179.096	-86.99%	4.162	3.669	-11.86%
$\bar{\mu}$	993.000	349.500	-64.80%	3.888	1.614	-58.49%	498.000	176.000	-64.66%	4.204	3.661	-12.90%
σ	3430.622	44.749	-98.70%	15.748	0.146	-99.07%	1715.143	22.374	-98.70%	0.255	0.048	-81.11%
						$c = 4.3$						
μ	4815.408	354.742	-92.63%	21.178	1.643	-92.24%	2408.996	178.782	-92.58%	4.077	3.669	-10.02%
$\bar{\mu}$	1312.000	352.000	-73.17%	4.994	1.633	-67.30%	657.500	177.500	-73.00%	4.128	3.662	-11.29%
σ	5284.368	45.618	-99.14%	24.051	0.159	-99.34%	2641.956	22.800	-99.14%	0.194	0.048	-75.32%
						$c = 4.1$						
μ	7623.002	354.372	-95.35%	33.850	1.647	-95.13%	3812.696	178.608	-95.32%	3.988	3.673	-7.91%
$\bar{\mu}$	4271.000	350.000	-91.81%	18.986	1.640	-91.36%	2137.000	176.500	-91.74%	4.026	3.667	-8.93%
σ	7680.157	45.064	-99.41%	34.972	0.155	-99.56%	3839.816	22.544	-99.41%	0.112	0.048	-57.58%

E.4 details 10,000 simulations of the presented planning problem in Fig. E.4b and Fig. E.4c. Here, it is evident that as the dimensional complexity increases, the true benefits of a specialised sampling scheme appear. Since the particular historical data are a good representation of the desired path, the proposed method is faster (by 57%) and produces lower cost paths at a significantly lower standard deviation (88% lower).

Obtaining lower-cost solutions, using the proposed method, for a problem such as the one posed by drone navigation also heavily outperforms the baseline. Three cost ($c = 4.5$, $c = 4.3$ and $c = 4.1$) thresholds were selected that lie within the range of what was produced by the feasible solutions of both methods (from Table E.4). Due to the sheer amount of compute time required by the baseline, the number of trials was reduced to 500. Table E.5 and Fig. E.8 detail the statistics related to obtaining a solution better than the cost thresholds mentioned above. Since the historical data are very representative of the desired paths, the proposed method does significantly better than the baseline. The baseline spends significant sampling effort exploring the entire space, where instead the rejection-free scheme hones its search. This results in greater speeds and overall consistency of the proposed method, since, as shown by the median and mean values of the baseline, there are a large number of outliers in the 500 trials that significantly impact the performance. By comparing the median values, the proposed method performs at least twice as well for $c = 4.5$ and $c = 4.3$, while for $c = 4.1$ it performs 11 times better.

E.5 Conclusions

This paper proposed a new learning-based sampling strategy to generate biased or approximately uniform samples of a given free space, while guaranteeing that no rejection sampling is required. Kernel density estimation is adopted to achieve a probabilistic non-parametric description of regions of the workspace where solutions of the motion planning problem are likely to exist. The kernel and bandwidth of the estimated kernel density were exploited to provide a guarantee-by-construction that all future states generated by sampling the KDE fall within the boundaries of the free space. The method was illustrated in two case studies using real historical data for 2D and 3D workspaces, collected from surface vessels and drones, respectively. Each case study contained detailed steps explaining how to generate the sampling spaces. Finally, motion planning problems were solved for both the ASV and the drone case studies, and extensive Monte Carlo simulations were performed to gather statistical data, which detailed the strengths of the method.

It is noteworthy that the proposed method only performs as well as the available

historical data. If the sought motion plan does not exist within the neighbourhood of the past behaviours, then the proposed method will perform worse than the baseline uniform sampling scheme.

Potential future work includes investigating whether or not pre-processing the data provides any performance improvement. It is speculated that for cases with highly application specific data, data augmentation or modification may improve the performance. Additionally, the statistical properties of the approximately uniform sampling scheme could be further investigated such that the uniformity of the sampled points could be accessed with respect to the underlying distribution.

Acknowledgment

E.6   References

[E1]   L. E. Kavraki, P. Svestka, J.-C. Latombe, and M. H. Overmars, "Probabilistic roadmaps for path planning in high-dimensional configuration spaces," *IEEE transactions on Robotics and Automation*, vol. 12, no. 4, pp. 566–580, 1996.

[E2]   L. E. Kavraki, M. N. Kolountzakis, and J.-C. Latombe, "Analysis of probabilistic roadmaps for path planning," *IEEE Transactions on Robotics and automation*, vol. 14, no. 1, pp. 166–171, 1998.

[E3]   R. Geraerts and M. H. Overmars, "A comparative study of probabilistic roadmap planners," *Algorithmic foundations of robotics V*, Springer, 2004, pp. 43–57.

[E4]   S. M. LaValle, "Rapidly-exploring random trees : A new tool for path planning," *The annual research report*, 1998.

[E5]   J. J. Kuffner and S. M. LaValle, "RRT-connect: An efficient approach to single-query path planning," *Proceedings 2000 ICRA. Millennium Conference. IEEE International Conference on Robotics and Automation. Symposia Proceedings (Cat. No. 00CH37065)*, IEEE, vol. 2, 2000, pp. 995–1001.

[E6]   S. M. LaValle and J. J. Kuffner, "Randomized Kinodynamic Planning," *The International Journal of Robotics Research*, vol. 20, no. 5, pp. 378–400, May 2001.

[E7]   S. Karaman and E. Frazzoli, "Sampling-based algorithms for optimal motion planning," *The international journal of robotics research*, vol. 30, no. 7, pp. 846–894, 2011.

[E8]   J. D. Gammell, S. S. Srinivasa, and T. D. Barfoot, "Batch informed trees (BIT*): Sampling-based optimal planning via the heuristically guided search of implicit random geometric graphs," *2015 IEEE international conference on robotics and automation (ICRA)*, IEEE, 2015, pp. 3067–3074.

[E9]   L. Janson, E. Schmerling, A. Clark, and M. Pavone, "Fast marching tree: A fast marching sampling-based method for optimal motion planning in many dimensions," *The International journal of robotics research*, vol. 34, no. 7, pp. 883–921, 2015.

[E10]   S. Choudhury, J. D. Gammell, T. D. Barfoot, S. S. Srinivasa, and S. Scherer, "Regionally accelerated batch informed trees (RABIT*): A framework to integrate local information into optimal path planning," *2016 IEEE International Conference on Robotics and Automation (ICRA)*, IEEE, 2016, pp. 4207–4214.

[E11]   M. P. Strub and J. D. Gammell, "Adaptively Informed Trees (AIT*): Fast asymptotically optimal path planning through adaptive heuristics," *2020 IEEE International Conference on Robotics and Automation (ICRA)*, IEEE, 2020, pp. 3191–3198.

[E12]   M. P. Strub and J. D. Gammell, "Advanced BIT* (ABIT*): Sampling-based planning with advanced graph-search techniques," *2020 IEEE International Conference on Robotics and Automation (ICRA)*, IEEE, 2020, pp. 130–136.

[E13]   S. Klemm, J. Oberländer, A. Hermann, A. Roennau, T. Schamm, J. M. Zollner, and R. Dillmann, "RRT*-Connect: Faster, asymptotically optimal motion planning," *2015 IEEE international conference on robotics and biomimetics (ROBIO)*, IEEE, 2015, pp. 1670–1677.

[E14]   D. Yi, M. A. Goodrich, and K. D. Seppi, "MORRF*: Sampling-based multi-objective motion planning," *Twenty-Fourth International Joint Conference on Artificial Intelligence*, 2015.

[E15]   M. Otte and E. Frazzoli, "RRT^X: Asymptotically optimal single-query sampling-based motion planning with quick replanning," *The International Journal of Robotics Research*, vol. 35, no. 7, pp. 797–822, 2016.

[E16]   L. G. D. Véras, F. L. Medeiros, and L. N. Guimaráes, "Systematic literature review of sampling process in rapidly-exploring random trees," *IEEE Access*, vol. 7, pp. 50 933–50 953, 2019.

[E17]   J. D. Gammell and M. P. Strub, "Asymptotically optimal sampling-based motion planning methods," *Annual Review of Control, Robotics, and Autonomous Systems*, vol. 4, pp. 295–318, 2021.

[E18]   Y. Abbasi-Yadkori, P. Bartlett, V. Gabillon, and A. Malek, "Hit-and-run for sampling and planning in non-convex spaces," *Artificial Intelligence and Statistics*, PMLR, 2017, pp. 888–895.

[E19]   T. T. Enevoldsen and R. Galeazzi, "Grounding-aware RRT* for Path Planning and Safe Navigation of Marine Crafts in Confined Waters," *13th IFAC Conference on Control Applications in Marine Systems, Robotics, and Vehicles (CAMS) 2021*, 2021.

[E20]   S. R. Lindemann and S. M. LaValle, "Current issues in sampling-based motion planning," *Robotics research. The eleventh international symposium*, Springer, 2005, pp. 36–54.

[E21]   L. Janson, E. Schmerling, and M. Pavone, "Monte carlo motion planning for robot trajectory optimization under uncertainty," *Robotics Research*, Springer, 2018, pp. 343–361.

[E22]   T. Osa, "Multimodal trajectory optimization for motion planning," *The International Journal of Robotics Research*, vol. 39, no. 8, pp. 983–1001, 2020.

[E23]   E. Schmerling and M. Pavone, "Evaluating trajectory collision probability through adaptive importance sampling for safe motion planning," *arXiv preprint arXiv:1609.05399*, 2016.

[E24]   J. D. Gammell, S. S. Srinivasa, and T. D. Barfoot, "Informed RRT*: Optimal sampling-based path planning focused via direct sampling of an admissible ellipsoidal heuristic," *2014 IEEE/RSJ International Conference on Intelligent Robots and Systems*, IEEE, 2014, pp. 2997–3004.

[E25]   A. Mandalika, R. Scalise, B. Hou, S. Choudhury, and S. S. Srinivasa, "Guided incremental local densification for accelerated sampling-based motion planning," *arXiv preprint arXiv:2104.05037*, 2021.

[E26]   T. T. Enevoldsen, C. Reinartz, and R. Galeazzi, "COLREGs-Informed RRT* for Collision Avoidance of Marine Crafts," *2021 International Conference on Robotics and Automation (ICRA)*, IEEE, 2021.

[E27] T. Kunz, A. Thomaz, and H. Christensen, "Hierarchical rejection sampling for informed kinodynamic planning in high-dimensional spaces," *2016 IEEE International Conference on Robotics and Automation (ICRA)*, IEEE, 2016, pp. 89–96.

[E28] D. Yi, R. Thakker, C. Gulino, O. Salzman, and S. Srinivasa, "Generalizing informed sampling for asymptotically-optimal sampling-based kinodynamic planning via markov chain monte carlo," *2018 IEEE International Conference on Robotics and Automation (ICRA)*, IEEE, 2018, pp. 7063–7070.

[E29] T. F. Iversen and L.-P. Ellekilde, "Kernel density estimation based self-learning sampling strategy for motion planning of repetitive tasks," *2016 IEEE/RSJ International Conference on Intelligent Robots and Systems (IROS)*, IEEE, 2016, pp. 1380–1387.

[E30] P. Lehner and A. Albu-Schäffer, "Repetition sampling for efficiently planning similar constrained manipulation tasks," *2017 IEEE/RSJ International Conference on Intelligent Robots and Systems (IROS)*, IEEE, 2017, pp. 2851–2856.

[E31] P. Lehner and A. Albu-Schäffer, "The repetition roadmap for repetitive constrained motion planning," *IEEE Robotics and Automation Letters*, vol. 3, no. 4, pp. 3884–3891, 2018.

[E32] C. Chamzas, A. Shrivastava, and L. E. Kavraki, "Using local experiences for global motion planning," *2019 International Conference on Robotics and Automation (ICRA)*, IEEE, 2019, pp. 8606–8612.

[E33] I. Baldwin and P. Newman, "Non-parametric learning for natural plan generation," *2010 IEEE/RSJ International Conference on Intelligent Robots and Systems*, IEEE, 2010, pp. 4311–4317.

[E34] Y. Dong, Y. Zhong, and J. Hong, "Knowledge-biased sampling-based path planning for automated vehicles parking," *IEEE Access*, vol. 8, pp. 156 818–156 827, 2020.

[E35] C. Zhang, J. Huh, and D. D. Lee, "Learning implicit sampling distributions for motion planning," *2018 IEEE/RSJ International Conference on Intelligent Robots and Systems (IROS)*, IEEE, 2018, pp. 3654–3661.

[E36] D. Hsu, J.-C. Latombe, and R. Motwani, "Path planning in expansive configuration spaces," *Proceedings of International Conference on Robotics and Automation*, IEEE, vol. 3, 1997, pp. 2719–2726.

[E37] D. Kim, Y. Kwon, and S.-E. Yoon, "Dancing PRM*: Simultaneous planning of sampling and optimization with configuration free space approximation," *2018 IEEE International Conference on Robotics and Automation (ICRA)*, IEEE, 2018, pp. 7071–7078.

[E38] J. Bialkowski, M. Otte, and E. Frazzoli, "Free-configuration biased sampling for motion planning," *2013 IEEE/RSJ International Conference on Intelligent Robots and Systems*, IEEE, 2013, pp. 1272–1279.

[E39] O. Arslan and P. Tsiotras, "Machine learning guided exploration for sampling-based motion planning algorithms," *2015 IEEE/RSJ International Conference on Intelligent Robots and Systems (IROS)*, IEEE, 2015, pp. 2646–2652.

[E40] S. S. Joshi and T. Panagiotis, "Non-parametric informed exploration for sampling-based motion planning," *2019 International Conference on Robotics and Automation (ICRA)*, IEEE, 2019, pp. 5915–5921.

[E41] B. Ichter, J. Harrison, and M. Pavone, "Learning sampling distributions for robot motion planning," *2018 IEEE International Conference on Robotics and Automation (ICRA)*, IEEE, 2018, pp. 7087–7094.

[E42] B. Ichter and M. Pavone, "Robot motion planning in learned latent spaces," *IEEE Robotics and Automation Letters*, vol. 4, no. 3, pp. 2407–2414, 2019.

[E43] J. Wang, W. Chi, C. Li, C. Wang, and M. Q.-H. Meng, "Neural RRT*: Learning-based optimal path planning," *IEEE Transactions on Automation Science and Engineering*, vol. 17, no. 4, pp. 1748–1758, 2020.

[E44] L. Li, Y. Miao, A. H. Qureshi, and M. C. Yip, "MPC-MPNet: Model-Predictive Motion Planning Networks for Fast, Near-Optimal Planning under Kinodynamic Constraints," *IEEE Robotics and Automation Letters*, vol. 6, no. 3, pp. 4496–4503, 2021.

[E45] A. Gramacki, *Nonparametric kernel density estimation and its computational aspects*. Springer, 2018.

[E46] D. W. Scott, *Multivariate density estimation: theory, practice, and visualization*. John Wiley & Sons, 2015.

[E47] B. W. Silverman, "Algorithm as 176: Kernel density estimation using the fast fourier transform," *Journal of the Royal Statistical Society. Series C (Applied Statistics)*, vol. 31, no. 1, pp. 93–99, 1982.

[E48] Z. I. Botev, J. F. Grotowski, and D. P. Kroese, "Kernel density estimation via diffusion," *The annals of Statistics*, vol. 38, no. 5, pp. 2916–2957, 2010.

[E49]   T. A. O'Brien, K. Kashinath, N. R. Cavanaugh, W. D. Collins, and J. P. O'Brien, "A fast and objective multidimensional kernel density estimation method: fastKDE," *Computational Statistics & Data Analysis*, vol. 101, pp. 148–160, 2016.

[E50]   A. Gramacki and J. Gramacki, "FFT-based fast computation of multivariate kernel density estimators with unconstrained bandwidth matrices," *Journal of Computational and Graphical Statistics*, vol. 26, no. 2, pp. 459–462, 2017.

[E51]   L. Devroye and L. Gyorfi, *Nonparametric Density Estimation: The L_1 View* (Wiley Interscience Series in Discrete Mathematics). Wiley, 1985.

[E52]   W. Härdle, M. Müller, S. Sperlich, A. Werwatz, *et al.*, *Nonparametric and semiparametric models*. Springer, 2004, vol. 1.

[E53]   T. T. Enevoldsen, M. Blanke, and R. Galeazzi, "Sampling-based collision and grounding avoidance for marine crafts," *Ocean Engineering*, vol. 261, p. 112 078, 2022. DOI: https://doi.org/10.1016/j.oceaneng.2022.112078.

[E54]   R. E. Andersen, M. Zajaczkowski, H. Jaiswal, J. Xu, W. Fan, and E. Boukas, "Depth-based deep learning for manhole detection in uav navigation," *2022 IEEE International Conference on Imaging Systems and Techniques (IST)*, 2022, pp. 1–6. DOI: 10.1109/IST55454.2022.9827720.

[E55]   T. Odland, *tommyod/KDEpy: Kernel Density Estimation in Python*, Dec. 2018. DOI: 10.5281/zenodo.2392268.

Paper F

Autonomy for Ferries and Harbour Buses: a Collision Avoidance Perspective

Thomas T. Enevoldsen[1][*], Mogens Blanke[1] and Roberto Galeazzi[1]

[1]Automation and Control Group, Department of Electrical and Photonics Engineering, Technical University of Denmark, DK-2800 Kgs. Lyngby, Denmark {tthen,mobl, roga}@dtu.dk

Abstract:

This paper provides a collision avoidance perspective to maritime autonomy, in the shift towards Maritime Autonomous Surface Ships (MASS). In particular, the paper presents the developments related to the Greenhoper, a Danish autonomous harbour bus. The collision and grounding avoidance scheme, called the Short Horizon Planner (SHP), is described and discussed in detail. Furthermore, the required autonomy stack for facilitating safe and rule-compliant collision avoidance is presented. The inherent difficulties relating to adhering to the COLREGs are outlined, highlighting some of the operational constraints and challenges within the space of autonomous ferries and harbour buses. Finally, collision and grounding avoidance is demonstrated using a simulation of the entire proposed autonomy stack.

F.1   Introduction

As the world's population continues to expand and the green transition accelerates, there is a growing demand for improved logistic and mobility capabilities. Autonomous transportation systems seek to increase efficiency, both in terms of availability, mobility, safety, and emissions. In recent times, rapid development has occurred within the space of maritime autonomy, with the first technological benefits emerging. In the beginning of 2022, the Japanese project, MEGURI2040, demonstrated autonomous capabilities onboard a container vessel. During fall 2021, Sea Machines launched a 1000nm autonomous voyage for their 11m long craft, showcasing the maturity of their technology within inner coastal waters. In fall 2022, the Norwegian autonomous ferry, Milliampere, was demonstrated, highlighting an important case study for inner-city mobility [F1]. These Maritime Autonomous Surface Ships (MASS) are prominent candidates to meet increasing mobility demands, strengthen connectivity to island societies, and reduce road congestion in major urban areas by opening their waterways for transport of goods and people. MASS will extend the availability of existing waterborne transportation services, and will open for new mobility on demand services. A major challenge in the shift towards autonomous vessels and systems is the complete adherence to the rules, regulations, and practises laid out by the preceding sailors and navigators.

In Denmark, ShippingLab represents the Danish initiative within autonomous waterborne transport, where the goal is to create Denmark's first autonomous and environmentally friendly ship. This effort has resulted in the Greenhopper, a 12.2m long battery operated double-ended catamaran, designed and built in Denmark. The vessel will facilitate the expansion and growth of the city of Aalborg, located in the northern part of the Danish peninsula, Jutland. It will cross the Limfjorden, with its journey lasting 5-7 minutes (580m).

Recent efforts within collision avoidance for marine autonomy focus on confined and inner coastal waters. In these waters, there are various efforts that concern computing trajectories in compliance with COLREGs 8 & 13-17. Bergman *et al.* [F2] demonstrated a two-step optimisation procedure, where a lattice-based planner computes suboptimal trajectories based on motion primitives that are refined by solving optimal control problems (OCP). Enevoldsen *et al.* [F3] presented a sampling-based method to calculate minimal route deviations, minimising cross-track error and speed loss. Thyri and Breivik [F4] detailed a collision avoidance scheme that assigns and uses control barrier functions for preventing ship domain violation, and thereby enforcing the COLREGs.

For the MilliAmpere [F1], Bitar *et al.* [F5] detailed a method consisting of the

(a) The Greenhopper: a Danish autonomous ferry.
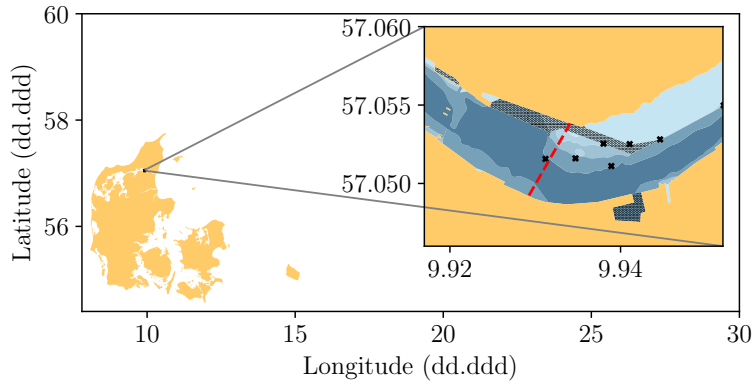
(b) The operational area at Limfjorden, Aalborg, Denmark. The dashed line is the nominal route, crosses buoys and hatched areas dredged locations. Darker blues are deeper contours.

Figure F.1: The Greenhopper vessel and its area of operation.

three aspects of an autonomous voyage: undocking, transit, and docking. Docking was dealt with using model predictive control, whereas the transit phase combined a hybrid A* with an OCP solver. Thyri *et al.* [F6] instead cast the problem as a velocity planning problem, by leveraging a set of pre-defined feasible paths. The planning phase then recomputes with respect to dynamic obstacles. The Dutch project Roboat seeks to implement an autonomous platform for urban mobility [F7], where in [F8] the system demonstrates its capabilities and basic adherence to COLREGs rule 13-15. For the Rhine river, Koschorrek *et al.* [F9] presented a system that used a hybrid A* to find feasible trajectories. Here, COLREGs are not directly considered because local law dictates that a ferry must yield for everything.

This paper proposes a collision avoidance scheme, the *Short Horizon Planner*

(SHP), designed for a fjord crossing ferry, such as the Greenhopper. The SHP considers the available manoeuvrability for precise obstacle avoidance, while partially adhering to the IMO COLREGs (rules 8 & 13-17). The role, purpose, and responsibility of the collision avoidance system within the autonomy stack is detailed and discussed, outlining apparent operational constraints in both the collision avoidance system and the remaining stack. The particular operation of the Greenhopper is detailed, highlighting the interplay between the SHP and the remaining autonomy stack.

F.2   System modelling and identification

The Greenhopper is propelled and manoeuvred by two azimuth thrusters, located fore and aft, at the centre line. It is equipped with four RGB cameras, eight Long Wavelength Infrared (LWIR) cameras, four W band and one X band radar, two 3D lidars, a GNSS, a gyro compass, an AIS transponder and an IMU. Sensors mounted on the mast can be seen in Fig. F.1a. A Voyage Control System (VCS) is responsible for executing steering and track control along a nominal route. The VCS will safely dock, undock, and carry out the voyage in nominal conditions. The nominal route can be modified by adding supplemental waypoints to the VCS, as safe navigation requires.

F.2.1   Surge velocity dynamics

Surge acceleration is the result of the balance between propeller forces and hull resistance.

With azimuth thrusters fore and aft, along ship thrust is,

$$T_x = T_{P,1} \cos(\phi_1) + T_{P,2} \cos(\phi_2) \tag{F.1}$$

where ϕ_i is the azimuth angle of thruster i and $T_{P,i}$ is propeller thrust.

Hull resistance consists of Stokes friction, linear in u, and pressure drag that is quadratic in $u|u|$. With mass and added mass in the left hand side factor, and thrust deduction t, surge dynamics reads,

$$(m - X_{\dot{u}})\dot{u} = (1 - t)T_x - X_u u - X_{u|u|} u|u|. \tag{F.2}$$

Introducing $T_x = \beta_s T_\%$ and $T_\%$ as commanded thrust percentage, (F.2) has the form,

$$\dot{u} = \beta T_\% - \alpha u - \gamma u|u| \tag{F.3}$$

with thrust scaling β, linear damping α, and quadratic damping γ. These are identified from full scale testing in the following section.
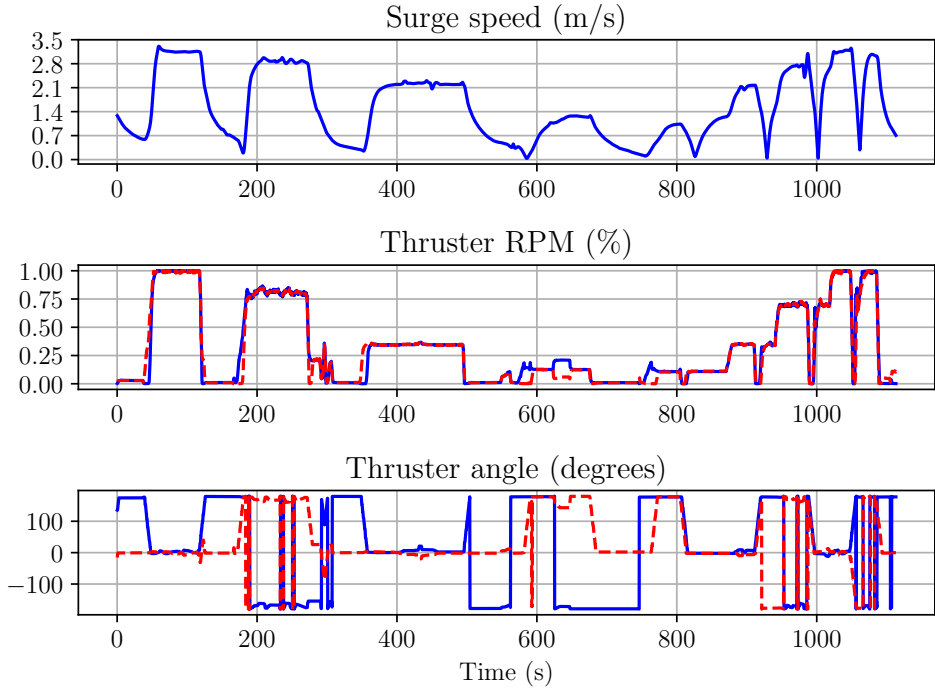
(a) Experimental data from the Greenhopper. $t = 0s$ to $t = 800s$ contains acceleration and deceleration experiments. From $t = 800s$ and onwards are recorded emergency stops at various speeds.
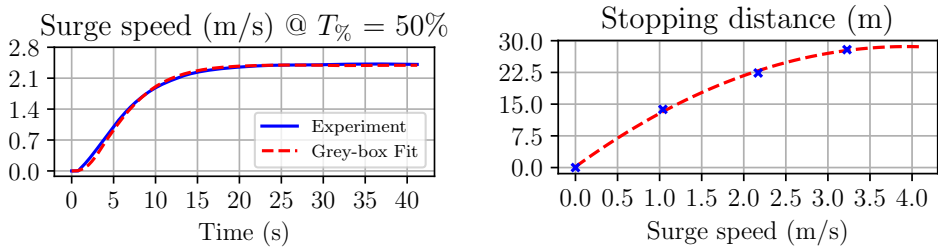
(b) Grey-box estimate of (F.3) at 50% thrust.

(c) Second order fit for the emergency stopping distances.

Figure F.2: Experiments and estimates from the Greenhopper.

F.2.2   Grey-box identification and analytical solution

The identification of (F.3) based on full-scale acceleration data revealed that due to the low speed regime, the particular hull form, and the propeller slip stream interaction with the pontoons of the catamaran hull, the nonlinear damping coefficient γ is hard to identify. The contribution of the term is essentially zero, on the basis of the available experimental data. Therefore, a linear model is pursued,

$$\dot{u} = \beta T_\% - \alpha u, \quad \dot{N} = \cos(\psi)\, u, \quad \dot{E} = \sin(\psi)\, u \tag{F.4}$$

where $T_\%$ and heading angle ψ are known and constant. The solutions to the linear ODEs are as follows

$$\begin{bmatrix} u(t) \\ N(t) \\ E(t) \end{bmatrix} = \begin{bmatrix} (1 - e^{-\alpha t})\frac{\beta}{\alpha} T_\% \\ \left(\frac{1}{\alpha^2} e^{-\alpha t} + \frac{1}{\alpha}t\right) T_\% \beta \cos(\psi) \\ \left(\frac{1}{\alpha^2} e^{-\alpha t} + \frac{1}{\alpha}t\right) T_\% \beta \sin(\psi) \end{bmatrix}. \tag{F.5}$$

The analytical solution is used to calculate a trajectory between two points in the north-east plane, simply by computing the arrival time t_f at the final point. The arrival time is obtained by setting the left-hand side of (F.5) to the desired point and solving for t. Once t_f is obtained, obtaining the trajectory is trivial.

F.3   Path planning and collision avoidance

The nominal path of the Greenhopper is described by two waypoints located on the north and south side of the fjord. In conditions with traffic, the objective is to find a path that connects either the nominal waypoints, or the current position of ownship and the goal in a collision-free and safe manner.

F.3.1   Spatio-temporal lattice planner

Let $\mathcal{X} \subseteq \mathbb{R}^3$ be the state space, with $\mathbf{x} \in \mathcal{X}$ and $\mathbf{x} = [E, N, t]^T$. $\mathcal{X}$ is divided into two subsets, the free space $\mathcal{X}_{\text{free}}$ and the obstacle space $\mathcal{X}_{\text{obs}}$, with $\mathcal{X}_{\text{free}} = \mathcal{X} \backslash \mathcal{X}_{\text{obs}}$. The objective is to find a sequence σ of states that minimises the cost function $c(\sigma)$, while connecting the starting state $\mathbf{x}_\text{s}$ and end state $\mathbf{x}_\text{e}$

$$\sigma^* = \underset{\sigma \in \Sigma}{\arg\min} \left\{ c(\sigma) \mid \sigma(0) = \mathbf{x}_\text{s}\,,\ \sigma(1) = \mathbf{x}_\text{e}\,,\ \forall s \in [0,1],\ \sigma(s) \in \mathcal{X}_{\text{free}} \right\}. \tag{F.6}$$

The obstacle subset $\mathcal{X}_{\text{obs}}$ is formed by the union over all constraints [F3], namely

$$\mathcal{X}_{\text{obs}} = \mathcal{X}_{\text{obs}}^{\text{OS}} \cup \mathcal{X}_{\text{obs}}^{\text{ENC}} \cup \mathcal{X}_{\text{obs}}^{\text{TV}}, \qquad \mathcal{X}_{\text{obs}}^{\text{TV}} = \bigcup_{i=1}^{n} \mathcal{X}_{\text{TV},i}(t) \tag{F.7}$$

with $\mathcal{X}_{\text{obs}}^{\text{OS}}$ containing states that violate manoeuvring constraints, $\mathcal{X}_{\text{obs}}^{\text{ENC}}$ the grounding and buoy collision states, and finally $\mathcal{X}_{\text{obs}}^{\text{TV}}$ the target vessel constraints, which is the union of n vessels, such that all n are considered simultaneously. The spatial constraints are encoded by the predicted trajectories of each target vessel ($\mathcal{X}_{\text{TV},i}(t)$).

A deterministic planning algorithm is proposed for building a directed graph. The starting state $\mathbf{x}_s$ is the position of ownship in the north-east plane at $t = 0$, and $\mathbf{x}_e$ is the current desired destination, at some unknown final time $t = t_f$. Consider a grid $\mathcal{G} = [\mathbf{G}_1, \dots, \mathbf{G}_m]^T \in \mathbb{R}^{m \times n}$, with rows $\mathbf{G}_i = [g_{i,1} \dots, g_{i,n}]$, where each row represents the depth towards the goal and the width of potential deviations, and each element $g_{i,j} \in \mathcal{G}$ represents a point in the north-east plane. The grid is pre-processed, in order to refine it, by modifying points $g_{i,j}$ that violate the environmental constraints, as follows $\bar{\mathcal{G}} = \mathcal{G} \backslash \mathcal{X}_{\text{obs}}^{\text{ENC}}$. A directed graph $\mathcal{T}$ with root $\mathbf{x}_s$ is built over $k = m + 1$ iterations. Two sets of nodes are formed, one with all current parent nodes $\mathcal{C}_p = \{\mathbf{x}_s\}$, which always contains the start $\mathbf{x}_s$, and a set for all current child nodes $\mathcal{C}_c = \{\mathbf{x}_e\}$ that always contains the end $\mathbf{x}_e$. At each iteration, the sets are modified by the grid rows, which dictates edges that are to be formed

$$
\begin{aligned}
&\mathcal{C}_p = \{\mathbf{x}_s\}, \mathcal{C}_c = \{\mathbf{x}_e, \mathbf{G}_k\} && \text{if } k = 1, \\
&\mathcal{C}_p = \{\mathbf{x}_s, \mathbf{G}_{k-1}\}, \mathcal{C}_c = \{\mathbf{x}_e, \mathbf{G}_k\} && \text{if } 1 < k < m + 1, \quad\quad \text{(F.8)} \\
&\mathcal{C}_p = \{\mathbf{x}_s, \mathbf{G}_{k-1}\}, \mathcal{C}_c = \{\mathbf{x}_e\} && \text{if } k = m + 1.
\end{aligned}
$$

Before adding a given edge to $\mathcal{T}$, the resulting trajectory between the two nodes is checked to see if it violates any constraints ($\mathcal{X}_{\text{obs}}$). The trajectory between two nodes is computed by forward simulating (F.5). Nodes in collision from $\mathcal{C}_c$ are discarded and omitted from $\mathcal{C}_p$.

F.3.2 Rules and regulations

Adherence to the rules and practises of safe navigation is fundamental for MASS. There is a general consensus that the most essential IMO COLREGs are rules 8 & 13-17. Rules 13-15 dictate the three most common vessel encounters: overtaking (13), head-on (14) and crossing (15). Rule 14 & 15 specifies that the give-way vessel must perform the manoeuvre toward the port side, where rule 13 allows passing on either side in a safe manner. Rule 16 & 17 dictate the behaviour of the give-way and stand-on vessel, see [F10].

In the literature, there is a consensus that partial adherence to the COLREGs is sufficient to demonstrate capable and safe navigation. Within confined waters, such as rivers and urban environments, additional complexities may arise. Rule 14 and 15 specifically apply between two power-driven vessels; therefore, if the system
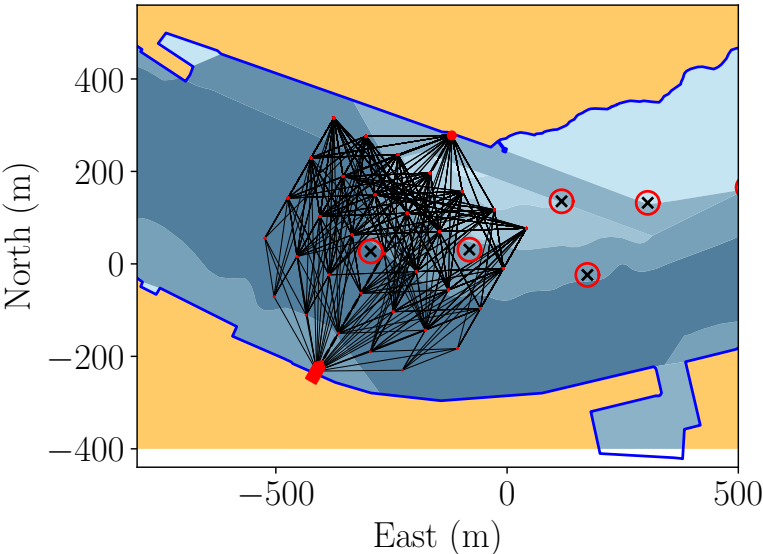
(a) Full lattice using a 7x5 grid.
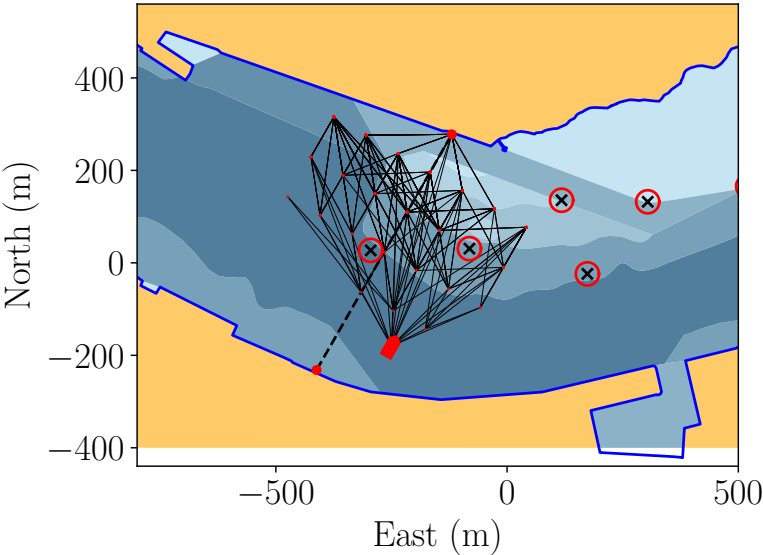
(b) Recomputing the lattice from an arbitrary location.

Figure F.3: The obstacle subset $\mathcal{X}_{\text{obs}}^{\text{ENC}}$ consists of the area surrounding the blue polygon (land and shallow waters) and the interior area of the red circles (buoys).
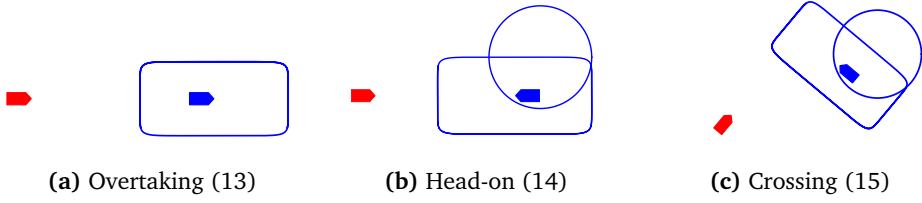
(a) Overtaking (13)   **(b)** Head-on (14)   **(c)** Crossing (15)

Figure F.4: Ship domains for COLREGs-compliance, dimensions are dependant on target vessel ship length.

encounters a sailboat, different rules and obligations apply. Furthermore, certain vessels may be restricted in their manoeuvrability. If a vessel is restricted, rule 9 applies, which states that a vessel less than 20m should give-way for a restricted vessel, even if according to rule 15 the target vessel is the give-way vessel. Hansen *et al.* [F11] used rule 9 within the decision making loop for a river crossing ferry, where its highlighted that simply following rule 15 without considering rule 9 may cause problems.

The complexity of the rule framework strongly depends on local laws (e.g. the Rhine River [F9]) for the particular waters. In Canadian waters, rule 15 is modified so that any vessel, with minor exceptions, crossing a river must yield to power-driven vessels travelling along it [F12]. According to §19 of Danish law on seafaring [F13], [F14], only three specific ferry routes must disregard the usual obligation to rule 15, and instead yield for any traffic the ferry may impede.

F.3.3 Ship domains for COLREGs-compliance

If MASS have adequate situation awareness, give-way and stand-on obligations can be enforced using Lamé curves [F3], see Fig. F.4. The curve for compliance with crossing and overtaking scenarios is given by

$$
\left| \frac{\cos(\psi(t))\Delta E_l(t) - \sin(\psi(t))\Delta N_l(t)}{a_L} \right|^p + \\
\left| \frac{\sin(\psi(t))\Delta E_l(t) + \cos(\psi(t))\Delta N_l(t)}{b_L} \right|^p \le 1
\tag{F.9}
$$

when used in conjunction with a circular constraint,

$$
\Delta E_c(t)^2 + \Delta N_c(t)^2 \le r_L^2
\tag{F.10}
$$

where a_L, b_L and r_L are scalar values based on the length of the target vessel and additional safety margins. The difference in coordinates at time t between the own ship and a given target vessel is used to evaluate the domains $\Delta E(t) =$
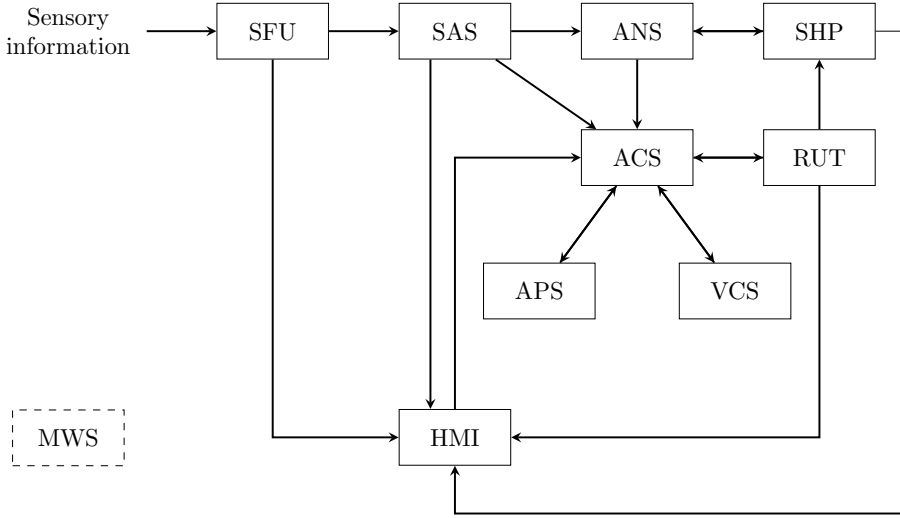
Figure F.5: Module interconnection within the autonomy stack.

$E(t) - E_{\text{TV}}(t) + E_\text{o}$, $\Delta N(t) = N(t) - N_{\text{TV}}(t) + N_\text{o}$ and $\bar{\psi}(t) = \psi_{\text{TV}}(t) + \psi_\text{o}$, where the offset is used to shift the elliptical and circular components of the domain,

$$
\begin{bmatrix} E_\text{o} \\ N_\text{o} \end{bmatrix} = \begin{bmatrix} \cos\left(-\bar{\psi}\right) & -\sin\left(-\bar{\psi}\right) \\ \sin\left(-\bar{\psi}\right) & \cos\left(-\bar{\psi}\right) \end{bmatrix} \begin{bmatrix} p_E \\ p_N \end{bmatrix}
\tag{F.11}
$$

with $p_E = 0$, and p_N equal to b_L in (F.9) and a_L in (F.10). For (F.9) and (F.10), the ψ_o is equal to 0 and $\frac{\pi}{2}$ respectively.

F.3.4   Safety margins

Ship length is commonly used to compute a safety margin with respect to other vessels. However, vessels navigating within inner coastal or confined waters are typically either sailboats or pleasure crafts, which are not obligated to carry an AIS transponder. Vessels of length greater than 20m are often required to have AIS. Therefore, it is necessary to select an adequate safety margin in the absence of an accurate ship length estimate. The safety margin is selected according to emergency stop manoeuvres (Fig. F.2a), such that a suitable distance is maintained to the target vessel, in instances with an erroneously perceived scenario. For the current transit speed of 3 knots, the required stopping distance is approximately 17.5m, therefore selecting 25m as the minimum ship length is ample distance.

F.4   The autonomy stack

The following section details the composition of the autonomy stack. The middleware is introduced and the purpose and responsibility of each module is outlined.

F.4.1   Middleware and autonomy stack features

Dittmann and Blanke [F15] investigated the regulatory framework and system requirements for the development and commissioning of MASS, highlighting some important considerations regarding reliability and redundancy. In addition, design choices and developments related to the custom middleware solution were detailed.

The autonomous system is composed of various modules, such that each block is compartmentalised and its interface clearly defined. Using a modular approach allows each part of the stack to be developed and tested individually, and also undergo strict stress and acceptance testing, before being rolled out and combined with the remaining system. The middleware facilitates publish–subscribe communication between modules, such that multiple modules can subscribe to the same module. Testing and simulation of various modules within the stack is achieved using a dedicated middleware simulator (MWS).

F.4.2   Module functionality and interconnection

The core of the stack consists of the Autonomous Coordination Supervisor (ACS), Autonomous Navigation Supervisor (ANS) and Autonomous Platform Supervisor (APS), which replace the traditional roles employed by the captain, navigator, and chief engineer [F16]. The ACS coordinates departures and exchanges routes with the route server (RUT), which stores the destination.

Effective and precise fused perception and sensory information is crucial for the remaining autonomous system. Human lookouts and navigators are replaced by an electronic outlook [F17] that uses cameras to detect and classify objects [F18]. The vision system is fused with the remaining sensors, producing a robust and resilient estimate of static and dynamic obstacles [F19], all of which is encapsulated by the Sensor Fusion (SFU) module. The estimated and fused states of the surrounding vessels can be augmented by a trajectory prediction scheme that uses information from the local area [F20]. However, the current stack only implements straight-line predictions. The Situation Awareness Service (SAS) is driven by information from the SFU, in order to maintain an overview of the unfolding scenario. Once a vessel violates set CPA and TCPA limits, the scenario is passed from SAS to the ANS, i.e. the 'navigator' is informed about the situation, and triggers the SHP for a route deviation. This ensures that the Greenhopper deals with the scenario in a timely

manner and with a reasonable safety margin. Details on the interaction between the SAS and ANS modules can be found in Hansen *et al.* [F21] and Papageorgiou *et al.* [F22]. A Human-machine Interface (HMI) visualises the SFU, RUT, SAS and SHP on an electronic navigational chart, with correct symbolism from IMO.

The SHP, originally introduced in Enevoldsen *et al.* [F3] as a generalised collision avoidance scheme for vessels in confined and inner coastal waters, is in this paper specialised for crossings, such as those encountered by the Greenhopper. The underlying planning scheme is implemented as described in Section F.3. As part of the autonomy stack, the SHP is tasked with computing rule-compliant, collision-, and grounding free passages for a given scenario at hand. Given an input consisting of own ship navigational data, predicted target vessel information, perceived COLREGs scenario (from the SFU-SAS-ANS) and the current destination (from RUT). The SHP reports within finite time whether a valid crossing exists and, if so, which sequence of waypoints must be followed to achieve it.

F.5   Demonstration and discussion

The autonomy stack and SHP is validated using software-in-the-loop testing by simulating the sensor fusion output. The results are visualised on the HMI, and generated while running the MWS, SAS, ANS, ACS, RUT and SHP modules. The MWS acts as both a vessel and SFU simulator. Figure F.6 shows a scenario in which the Greenhopper departs the southern harbour, following the nominally planned route. As the vessel is underway, two target vessels approach from the starboard side. The CPA for the southernmost target vessel is greater than the safety limit and is therefore not considered. However, the second target vessel violates the CPA limit; therefore, once TCPA falls below the chosen limit, the SHP is triggered and a route deviation is performed. Executing the deviation allows the Greenhopper to safely avoid the target vessel before reaching its destination at the northern point of the fjord.

A fundamental requirement for adhering to the COLREGs is an adequate estimate of the scenario at hand. Most systems, including the proposed one, break down if their assumptions do not hold. Most often, MASS depend on AIS for identifying vessel type and size, but in waters as those navigated by the Greenhopper and other autonomous ferries, a vast majority operate without AIS (due to being a leisure craft or other exemptions). It is therefore crucial that the perception system can classify if the perceived vessel is power-driven or not and is capable of determining whether a vessel is manoeuvrability restricted. Otherwise, the COLREGs cannot be applied correctly. For safe navigation, this is a major defect, since the target vessels
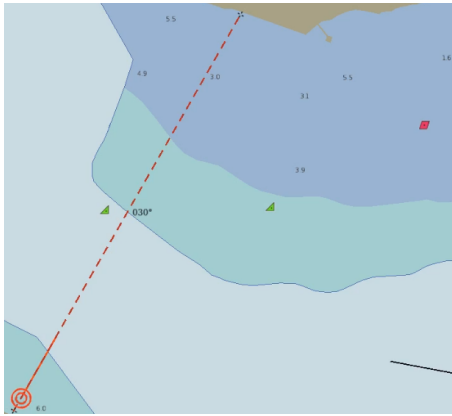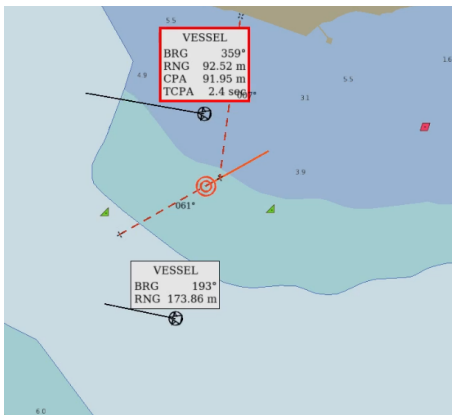
(a) t=10s
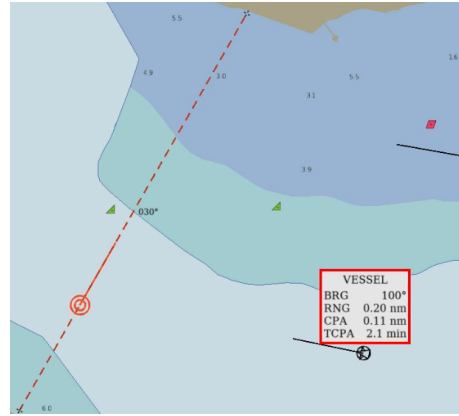
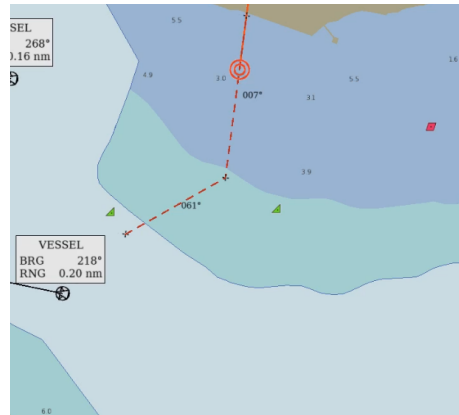**(b)** t=1m40s

(c) t=2m40s

(d) t=2m47s

(e) t=4m16s

(f) t=5m58s

Figure F.6: Simulated demonstration of the SHP with most of the autonomy stack. The Greenhopper is departing the southern harbour, following the nominally planned path. A manoeuvre is required while underway, as two other vessels approach from starboard.

are commanded by humans, who expect that any vessel they encounter adheres and acts according to the COLREGs, and if a severe risk of collision occurs, knows how to mitigate or lessen its severity. If the perceived scenario is correct, the proposed collision avoidance strategy can, in a deterministic fashion and within a finite time, report whether or not a path deviation exists within the chosen safety limits. If no solution exists during the voyage, the issue is raised to the ACS, which must be capable of correctly dealing with such an emergency situation, either by calling for help from a Remote Control Centre (RCC) or by stopping the vessel and signalling the surroundings that an emergency is unfolding.

F.6   Conclusion

The paper presented a collision avoidance perspective to autonomous ferries and harbour buses. A Danish autonomous ferry initiative, the Greenhopper, was introduced, and its autonomy stack was detailed and discussed. A deterministic collision avoidance strategy was presented, as well as simple ship domains for enforcing giveway responsibilities. The importance of a well-functioning and sufficiently accurate estimate of the unfolding situation was discussed in great detail. In conclusion, to navigate according to the COLREGs and safe navigation practises, the target vessels must be correctly classified in terms of vessel type and manoeuvrability.

Future work includes field verification of the proposed SHP in conjunction with the remaining autonomy stack. Once verified, the final steps towards fully commissioning the ferry for autonomous operation must be undertaken.

Acknowledgements

F.7 References

[F1] E. F. Brekke, E. Eide, B. H. Eriksen, E. F. Wilthil, M. Breivik, E. Skjellaug, Ø. K. Helgesen, A. M. Lekkas, A. B. Martinsen, E. H. Thyri, *et al.*, "Milliampere: An autonomous ferry prototype," *Journal of Physics: Conf. Series*, vol. 2311, 2022, p. 012 029.

[F2] K. Bergman, O. Ljungqvist, J. Linder, and D. Axehill, "A colregs-compliant motion planner for autonomous maneuvering of marine vessels in complex environments," *arXiv preprint arXiv:2012.12145*, 2020.

[F3] T. T. Enevoldsen, M. Blanke, and R. Galeazzi, "Sampling-based collision and grounding avoidance for marine crafts," *Ocean Engineering*, vol. 261, p. 112 078, 2022. DOI: https://doi.org/10.1016/j.oceaneng.2022.112078.

[F4] E. H. Thyri and M. Breivik, "A domain-based and reactive colav method with a partially colregs-compliant domain for asvs operating in confined waters," *Field Robotics*, vol. 2, pp. 637–677, 2022.

[F5] G. Bitar, B. H. Eriksen, A. M. Lekkas, and M. Breivik, "Three-phase automatic crossing for a passenger ferry with field trials," *2021 European Control Conference (ECC)*, IEEE, 2021, pp. 2271–2277.

[F6] E. H. Thyri, M. Breivik, and A. M. Lekkas, "A path-velocity decomposition approach to collision avoidance for autonomous passenger ferries in confined waters," *IFAC-PapersOnLine*, vol. 53, no. 2, pp. 14 628–14 635, 2020.

[F7] W. Wang, T. Shan, P. Leoni, D. Fernández-Gutiérrez, D. Meyers, C. Ratti, and D. Rus, "Roboat II: A novel autonomous surface vessel for urban environments," *2020 IEEE/RSJ Int. Conf. on Intelligent Robots and Systems (IROS)*, IEEE, 2020, pp. 1740–1747.

[F8] J. de Vries, E. Trevisan, J. van der Toorn, T. Das, B. Brito, and J. Alonso-Mora, "Regulations aware motion planning for autonomous surface vessels in urban canals," *2022 Int. Conf. on Robotics and Automation (ICRA)*, 2022, pp. 3291–3297. DOI: 10.1109/ICRA46639.2022.9811608.

[F9] P. Koschorrek, M. Kosch, M. Nitsch, D. Abel, and D. Jürgens, "Towards semi-autonomous operation of an over-actuated river ferry," *Automatisierungstechnik*, vol. 70, no. 5, pp. 433–443, 2022. DOI: 10.1515/auto-2021-0152.

[F10] A. N. Cockcroft and J. N. F. Lameijer, *Guide to the collision avoidance rules*. Elsevier, 2003.

[F11] P. N. Hansen, T. T. Enevoldsen, D. Papageorgiou, and M. Blanke, "Autonomous Navigation in Confined Waters–A COLREGs Rule 9 Compliant Framework," *arXiv preprint arXiv:2207.08227*, 2022.

[F12] CSA, *Collision Regulations, C.R.C., c. 1416, Canada Shipping Act (CSA), 2001*, `https://laws-lois.justice.gc.ca/PDF/C.R.C.,_c._1416.pdf`, 2001.

[F13] Søfartsstyrelsen, *Bekendtgørelse om sejlads m.m. i visse danske farvande (BEK nr 656 af 20/05/2020)*, 2020.

[F14] Søfartsstyrelsen, *Bekendtgørelse om sejlads på Limfjorden mellem Egholm og Kattegat (BEK nr 953 af 18/12/1991)*, 1991.

[F15] K. Dittmann and M. Blanke, "Risk mitigation by design of autonomous maritime automation systems," *Automatisierungstechnik*, vol. 70, no. 5, pp. 469–481, May 2022. DOI: `10.1515/auto-2021-0151`.

[F16] K. Dittmann, P. N. Hansen, D. Papageorgiou, and M. Blanke, "Autonomy for ships: A sovereign agents architecture for reliability and safety by design," *IEEE Xplore-Proc. IEEE SysTol*, 2021.

[F17] M. Blanke, S. Hansen, J. D. Stets, T. Koester, J. Brøsted, A. L. Maurin, N. Nykvist, J. Bang, and D. M. Authority, "Outlook for navigation–comparing human performance with a robotic solution," *Proc. of ICMASS*, 2018.

[F18] F. E. T. Schöller, M. Blanke, M. K. Plenge-Feidenhans, and L. Nalpantidis, "Vision-based object tracking in marine environments using features from neural network detections," *IFAC-PapersOnLine*, vol. 53, no. 2, pp. 14 517–14 523, 2020.

[F19] D. Dagdilelis, M. Blanke, R. H. Andersen, and R. Galeazzi, "Cyber-resilience for marine navigation by information fusion and change detection," *Ocean Engineering*, vol. 266, p. 112 605, 2022. DOI: `https://doi.org/10.1016/j.oceaneng.2022.112605`.

[F20] F. E. Schöller, T. T. Enevoldsen, J. B. Becktor, and P. N. Hansen, "Trajectory prediction for marine vessels using historical ais heatmaps and long short-term memory networks," *IFAC-PapersOnLine*, vol. 54, no. 16, pp. 83–89, 2021.

[F21] P. N. Hansen, D. Papageorgiou, M. Blanke, R. Galeazzi, M. Lützen, J. Mogensen, M. Bennedsen, and D. Hansen, "COLREGs-based Situation Awareness for Marine Vessels-a Discrete Event Systems Approach," *IFAC-PapersOnLine*, vol. 53, no. 2, pp. 14 501–14 508, 2020. DOI: `10.1016/j.ifacol.2020.12.1453`.

[F22]   D. Papageorgiou, P. N. Hansen, K. Dittmann, and M. Blanke, "Anticipation of ship behaviours in multi-vessel scenarios," *Ocean Engineering*, vol. 266, p. 112 777, 2022. DOI: https://doi.org/10.1016/j.oceaneng.2022.112777.